



*Faculty of Engineering, Computer and Mathematical Sciences*

SCHOOL OF MECHANICAL ENGINEERING

# **PERFORMANCE BENEFITS OF CUSTOMISED SEATING INTERFACES FOR ELITE WHEELCHAIR RACING ATHLETES**

AMY LEWIS

A thesis submitted in fulfilment of the requirements for the degree of

Doctor of Philosophy

July 2018



---

# DECLARATION

I certify that this work contains no material which has been accepted for the award of any other degree or diploma in my name, in any university or other tertiary institution and, to the best of my knowledge and belief, contains no material previously published or written by another person, except where due reference has been made in the text. In addition, I certify that no part of this work will, in the future, be used in a submission in my name, for any other degree or diploma in any university or other tertiary institution without the prior approval of the University of Adelaide and where applicable, any partner institution responsible for the joint-award of this degree.

I acknowledge that copyright of published works contained within this thesis resides with the copyright holder(s) of those works.

I also give permission for the digital version of my thesis to be made available on the web, via the University's digital research repository, the Library Search and also through web search engines, unless permission has been granted by the University to restrict access for a period of time.

I acknowledge the support I have received for my research through the provision of an Australian Government Research Training Program Scholarship.

---

SIGNED

---

DATE

---

# ACKNOWLEDGEMENTS

Thank you to all those who have shared this journey for me and fostering my growth not only within this PhD but within life itself. I am so grateful for all the support I have gotten, and for everyone who has made this journey an enjoyable one.

I would like to especially thank my parents, for providing me more than I ever needed, but all I ever wanted. You have given me the capacity to be brilliant, and I hope that I have, and continue to make you proud.

To my supervisors, thank you for the endless hours you have given me. I certainly would not have gotten here without you!

To my friends, thank you for making a PhD more than just a job and giving me a reason to be excited about coming into the office each day. Moreover, thank you, Jason, for being my inspiration, and challenging me to be the best I can be. It has been an honour growing through this journey beside you.

---

# ABSTRACT

The limited customisation in commercially available wheelchairs does not always appropriately accommodate the anthropometric variations resulting from specific impairment. Wheelchair racing athletes demonstrate up to 3.8% total body mass greater in the upper extremities, and up 9.8% total body mass reductions in their lower extremities, and between-limb asymmetries of 62.4%. As a consequence, athletes may not have the stable base of support required for optimal propulsion. The optimisation of an entire wheelchair to match unique athlete geometry is both time consuming and costly, as wheelchairs cost over \$2000 each. The use of assistive technology can provide an efficient transition between the commercially available equipment and the unique athlete anthropometry. Customised seating interfaces offer a time and cost effective solution, facilitating regular modifications to satisfy athlete growth. These solutions have been used extensively in clinical applications for enhanced stress distribution and injury prevention at the seating interface; however, they have not yet been applied to sporting contexts. The goal of this research was to investigate the performance impact of customised seating interfaces on wheelchair racing propulsion technique. Supplementary goals included the development of practically viable instrumentation solutions and a musculoskeletal model representative of the unique wheelchair racing athlete anthropometries and physical capabilities to assess injury risk to analyse performance impact holistically.

The research was split into four main themes:

1. Verification of the importance of the seating interface relative to other key performance parameters such as aerodynamics and glove selection.
2. Instrumentation of the hand-pushrim and seating interfaces
3. Development of a musculoskeletal model
4. Computational modelling of performance and injury risk

Computational modelling was performed in the OpenSim environment which coupled kinematic inputs from 3D motion capture (VICON Bonita V16; Oxford Metrics, Oxford, United Kingdom), with kinetic inputs from a pressure mat at the seating interface (XSensor LX100; Calgary, Alberta, Canada) and inertial measurement units (IMUs) (I Measure U; New Zealand) to estimate the hand-interface interactions. This was achieved using Newton's Second Law, incorporating athlete-specific mass data (from the analysis DXA scans), and acceleration measured from the IMU.

---

Customised seating interfaces reduced the undesirable peak translations of the knee by up to 41.8% and lateral translation of the spine by 33.4%. These translated towards enhanced performance, with an average performance time reduction of 29.8 s (3.7% race time) in the eight international competitions following the inclusion of the customised seating interface. Additionally, athletes using cushioned seating interfaces had reduced peak pressures at the seating interface as compared to those without the interface. Instrumentation can be used outside the laboratory environments, and can, therefore, be applied in the daily training environment to optimise performance preparation.

This research provided foundation work for the use of computational biomechanical analyses for the holistic assessment of wheelchair racing performance. Whilst this research has demonstrated the potential impact computational modelling approaches can have on the performance preparation of athletes, some areas for further refinement have been identified. Future research into the processing of IMU data and the validation of musculoskeletal models for wheelchair racing athletes are the critical areas for improvement. Once achieved, the computational modelling approaches explored in this research can positively impact performance outcome, particularly when coupled with the optimisation of equipment, such as customised seating interfaces.

---

# CONTENTS

<b>LIST OF FIGURES</b>	<b>X</b>
<b>LIST OF TABLES</b>	<b>XVII</b>
<b>CHAPTER ONE: INTRODUCTION</b>	<b>1</b>
1.1 Wheelchair Racing Propulsion	2
1.2 Sporting Wheelchair Design	4
<b>CHAPTER TWO: BACKGROUND</b>	<b>7</b>
2.1 Physical Impairments of Wheelchair Racing Athletes	8
2.2 Wheelchair Racing Equipment	12
2.3 Biomechanical Analysis of Performance	18
2.4 Wheelchair Instrumentation	23
2.5 Aims and Objectives	28
2.6 Significance	29
2.7 Contributions and Organisation of Thesis	31
2.8 Research Output	32
<b>CHAPTER THREE: HOW IMPORTANT IS THE SEATING INTERFACE TO ATHLETE PERFORMANCE?</b>	<b>34</b>
3.1 Athlete Characteristics	36
3.2 Does Glove Type Influence Wheelchair Propulsion Symmetry in Junior Athletes?	39
3.3 The Optimisation of Trunk Position for the 2016 Rio Paralympic Wheelchair Racing Finals	43
3.4 Implications and Conclusion	50
<b>CHAPTER FOUR: WHEELCHAIR INSTRUMENTATION USING IMUs</b>	<b>52</b>
4.1 Characteristic Response from IMUs Measuring Wheelchair Propulsion at Various Placement Locations	55
4.2 Methods of Collecting Wheelchair Racing Performance Data Using IMUs	63
4.3 Does the Placement of IMUs Affect the Macroscopic Measurement of Acceleration in Wheelchair Sports?	68
4.4 Intra Stroke Profiling of Wheelchair Propulsion Using IMUs, and the Influence of Equipment	77
4.5 The Validation of IMUs on Estimating Torque Production of Wheelchair Racing Athletes	83
4.6 Discussion	95
4.7 Implications and Conclusion	96

---

<b>CHAPTER FIVE: WHEELCHAIR INSTRUMENTATION USING A PRESSURE MAT</b>	<b>98</b>
5.1 Methods of Collecting Wheelchair Racing Performance Data Using a Pressure Mat	100
5.2 Can a Commercially Available Pressure Mat Effectively Measure Interactions Acting at the Seating Interface?	102
5.3 Effect of Seating Cushions on Pressure Distribution	111
5.4 Changes in Leg Pressure During Modes of Racing Wheelchair Propulsion	114
5.5 Discussion	120
5.6 Implications and Conclusions	121
<b>CHAPTER SIX: DEVELOPMENT OF A SUBJECT-SPECIFIC, 3D MUSCULOSKELETAL MODEL</b>	<b>123</b>
6.1 Processing Of DXA Scans For the Calculation of Body Segment Inertial Parameters	126
6.2 The Effect of Altering Intensity Thresholds in DXA Scans on the Calculations of Body Segment Masses	132
6.3 Mass Distribution of Wheelchair Athletes Assessed Using DXA Scans	139
6.4 A Strategy for Estimating Maximum Isometric Force Generating Capacity of Wheelchair Racing Athletes	147
6.5 Discussion	155
6.6 Implications and Conclusion	157
<b>CHAPTER SEVEN: QUANTIFYING THE MECHANICS OF WHEELCHAIR PROPULSION USING SIMULATION</b>	<b>159</b>
7.1 Injury Prevention of Elite Wheelchair Racing Athletes Using Simulation Approaches	161
7.2 Influence of Customised Seating Interfaces on Lower Extremity Wheelchair Racing Kinematics: A Case Study	172
7.3 Implications and Conclusion	182
<b>CHAPTER EIGHT: CONCLUSION</b>	<b>183</b>
8.1 Overview of the Experimental Chapters	183
8.2 Contribution to Scientific Understanding and Future Directions	192
8.3 Concluding Remarks	196
<b>REFERENCES</b>	<b>198</b>
<b>APPENDIX A: COMPUTATIONAL MODELLING IN OPENSIM</b>	<b>217</b>
A.1 Inverse Kinematics	218
A.2 Inverse Dynamics	221
A.3 Static Optimisation	224
A.4 Conclusion	226

---



---

<b>APPENDIX B: MUSCULOSKELETAL MODEL DEVELOPMENT</b>	<b>227</b>
B.1 Subject-Specific Modelling Approaches	229
B.2 Perturbation of Musculoskeletal Model Parameters	231
B.3 Estimating Body Segment Inertial Parameters	232
B.4 Estimating Maximum Force Generating Capacity of Skeletal Muscles	235
B.5 Estimating Joint Reference Frames	236
<b>APPENDIX C: VALIDATION AND VERIFICATION OF INVERSE DYNAMICS MODELS</b>	<b>237</b>
C.1 Definition of Reserve Actuators	238
C.2 Verification of Musculoskeletal Model Adaptions for use with Wheelchair Racing Athletes	240
C.3 Upper Extremity Muscle Demand of Wheelchair Racing Propulsion Technique	244

---

# LIST OF FIGURES

<b>CHAPTER ONE: INTRODUCTION</b>	<b>1</b>
Figure 1.1: Wheelchair racing athletes assume a kneeling posture, and contact the pushrims using a striking motion.	2
Figure 1.2: Free body diagram of the propulsion phase as presented by Fuss. <sup>11</sup>	3
Figure 1.3: Free body diagram of the recovery phase as presented by Fuss. <sup>11</sup>	4
<b>CHAPTER TWO: BACKGROUND</b>	<b>7</b>
Figure 2.1: Peak isometric force measurements for shoulder movements (abduction, adduction, internal and external rotation) at a variety of speeds (60 °/sec, 180 °/sec and 300 °/sec) for wheelchair using and non-wheelchair using athletic and everyday populations. References presented in Table 2.2.	11
Figure 2.2: The three wheel types used in wheelchair racing. From left to right: Carbon disc, carbon aero, spoked.	13
Figure 2.3: Schematic outline of research demonstrating how each of the sub-studies contribute to the four research aims addressing the main aim of the research.	30
<b>CHAPTER THREE: HOW IMPORTANT IS THE SEATING INTERFACE TO ATHLETE PERFORMANCE?</b>	<b>34</b>
Figure 3.1 Relevance of the Chapter 3 to the fundamental research question.	36
Figure 3.2: Representative force curves (in AP direction) from a single push, normalised by system (athlete + wheelchair) mass.	41
Figure 3.3: Differences in the symmetry of force development (Asymmetry Index, Equation 3.1).	42
Figure 3.4: Trunk motion categorisation (based on trunk position at the top of the stroke).	45
Figure 3.5: Example of processed images used for frontal area estimation of a low (A) and high (B) classified athlete.	45
Figure 3.6: Influence of vertical position on athlete finishing place for both male and female athletes.	46
Figure 3.7: Break down of trunk position and finishing position according to race distance.	47
Figure 3.8: Influence of stroke count on vertical motion and finishing position.	48

---

<b>CHAPTER FOUR: WHEELCHAIR INSTRUMENTATION USING IMUs</b>	<b>52</b>
Figure 4.1 Relevance of the Chapter 4 to the fundamental research question.	54
Figure 4.2: Schematic demonstrating how IMUs were coupled to the wheel.	57
Figure 4.3: Example of IMU synchronisation as performed through comparing impact peaks.	57
Figure 4.4: Exemplar data from the IMU at different placement locations on the wheelchair. Contacts indicated by vertical dashed lines.	58
Figure 4.5: Characteristic acceleration data from IMU located on the wheelchair frame and hand.	59
Figure 4.6: Inter- and intra- rater reliability of contact identification between two experienced raters. IMU data obtained from wheelchair wheel.	60
Figure 4.7: Directional bias in video digitisation approaches, based on IMU located on the wheelchair wheel.	60
Figure 4.8: Influence of centripetal acceleration in IMU measurements located at different radii (2.8 cm, 10.4 cm, and 24.3 cm) on a wheel.	61
Figure 4.9: Testing set up. A) Custom clamp (circled) keeping wheelchair on the treadmill; B) IMU locations (circled).	63
Figure 4.10: IMU (square) mounting locations and reflective marker (circle) positioning. An additional marker was located atop the WRA IMU. A) Rear view: demonstrates frame (axle housing) placements (FL, FR). B) Right side view: highlights where IMUs were located on the wheel axle (WLA, WRA), pushrim (WLM, WRM), and outer rim (WLR, WRR). The left wheel was instrumented identically.	64
Figure 4.11: Tracking and Scaling marker placements used to actuate a musculoskeletal model with the Inverse Kinematics tool in the OpenSim environment.	66
Figure 4.12: Comparison of motion capture data and its derivatives over 15 push cycles, for the marker at the base of 2nd metacarpal joint on the left hand for athlete E at 22 km/hr.	67
Figure 4.13: Comparison of data from High SNR (Athlete F, 28 km/hr) and Low SNR signals (Athlete C, 22 km/hr).	69
Figure 4.14: Typical resultant acceleration patterns from Athlete F (29 km/hr) for verifying the four IMU placement locations (Frame, Axle, Pushrim and Outer Rim) against the reference data (motion capture), which was used to determine the acceleration of the hand.	70
Figure 4.15: Detection rate of false positive (FP) and false negative (FN) contact recordings across the four main placement locations.	72
Figure 4.16: Comparison of cycle times (s) estimated by IMUs against reference system (motion capture) for 523 push cycles. Signal to noise ratio (SNR) and correlation values ( $r$ ) from all trials and conditions for each athlete are labelled on each graph. IMUs were not located on the Pushrim for Athlete I.	73

---

---

Figure 4.17: Comparison of cycle times (s) estimated by IMUs against reference system (motion capture) for 127 push cycles for athletes with a coordination impairment. Signal to noise ratio (SNR) and correlation values ( $r$ ) from all trials and conditions for each athlete are labelled on each graph.	74
Figure 4.18: Representative example of acceleration trace demonstrating the detection of contact points with an IMU compared to motion capture, however, issues with the identification of release.	79
Figure 4.19: Capability assessment of the accuracy of the IMU-based contact detection methodology across varying athlete characteristics.	80
Figure 4.20: Comparison of different processing methods which can be used to improve the detection of release points.	81
Figure 4.21: Instrumentation configuration, demonstrating the placement locations of each of the three IMUs, and the chair on top of the force plates, demonstrating the wheels each starting on a different force plate.	85
Figure 4.22: Power spectral density of resultant acceleration signals from all athletes for both the acceleration and steady-state conditions for determining appropriate cut-off frequencies for the filtering of IMU data.	86
Figure 4.23: Selection of most appropriate cut-off frequency. The blue line represents filtered data (at the specified cut off frequency). Higher cut off frequencies demonstrates a closer fit between data sets.	87
Figure 4.24: Example of two athlete data in three dimensions (IMU data: solid lines; force plate data: dotted line) for a good (right) and poor (left) comparison of data in the AP direction. Body mass has been removed in the vertical (FV) direction. N.B. starting time on the x-axis included calibration of the force plates and the audible three-command cue for start of motion.	88
Figure 4.25: Bland Altman Plots of Agreement for a Start trial for each of the kinetic parameters for each athlete in each primary direction.	90
Figure 4.26: Comparison of steady-state data as recorded by IMUs to literature. Data from the literature is below 3 m/s are representative of manual wheelchair propulsion, while athlete data is above.	91
Figure 4.27: Comparison of raw and filtered steady state and acceleration data demonstrating a clear difference in magnitude of acceleration data with movement speed, and how the impact peaks used in Sections 4.1 through 4.4 relate to the force profile.	94

## **CHAPTER FIVE: WHEELCHAIR INSTRUMENTATION USING A PRESSURE MAT** **98**

Figure 5.1: Relevance of the Chapter 5 to the fundamental research question.	100
Figure 5.2: Placement of a pressure mat in two different wheelchairs (A and B). Tablet demonstrates no apparent singularities from placement.	101

---

Figure 5.3: Illinois Agility Test used in wheelchair rugby agility trials, with specific data analysed from the weaving section, as evident in the middle of the Figure.	105
Figure 5.4: Inter-individual variation of seating pressure while stationary for a single timestamp.	106
Figure 5.5: Comparison of average pressure, peak pressure and contact area for a single wheelchair racing and a single wheelchair rugby athlete.	107
Figure 5.6: Variation of magnitude and location of pressure for Athlete F (wheelchair racing) during steady-state propulsion (Top), and acceleration (Bottom) demonstrating that under non-constant velocity propulsion, the pressure at the athlete interface is not consistent between the recovery phase (left) and propulsion phase (right).	108
Figure 5.7: Variation in magnitude and location of peak pressures during agility tasks for a single wheelchair rugby athlete at a single time instant demonstrating seating pressure is not constant under non-linear conditions	109
Figure 5.8: Exemplar data of seating pressure across three athletes, obtained as a static measure before data collection.	112
Figure 5.9: Exemplar data from two athletes demonstrating the influence of foam cushions on average pressure, peak pressure and contact area. Data are presented as a mean of all athletes who use or do not use foam seating cushions.	112
Figure 5.10: Transient behaviour of average pressure and contact area for a single athlete (Athlete F) during steady state propulsion on a track and treadmill, acceleration on the track, and a starting motion.	116
Figure 5.11: Variation in pressure for a single timestamp across different modes of propulsion. Panels represent the different directions of pressure measured by the pressure mat.	117
Figure 5.12: Variability of average pressure and contact area during different modes of propulsion (track steady-state, track acceleration, start, treadmill steady-state), compared to the minimum value for a single athlete (Athlete F).	118
<b>CHAPTER SIX: DEVELOPMENT OF A SUBJECT-SPECIFIC, 3D MUSCULOSKELETAL MODEL</b>	<b>123</b>
Figure 6.1: Relevance of the Chapter 6 to the fundamental research question.	125
Figure 6.2: Example of DXA scan images delineated into the fourteen segments used in this research. A) provides an example of a high attenuation image which is inclusive of soft tissue mass. B) provides an example of the low attenuation image which shows the skeletal structure.	127
Figure 6.3: Musculoskeletal model used in research, highlighting the muscles modelled and marker placements used to actuate the model.	128
Figure 6.4: A) Example of a DXA scan, B) the histogram with default thresholds and C) the thresholds extended to maximum.	133

---

---

Figure 6.5: Comparison of the distribution of pixels across the majority of DXA scan data.	133
Figure 6.6: Threshold protocols for the high attenuation (soft tissue: top) and low attenuation (bone: bottom).	134
Figure 6.7: Comparison of DXA scan data due to different threshold intensities.	135
Figure 6.8 Differences in mass segments based on alterations in intensity.	136
Figure 6.9: Comparison of body mass distribution based on threshold intensity protocol.	136
Figure 6.10: Propulsion cycle modelled in OpenSim using the upper extremity dynamic model. Pink dots represent markers.	137
Figure 6.11: Influence of segment mass definition on inverse dynamics results (joint reaction torques).	137
Figure 6.12: Body mass distribution of all athletes. Thigh and shank segments of Athlete I were excluded from analysis due to the presence of overlapping limb segments.	141
Figure 6.13: Appendicular mass asymmetry indices calculated from DXA data. Positive values indicate right side bias, with larger magnitudes demonstrating larger asymmetry.	141
Figure 6.14: Population-based averages for body mass distribution.	142
Figure 6.15: Segment masses as presented as a percentage of total body mass (mean of left and right data).	142
Figure 6.16: Variation in joint reaction moments calculated using inverse dynamics, between athlete-specific and total body mass-matched scaled models.	144
Figure 6.17: Comparison of muscle and reserve actuator contributions to activation and force, for Athlete I at 26 km/hr. Each data point corresponds to the activation or force of each muscle or reserve actuator in the system per time stamp (0.004 s) over the simulation period. Activation has been normalised against total activation.	150
Figure 6.18: Comparison of the difference in muscle activation and force between successive scaling factors. Data are presented as a percentage of the mean value of muscle activation and force for scaling factors 1-4.	151
Figure 6.19: The contribution of the reserve actuators varies with increasing scaling factor.	152
 <b>CHAPTER SEVEN: QUANTIFYING THE MECHANICS OF WHEELCHAIR PROPULSION USING SIMULATION</b>	
Figure 7.1: Relevance of the Chapter 7 to the fundamental research question.	160
Figure 7.2: Joint range of motions explored in this investigation.	163
Figure 7.3: Example of a computational model of wheelchair racing propulsion. Arrows demonstrate the direction and magnitude of applied forces.	164
Figure 7.4: Kinematic comparison of motion for Athlete E (left) and Athlete I (right).	166

---

---

Figure 7.5: Torso rotation to the right side during propulsion. The dashed line between the centre of spine and sternum.	168
Figure 7.6: Amalgamation of existing verified models, including the Upper Extremity (top left), <sup>164</sup> Wrist, <sup>331</sup> and Lower Extremity <sup>332</sup> to produce a full body model.	169
Figure 7.7: Scapula movement during propulsion from a top view (top) and rear view (bottom). Data is from Athlete J (Section 7.2).	170
Figure 7.8: Comparison of reaction force estimates for unlocked (top) and locked (bottom) scapulothoracic joints, which resulted in the large overestimation of error in the results for Athlete I at 27 km/hr.	171
Figure 7.9: Marker (circles) configuration on A) the wheelchair frame (four, front two occluded) and B) wheel (five, same on both wheels).	174
Figure 7.10: Motion capture marker placement on an athlete.	174
Figure 7.11: Cyclograms demonstrating reduced asymmetries at the hand during steady state conditions due to a customised seating interface.	177
Figure 7.12: Cyclograms, demonstrating reduced asymmetries at the hand and elbow through the inclusion of the customised seating interface under race start conditions.	178
Figure 7.13: Violin plots demonstrating joint reaction moments differ between left (blue) and right (yellow) limbs during steady-state motion. The width of the violin plot for a particular moment indicates its relative frequency in the distribution.	179
Figure 7.14: Violin plots demonstrating joint reaction moments differ between left (blue) and right (yellow) limbs during a starting motion.	179
Figure 7.15: Performance impact of customised seating interfaces on performance. Dashed lines indicate mean time. Values are omitted to retain athlete anonymity.	180
<b>CHAPTER EIGHT: CONCLUSION</b>	<b>183</b>
Figure 8.1: Relation of key research aims to overall research aim.	184
<b>REFERENCES</b>	<b>198</b>
<b>APPENDIX A: COMPUTATIONAL MODELLING IN OPENSIM</b>	<b>217</b>
Figure A.1: Flowchart of the modelling process demonstrating the required inputs (left, dark boxes), the processes (outlined boxes), and the resulting outputs (right, light boxes).	218
Figure A.2: Required inputs for inverse kinematics calculations and the resulting output measures (right).	219

---

---

Figure A.3: Required inputs for inverse dynamics calculations and the resulting output measures.	221
Figure A.4: Required inputs for Static Optimisation calculations and the resulting output measures. Yellow boxes contain the required input parameters, and range boxes are the computational tool employed by OpenSim.	225
<b>APPENDIX B: MUSCULOSKELETAL MODEL DEVELOPMENT</b>	<b>227</b>
<b>APPENDIX C: VALIDATION AND VERIFICATION OF INVERSE DYNAMICS MODELS</b>	<b>237</b>
Figure C.1: Comparison of reserve actuator with defining various levels of optimal force in reserve actuators.	239
Figure C.2: Differences in reaction forces or moments for each of the modelled ROM for scaled values compared to default.	242
Figure C.3: Average (left) and maximum (right) instantaneous stress for the simulated muscles during wheelchair racing propulsion for Athlete E at 22 km/hr.	246
Figure C.4: Muscle force during propulsion (shaded) and recovery phases. Darker regions mean more muscles being recruited to complete the task.	247



---

# LIST OF TABLES

<b>CHAPTER ONE: INTRODUCTION</b>	<b>1</b>
<b>CHAPTER TWO: BACKGROUND</b>	<b>7</b>
Table 2.1: Classification profiles for wheelchair racing athletes competing in athletics, and the corresponding physical impairments. Data presented in this table is based upon the World Para-Athletics Classification Rules and Regulations. <sup>21</sup>	8
Table 2.2: Reference detail for Figure 2.1.	11
Table 2.3: Paralympic Sports Australian Athletes compete in which require performance equipment. Data compiled from the author based on information found online and from discussions with Australian Paralympic Committee Staff.	14
Table 2.4: List of literature summarising how musculoskeletal models have been used in wheelchair research.	22
Table 2.5: Bespoke instrumentation solutions currently used to measure wheelchair kinematics.	26
<b>CHAPTER THREE: HOW IMPORTANT IS THE SEATING INTERFACE TO ATHLETE PERFORMANCE?</b>	<b>34</b>
Table 3.1: Athlete information. Speed is only listed for athletes who performed steady-state propulsion on a treadmill (Section 4.2)	37
Table 3.2: Population sample for each experimental simulation. No athletes were used in study 3.3 which was a review of video (YouTube), or in Section 4.1 which involved pilot testing.	38
Table 3.3: Comparison of gloved and non-gloved conditions between classifications and glove type (hard or soft). Data are presented as an absolute percentage difference from perfect symmetry (mean $\pm$ SD). Larger magnitudes indicating a more considerable difference between hands.	41
Table 3.4: Possible male time reductions if athletes maintained a low trunk position.	48

---

<b>CHAPTER FOUR: WHEELCHAIR INSTRUMENTATION USING IMUs</b>	<b>52</b>
Table 4.1 Reliability of IMUs in contact timings, data presented as mean time $\pm$ SD.	59
Table 4.2: Relevant athlete demographics for the five athletes in this study. Further characteristics were presented previously in Table 3.1.	69
Table 4.3: Summary statistics demonstrating the quality of agreement between methods (conventional versus IMU) for each IMU placement location. Quality of agreement is shown visually through shading, yellow (good) through blue (poor). High SD values of Athlete F are attributed to the different propulsion strategy, including swing throughs (cycle time $\sim$ 1.3 s), which the athlete used for efficiency. No IMUs were located on the pushrim for Athlete I.	75
Table 4.4: Precision and bias between IMU estimates and force plate data. RFD data were not presented as % mean due to the small denominator.	89
<b>CHAPTER FIVE: WHEELCHAIR INSTRUMENTATION USING A PRESSURE MAT</b>	<b>98</b>
Table 5.1: Coefficient of variation measures in average pressure, peak pressure and contact area, demonstrating inter-individual variation between modes of propulsion.	107
Table 5.2: Comparison of average pressure, peak pressure and contact area (mean $\pm$ SD) during the propulsion and recovery phase when a seating cushion was not, and was used. Data are presented as the average of all athletes.	113
Table 5.3: Differences in average pressure and contact area between modes of propulsion (track steady-state, track acceleration, start, treadmill steady-state).	118
<b>CHAPTER SIX: DEVELOPMENT OF A SUBJECT-SPECIFIC, 3D MUSCULOSKELETAL MODEL</b>	<b>123</b>
Table 6.1: Relevant athlete characteristics. Further elaboration can be found in Table 3.1.	126
Table 6.2: Changes in segment mass based on intensity threshold protocol.	136
Table 6.3: Differences in mass distribution of the computational model between scaling approaches (actual and generic).	143
<b>CHAPTER SEVEN: QUANTIFYING THE MECHANICS OF WHEELCHAIR PROPULSION USING SIMULATION</b>	<b>159</b>
Table 7.1: Kinematic and kinetic characteristics of propulsion presented for Athlete E as mean $\pm$ SD; n represents the number of push cycles recorded. Contact and Release angles are presented to no decimal places to reflect the precision of the collected data.	165

---

---

Table 7.2: Kinematic and kinetic characteristics of propulsion presented for Athlete I as mean $\pm$ SD; n represents the number of push cycles recorded. Contact and Release angles are presented to no decimal places to reflect the precision of the collected data.	165
Table 7.3: Statistical significance for shoulder reaction moments with kinematic parameters.	166
Table 7.4: Changes in forwards knee motion between old and new seating conditions. Positive values indicate a reduction in movement (post).	177
<b>CHAPTER EIGHT: CONCLUSION</b>	<b>183</b>
Table 8.1: Key findings from Chapter Three: How important is the seating interface to athlete performance?	185
Table 8.2: Key findings from Chapter Four: Instrumentation using IMUs.	187
Table 8.3: Key findings from Chapter Five: Instrumentation using a pressure mat.	189
Table 8.4: Key findings from Chapter Six: Development of a subject-specific, 3D, musculoskeletal model.	190
Table 8.5: Key findings from Chapter Seven: Quantify the mechanics of wheelchair racing propulsion using simulation.	191
<b>REFERENCES</b>	<b>198</b>
<b>APPENDIX A: COMPUTATIONAL MODELLING IN OPENSIM</b>	<b>217</b>
Table A.1: Observed kinematic uncertainties and impact on the model and ensuing calculations.	220
Table A.2: Observed kinetic uncertainties and impact on the model and ensuing calculations.	223
<b>APPENDIX B: MUSCULOSKELETAL MODEL DEVELOPMENT</b>	<b>227</b>
Table B.1: Required parameters for the development of a computational model in the OpenSim environment. List of computational counterparts acquired from the XML file for the gait 2392_scaled. Osim file. <sup>128-132</sup>	228
Table B.2: Source of BSIP in the most common shoulder and upper extremity models, demonstrating the reliance on cadaver studies, despite the questions in the literature regarding their reliability.	229
Table B.3: Model definition result errors as presented in the literature.	230

---

---

Table B.4: Limitations and specific applications of a number of direct BSIP estimation methods performed <i>ex vivo</i> .	233
Table B.5: Limitations and specific applications of a number of direct BSIP estimation methods performed <i>in vivo</i> .	233
Table B.6: Limitations and specific applications of a number of indirect BSIP estimation methods performed <i>in vivo</i> using regression equations.	234
Table B.7: Limitations and specific applications of a number of indirect BSIP estimation methods performed <i>in vivo</i> using geometric models.	234
Table B.8: Estimation procedures for muscle physical cross-sectional area (PCSA).	235
<b>APPENDIX C: VALIDATION AND VERIFICATION OF INVERSE DYNAMICS MODELS</b>	<b>237</b>
Table C.1: Mean absolute RMS differences between original and scaled conditions on static optimisation when scapula scaled.	243
Table C.2: Muscles and the number of muscle elements modelled in computational modelling and EMG literature.	245

---

## CHAPTER ONE:

# INTRODUCTION

---

Wheelchair racing is a sport within the stream of athletics and triathlon (running) open to athletes with a physical impairment. Athletes propel a specialised wheelchair on either a track surface (Athletics: 100 m, 200 m 400 m, 800 m, 1,500 m, 5,000 m, 10,000 m, 4 × 100 m relay and 4 × 400 m relay) or a road surface (Marathon: 42,195 m, triathlon 5,000 m). Australia has a rich history in both athletics and triathlon at an international level. This includes Louise Savage (9 Gold and 4 Silver Paralympic medals between 1992 and 2004) and Kurt Fearnley (3 Gold, 7 Silver and 3 Bronze Paralympic medals between 2000 and 2016) in athletics, as well as Bill Chaffey in triathlon, who has won gold at the World Championships five times between 2009 and 2015.

Wheelchair racing first appeared in an international games for the disabled in 1960, in Rome, Italy.<sup>1</sup> Since its establishment, performance times have improved dramatically. The men's 1,500 m times have dropped from 3:58.50 (minutes : seconds . hundredths) at the 1984 Summer Olympics,<sup>2</sup> to 2:51.84, which was the fastest official time recorded by a wheelchair racer at the end of 2017. While sporting outcome is primarily a reflection of athletic ability, the effective integration of modern technologies may have also contributed to the significant drop in performance time over the last 35 years.

The use of aluminium, titanium or composite materials make wheelchairs lighter and stiffer, to become faster and more responsive,<sup>3</sup> which is beneficial for performance. An exploration into further performance and equipment optimisation is crucial to maintain current competitive advantages and success over international competitors and to assist with the improved performance of developing athletes. The integration of science and technology into wheelchair sports is relatively novel, making substantial performance gains easily obtained. Additionally, the majority of wheelchair-related literature to date has been clinical.

### 1.1 WHEELCHAIR RACING PROPULSION

Wheelchair racing propulsion technique is different to the conventional grab and push technique of conventional manual wheelchair propulsion (Figure 1.1).<sup>4</sup> Wheelchair racers instead use more of a striking motion between the hand (which is protected through a glove), and the push-rim (located on top of the rear wheels).<sup>5</sup> This rubber pushrim has a diameter between 12" (304.8 mm) and 16" (406.4 mm), as compared with overall wheel diameter (29", 622 mm)<sup>6</sup>. The ratio of these two measurements acts as the gearing system for the wheelchair.<sup>7</sup> The pushrim surface can be modified with fabric tape or adhesives to increase the surface roughness, and hence increase traction between the hand and pushrim to improve force transfer to the wheelchair.<sup>7</sup> As athletes are not gripping the wheels, they can have a higher cadence, allowing them to reach greater peak speeds.

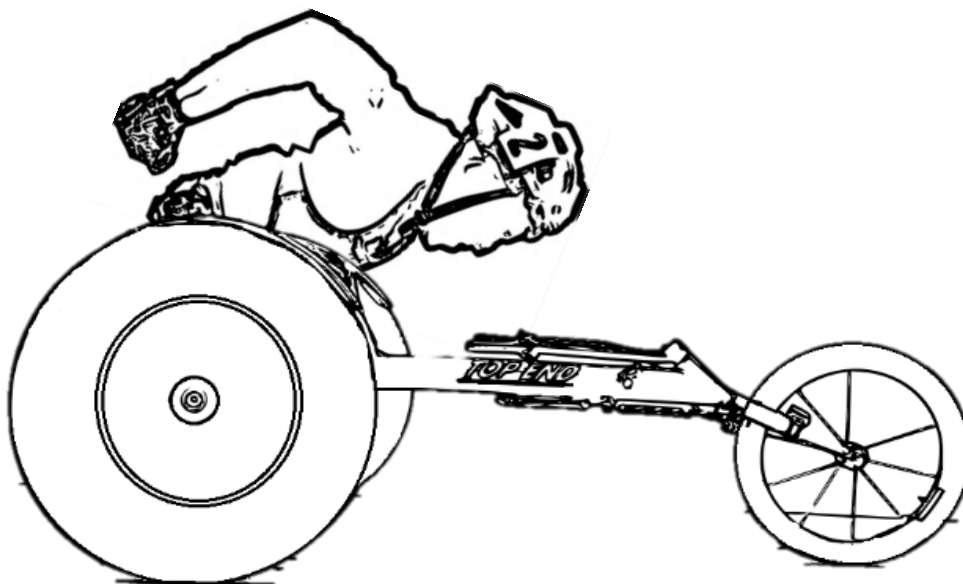


Figure 1.1: Wheelchair racing athletes assume a kneeling posture, and contact the pushrims using a striking motion.

Athletes assume a kneeling posture for propulsion, and as such, the seating interface is at the shins, rather than at the ischial tuberosities seen in conventional, upright postures. This position promotes power transfer to the pushrims<sup>3</sup> and substantially reduces athlete frontal area by 46% (0.37 m<sup>2</sup> conventional, upright postures,<sup>8</sup> but just 0.17 m<sup>2</sup> in a racing wheelchair).<sup>9</sup> Due to reduced aerodynamic drag, power reductions of 16.6% were identified for athletes assuming the aerodynamically optimised racing position (with a hyperextended neck) as compared to an upright position. A flexed head position (looking up) requires 1.75% greater power than a hyperextended neck position.<sup>9</sup>

Wheelchair propulsion is a closed loop cyclic motion, where the legs are rigidly secured within the seat, presumably exhibiting a quasi-static movement, while the arms demonstrate a highly dynamic motion. Propulsion can be separated into two fundamental phases: propulsion and recovery.<sup>10</sup> Force transfer between the athlete and wheelchair occurs during the propulsion phase. During the recovery phase, athletes return to a position ready for the next hand contact (initiating the start of the following propulsion phase). There is no single “optimum” technique, with athletes optimising their technique based on their unique physical capabilities.

To optimise individual performance, athletes must successfully execute the mechanical demands of propulsion (overcoming the athlete-wheelchair moment of inertia) to overcome the resistive forces acting on the system. The two main resistive forces acting on this system include rolling resistance ( $F_{\text{Rolling}}$ ) and aerodynamic resistance ( $F_{\text{Drag}}$ ) as presented in the free body diagrams in Figure 1.2 and Figure 1.3. These are in horizontal equilibrium with the inertial forces ( $F_{\text{Inertial}}$ ) and the force applied to the ground by the rear wheels ( $F_{\text{Applied}}$ ). Further information can be found in the literature by Fuss.<sup>11</sup>

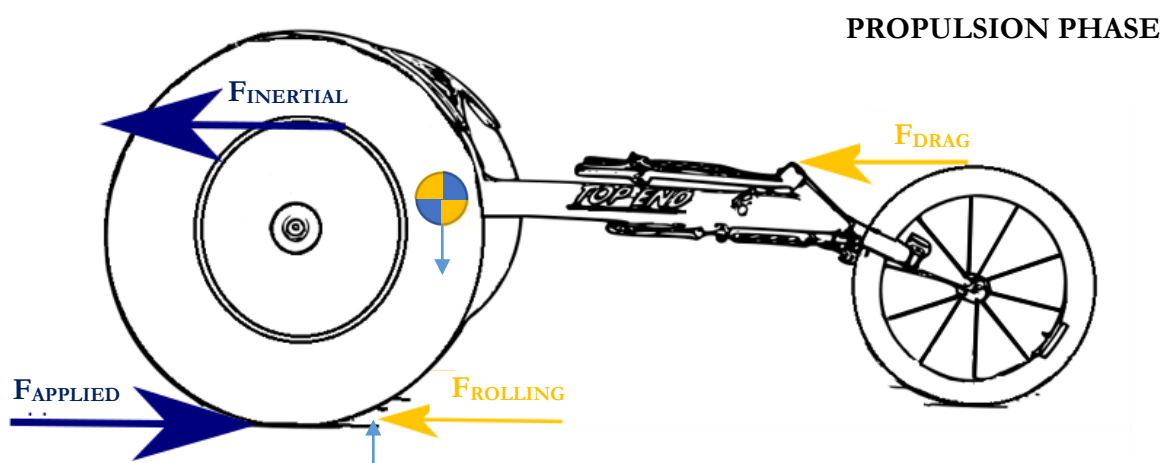


Figure 1.2: Free body diagram of the propulsion phase as presented by Fuss.<sup>11</sup>

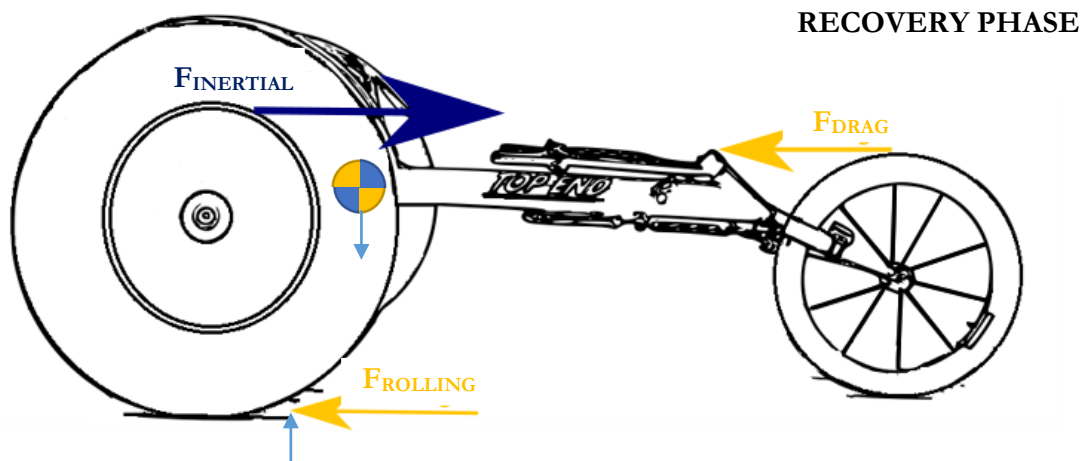


Figure 1.3: Free body diagram of the recovery phase as presented by Fuss.<sup>11</sup>

Rolling resistance in wheelchair racing is the more significant source of resistive drag, being between 65% and 75% of total resistance (depending on speed), with aerodynamics being the remaining 35% to 25%.<sup>9</sup> Overcoming these resistive forces is achieved through ensuring optimum friction between the hand, glove and pushrim; and applying maximal propulsive force over an optimum path.<sup>12</sup>

## 1.2 SPORTING WHEELCHAIR DESIGN

Sporting-specific wheelchair designs are performance driven to effectively balance the competing key design requirements of strength, stability, aerodynamics, and agility. Athletes began to modify their wheelchairs for specific sports in the 1970s,<sup>1</sup> with the first three-wheeled racing wheelchair design developed in 1990.<sup>6</sup> Modern materials and manufacturing techniques also mean aluminium and carbon fibre are used in the construction of the chassis to achieve a lightweight frame (between 4.5 kg and 8.2 kg)<sup>1, 11, 13, 14</sup> without compromised structural integrity and stiffness.<sup>15</sup> Use of lightweight materials has large implications on performance as additional mass in the athlete-wheelchair system is detrimental.<sup>11</sup>

The importance of each of the design requirements varies across wheelchair sports, as is reflected in the considerable differences in chassis design. For example, wheelchair mass and aerodynamics are of paramount importance to wheelchair racing as these assist in optimising linear velocity and acceleration. However, athletes in ball sports are more concerned with mobility, with wheelchair rugby also requiring a high stiffness chassis to withstand the frequent collisions. This translates to an increased rugby wheelchair mass (17.2 kg).<sup>16</sup> As a point of comparison, conventional wheelchairs have a mass up to up to 18 kg<sup>1</sup> (ultralightweight wheelchairs <13.6 kg; lightweight chair <15.5 kg).<sup>17</sup>



---

Some distinguishing features of wheelchair racing chairs include the tubular tires, lightweight rims, precision hubs, and large rear wheels with smaller pushrims.<sup>1</sup> The rear wheels are cambered to increase stability by providing a broader base of contact (although at the detriment of increased rolling resistance). Commercially-available wheelchairs allow limited customisation in configuration. A popular brand of wheelchair amongst Australian athletes (Invacare, Ohio, United States of America), allows athlete-specific prescription of upper and lower frame width, cage depth, knee width, and height, kneel depth and front and rear seat height.<sup>6</sup> Additionally, athletes can opt for an elongated front fork to further enhance stability. However, the increased length decreases the manoeuvrability of the wheelchair, and so athlete-specific wheelchair prescription is required. Triathlon athletes compete using the same equipment as wheelchair racers.

The degree of customisation available in commercially available chairs does not always accommodate the anthropometric variations resulting from specific impairment sufficiently. For example, athletes with amputation or substantial loss of skeletal muscle tissue (on either one or both legs) are likely to have a seating cavity which is too large. As a result, athletes may move relative to the seat, like running in a pair of shoes which is too large.

The relationship between chair geometry, athlete anthropometry, and track characteristics is key to improved performance.<sup>1</sup> Athletes with different levels of injury have demonstrated distinct differences in stroke kinematics,<sup>18</sup> and adopt wheelchair designs and seating postures which best optimise balance and performance. As para-athletes present with varying levels of skeletal muscle tissue and bone, they all sit differently within the seat.

The optimisation of an entire wheelchair to unique athlete geometry is both time-consuming and costly. Additionally, it precludes replacements to accommodate any anthropometric changes (such as loss or gain of skeletal muscle tissue). The use of assistive technology can provide an efficient transition between the commercially available equipment and the unique athlete anthropometry to improve the performance of the athlete-wheelchair system as a whole. For example, seating inserts provide a time- and cost-effective solution, which facilitate regular modifications to satisfy athlete growth. These solutions have been used extensively in clinical applications for enhanced stress distribution and injury prevention at the seating interface, but not in sporting applications.

Moulding cushions to exactly match an athlete's geometry can artificially return the tissue lost by impairment. Increased support is achieved through custom contouring of the cushion to match athlete-specific anthropometric adaptations owing to physical impairment. A customised seating interface can benefit acceleration, power, and mobility as a consequence of the increased conformity and maximisation of the contact surface area between the buttocks and seat.<sup>19</sup>

Despite these benefits; no literature presents what the influence of customised seating interfaces is on sporting performance. Anecdotal coach and athlete feedback indicates an investigation into the use of customised seating interfaces for sporting performance is warranted.<sup>19</sup> This led to the fundamental question of this research; what performance effect do customised seating interfaces have on wheelchair racing athletes? To understand the performance impact of customised seating however, further investigation into appropriate measurement tools (instrumentation) and biomechanical analytical techniques (computational modelling) are required.

---

## CHAPTER TWO:

# BACKGROUND

---

There are twenty-three summer Paralympic sports (as at January 2019), which are contested by athletes having a physical, visual or learning impairment. This research is focused only on athletes having a physical impairment. The ten eligible physical impairment types include; impaired muscle power, reduced passive range of movement, limb deficiency, leg length difference, short stature, hypertonia, ataxia, athetosis, and visual impairment.<sup>20</sup> Of the twenty-three sports, four are dedicated wheelchair sports (basketball, fencing, rugby, and tennis), with wheelchair athletes also eligible to compete within classifications of other sports (athletics and table tennis, for example). This chapter will provide a background of wheelchair racing, including the physical impairments of athletes competing in the sport and the equipment required for competition, and highlight the need for customised seating interfaces. Additionally, the methods currently being used for the biomechanical analysis will be revealed, with insight as to how they can be improved to more accurately quantify any technical changes resulting from the inclusion of customised seating interfaces.

## 2.1 PHYSICAL IMPAIRMENTS OF WHEELCHAIR RACING ATHLETES

To be eligible to compete in para-athletics, athletes must present with a physical impairment which is the direct result of a health condition or injury.<sup>21</sup> These relate to either compromised muscular control or impaired muscle power.<sup>22</sup> Para sports are governed through a classification system to reduce the inequalities between functionality, promoting more equal opportunities for athletes to excel. The specific classifications for wheelchair racing are presented in Table 2.1. Lower classifications (i.e. T31) have less functional mobility than athletes in a higher classification (i.e. T34).

Table 2.1: Classification profiles for wheelchair racing athletes competing in athletics, and the corresponding physical impairments. Data presented in this table is based upon the World Para-Athletics Classification Rules and Regulations.<sup>21</sup>

		<b>Lower Extremity Function</b>	<b>Trunk Control</b>	<b>Upper Extremity and Hand Function</b>
Compromised Muscular Control	T31	A demonstrable degree of function in one or both lower limbs.	Fair static control. Poor dynamic trunk control.	Hand severe to moderate involvement.
	T32	Poor functional strength in all limbs.	Fair static control. Poor dynamic trunk control.	Hand severe to moderate involvement.
	T33	Some demonstrable function. Spasticity grade 4-3.	Fair trunk control, but forward trunk motion often limited to extensor tone. Spasticity grade 2+.	Moderate limitation spasticity grade 2+. Poor finger dexterity.
	T34	Moderate to severe involvement. Spasticity grade 4 -3.	Minimal limitation of trunk movements.	The upper limbs often show regular functional strength.
Impaired Muscle Power	T51	N/A	N/A	Decreased shoulder muscle power.
	T52	N/A	No trunk function.	Normal shoulder, elbow and wrist muscle power. Poor to normal muscle of fingers.
	T53	No lower spinal muscle activity.	No abdominal activity.	Normal arm muscle power.
	T54	May have significant leg muscle power.	Partial trunk control to normal trunk control.	Normal arm muscle power.

N/A: No mention in documentation, however based on similar activity limitations (T51: complete spinal cord injury at level C5-6, T52: complete cord injury at C7-8), it can be presumed that there is no function.

---

### 2.1.1 INDIVIDUALS WITH COMPROMISED MUSCULAR CONTROL

Athletes classified as T31 – T34 have compromised muscular control, and present with either hypertonia (high muscle tone), athetosis (involuntary contractions of muscles) or ataxia (impaired control of voluntary movement). Such impairments are the result of health conditions including cerebral palsy, and multiple sclerosis however they also may be acquired from stroke or acquired brain injury.<sup>21</sup>

- **Hypertonia** (resulting from cerebral palsy, stroke, acquired brain injury or multiple sclerosis).<sup>21</sup> Clinically, there are two forms of hypertonia; spastic and dystonic.<sup>23</sup> A simplified definition of spasticity-related hypertonia is the premature and/or exaggerated muscle contraction (which may resist the passive stretch) as a consequence of the absence of modulation of the stretch reflex.<sup>24</sup> Dystonia, however, relates to sustained contractions of muscles which may result in abnormal posture, and contribute to joint stiffness.<sup>25</sup>
- **Ataxia** (resulting from cerebral palsy, brain injury, Friedreich’s ataxia, multiple sclerosis or spinocerebellar ataxia).<sup>21</sup> Ataxia is the result of a damaged, or dysfunctional cerebellum, which is vital in maintaining static and dynamic balance and modulating muscle activity.<sup>25</sup>
- **Athetosis** (resulting from damage to motor control centres of the brain from the result of cerebral palsy, stroke or traumatic brain injury).<sup>21</sup> Athetosis is characterised by involuntary movement of the fingers and toes, an inability to be still (swaying), and characteristic athetoid posturing of limbs and the trunk.<sup>21</sup>

### 2.1.2 INDIVIDUALS WITH IMPAIRED MUSCLE POWER

Athletes classified as T51 – T54 have impaired muscle power (resulting from spinal cord injury, muscular dystrophy and spina bifida, for example), reduced passive range of movement and congenital or traumatic leg length difference.<sup>21</sup>

- **Spinal Cord Injury** (resulting from trauma). Athletes with spinal cord injury have compromised voluntary movement and sensory function<sup>26</sup> below their lesion level,<sup>27</sup> and altered skeletal muscle properties<sup>28</sup> as a result of the inhibited neural pathways. The extent of the impairment is related to the physical activity level, completeness of the spinal cord lesion<sup>29</sup> and time post-injury.<sup>30</sup>
- **Muscular Dystrophy.** The exercise capacity of individuals with muscular dystrophy is limited.<sup>31</sup> Additional pulmonary limitations extend to perceived shortness of breath during cardiopulmonary testing, and hypotensive response.

- **Brachial Plexus Injury** is the most common peripheral nervous system injury,<sup>32</sup> with resulting neurological symptoms including numbness, tingling and pain in the upper extremity.<sup>33</sup>
- **Polio.** Muscular paralysis from the poliomyelitis virus on the spinal cord. Athletes with polio have a rapid onset of fatigue (in weakened muscles)<sup>31</sup> which limits their physiological capacity.
- **Spina Bifida** (congenital). Athletes with spina bifida have incomplete development of the brain, spinal cord, and their protective coverings, resulting in tone changes and balance issues.<sup>34</sup>
- **Guillain-Barré Syndrome** is a non-traumatic peripheral neuropathy characterised by rapidly progressive weakness and sensory loss.<sup>35</sup>

### 2.1.3 ADDITIONAL IMPAIRMENT TYPES

Wheelchair racing athletes may also present with

- **Limb Deficiency** resulting from amputation which is the result of trauma or congenital limb deficiency.<sup>21</sup> The minimum impairment criteria imposed by the World Para Athletics Classifications require at least half of the foot to be missing to be eligible for competition.<sup>21</sup>
- **Impaired Passive Range of Movement** resulting from arthrogyposis, ankyloses, or post burns joint contractures.<sup>21</sup>
- **Leg Length Difference** resulting from congenital or traumatic causes of bone shortening in one leg.<sup>21</sup>

### 2.1.4 PHYSICAL IMPAIRMENTS OF TRIATHLON ATHLETES

Within triathlon, athletes compete in six classifications with seven impairment types,<sup>36</sup> including impaired muscle power and vision impairment (athletes are led by a guide). One classification exists for athletes requiring a wheelchair during the run segment.<sup>37</sup> Within this classification, there exist two subclasses separating the impairment level: H<sub>1</sub> and H<sub>2</sub>, who are more and less impaired, respectively.

### 2.1.5 HOW STRENGTHS OF WHEELCHAIR ATHLETES DIFFER TO ABLE-BODIED POPULATIONS

It is commonly accepted that in general, athletes have greater strength capacity than non-active individuals.<sup>38</sup> This is due to physiological enhancement following the extensive physical training as part of training and competition.<sup>39, 40</sup> However, further physical adaptation results from impairment. Differences in both physiological and biomechanical (power production) have been demonstrated for manual wheelchair users with and without upper limb impairment.<sup>41</sup> More specifically, Mulroy et al. <sup>26</sup>

have shown significant differences in both speed and cycle distance between paraplegics and tetraplegics at comparable cadence. Therefore, the strength of wheelchair athletes may differ considerably to that of an able-bodied population due to both their physical training and impairment.

Maximum strength can be assessed objectively during an isometric contraction.<sup>42</sup> A survey of the literature has revealed similarities in isokinetic measurements between wheelchair athletes and able-bodied, non-athletic individuals (Figure 2.1, Table 2.2).<sup>43-49</sup> These findings are consistent with the literature of Haisma et al.<sup>50</sup> (as cited in Phillips *et al.*<sup>51</sup>) which demonstrated comparable shoulder strengths of people with paraplegia against age and gender-matched able-bodied populations.

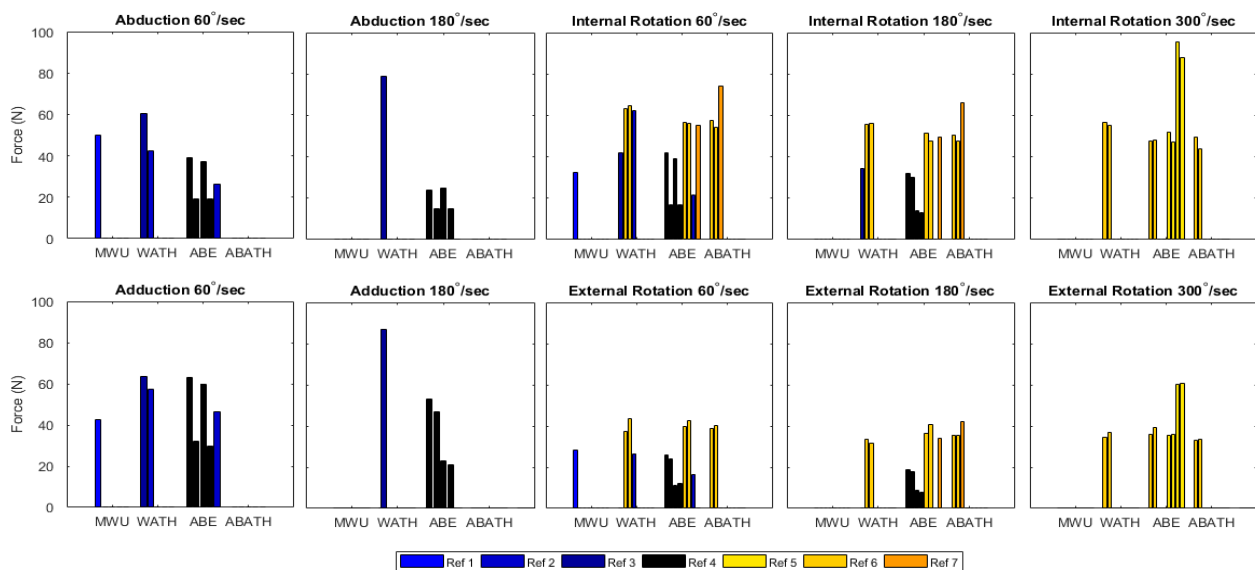









Figure 2.1: Peak isometric force measurements for shoulder movements (abduction, adduction, internal and external rotation) at a variety of speeds (60 °/sec, 180 °/sec and 300 °/sec) for wheelchair using and non-wheelchair using athletic and everyday populations. References presented in Table 2.2.

Table 2.2: Reference detail for Figure 2.1.

Reference	W/AB	Ath/Ev	M/F	N
 1: Ambrosio et al. <sup>43</sup>	W	EV	NA	22
 2: Burnham et al. <sup>44</sup>	W	ATH	M	19
 3: Miyahara et al. <sup>45</sup>	W	ATH	NA	8
 4: Connelly et al. <sup>49</sup>	AB	EV	M	19
	AB	EV	F	19
 5: Ellenbacker & Mattallino <sup>46</sup>	AB	ATH	M	125
	AB	EV	M	12
 6: Bernard et al. <sup>47</sup>	AB	ATH	M	15
	W	ATH	M	21
	AB	EV	M	22
 7: Ruivo et al. <sup>48</sup>	AB	EV	M	22
	AB	EV	M	22

W = wheelchair using, AB = able-bodied, Ath = athlete, Ev = non-athletic, M = male, F = female, N = number of participants.

Increased abduction forces at the shoulder, particularly at higher rotation speeds (120 °/s) are observed for wheelchair athletes in contrast to able-bodied individuals (Figure 2.1). While these differences are within the same order of magnitude, the consistently greater forces may be indicative of a greater maximum isometric force generating capacity for wheelchair users as compared with the able-bodied, non-athletic populations. Notable differences in parameters between populations may compromise the reliability of the results of the biomechanical simulation. This highlights the need for the use of subject-specific maximum isometric force generating capacity parameters for the computational analysis of wheelchair racing athletes to ensure the governing properties of the musculoskeletal model reflect the athlete characteristics as much as possible.

The comparable magnitude of isometric strengths observed between populations suggests that the underlying force-velocity parameters of the muscles are retained. This supports literature by Haisma et al.<sup>50</sup> who demonstrated comparable upper extremity muscle strength and respiratory function of a paraplegic population with the able-bodied population examined. These similarities may be due to no pathological conditions being present in the upper extremity of people with paraplegia. This suggests the theory that although the magnitude of force-generating capacity may require adaptation, the governing principles of muscle (for example, force-velocity relationships) are maintained in unaffected skeletal tissue following spinal cord injury. Therefore, for computational analysis, typical able-bodied force-velocity relationships as found in literature can be used for athletes classified as T53, T54, and T34, meaning the derivation of new governing muscle relationships is not required. This assumption, however, would not be appropriate for athletes classified as T51 for example (decrease of shoulder muscle power, especially pectoralis major and triceps)<sup>22</sup> nor could it be extrapolated to quadriplegic athletes, who have varying levels of impairment to the upper extremity.

### 2.2 WHEELCHAIR RACING EQUIPMENT

To compete, athletes require a specialised racing wheelchair, wheels, and gloves. There exists some capacity to manipulate each of these equipment selections to enhance acceleration and velocity (wheelchair and wheels), and the force transmission to the wheelchair (gloves). There are three principal wheel types used by wheelchair racers: spoked, aero spoke, and disc (Figure 2.2), of which the latter two are constructed from carbon fibre. Athletes opt to use the different wheels based on their aerodynamic response. Disc wheels are lighter and more aerodynamic, while spoked wheels have better handling characteristics, as the solid disc wheels act like sails when strong crosswinds are present. Video analysis of the Rio 2016 Paralympics finals (available through YouTube), revealed 2.7% of athletes used spoked wheels, close to 40% used aero spoke, and the remaining 57.3% used disc wheels.



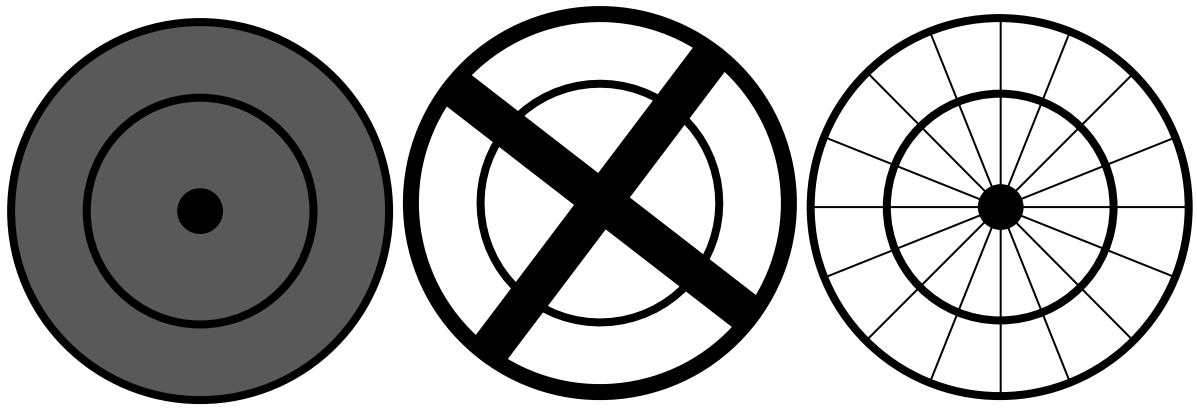


Figure 2.2: The three wheel types used in wheelchair racing. From left to right: Carbon disc, carbon aero, spoked.

Gloves are used: for protection of the fingers and thumbs, to maintain optimum hand position, and to provide grip against the pushrim surface.<sup>52</sup> Athletes can opt to either use a soft, leather glove, or hard thermoplastic glove which is moulded to the hand directly. Athletes select gloves based on personal preference. Performance benefits using hard gloves include greater peak velocities under sprint conditions with larger peak forces as compared with soft gloves.<sup>53</sup> Presumably, this is a result of the increased stiffness at the hand-pushrim interface. Soft gloves, however, give the benefit of additional damping for protection and comfort. An analysis of the Rio 2016 Paralympics demonstrated that an even distribution of glove type was used by the athletes making finals (athletes used either a soft or hard glove). Australian athletes typically used thermoplastic gloves, and athletes in T31-34 classifications more frequently opting to use the soft, leather gloves. It is feasible that the preference of soft gloves in this classification group is a consequence of the coordination impairment, with the soft gloves being more favourable for inconsistent hand positioning than the custom moulded thermoplastic counterparts.

### 2.2.1 ASSISTIVE EQUIPMENT AND TECHNOLOGY

The biomechanical and physiological variation between athletes leads to a variation in how athletes interact with their equipment. Para-athletes may require assistive equipment to return the range of motion which is either lost or reduced through illness, injury, or congenital disability. Assistive equipment is fundamental for athletes to compete. Ingenious engineering maximises the musculoskeletal capabilities of an individual to help an athlete gain a competitive advantage. The assistive technology used in sports at the summer Paralympic Games is summarised in Table 2.3.

## 2. BACKGROUND

Table 2.3: Paralympic Sports Australian Athletes compete in which require performance equipment. Data compiled from the author based on information found online and from discussions with Australian Paralympic Committee Staff.

	<b>Athlete Interfaces</b>	<b>Prosthetics and Orthotics</b>	<b>Wheelchairs</b>	<b>Throwing Frames</b>
Archery	•	•	•	•
Para Athletics	•	•	•	•
Badminton	•	•	•	
Boccia	•		•	
Canoe	•	•		
Cycling	•	•	•	
Equestrian	•	•		
Football 5-A-Side				
Goalball				
Judo				
Para Dance Sport	•		•	
Para Powerlifting				
Rowing	•	•		
Sailing	•	•		
Shooting	•	•	•	
Sitting Volleyball				
Para-Swimming				
Table Tennis	•	•	•	
Taekwondo				
Triathlon	•	•	•	
Wheelchair Basketball	•	•	•	
Wheelchair Fencing	•		•	
Wheelchair Rugby	•	•	•	
Wheelchair Tennis	•	•	•	
Total Sports	17	14	13	2

With recent technological advances, it is possible for equipment to provide performance enhancement. To ensure any equipment (both able-bodied and adapted), does not offer a competitive advantage exceeding human capabilities, the governing sporting body establishes a set of rules for athletes to comply with. Rules are updated with emerging technology and innovation. However, as wheelchair racing is a relatively modern sport, and does not have the rich sports science history of sports such as cycling, equipment guidelines remain broad. Relevant requirements of equipment for use in wheelchair racing, as described by IPC (International Paralympic Committee) Athletics,<sup>54</sup> include:

*“Rule 159 Para 2: no part of the body of the chair may extend forwards beyond the hub of the front wheel and be wider than the inside of the hubs of the rear two wheels. The maximum height from the ground of the main body of the chair shall be 50cm.”*

---

*“Rule 159 Para 9: no part of the chair may protrude behind the vertical plane of the back edge of the rear tyres.”*

Athlete interfaces include any surface where the athlete interacts with their equipment. For wheelchair racing, there are two interfaces. One is at the pushrim; when the hands are in contact with the wheel, and the other is at the seating interface; which, due to the kneeling posture, is underneath the shins. A considerable amount of literature, both clinical and applied, has been published into the optimisation of the athlete-pushrim interactions to maximise movement efficiency.<sup>55-64</sup> Less literature surrounds the interactions at the seating interface, despite these being demonstrated to influence propulsion.

Closed chain constraints mean the kinematics of the upper extremity are inextricably linked with dynamics at the seating interface, such as pressure distribution. Changes in pressure distribution at the seating interface can result from propulsion kinematics and kinetics during the push phase and recovery phase, or through wheelchair configuration. One primary cause of this variation between athletes is the level of trunk function present, which is consistently used in classification to differentiate between different groups.<sup>22</sup> Dynamic trunk control is important in the context of upper extremity force generation, particularly concerning the inertial effects associated with the head-arm-trunk segments. This can potentially lead to a competitive advantage, through increased trunk rotation,<sup>64</sup> and greater push angle, which has been demonstrated to improve performance.<sup>65</sup> Importantly, the centre of force at the seating interface has been demonstrated (using a pressure mat) to translate throughout a stroke during manual wheelchair propulsion.<sup>66</sup> While potential benefits to force application may result from trunk function, as the propulsion action causes variation in this centre of force and, potential momentary instabilities at the seating interface may exist.

Instabilities at the seating interface can increase unwanted motion at higher levels, which can place additional stresses on the upper extremity, increasing the risk of injury (as literature has suggested shoulder injuries result from the repetitive, high shoulder forces required in wheelchair propulsion),<sup>63, 67-69</sup> or introduce spatiotemporal asymmetries during propulsion which can result in steering difficulties.<sup>70</sup> As both of these are undesirable, manipulation of the seating posture of the athlete to enhance stability has been advocated,<sup>71</sup> with the degree of customisation related to each sport and the type of wheelchair used. Increased conformity at the pelvis can reduce slip at the athlete-wheelchair interface, dramatically increasing the component of applied energy into useful power. Achieving this increased conformity can be the result of seating and postural support customisation.<sup>72</sup>

Despite these performance benefits, the main focus of literature surrounding athlete-wheelchair interactions to date is the prevention of pressure ulcers among wheelchair users. This is likely due to the prevalence of pressure ulcers in seated persons ranges up to 60%, which results in both pain and systemic illness,<sup>73</sup> having a detrimental impact on their livelihoods. Injuries are caused due to the prolonged and excessive pressure applied to the blood and lymphatic cells underlying the skin,<sup>74</sup> with the reduced sensation of the lower extremity leading to insensitivity to pain or discomfort.<sup>75</sup> Pressure ulcers develop in the deep tissues, and are hence hard to detect until they reach the skin surface,<sup>76</sup> by which time the damage to tissue has already occurred, and athletes would be unable to train or compete.

Non-conformity at the seating interface promotes lower limb movement, generating frictional rubbing. Pressure sores are referred to as deep tissue injuries which emanate from sustained, localised mechanical compression as well as shear and tension deformations which result from the impinging bony prominences on the gluteal muscles.<sup>77-79</sup> A clinically relevant pressure of 32 mmHg (4.3 kPa) can be attributed to a compression-induced muscle cell degeneration in the skeletal tissue of mice.<sup>80</sup> This level of compression has been considered by clinicians as a causal factor of pressure ulcers.<sup>80</sup> This was supported in other literature, with further recommendations that pressure should not exceed 60 mmHg (8 kPa), which is generally assumed to be the limit of tissue viability.<sup>81</sup> Cellular breakdown is not only associated with the magnitude of applied pressures but also duration. Significant cell break down has been demonstrated to occur in the skeletal tissue of mice after two hours of sustained compression,<sup>80</sup> which can be comparable to the length of an athlete training session.

### 2.2.2 CUSTOMISED SEATING INTERFACES

Athletes may customise frame width, depth, height and axle position of their wheelchair<sup>82</sup> for an optimised position which is both stable and powerful. Additionally, athletes have some flexibility in the design of the wheelchair chassis to satisfy their unique characteristics best. This includes wheelchair length, cage depth, kneel depth, and front and rear seat height.<sup>6</sup> While these can be used to alleviate the effect on performance from some of the idiosyncrasies of the athlete, it is common for poor interfacing to exist between the athlete and the seat.

The Great Britain wheelchair basketball team competed at the London 2012 Paralympics with the first tailor-made 3D printed seats.<sup>83</sup> Eight athletes (four male, four female) participated in these chairs, which were created from 3D body scans and computer-aided design technology, before being manufactured using selective laser sintering. Widespread improvements in speed, acceleration, and manoeuvrability were identified from preliminary testing.<sup>84</sup> Despite these performance benefits, the complete customisation allows minimal flexibility when it comes to changes in athlete anthropometry,

---

such as through growth. Sport-specific wheelchairs are expensive, with high-end basketball wheelchairs costing between CAD 2,500 and 5,000.<sup>85</sup> Therefore, athletes do not purchase new wheelchairs frequently, and so the development of removable interfaces provides a cheaper alternative.

The most common customised seating interface is a foam cushion, which has been used in clinical literature and applications for the prevention of pressure sore injuries. The increased comfort, supportive contact area provided by customised seating interfaces dissipates high shear stresses, enhances load distribution, and minimises internal gluteal stresses and strains over the ischial tuberosities.<sup>86-88</sup> Customised seating may provide a stable base of support for dynamic sitting,<sup>52</sup> assist in enhancing body alignment, and alleviate pressure to reduce the likelihood of obtaining a pressure-related injury.<sup>89</sup>

Customised seating interfaces can also be created from many different materials, however, are typically either a viscoelastic foam or polymeric gel. Foams provide good conformity (as they can be cut into any shape), firm support, with multiple stiffness grades, while gel packs are standard sizes and do not demonstrate the elastic properties of the foams.<sup>74</sup> Different materials have varying levels of effectiveness with regards to relieving pressure,<sup>90</sup> and comfort.<sup>81</sup> When combined, various performance and comfort characteristics can be further improved.<sup>79</sup> These characteristics are dependent upon the intended use. For clinical interfaces, comfort is a high priority, however for athletic interfaces, performance is the fundamental consideration, and comfort may be compromised to support this performance.

Athletes can also include contoured foam cushions into the seating interface of their sports wheelchair to account for anthropometric idiosyncrasies. The priority for wheelchair athletes is performance. Customised seating interfaces (and seating configuration) provide a number of performance-based benefits, including: improved head control, posture, reach, grasping and functional capabilities,<sup>86</sup> stability,<sup>79</sup> and reduced interface friction,<sup>79</sup> better energy transfer efficiency, injury mitigation, and optimised balance and orientation for enhanced forward movement,<sup>91</sup> allowing maximum force transfer through the entire range of motion.<sup>92</sup>

The inclusion of foam inserts, as well as manipulating wheelchair set up parameters, affects athlete-wheelchair interactions, specifically the pressure acting at the seat. All adaptations to the seating interface can influence the interactions between the athlete and wheelchair. Apart from anecdotal feedback, there have been few comparative studies surrounding the performance of removable postural supports for individuals with SCI.<sup>79</sup> Additionally, there is a lack of qualitative support for how athlete performance is adapted from the inclusion of customised seating interfaces in wheelchair sports.<sup>19</sup> For example, customised seating interfaces having excessive conformity allow minimal

positional error and no tolerance for dynamic movement at the pelvis,<sup>91</sup> which may be at the detriment of performance. Further biomechanical investigation into how customised seating can be effectively integrated into sporting wheelchairs is hence warranted.

### 2.3 BIOMECHANICAL ANALYSIS OF PERFORMANCE

Performance can be measured directly using a stopwatch. However, this outcome-centric approach does not provide insight into the aetiology of performance. This precludes the ability to understand whether gains are optimised, how well they can be generalised across the elite wheelchair racing population, and most importantly, whether there are any associated injury risks. Without understanding the mechanics of movement, the integration of sporting technology will have minimal impact.

Wheelchair instrumentation can highlight propulsion asymmetries (which are detrimental to performance)<sup>70, 93-95</sup> and aid in understanding how propulsion can be made more efficient (such as through increased rate of force development, or change the direction of applied forces).<sup>96-99</sup> These tools can improve performance preparation to benefit outcome. However, another aspect of performance preparation is managing injury risk (through monitoring shoulder load)<sup>47, 100-102</sup> to ensure competitive longevity.

Manual wheelchair propulsion literature is commonly performed at self-directed speeds, between 1-1.1m/s. However, these are substantially less than speeds produced by wheelchair racing athletes, who can reach average speeds of up to 8.6 m/s.<sup>20</sup> Increased speed is likely to impact these results, particularly concerning kinematic hand patterns due to differences between manual and racing propulsion.<sup>58, 103, 104</sup> Based on the observed trends with hip loading compared when walking and running,<sup>105</sup> it can also be presumed shoulder joint loading will differ at varying speeds. Muscle activity and muscle strain are also anticipated to increase, but by an unknown magnitude.

Biomechanical modelling of wheelchair propulsion can be performed to varying levels of complexity. A simplified analysis was performed by Lombardi and Dedini,<sup>106</sup> using Newton-Euler and Jourdain equations to determine the dynamic behaviour of the upper extremity during motion. This literature estimated joint load and the inertial efforts required by wheelchair propulsion.

Obtaining joint reaction forces *in vivo* are not experimentally feasible<sup>107</sup> as they would require highly invasive and potentially harmful instrumentation to collect the data needed.<sup>108-110</sup> For example, the collection of *in vitro* intersegmental joint loads requires the surgical implantation of specialised

---

instrumentation. Although instrumented implants have developed substantially since the first use in 1966,<sup>111</sup> they are still not suitable for use within an elite, athletic, wheelchair propulsion.

Although biomechanical modelling using multi-segment approaches is highly efficient, it is inherently limited by the number of assumptions required, the neglect (or over-simplification) of muscular contribution, and in some cases, the restriction of the analysis to only two dimensions (e.g. <sup>106</sup>). The inclusion of the muscular system better facilitates an understanding of the level in which each musculoskeletal element impacts movement.<sup>112</sup> Understanding these constraints is crucial, and when neglected will result in ineffective treatment of movement abnormalities or technique adaptations.

The biomechanics of sporting wheelchair propulsion have been studied in depth, including the contribution of the muscles towards motion.<sup>12, 18, 64, 65, 97, 113-119</sup> Benefits of modelling muscular contributions were presented by Hamner et al.,<sup>120</sup> who generated a more systematic methodology for determining the muscular contributions to both the support and propulsion phases of a running gait cycle.<sup>121, 122</sup> Wheelchair racing propulsion is a physically straining,<sup>123</sup> and highly dynamic activity, utilising many of the upper extremity and back musculature. As such, the biomechanical evaluation of both the efficiency and risk of injury to these muscles through changes in technique (specifically as a consequence of adapted seating position) is required. One such method for achieving this is through the use of computational modelling.

### 2.3.1 COMPUTATIONAL MODELLING OF WHEELCHAIR PROPULSION

Computational modelling approaches enhance the understanding of the interactions and relationships within the musculoskeletal system.<sup>107</sup> They have been used to identify the pathomechanics and extent of movement disorders,<sup>124, 125</sup> optimise athletic performance,<sup>107</sup> and diagnose and evaluate patient-specific targeted treatments.<sup>126</sup> Modelling applications have positively impacted the approaches to the clinical treatment of cerebral palsy, lower extremity amputees, and osteoarthritis.<sup>127-132</sup> Indirect performance benefits are gained through injury mitigation and maximising competitive longevity.

Commercially available modelling platforms provide environments which are equipped to handle the complex mathematics required to model the musculoskeletal system. These packages also handle the inclusion of subject-specific geometries in three dimensional, full body, transient analyses. An example of such software is OpenSim, which provides an interactive open-source platform for creating sophisticated models.<sup>112, 133</sup> Although other platforms also exist for performing computational biomechanical analyses, OpenSim will be used as a foundation for the remainder of the review due to its prevalence and popularity in the literature.<sup>134</sup> While each software package has different coverage

of different features for their intended users; they have more similarities than differences and a standard workflow across all of them can be recognised. This workflow is highlighted in Appendix A.

### 2.3.2 MUSCULOSKELETAL MODELS OF WHEELCHAIR RACING ATHLETES

The computational model requires three input data sets; marker-based or segment-based kinematics, a musculoskeletal model containing the inertial and geometrical representation of the athlete, and the kinetics (applied and reaction forces) of propulsion. Musculoskeletal models currently available in OpenSim for the upper extremity are developed using able-bodied, non-athletic parameters. For example, the generic 3DGaitModel2392 (a lower extremity model with 23 degrees of freedom, and 92 musculotendon actuators) represents an adult subject of height 1.8 m and mass of 75 kg.<sup>135-139</sup> Due to the presence of biological variation between wheelchair racing athletes and able-bodied, non-athletic individuals, small discrepancies between these populations are to be expected. For this review, the term ‘error’ refers to the level of disagreement between the theoretically defined and physical parameters, while ‘accuracy’ refers to their agreement. For example, a high error would be expected when estimating inertial properties of an amputated limb (using anthropometric data from an able-bodied population), while greater accuracy would be anticipated from subject-specific modelling procedures.

The use of generic parameters in computational modelling has been questioned in the literature due to the limited generalisation to the broader population.<sup>140-143</sup> For example, percent root mean squared errors greater than 25.0% have been demonstrated in the measurement of thigh segment masses of able-bodied living subjects compared with dual-energy X-Ray absorptiometry (DXA) obtained values.<sup>144</sup> These differences were observed against popular cadaver research (% root mean square error (%RMSE) = 27.7%, females 19 – 30 years)<sup>145</sup> and a mathematical inertial model (%RMSE = 25.8%, females 19 – 30 years),<sup>146</sup> which is based on experimentally determined mass distributions and anthropometry. As these differences are apparent between two like populations (able-bodied and non-athletic), it can be inferred that athletes demonstrating physical impairments are likely to present greater variances. For example, it has been demonstrated that wheelchair athletes have significantly more lean mass in their arms compared to a reference population.<sup>147</sup> Although the variation of body segment inertial parameters defined in a model has been demonstrated to influence simulation accuracy,<sup>141, 148, 149</sup> the influence of their variation due to age, size, or physical deformation on input parameters is currently unknown.<sup>124, 130</sup>

Generic musculoskeletal models are derived for average geometries (Appendix B), and hence require scaling before use to reflect the subject-specific geometry. These processes are embedded within the OpenSim workflow to alter segment masses and lengths with respect to total body mass and height



---

while retaining overall proportions. Body segment lengths are defined by minimising the distance between the experimental surface markers and the virtual marker locations on the model.<sup>133, 150, 151</sup> It is clear that these procedures do not accommodate inter-individual anthropometric variations, particularly when considering musculoskeletal impairments. As poor scaling approaches generate a skeletal model which poorly reflects a subject's anthropometry, inverse kinematics and dynamics computations can be affected.<sup>140</sup> Subject-specific parameters (including body segment lengths, mass distribution and the identification of functional joint centres) should be ascertained,<sup>152</sup> as accurate input anatomic details improve the reliability of model estimates.<sup>153</sup> However, Mogk et al.<sup>154</sup> have identified that model adjustments are still often estimated from generic parameters. Additionally, the extent of errors introduced by adjusting individual parameters is currently unknown.<sup>124</sup>

The presence of uncertainties within biomechanical modelling approaches is widely acknowledged in the literature.<sup>155</sup> Engel et al.<sup>156</sup> has stated that the field of biomechanics is severely restricted by the inability to measure internal forces and pressure, due to ethical reasons. Therefore, unlike other mechanical systems, estimations of the function and contribution of musculoskeletal elements are required. The uncertainties arising from measurement error and parametric estimation can significantly affect the interpretation of results,<sup>153</sup> as these errors propagate throughout the sequential process of computational modelling. The only literature of note demonstrating the propagation of errors through successive simulation studies was performed by Myers et al.<sup>153</sup> Findings from this study demonstrated movement artefact errors (defined as skin and soft tissue movement relative to the underlying bone) grew from 1.8 times to 4.0 times larger than marker placement error between calculation of joint kinematics and moments. Additionally, muscle force outputs were observed to be highly sensitive to changes in maximum isometric force and tendon slack length. Understanding the magnitude of errors and the reliability of outputs is crucial for applying the results to real-world situations. For example, poorly defined parameters may lead to false negative load monitoring data, indicating techniques do not pose an injury risk, when in fact they do. Consequently, accurate methods of kinematic and kinetic data measurement and definition of musculoskeletal model inputs are required.

The considerable time requirements for customised model development commonly restrict investigations to case studies or studies with low subject numbers. For example, Donnelly et al.<sup>157</sup> noted that the experimental and computational time required to process a single simulation was 36 hours, which they suggested was a limitation to the application of current in-silico subject-specific techniques. As a result, analyses are performed on very specific populations, increasing the potential for the presence of sampling effects and consequently for obtaining false positives. For example, athletic populations would have significantly higher force generating capacity in their muscles than

non-athletic populations. This, in turn, creates a trade-off between modelling accuracy and complexity for reliable and generalisable data.<sup>158</sup>

Musculoskeletal modelling of the upper extremity is an evolving field, with only a few comprehensive musculoskeletal models currently developed.<sup>159</sup> Bolsterlee et al.<sup>159</sup> has identified seven commonly used large-scale models, including scapular and clavicular motions: the Swedish shoulder model,<sup>160, 161</sup> the Delft shoulder and elbow model,<sup>162, 163</sup> the Newcastle shoulder model,<sup>100</sup> Holzbaur's upper extremity model,<sup>164</sup> the Anybody upper extremity model,<sup>165</sup> Garner's model,<sup>166</sup> and Dickerson's model.<sup>167</sup> Of these models, Odle<sup>168</sup> has identified two of these models (Delft shoulder and elbow model, Anybody upper extremity model), and two other models (SIMM Upper extremity and Dutch Shoulder and Elbow model) which have been used for the biomechanical analysis of wheelchair propulsion in the literature (Table 2.4). The majority of previous modelling literature has been performed on manual wheelchair propulsion (Table 2.4). Although one example presented in Table 2.4 used wheelchair athletes,<sup>169</sup> it is clear that the application of modelling to wheelchair racing athletes is novel. Further detail regarding the development of a musculoskeletal model and the corresponding errors from poor model development are summarised in Appendix B.

Table 2.4: List of literature summarising how musculoskeletal models have been used in wheelchair research.

Reference Publication	Population Sample	Model Used
van Drongelen et al. <sup>170</sup>	5 able-bodied, 8 paraplegia, 4 tetraplegia	Delft Shoulder and Elbow
van Drongelen et al. <sup>171</sup>	5 able-bodied, 8 paraplegia, 4 tetraplegia	Delft Shoulder and Elbow
Veeger et al. <sup>169</sup>	3 wheelchair athletes	Delft Shoulder and Elbow
Veeger et al. <sup>169</sup>	1 able-bodied, 2 paraplegia	Delft Shoulder and Elbow
Dubowsky et al. <sup>101</sup>	2 paraplegia, 1 able-body	AnyBody, based on the Dutch Shoulder Model
Sullivan et al. <sup>172</sup>	1 wheelchair user	AnyBody
Sullivan et al. <sup>173</sup>		AnyBody
Morrow et al. <sup>174</sup>	12 paraplegia	SIMM, based on Holzbauer's Upper Extremity Model
Rankin et al. <sup>175</sup>	1 paraplegia	SIMM, based on Holzbauer's Upper Extremity Model
Rankin et al. <sup>176</sup>	12 paraplegia	SIMM, based on Holzbauer's Upper Extremity Model

---

Few musculoskeletal models have been explicitly designed to represent the physically disabled population. Furthermore, the few models developed to address the gap are representative of non-active tetraplegics who differ quite substantially from paraplegic athletes. For example, it has been demonstrated that tetraplegics with high cervical level spinal lesions have compromised shoulder strength, being just 50% of that of individuals with paraplegia or able-bodied individuals.<sup>50, 51, 177</sup> Consequently, the musculoskeletal models used for the assessment of propulsion biomechanics in individuals with spinal cord injury have been weakened, by reducing the defined maximum isometric force capability of muscles.<sup>170, 178</sup> Aforementioned differences in strength capabilities (Section 2.1.5) suggest that the weakened musculoskeletal models representative of individuals with tetraplegia should be used with caution for wheelchair racing athletes.

## **2.4 WHEELCHAIR INSTRUMENTATION**

Performance data (both kinetic and kinematic) are required to drive computational models. Kinematic data is measured using motion capture. For wheelchair racing, there are two kinetic inputs required: the propulsive forces applied by the hands, and the reaction forces acting at the seating interface. Instrumentation must be unobtrusive to performance and capable of being used in training or competition environments to ensure the relevance of measured data. Traditionally, force platforms are considered as the gold standard method of force measurement, while video digitisation is the gold standard for kinematic analysis.

Giltsdorf et al.<sup>179</sup> utilised a force plate located directly on the seat, to compare seating forces of two types of cushion. Force plates, however, are not appropriate for use outdoors, nor would force plates fit in the seating interface of smaller wheelchair racing frames. Furthermore, despite the frequent use of video digitisation for the measurement of sporting wheelchair kinematics,<sup>180-182</sup> such methods are practically limited. This is due to their high user subjectivity, dependence on evaluator experience, and substantial processing times required for reliable analysis. Further limitations extend to constrained capture volumes and may restrict testing to be laboratory-based, which have previously been criticised.<sup>183, 184</sup> Consequently, innovative instrumentation solutions are required for the in-field measurement of wheelchair propulsion kinetics, both at the propulsive interface and seating interfaces.

### **2.4.1 PROPULSIVE FORCES**

The magnitude of mean and peak forces throughout a push cycle in both wheelchair racing and manual wheelchair propulsion have been measured extensively in the literature. Numerous studies have used

custom dynamometers for the measurement of propulsion torque and power.<sup>185</sup> It has been suggested that ergometers mounted on dynamometers are widely used as a measurement tool as body movement is better controlled and more accurately assessed in a laboratory-based environment.<sup>186, 187</sup> However, other reviews have criticised their use as they are not representative of overground propulsion.

Wheel-based measurement systems facilitate the collection of propulsion kinetics across different terrain and require little to no acclimatisation period.<sup>188</sup> An advantage of these over dynamometers, is that they allow the overground assessment of wheelchair propulsion. The most frequently implemented wheel-based measurement system is the SMARTWheel (Three Rivers Holdings, Inc, Mesa, Arizona).<sup>189, 190</sup> This is a commercially available force and torque sensing pushrim and has been used to examine the three-dimensional propulsive forces, moments and spatiotemporal characteristics of propulsion.<sup>60, 62, 70, 96, 188, 191-193</sup> The SMARTWheel itself is comprised of three aluminium beams each instrumented with a full strain gauge bridge. A four-channel mercury slip-ring is used for signal transmission of the rotating wheel. An A/D (analogue to digital) board, and 15V commercial power supply are fastened to the wheel, with an optical encoder used to detect the position of the sensor beams, with respect to the top dead centre of the wheel.<sup>190</sup> Although the SMARTWheel has been used extensively in clinical research, it is not conducive to sporting applications, preventing its use in the regular analysis of wheelchair racing propulsion.

Each SMARTWheel has a mass of 4.9 kg,<sup>194</sup> which is comparable to total wheelchair mass (between 4.5 and 8.2 kg).<sup>1, 11, 13, 14</sup> Wheelchair mass is directly related to winning time,<sup>11</sup> with 1 kg of non-functional athlete-wheelchair mass demonstrated to slow an athlete by up to 0.13 s over a 100 m race.<sup>11, 195</sup> Performance reductions are due to the altered mass distribution, increased rolling resistance, and corresponding adaptations to propulsion kinematics.<sup>11, 196-199</sup> Medals were attained within a time frame of 0.28% of the winning time for the women's T54 1,500 m race at the London 2012 Paralympics.<sup>200</sup> At the Rio 2016 Paralympics, the difference between gold and silver for the men's (T54) 100 m and 400 m races was 0.20 s and 0.14 s, respectively, and just 0.13 s for the women's 100 m.<sup>20</sup> The necessity of lightweight instrumentation solutions is evidenced through the comparable differences in finishing times with reported losses from 1 kg of additional mass. It is important to highlight that the relative importance of the mass of instrumentation varies between sports. As wheelchair racing chairs have a mass which is approximately one-quarter of wheelchair rugby chair mass (17.2 kg)<sup>16</sup> instrumentation mass has a much higher importance in wheelchair racing than other wheelchairs. This is supported in the literature by Bednarczyk and Sanderson<sup>201</sup> who demonstrated that adding 5 to 10 kg of mass to low-mass manual wheelchair system did not change wheeling kinematics on level ground, at low speeds, and for short distances.

---

The ratio of the pushrim diameter relative to wheel diameter serves as the gearing system of the wheelchair, which is individually selected to best satisfy the unique power and velocity requirements of an athlete. Athletes choose rear wheel sizes of 700c (622 mm diameter) or 26" (660.4 mm), and pushrim diameters of 12" (304.8 mm), 13" (330.2 mm), 14" (355.6 mm), 15" (381.0 mm) or 16" (406.4 mm).<sup>6</sup> The fixed pushrim diameter of the SMARTWheel may not match an athlete's normal configuration, which may influence their performance. Additionally, the pushrim is not present in all wheelchair sports (e.g., wheelchair rugby), limiting its generalisation across all wheelchair sports.

A low-cost and lightweight alternative to the SMARTWheel is the Sensewheel Mark 1 (Movement Metrics, London, UK), which was used by Symonds et al.<sup>202</sup> and Symonds et al.<sup>203</sup>. This system is comprised of three load cells, each containing eight strain gauges with local amplifiers. Accelerometers were included to measure wheel angle for coordinate transformation, with a gyroscope used to measure wheel rotation speed. A telemeter was mounted at the wheel hub for data transmission.<sup>203</sup> This system has been used for manual wheelchair propulsion currently, requiring a pillar connected pushrim type of wheel, and no camber, and so is incompatible with wheelchair racing chairs.

Another commercially available alternative is a PowerTap, which is a hub driven power meter used in cycling. A PowerTap measures power output through eight strain gauges at the hub, with data transmitted using a radio-frequency signal to the receiver.<sup>204</sup> This system only has a recording frequency of up to 12 Hz.<sup>205</sup> As literature has shown that contact time between the hand and pushrim can be just 0.45 s for steady-state propulsion, and 0.82 s for the first stroke from stationary,<sup>116</sup> such a low recording frequency may not be appropriate. From this, it can be suggested that commercially available force sensors are not compatible with wheelchair racing propulsion. Consequently, the exploration of new technologies capable of providing a practical solution for applied practice is warranted.

A range of bespoke instrumentation solutions have been used in the literature (Table 2.5). Sabick et al.<sup>206</sup> used a custom instrumented handrim assembly comprised of a 6-component load cell, and data logger fixed to the wheel. Alternatively, Newsam et al.<sup>207</sup> and Kulig et al.<sup>208</sup> introduced a strain gauge force transducer for determining forces and torque applied to the pushrim to identify the start and end of the contact. Additionally, bespoke instrumentation solutions, including optical encoders,<sup>209</sup> electric generators,<sup>210</sup> gyroscopes<sup>211</sup> and six degree of freedom (DoF) inertial measurement units (IMU) attached to the wheelchair frame,<sup>212</sup> have all been used for the measurement of wheelchair speed. Turning radius has also been examined using a smartphone embedded with a 6DoF IMU.<sup>213</sup>

Lemerle et al.<sup>214</sup> have also examined hand-based instrumentation and established that capacitive sensors were unable to assess the coupling forces (gripping and push) of propulsion, with errors of up to 80% as compared to load cell measurements. Errors were due to the extreme difficulty in precisely

measuring the location and orientation of every sensor element during contact. Additional errors may result from the high impact nature of wheelchair racing propulsion, hand temperature at the end of an effort, and the restriction on movement on the hand as sensors are less flexible than skin.

Table 2.5: Bespoke instrumentation solutions currently used to measure wheelchair kinematics.

Sensor	Variable	Location	References
Strain Gauges	Torque applied to the pushrim	Connections between pushrim and wheel	Asato et al. <sup>190</sup> Rodgers et al. <sup>215</sup> Robertson et al. <sup>62</sup> Cooper et al. <sup>99</sup> Goosey-Tolfrey et al. <sup>195</sup> Newsam et al. <sup>207</sup> Kulig et al. <sup>208</sup>
6-Component Load Cell	Orthogonal force and moment applied to pushrim	Pushrim	Sabick et al. <sup>206</sup>
Optical Encoders	Speed		Moss et al. <sup>209</sup>
Electric Goniometers	Speed		Fuss and Ow <sup>210</sup>
Gyroscopes	Speed		Chua et al. <sup>211</sup>
6DoF IMU	Speed	Wheelchair frame	Usma-Alvarez et al. <sup>212</sup>
Smart Phone with Embedded 6DoF IMU	Turning radius	Each wheel	Fuss et al. <sup>213</sup>
	Speed, # of pushes	Frame and wheels	Van der Slikke et al. <sup>180</sup>
	Speed, frame displacement, frame rotation	Frame and wheels	Van der Slikke et al. <sup>216</sup>
	Velocity, heading, ground distance covered, motion trajectory of wheelchair	Wheel	Pansiot et al. <sup>217</sup>
	Propulsion timing and coordination	Wheelchair and wrist	Bergamini et al. <sup>218</sup>

Strain gauges are some of the most frequently utilised sensors for the measurement of applied forces and torques at the handrim (Table 2.5). Although useful, these solutions can become bulky through the creation of custom mounting, and the inclusion of a data logger to ensure the system is wireless. Although there is high confidence in the output data, it may not satisfy the semi-embedded requirement of instrumentation solutions to adapt to different pushrim diameters. Additionally, such configurations may require permanent fastening (resulting in an exclusive set of testing wheels), and therefore the generalisability of the solution across multiple athletes is limited. To promote the regular use of instrumentation in the daily training environment, a system which is easily mounted (and removed) and operated by coaches, biomechanists and athletes is preferable.

---

An emerging trend in sporting instrumentation is the use of wearable technologies. These are explicitly designed to be both lightweight and minimally obtrusive to capture performance information during regular movement. One of the primary wearable sensors is the IMU. Success in the measurement of position, velocity, acceleration, parameters related to propulsion timing, the progression of force, and coordination has been demonstrated when using IMUs in multiple wheelchair sports,<sup>180, 216-218</sup> without constraining athlete movement.<sup>218</sup> Following the development of analysis software, data processing can become semi-automated, substantially reducing the computational requirements, as compared with the current gold standard measurement method of manual video digitisation.<sup>180</sup> From a practical perspective, IMUs provide a lightweight solution (12 gm/sensor),<sup>219</sup> which have wireless data transmission (within 10 m range via Bluetooth) and semi-embedded (quickly connected to or detached from the equipment) solution, which can be inexpensive, and operated both indoors and outdoors. Despite all these benefits however, IMUs are yet to be used for kinetic estimations, within the sport of wheelchair racing, current applications of IMUs have been limited to kinematic analysis. Although the application of IMUs for estimating kinetics within wheelchair racing is relatively novel, their use in other sports, such as the commercial Push Band used in weightlifting has been well established, justifying their investigation within this research.

In the absence of measuring kinetic information directly, modelling techniques can be used to understand wheelchair propulsion biomechanics. Kinetic data have been estimated using modelling techniques both in two dimensions,<sup>187, 220</sup> and three dimensions.<sup>116, 207</sup> Modelling approaches have also been employed to calculate braking force as calculated by taking into account the resistance of the front and rear wheels,<sup>221</sup> or the influence of mass on performance.<sup>11</sup> This was not performed as part of this research, and so further detail into these approaches will not be provided.

#### 2.4.2 SEATING INTERFACE

Pressure mats are the most commonly implemented measurement tool in the literature for the measurement of seating interface pressure,<sup>93, 222, 223</sup> monitoring changes in pressure due to athlete positioning,<sup>224, 225</sup> and for the use of cushions for pressure relief.<sup>81, 90, 226</sup> Pressure mapping technology measures the magnitude and distribution of pressure across the seat.<sup>79, 90, 222, 224, 225, 227-229</sup> While these applications are predominantly clinically based; pressure mapping technology has also been used for monitoring pelvic movement<sup>227</sup> and monitoring changes in pressure due to the use of customised seating interfaces in wheelchair using populations.<sup>74, 81</sup>

The pliable surface and lightweight nature of the pressure mat makes it particularly well suited to sports wheelchairs, and can adapt to different radii of curvature and length measurements present between

different seating buckets, and on contoured foam cushions. Additionally, the wireless transmission capabilities present good compliance with sport specific requirements to ensure regular athlete motion is not compromised.

Although pressure mats do not directly measure forces, which are required for performance review and input into computational modelling approaches, they have demonstrated success in measuring reaction forces of running and walking.<sup>230, 231</sup> A comparison of the use of a pressure mat with a force platform, revealed both technologies were equally useful in assessing seated postural control.<sup>232</sup> Additionally, pressure mapping technology has demonstrated success for clinical based load monitoring literature<sup>233</sup> and measuring reaction forces.<sup>231</sup>

### 2.5 AIMS AND OBJECTIVES

This research aimed to assess the effectiveness of customised seating interfaces on linear wheelchair performance through computational biomechanical modelling. Foundation work has been able to provide a handful of athletes with seating interfaces; however, the methods for quantifying changes in performance are still required. Four key objectives were established to achieve these aims, which are detailed below, with the interrelation between these aims summarised in Figure 2.3:

#### **Aim 1: Understand how various aspects of wheelchair racing technique and equipment at the seating interface relate to performance.**

A meaningful change in performance is required to justify the cost of the initial manufacture of customised seating interface and the continued research into its optimisation. As such it is imperative to understand how the different aspects of athlete technique and equipment relate to an athlete's overall performance to ascertain the potential performance advantages an athlete may gain from the use of a customised seating interface.

#### **Aim 2: Develop instrumentation tools capable of in-field data measurement.**

Commercially available instrumented wheels currently used in clinical research are not appropriate for use on a racing wheelchair as they alter natural athlete propulsion. A bespoke instrumentation solution must be developed to obtain the kinetic components of performance required as an input to the biomechanical model. This solution must be easily mounted to the



---

wheelchair, having little mass, wireless capabilities, and embedded use, so as not to interfere with regular athlete performance, and facilitate consistent athlete usage.

**Aim 3: Develop a subject-specific, 3D computational model.**

Existing musculoskeletal models used in biomechanical modelling techniques are yet to incorporate the tissue adaptations associated with para-athletes, limiting the relevance of obtained findings. Due to the anthropometric variation in the lower extremities of wheelchair racing athletes, it is anticipated that current models, based on generic anthropometric data will overestimate the inertial and force-generating ability of an individual, while the converse is true for the upper extremity. Additionally, the complete systematic analysis of the mechanics of movement with the relationship with equipment is yet to be performed.

**Aim 4: Quantify the mechanics of wheelchair racing using simulation.**

The primary focus of this research is to understand whether the inclusion of customised seating interfaces increase injury risk and to quantify the potential performance advantage. Traditional measurement approaches can analyse performance outcome, however, are incapable of detailing how the outcome was achieved. A subject-specific computational modelling approach, using the instrumentation techniques and musculoskeletal model developed in Aim 2 and Aim 3 are capable of answering these questions.

## **2.6 SIGNIFICANCE**

Use of coupled kinematic and kinetic performance analysis utilising computational biomechanical modelling can provide an objective and precise measurement of the difference in performance due to the use of customised seating interfaces. Such a process can identify the magnitude and efficiency of applied loads, as well as how this translates into muscular loading and the reaction forces acting at the joints. This research will be of significant benefit to athlete preparation, demonstrating how technique can be optimised and how injury risks can be minimised. Wheelchair racing has demonstrated to have the highest incidence of soft tissue injury amongst wheelchair sports.<sup>234</sup> For example, the prevalence of shoulder pain in individuals with spinal cord injury (SCI) is between 31% and 73%.<sup>235</sup>

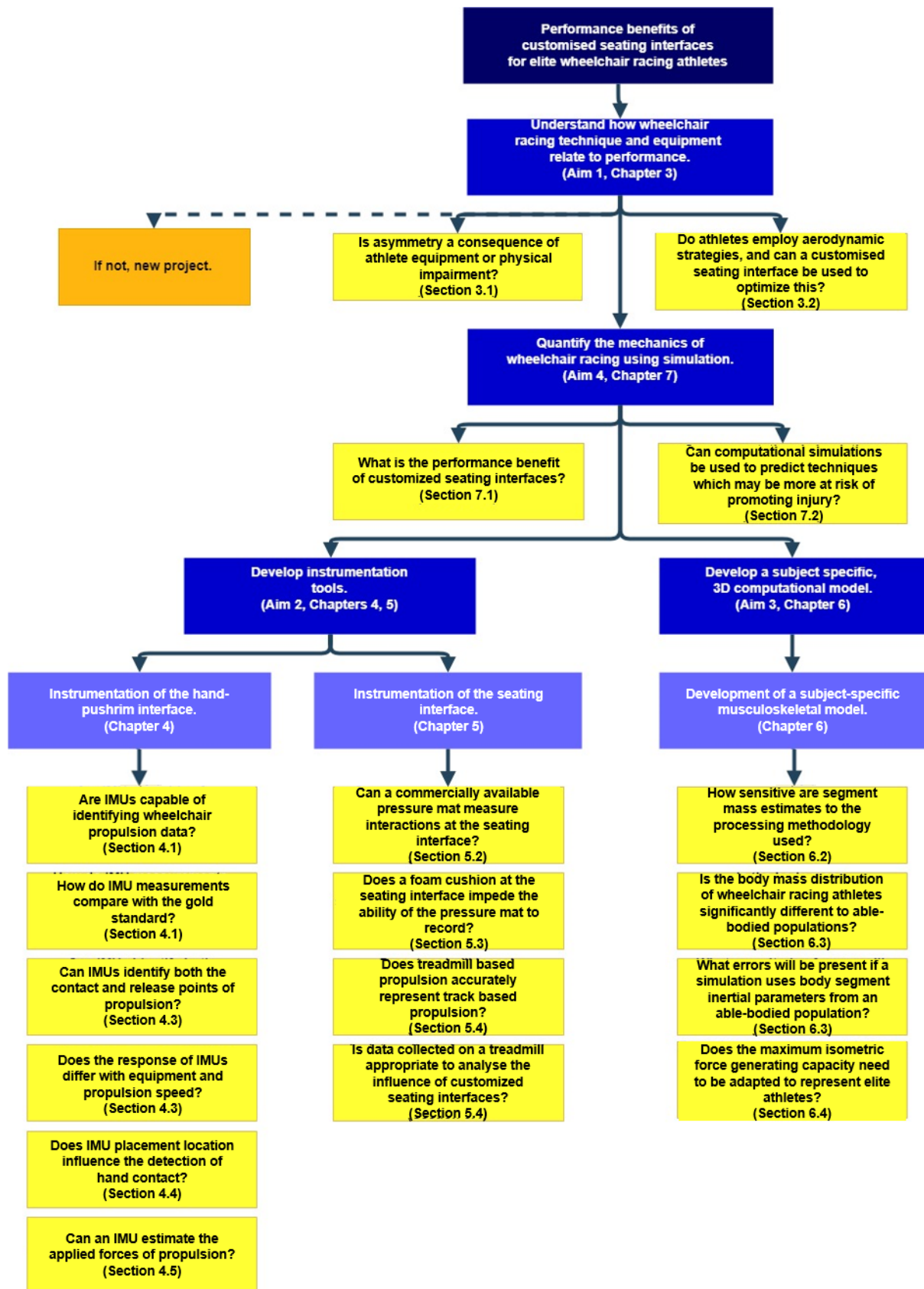


Figure 2.3: Schematic outline of research demonstrating how each of the sub-studies contribute to the four research aims addressing the main aim of the research; to identify the performance benefits of customised seating interfaces on wheelchair racing performance.

---

The methods developed in this research can also be used to benefit a greater range of athletes in multiple other sports, as well as assist manual wheelchair users better execute tasks of daily living and ambulation.

In addition, supplementary benefits are gained through the completion of intermediate aims of this research. Limited biomechanical performance feedback to the wheelchair racing athletes in this research is currently provided, specifically on track surfaces, and with regards to kinetic aspects of performance. As a result, athletes, coaches, and biomechanists are reliant on qualitative perceptions of performance to make informed decisions regarding changes in equipment and technique. The instrumentation developed within this research could thus have considerable practical implications on performance preparation.

## **2.7 CONTRIBUTIONS AND ORGANISATION OF THESIS**

To the best of the author's knowledge, there has been no computational literature published regarding the biomechanics of wheelchair racing, and how it is affected by the implementation of customised seating interfaces. These investigations will make a considerable contribution to Paralympic wheelchair racing, dramatically improving the way Paralympic coaches conduct daily training.

The remainder of the thesis is broken into five experimental chapters (Chapters Three to Seven), describing the engineering solutions used to answer each of the four principal objectives documented previously. The potential performance impact of customised seating interfaces, relative to athlete equipment and technique is first established in Chapter Three (Aim 1). Chapter Four then investigates the instrumentation of the hand-pushrim interface using IMUs. The effects of placement, athlete equipment and propulsion style on recording accuracy were analysed to understand the robustness of the IMU as a solution before investigating the capacity to estimate input forces using IMUs. Chapter Five builds on Chapter Four, examining the ability for a commercially available pressure mat to measure the interactions at the athlete-seating interface. Together, these chapters address the second aim of the thesis in developing instrumentation tools capable of in-field data measurement. Chapter Six outlines how a subject-specific, 3D computational model (Aim 3) can be generated from DXA scans. The findings from Chapters Three to Six provide the foundation for Chapter Seven, which quantifies the mechanics of wheelchair racing propulsion using computational biomechanical simulation (Aim 4). The final experimental chapter investigates how computational modelling approaches can be used to support performance analysis and reduction of injuries. Each of these chapters is comprised of some smaller investigations, which have been published, presented at conferences, or are currently under review.

## 2.8 RESEARCH OUTPUT

To date, the research for this thesis has produced many research outputs that have been published in peer review outputs. These can be summarised as follows:

### 2.8.1 JOURNAL PAPERS

1. Lewis, AR., Haydon, DS., Phillips, EJ., Grimshaw, PN., Pinder, R., Winter, J., Robertson, WSP. & Portus, M. 2017. Placement effects of inertial measurement units on contact identification in wheelchair racing. *Sports Biomechanics*. Under review
2. Lewis, AR., Phillips, EJ., Robertson, WSP., Grimshaw, PN., Portus, M. & Winter, J. 2018. A practical assessment of wheelchair racing performance kinetics. *Sports Biomechanics*. Under review
3. Lewis, AR., Haydon, DS., Phillips, EJ., Grimshaw, PN., Pinder, R., Winter, J., Robertson, WSP. & Portus, M. 2018. Monitoring seating interface pressure in wheelchair sports. *Sports Engineering*. doi: 10.1007/s12283-018-0272-3
4. Lewis, AR., Robertson, WSP., Phillips, EJ., Grimshaw, PN. & Portus, M. 2017. The effects of personalised versus generic scaling of body segment masses on joint torques during stationary wheelchair racing. *Journal of Biomechanical Engineering*. Under review
5. Lewis, AR., Robertson, WSP., Phillips, EJ., Grimshaw, PN. & Portus, M. 2017. Estimating the maximum isometric force generating capacity of wheelchair racing athletes for simulation purposes. *Journal of Applied Biomechanics*. Under review
6. Lewis, AR., Robertson, WSP., Phillips, EJ., Grimshaw, PN. & Portus, M. 2018. Influence of customised seating interfaces on wheelchair racing athletes; A case study. *International Journal of Sports Physiology and Performance*. Under review

### 2.8.2 CONFERENCE PROCEEDINGS

7. Lewis, AR., Phillips, EJ., Robertson, WSP., Grimshaw, PN. & Portus, M. 2018. Intra-stroke profiling of wheelchair propulsion using inertial measurement units. *Proceedings*. 2(6). 256. doi: 10.3390/proceedings2060256
8. Lewis, AR., Phillips, EJ., Robertson, WSP., Grimshaw, PN. & Portus, M. 2018. Injury prevention of elite wheelchair racing athletes using simulation approaches. *Proceedings*. 2(6). 255. doi: 10.3390/proceedings2060255

---

### 2.8.3 CONFERENCE PRESENTATIONS

9. Lewis, AR., Phillips, EJ., Periac, F., Portus, M., Grimshaw, PN. & Robertson, WSP. 2017. Does glove type influence wheelchair propulsion symmetry in junior athletes. Presented at the 26<sup>th</sup> conference of the International Society of Biomechanics, Brisbane, Australia, 23-27 July 2017.
10. Lewis, AR., Phillips, EJ., Moore, V., Bartram, JC., Grimshaw, PN., Portus, M. & Robertson, WSP. 2017. The Trunk Position for the 2016 Rio Paralympic wheelchair racing finals. Presented at the 25<sup>th</sup> conference of the International Society of Biomechanics in Sports, Cologne, Germany, 14-18 June 2017.
11. Lewis, AR., Phillips, EJ., Grimshaw, PN., Portus, M. & Robertson, WSP. 2017. Effect of seating cushions on pressure distribution in wheelchair racing. Presented at the 25<sup>th</sup> conference of the International Society of Biomechanics in Sports, Cologne, Germany, 14-18 June 2017.
12. Lewis, AR., Phillips, EJ., Portus, M., Grimshaw, PN. & Robertson, WSP. 2017. Changes in leg pressure during modes of racing wheelchair propulsion. Presented at the 26<sup>th</sup> conference of the International Society of Biomechanics, Brisbane, Australia, 23-27 July 2017.
13. Lewis, AR., Robertson, WSP., Grimshaw, PN., Phillips, EJ. & Portus, M. 2017. Body segment mass differences from altering intensity thresholds in Dual-Energy X-Ray Absorptiometry scans. Presented at the XVI International Symposium on Computer Simulation in Biomechanics, Gold Coast, Australia, 20-22 July 2017.
14. Lewis, AR., Haydon, DS., Grimshaw, PN., Robertson, WSP., Phillips, EJ. & Portus, M. 2016. The effect of inertial measurement unit placement on acceleration measurements on wheelchairs. Presented at the 10th Australasian Biomechanics Conference, Melbourne, Australia, 4-6 December 2016.

---

---

## CHAPTER THREE:

# HOW IMPORTANT IS THE SEATING INTERFACE TO ATHLETE PERFORMANCE?

---

To justify the critical analysis of customised seating interfaces, it is essential to understand their overall impact relative to all other elements impacting performance. For example, interactions at the hand-pushrim interface have a substantial effect on propulsion performance. Athlete-wheelchair velocity (and hence forwards motion in straight-line pushing) is the result of energy transfer from the athlete to their wheelchair. Maximising this velocity can be achieved through increasing the power application over longer contact ranges and increasing mechanical efficiency. Ensuring maximal power output from

---

each hand (symmetry) may improve the mechanical efficiency of motion. Asymmetrical propulsion may result from kinematic error, or possibly through poor equipment (glove) interfacing.

Aerodynamic effects also require consideration, as it is plausible that through the inclusion of a customised seating interface, the frontal area may increase considerably, resulting in a more significant drag coefficient and hence resistive forces. Although athletes may be in a position where they are capable of producing more power, they may require all of this power, and more, to overcome the additional resistive forces. Resistive forces due to aerodynamic drag are substantial in sports (up to 90% of drag forces in cycling).<sup>236</sup> In the absence of wind tunnel testing, the aerodynamic strategies employed during wheelchair racing events and whether slight changes to the frontal area, caused by a change in seating position impact performance can be investigated.

The content presented in this chapter addresses the first aim of this research to understand how various aspects of wheelchair racing technique and equipment and how these all contribute to performance. Hence the potential performance impact from the inclusion of customised seating interface can be inferred. This chapter is split into two experimental studies, to improve the understanding of how wheelchair racing technique and equipment relate to performance, and highlight whether customised seating interfaces have the potential of providing substantial performance gains. The relevance of this chapter in relation to the overall research questions are presented in Figure 3.1.

### **Does glove type influence wheelchair propulsion symmetry in junior athletes?**

#### **(Section 3.1)**

*Research Question:*

- Is asymmetry a consequence of athlete equipment or physical impairment?

### **The optimisation of trunk position for the 2016 Rio Paralympic wheelchair racing finals.**

#### **(Section 3.2)**

*Research Question:*

- Do athletes employ aerodynamic strategies, and can a customised seating interface be used to optimise this?

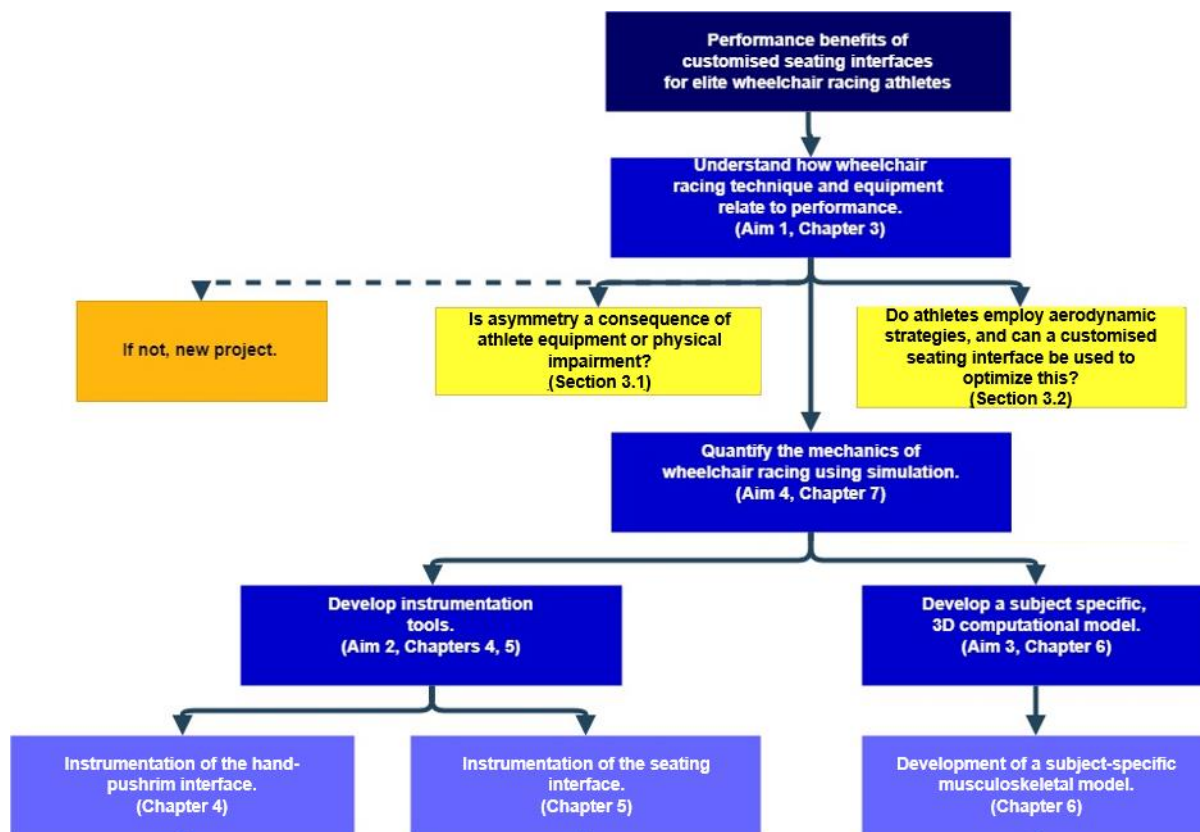


Figure 3.1 Relevance of the Chapter 3 (How important is the seating interface to athlete performance?) to the fundamental research question; what is the performance impact of customised seating interfaces on wheelchair racing propulsion?

### 3.1 ATHLETE CHARACTERISTICS

A total of thirteen athletes were investigated as part of the research in this thesis (Table 3.1). The majority of athletes were from wheelchair racing and triathlon. For these athletes, two key inclusion criteria in the participant recruitment process included the use of elite athletes, and that no visible upper extremity neurological conditions were present. The population sample demonstrated different equipment (wheel type: disc or spoke, glove type: leather or thermoplastic), classification (spinal cord injury or cerebral palsy), gender (male and female) and experience (senior and junior). Two additional athletes were used from the Wheelchair Rugby national program as a point of comparison within a single study. These athletes were either classified as a 2.0 point (limited trunk function, impairment has a mid-range effect on performance) or 3.0 point (partial trunk function, impairment has a smaller impact on performance).



For wheelchair racing athletes, this research was restricted to athletes only presenting with physical impairment and fair to good functional strength in the arms. Athletes had either no trunk function (T53:  $n = 1$ ) or partial to full trunk power (T54:  $n = 4$ ) with possible leg function, as well as no lower spinal muscle activity (T34:  $n = 2$ ).<sup>22</sup> Two triathlon athletes classified as PT1 (athletes predominantly using a wheelchair for daily ambulation)<sup>237</sup> also formed part of the population sample. One athlete was competitive in both wheelchair racing, and triathlon at the time of data collection.

Table 3.1: Athlete information. Speed is only listed for athletes who performed steady-state propulsion on a treadmill (Section 4.2)

Athlete	Sport	Classification	Sex	Impairment	Mass (kg)	Speed (km/hr)	Age	Glove Type	Wheel Type
A	WRac	T34	M	Hereditary Spastic Paraplegia	62.5	19,20	Junior	Soft	Aero
B	WRac	T34	M	Cerebral Palsy	60.1	21,22	Junior	Soft	Disc
C	WRac	T54	M	Spina Bifida	54.3	22,23	Junior	Hard	Spoke
D	WRac	T54	M	Spina Bifida	87.9	26,27	Junior	Soft	Spoke
E	WRac	T54, PT1	F	SCI (acq)	60.3	22,23,24	Senior	Hard	Disc
F	WRac	T54	M	Congenital Limb Def.	62.2	28,29,30	Senior	Hard	Disc
G	WRug	2.0 point	M	SCI (acq)	92.9	N/A	Senior	Soft	Disc
H	WRug	3.0 point	M	SCI (acq)	77.8	N/A	Senior	Soft	Disc
I	WRac	T53	F	Paraplegia	54.4	26,27,28	Senior	Hard	Disc
J	PTri	PT1	M	Incomplete paraplegia	67.1	32 SPM	Senior	Hard	Disc
K	PTri	PT1	M	Incomplete paraplegia	73.8	N/A	Senior	Hard	Disc
L	WRac	T53	M	Spina Bifida	62.0	N/A	Senior	Hard	Disc
M	WRac	T54	M	Paraplegia	56.2	N/A	Senior	Hard	Disc

WRac: wheelchair racing, WRug wheelchair rugby, PTri: paratriathlon, acq: acquired, SPM: strokes per minute. No specified speed for WRug athletes.

Throughout each of the studies presented, a subset of these athletes were used. Table 3.2 summarises the subset of athletes used for each of the individual analyses comprising this research.

### 3. HOW IMPORTANT IS THE SEATING INTERFACE TO ATHLETE PERFORMANCE?

Table 3.2: Population sample for each experimental simulation. No athletes were used in study 3.3 which was a review of video (YouTube), or in Section 4.1 which involved pilot testing.

Athlete	3.2	3.3*	4.1*	4.3	4.4	4.5	5.2	5.3	5.4	6.2	6.3	6.4	7.1	7.2
A	•			•	•	•	•	•						
B	•			•	•	•	•	•						
C	•				•	•	•	•						
D	•				•	•	•	•						
E				•	•	•	•	•		•	•	•	•	
F				•	•	•	•	•	•					
G							•							
H							•							
I				•	•	•				•	•	•	•	
J														•
K										•	•			
L										•	•			
M										•	•			

A small population sample was utilised due to the nature of the elite wheelchair athlete population and the sizeable inter-athlete variability in both the physical impairments and capabilities within the same classification. For example; literature has demonstrated kinematic variation for experience,<sup>238</sup> gender,<sup>239</sup> and classification.<sup>240</sup> It is unlikely that appropriate generalisations will be able to be established for all elite wheelchair racing athletes, and hence the use of a small population is not limiting to this research.

Able-bodied individuals were not recruited to increase sample size as biomechanical variations have been reported between experienced and inexperienced (able-bodied, non-wheelchair users) wheelchair propulsion, influencing 30 s agility, 1 min distance test, and 10 m sprint performance.<sup>241</sup> Additionally, differences in the kinematic technique of manual wheelchair users compared with novices (including able-bodied, non-athletic population samples) has been demonstrated.<sup>202, 238</sup>

---

## 3.2 DOES GLOVE TYPE INFLUENCE WHEELCHAIR PROPULSION SYMMETRY IN JUNIOR ATHLETES?

### 3.2.1 INTRODUCTION

For wheelchair propulsion, kinematic<sup>114</sup> and kinetic<sup>94</sup> asymmetries are commonly documented and have negative implications on steering,<sup>194</sup> and thus are considered to be undesirable for performance. These asymmetries are frequently assumed to be the consequence of a musculoskeletal or anatomical imbalance,<sup>95</sup> resulting from spinal cord injury or another physical impairment. The aetiology of these abnormal motions and methods for their mitigation, such as strength and conditioning have been readily explored. However, literature has yet to confirm whether the aetiology of these asymmetries is purely a consequence of the geometry and impairment of an athlete, or how well athlete's equipment fits their unique anthropometry (wheelchair and gloves). For example, spatial and temporal hand asymmetries may be the result of either musculoskeletal bias in the upper extremity or due to ill-fitting gloves, preventing maximum force transfer to the chair.

Gloves used in wheelchair racing increase the contact area between the hands and pushrim, to improve the effectiveness of force transfer to the chair, while protecting the hands from repeated high impact.<sup>97</sup> These gloves can be either custom thermoplastic hard gloves, which most elite racers use, or soft leather. Hard gloves have been demonstrated to use less impulse and peak torque to maintain the same speed, which may mean they are more efficient than the soft glove counterpart.<sup>53</sup> These hard gloves are custom made, using 3D scanning and printing methodologies. Typically, however, only one hand is scanned, with the design mirrored to fit the other hand, commonly meaning one fits better than the other. Conversely, soft gloves can sometimes be customised. This study aimed to compare gloved (hard and soft) and un-gloved starting conditions on a stationary wheelchair racing start and whether this altered the distribution, rate of force development, or direction of force application. It was hypothesised that significant differences would be observed in kinetic symmetry between gloved and non-gloved trials.

### 3.2.2 METHODS

#### *Athlete Selection*

National level junior wheelchair racing athletes (Athletes A – D), classified as T34 (cerebral palsy,  $n = 2$ ), and T54 (spinal cord injury,  $n = 2$ ) formed the population sample.

#### *Experimental Propulsion Task*

All athletes performed four stationary starts under two conditions: gloved and non-gloved. Starts were conducted in laboratory settings, on a Mondo track surface. An audible three-command start was provided to the athletes, to represent a race start.

#### *Measurement System*

Three force plates operating at 1 kHz (Kistler 9281B-11, Switzerland), were embedded beneath a Mondo track surface to measure the ground reaction force of each wheel independently.

#### *Data Processing*

Data were low pass filtered (Butterworth, bidirectional, -6dB cut-off frequency 20 Hz),<sup>242</sup> and normalised to system (athlete + wheelchair) weight using MATLAB R2017a (Mathworks, USA). Force parameters of interest included peak force ( $F_{ML}$ ;  $F_{AP}$ ;  $F_V$ ), the rate of force development (RFD), propulsive impulse (PI), and time to peak force (TPF). Data are expressed as a ratio of left and right measures (Equation 3.1), with positive values indicating right-side dominance). For data collected on the left force plate,  $F_{ML}$  was multiplied by -1 to support direct comparison with data collected on the right force plate. Independent samples t-tests determined the influence of glove status and athlete classification on each of the dependent variables. Statistical analysis was performed using IBM SPSS Statistics 24 Software for Windows (SPSS Inc., Chicago, IL USA), with a significance level of  $\alpha = 0.05$ .

$$100\% \times 2 \frac{(Right-Left)}{(Right+Left)} \quad \text{Equation 3.1}$$

### 3.2.3 RESULTS

Athletes demonstrated variability over the first stroke with clear differences between left and right hands for both gloved and non-gloved conditions (Figure 3.2). Excluding the non-gloved trial for Athlete A, the magnitude of the applied forces remains relatively constant between hands, across tests. Force transmission differed considerably between athletes. Athletes typically had longer push phases with their right hand than their left hand for the gloved conditions (excluding Athlete D, Figure 3.2). For the T34 athletes, Athlete A was more symmetrical wearing gloves, while Athlete B was more symmetric without wearing gloves. T54 athletes demonstrated a two-phase stroke, while the T34 athletes with soft gloves, who exhibits a single peak.

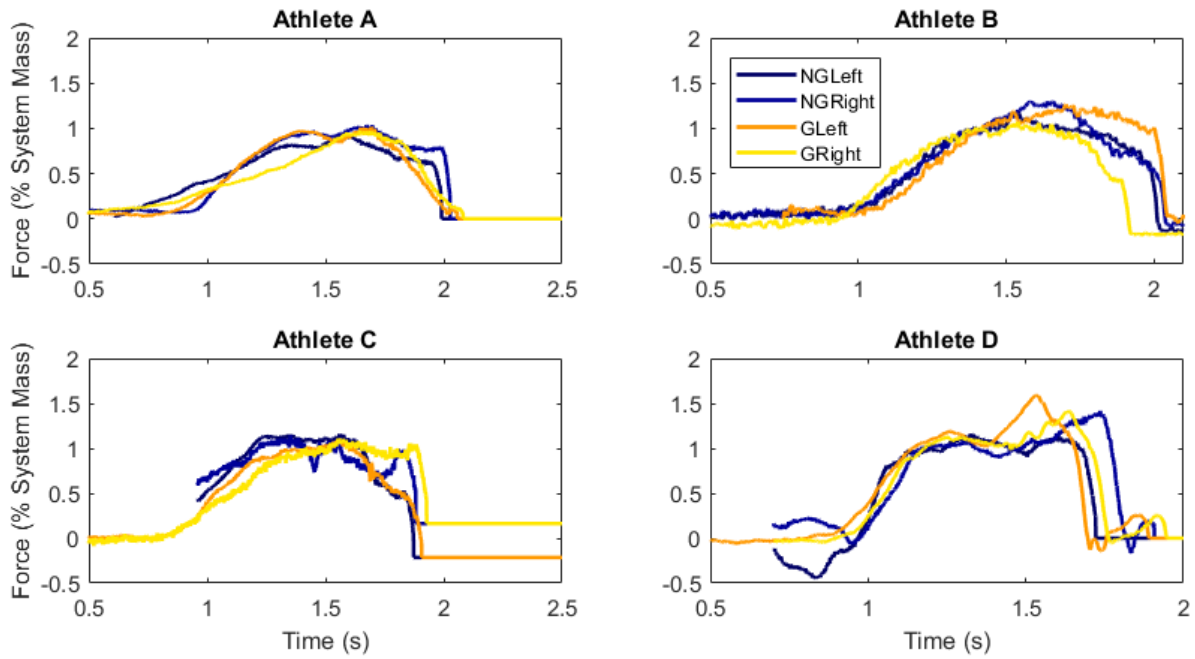


Figure 3.2: Representative force curves (in AP direction) from a single push, normalised by system (athlete + wheelchair) mass.

Parameters of interest are quantified in Table 3.3, which is presented as mean  $\pm$  SD, with statistical significance identified for  $F_{AP}$  ( $p = .031$ ) when comparing the gloved condition only. As a cohort, it can be considered that for most aspects of force generation, the use of either a hard or soft glove does not have a significant impact on symmetry.

Table 3.3: Comparison of gloved and non-gloved conditions between classifications and glove type (hard or soft). Data are presented as an absolute percentage difference from perfect symmetry (mean  $\pm$  SD). Larger magnitudes indicating a more considerable difference between hands.

	Hard Glove	Soft Glove	T34	T54
$F_{ML}$ (N)	$-6.3 \pm 4.1$	$10.6 \pm 15.5$	$7.8 \pm 12.3$	$3.1 \pm 19.5$
$F_{AP}$ (N)	$1.2 \pm 4.7$	$-8.0 \pm 7.2$	$-5.6 \pm 5.8$	$-5.0 \pm 10.4$
$F_V$ (N)	$-34.0 \pm 2.4$	$-0.5 \pm 4.1$	$0.5 \pm 3.9$	$-4.1 \pm 2.3$
RFD (N/s)	$16.5 \pm 4.8$	$15.3 \pm 13.3$	$15.2 \pm 12.5$	$16.3 \pm 10.7$
PS (N.s)	$1.8 \pm 2.5$	$3.9 \pm 8.3$	$5.1 \pm 7.7$	$0.9 \pm 6.1$
TPF (s)	$-3.4 \pm 8.6$	$1.3 \pm 10.8$	$4.2 \pm 8.4$	$-5.8 \pm 10.1$

ML: mediolateral, AP: anterior-posterior, V: vertical.

Significant differences were observed between classifications for  $F_V$  ( $p = .024$ ), with non-significant, yet considerable differences also found for time to peak force ( $p = .066$ ) when comparing both the gloved and non-gloved conditions. Differences in the symmetry of force development between

classifications are observed in Figure 3.3. Differences are possibly attributable to the greater physical strength of T54 athletes, which is reflected through faster winning times.<sup>243</sup> Thus, it can be extrapolated that if athlete speed affects the influence of gloves, proper fitting gloves will be important for senior-elite athletes.

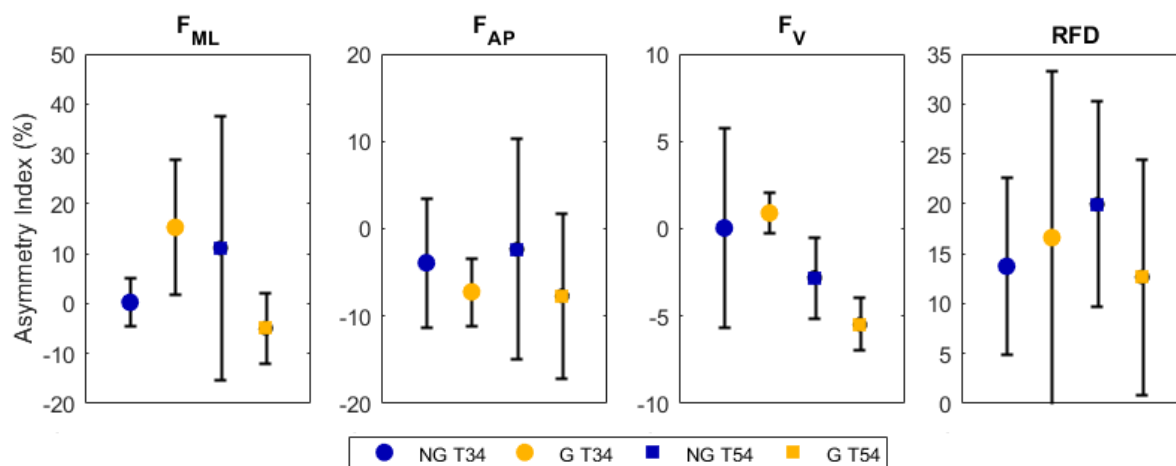


Figure 3.3: Differences in the symmetry of force development (Asymmetry Index, Equation 3.1).

### 3.2.4 DISCUSSION

Considerable inter- and intra- athlete variability was observed in the elite, junior wheelchair racing athletes tested under both the gloved and un-gloved conditions for all variables. This variability cannot be associated with glove type, as there was an even split in the use of hard and soft gloves used for athletes classified as T54. Differences may be present for more experienced senior athletes, who do have more consistent start patterns and who are less easily trained out of poor movement patterns. Substantial differences between classifications were observed, as expected, with T54 athletes more affected by glove type.

High levels of inter- and intra-athlete variability were demonstrated through the large error bounds of Figure 3.3, with the substantial differences between athlete classifications attributed to physical functionality. Although junior athletes have more variability than senior athletes, the athletes in this study were highly trained, suggesting the skill is highly variable in both novices and experts. The influence of glove type may be more conclusive for a more refined skill, such as steady-state propulsion.

As gloves were not found to contribute to athlete asymmetries substantially, it can be considered that these are more of a consequence of physical impairment and geometry. This highlights the potential impact that customised seating interfaces may have on performance if they are capable of reducing these athlete asymmetries.

---

### 3.2.5 CONCLUSION

Considerable variability was observed amongst all athletes suggesting the possibility for further optimisation of both technique and the athlete-pushrim interfacing. Symmetry was not significantly affected by glove selection, highlighting the potential performance impact of customised seating interfaces for wheelchair racing athletes as asymmetries are likely a consequence of physical impairment and geometry, thus highlighting the potential performance impact of customised seating interfaces for wheelchair racing athletes.

## 3.3 THE OPTIMISATION OF TRUNK POSITION FOR THE 2016 RIO PARALYMPIC WHEELCHAIR RACING FINALS

### 3.3.1 INTRODUCTION

Performance in wheelchair racing is speed dependant,<sup>244</sup> with winning velocities being the result of the maximisation of physical capabilities, while reducing resistive forces (rolling friction:  $F_R$  and aerodynamic drag:  $F_D$ ).<sup>245</sup> Highly trained athletes have limited potential for further physical gains, particularly those with physical impairments, making aerodynamic improvements more readily available. Based on the well-established  $F_D$  relationship (Equation 3.2),<sup>245</sup> to reduce aerodynamic resistance athletes must minimise their frontal area.

$$F_D = 0.5\rho A_d v^2 C_D \quad \text{Equation 3.2}$$

Where  $\rho$  is the air density,

$A_d$  is the frontal area,

$v^2$  is athlete velocity, and

$C_D$  is the drag coefficient.

Aerodynamically optimised wheelchairs reduce frontal area by almost half (0.37 m<sup>2</sup> in upright positions in conventional chairs<sup>8</sup> as compared to 0.17m<sup>2</sup> for the same position in a racing wheelchair<sup>9</sup>), with further reductions obtained through body positioning. Cycling literature has demonstrated that a flexed upper trunk position reduces frontal area by 20–29%;<sup>246</sup> however, the same position has only a 3-4% improvement in wheelchair racing.<sup>247</sup> This difference may be the consequence of wheelchair athletes using arms for propulsion, compromising athlete aerodynamics with each stroke.

### 3. HOW IMPORTANT IS THE SEATING INTERFACE TO ATHLETE PERFORMANCE?

---

Two distinct wheelchair propulsion strategies exist; high stroke count (frequency) or high power. A frequency strategy is more aerodynamic but may have limited contact range, and thus may generate lower momentum. A high power strategy, however, increases frontal area (during recovery), as athletes increase vertical trunk motion in order to contact the pushrim as close to the top as possible and maximise input torque.<sup>248</sup> Athletes will typically adopt a technique thought to best suit their specific physical capabilities. As the recovery phase can range between 49.6% and 78.4% of stroke time throughout a 100 m race,<sup>249</sup> poor aerodynamic technique can be detrimental.

This study examined the propulsion methods used by wheelchair racing finalists in the 100 m – 5,000 m Track events at the 2016 Rio Paralympic Games to determine whether any relationships exist between athlete placings, and technique, specifically concerning trunk position. It was hypothesised that there would be clear aerodynamic strategies utilised by athletes who medal more often.

#### 3.3.2 METHODS

Male and female athletes with a T54 classification; those with paraplegia, having normal hand and arm function, normal or limited trunk function, and no leg function,<sup>22</sup> formed the population sample. Athlete performance, over each distance final (100 m, 200 m, 400 m, 1,500 m, and 5,000 m) was analysed independently ( $n = 87$ ; males  $n = 43$ , females  $n = 44$ ). Race times were obtained from the official website of the Paralympic Movement (<http://www.paralympic.org/>), with video data obtained from the public domain (<https://www.youtube.com/>). Ethical approval was obtained from the University of Adelaide Human Research Ethics Committee.

Peak vertical range of trunk motion (during the recovery phase) and stroke count over the final 100 m of racing was documented. Athletes were manually classified into one of three groups (Figure 3.4) based on visual inspection: low-trunk remains parallel to track surface; moderate-thoracic region elevates from lower extremity, hyperextended neck position; high-trunk opens fully, neck flexed). Intra-rater reliability measures were performed to ensure consistency of classification and stroke count and were conducted using IBM SPSS Statistics 24 Software for Windows. The impact of trunk position on stroke count and finishing position was established using a linear trendline in Microsoft Excel 2013.



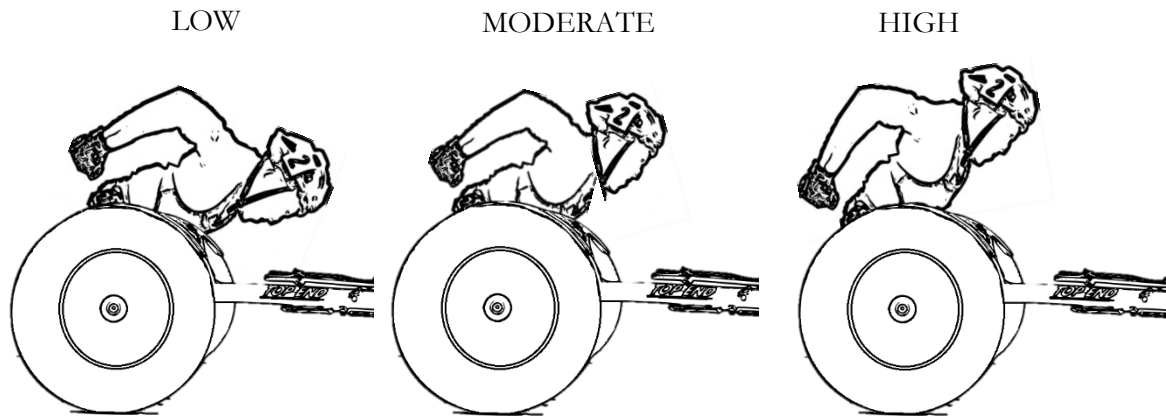


Figure 3.4: Trunk motion categorisation (based on trunk position at the top of the stroke). Low: trunk remains parallel to track surface, Moderate: thoracic region rises from lower extremity, the head remains tucked, High: trunk opens fully, head un-tucked.

Theoretical race times were calculated for moderate and high classified athletes, using an  $F_D$  measure calculated from the frontal area of low athletes. Effective frontal area of the athletes was estimated using still images (5,000 m and marathon races) in the frontal plane; to prevent parallax errors. Background pixels of each image were removed (Figure 3.5). For image calibration, it was assumed athletes used a standard 22" front wheel. This enabled a measure of pixels per square metre, and thus an estimate of athlete frontal area. Percentage difference to the mean measure of the frontal area from the low classified group was obtained. The frontal area presented in the literature by Barbosa et al<sup>9</sup> was scaled to this difference.  $F_D$  was calculated using average velocity over the duration of the race (as final 100 m split times were not available), and assuming air density to be 1.2 kg/m<sup>3</sup>.<sup>9</sup> It was assumed reductions in  $F_D$  did not impact other stroke characteristics when estimating theoretical race time.

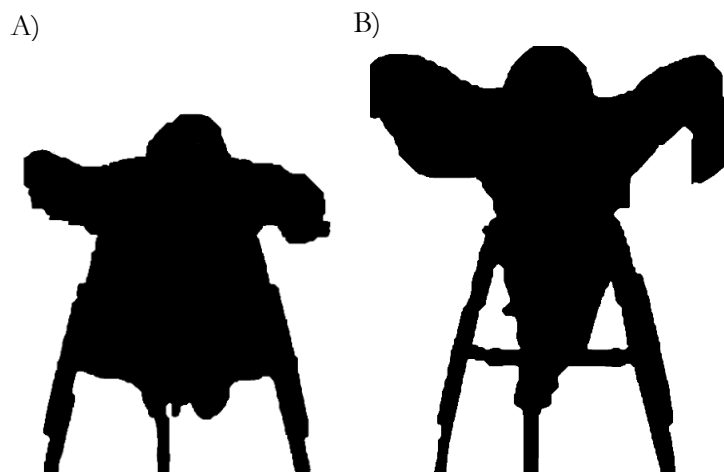


Figure 3.5: Example of processed images used for frontal area estimation of a low (A) and high (B) classified athlete.

## 3.3.3 RESULTS

Excellent intra-rater reliability was observed for the manual digitisation of classification (intra-class correlation coefficient (ICC) > 0.89) and stroke count (ICC > 0.99). Female athletes demonstrated a clear trend of a high vertical range of motion not medalling, with medallists more frequently assuming a low or moderate position (Figure 3.6). The same trend was not observed for male athletes, with no preference observed in sprint or endurance events. A higher number of male athletes ( $n = 9$ ) utilised high positions, as compared with females ( $n = 4$ ).

However, a low position was not always observed to be beneficial to performance, however, with all male 7<sup>th</sup> placegetters, and 80% of the female 8<sup>th</sup> place getters (4 out of 5) assuming a low position. Consequently, it can be observed that assuming a low position (for both male and female athletes) does not guarantee improved performance.

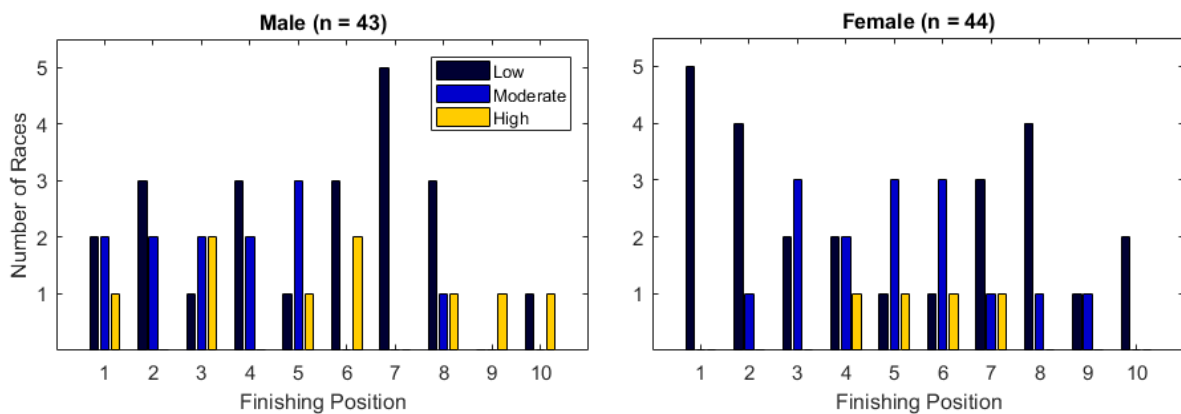


Figure 3.6: Influence of vertical position on athlete finishing place for both male and female athletes.

For the 100 m sprint, the majority of athletes (7 out of 8) assumed a low position for both males and females (Figure 3.7), while males predominantly assumed a moderate ( $n = 3$ ) and high ( $n = 3$ ) position for the 400 m. No trends were observed across other race distances.

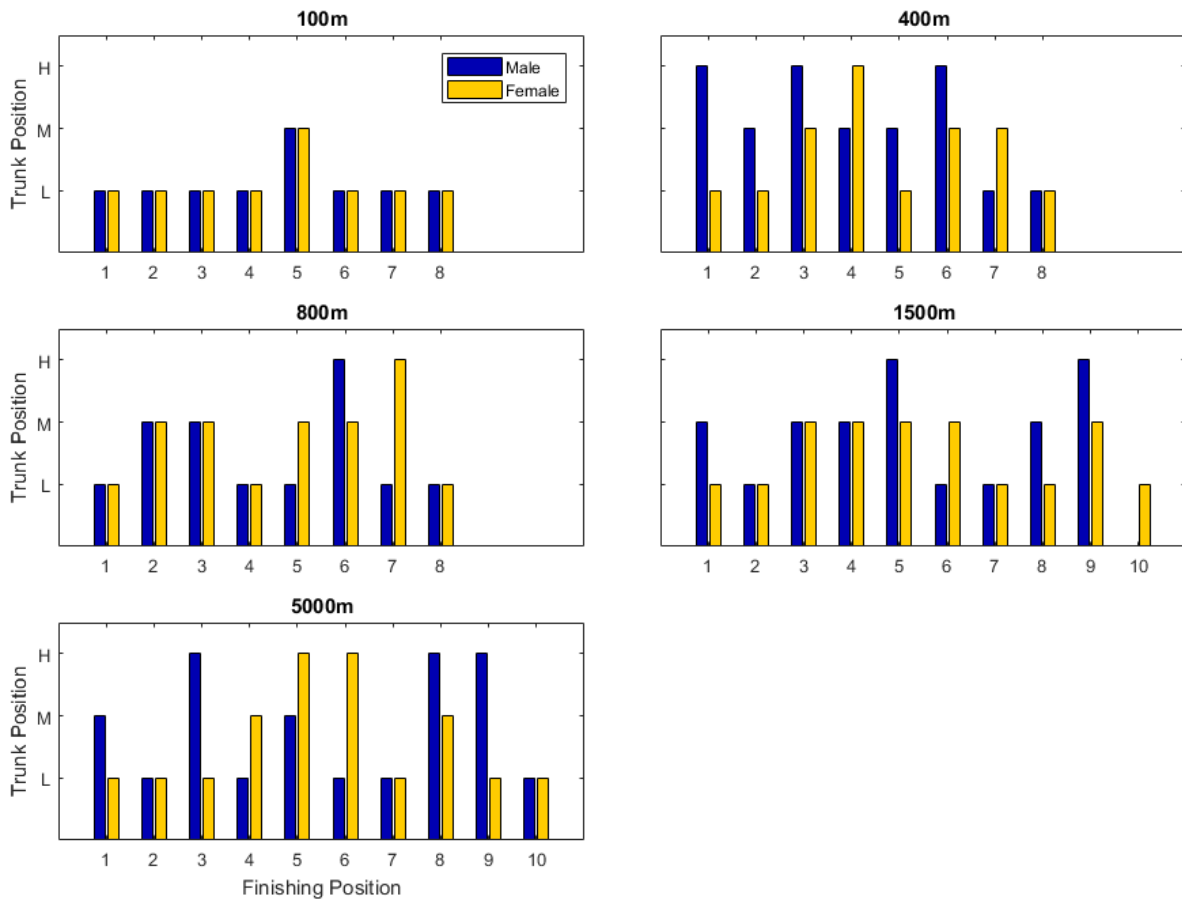


Figure 3.7: Break down of trunk position and finishing position according to race distance. L: low, M: moderate, H: high.

Females assuming a low vertical trunk motion have a higher stroke count over the final 100 m assessed (Figure 3.8). However, males are less consistent, with some athletes having a low position, as well as a low stroke count, potentially suggesting an optimised kinematic technique

Weak negative interactions were observed between a vertical range of trunk motion and stroke count (Figure 3.8) for both males ( $R^2 = 0.30$ ) and females ( $R^2 = 0.17$ ). Weak interactions were also observed between stroke count and finishing position, which was positive for males ( $R^2 = 0.11$ ) and negative for females ( $R^2 = 0.17$ ). The weakness of the correlations suggests that variation exists between athletes, which can be expected due to the different physical functionalities within this population.

### 3. HOW IMPORTANT IS THE SEATING INTERFACE TO ATHLETE PERFORMANCE?

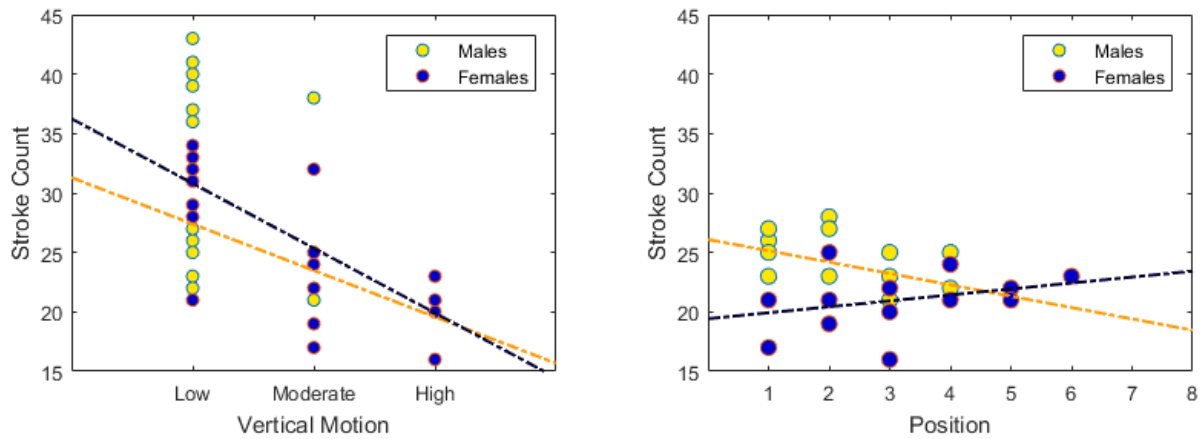


Figure 3.8: Influence of stroke count on vertical motion (left) and finishing position (right). Dashed lines show the line of best fit for male and female data sets. N.B. Data for 100 m race excluded for the right plot based on different race tactics.

Athletes classified as moderate and high vertical trunk range of motion displayed respective frontal area 113.2% and 147.0% greater than that of a low athlete. Estimated race times of moderate and high athletes modelled using a low  $F_D$  are presented in Table 3.4. Reductions in race times were meaningful, with all athletes improving their performance outcome, under the assumption that force generating capacity was not compromised.

Table 3.4: Possible male time reductions if athletes maintained a low trunk position.

Height	100 m ( $n = 16$ )	400 m ( $n = 16$ )	800 m ( $n = 16$ )	1,500 m ( $n = 19$ )	5,000 m ( $n = 19$ )
Moderate	0.9*	$2.8 \pm 0.7$	$5.7 \pm 0.0$	$10.9 \pm 0.0$	$39.8 \pm 0.0$
High	N/A	$8.3 \pm 0.1$	$16.7^*$	$31.9 \pm 0.0$	$116.2 \pm 0.1$

\* Denotes single athlete with specific position during the event.

#### 3.3.4 DISCUSSION

A retrospective analysis of the influence of vertical trunk motion on finals placing of T54 athletes at the 2016 Rio Paralympics was performed in this study. Females tended to show a greater reliance on aerodynamic positioning than males. A positive relationship between stroke count and finishing position was observed for male athletes only. This highlights the balance between aerodynamics and physical capabilities, as low stroke counts can be considered as being associated with a more powerful technique.

---

For males, this aerodynamic position does not appear the decisive factor for winning a race. Females however were more likely to win with improved aerodynamic positions. Males can potentially better overcome the additional resistive forces of poor aerodynamic positioning due to their enhanced strength capabilities. However, this study demonstrates that if already powerful athletes can adopt low positions, without compromising their power generating capabilities, they will increase their potential for winning. Over-correction of aerodynamic positioning may ultimately adapt technique towards that of a T53 athlete, who has no trunk function and hence is forced to adopt a low position. However, T53 athletes typically have slower finishing times. Therefore, aerodynamics must not be optimised in isolation. Further exploration into upper extremity joint kinematics applied kinetics and contact parameters (contact and release angles) should be performed across athletes demonstrating low vertical trunk motion to ascertain relationships with athlete speed, to ensure peak force generating capacity is not compromised from the reduced push length on the wheel.

Low positions were used more frequently in the 100 m race, likely due to the negligible steering requirements (manoeuvring the bend, and avoiding other athletes). However, some athletes still presented moderate frontal areas, which may be due to the presence of leg mass preventing athletes from obtaining optimal positions. Wheelchair racing chairs are yet to have the capacity for changing seating inclination, despite being within sports guidelines. This is however under investigation in other wheelchair sports.<sup>181</sup> Forward-inclined seats may counteract this presence of leg mass, while also placing athletes in a more powerful position for propulsion.

Tabulated reductions in time overestimate actual benefits, as they assume athletes maintain a low position throughout the race, with no compromise in power generation, which is implausible due to the steering requirements around the track. Additionally, peak vertical trunk motion varies considerably throughout a race, particularly when drafting, whereby athletes assume lower positioning, suggesting the limitation of assessing only the final 100 m sprint, where athletes may adapt their technique. This limitation arose from the limited footage available. Classification of trunk height and calculation of frontal area may have been impacted by human error. However, intra-rater reliability measures were obtained to ensure these effects were minimal.

Further investigations could optimise the individual power and aerodynamic balance, taking into consideration unique strength, physiology, and physical capabilities. Additionally, with more footage, the presented trends could be investigated over the duration of a race for a broader range of athletes, particularly comparing those who do and do not make finals, and competitions where headwinds were considered influential. Such assessments were limited in this study as no high-speed footage was

available. These same limitations prevented the quantification of the frontal area of all athletes, which would have assisted in providing a more reliable athlete classification methodology.

#### 3.3.5 CONCLUSION

This study assessed the vertical trunk motion of male and female T54 classified wheelchair racing finalists at the 2016 Paralympics in Rio. Winning female athletes were identified as using more aerodynamic positions, while more variation in aerodynamic, and non-aerodynamic postures were identified in the male athletes. This difference in aerodynamic prioritisation is due to their increased ability for force production, and hence optimal position for each athlete may differ and thus requires further kinematic exploration.

#### 3.4 IMPLICATIONS AND CONCLUSION

The optimisation of wheelchair racing technique is reliant on the development of athlete equipment, technique, and physiology. From an engineering perspective, the two key factors able to be changed include equipment and methods for analysing performance.

The optimisation of the seating interface (through the inclusion of customised seating interfaces) may be considered as having a more significant impact on performance than changing athlete gloves (Section 3.2). As mentioned previously, the low cost of manufacture, ease of production, and customisation of seating interfaces make it a mostly generalisable solution, not only to wheelchair racing athletes, but to other athletes, and manual wheelchair users, with anticipated high impact.

The inclusion of a customised seating interface has the potential to increase athlete frontal area during the process of creating a more stable base of support. For females, this has the potential to detriment performance, however, may have less of an impact for males (Section 3.3). Excessive athlete elevation should also be avoided to ensure that stability within the chair is not compromised as a consequence of having a high centre of mass.

The presence of leg mass may disadvantage some athletes aerodynamically, as they will not be able to assume a completely horizontal position. Currently, racing wheelchair frame design does not allow for the inclination of seating buckets to accommodate the legs. However, by custom moulding of the customised seating interface, athletes can gain a more stable position, as well as one which is possibly more aerodynamic, by forming the inclined surface through the cushion. As the observed time savings

---

between high and low aerodynamic strategies are meaningful, the use of customised seating interfaces for performance seating can demonstrate significant results.

*Key Findings:*

- Glove selection did not considerably impact the degree of symmetry during a starting motion.
- The starting motion is a highly variable task.
- The aerodynamic position is important for females but less so for males, based on different technical strategies used, possibly based on strength.
- Significant time savings can be made if an aerodynamic position is adopted, with no loss in power generation.
- Aerodynamic positions did not always improve performance, with a balance of aerodynamics and power required.

*Implications:*

- Considerable variability in force generation over the first push suggests further optimisation for athlete interaction with the pushrim (for more effective force transfer) is possible.
- Glove use may provide a more significant impact for stronger, and elite level athletes, and can potentially influence competition outcome.
- Although aerodynamics were not identified as the winning factor for males, improved aerodynamics, with no compromise to power generating capabilities can increase the potential of winning.
- For males, aerodynamic positioning is not everything, and performance improvement requires a change in kinematic propulsion style or equipment.
- Overcorrection of aerodynamic positioning may artificially increase impairment, meaning athletes must select a technique best suited to their capabilities.

---

## CHAPTER FOUR:

# WHEELCHAIR INSTRUMENTATION USING IMUs

---

To comprehensively analyse the biomechanical influence of customised seating interfaces on wheelchair racing performance using computational modelling approaches, three key inputs are required: kinematic data, kinetic data and a musculoskeletal model containing relevant geometries. Within wheelchair racing, there are two main kinetic sources requiring measurement of the dynamic interactions between the hand and the pushrim, and the quasi-static interactions at the athlete-wheelchair interface. As stated in the Literature Review (Chapter Two), the most commonly implemented (commercially available) instrumented wheel used in clinical based literature is not conducive to sporting performance. Consequently, the kinetic measurement of wheelchair racing propulsion is limited due to the lack of practically viable instrumentation solutions available for use with sporting applications. From a performance perspective, instrumentation solutions are constrained by mass, as this has been shown to have a significant influence on performance.



---

The limitations in the ability to measure the applied forces during wheelchair racing led to the creation of the first aim of this research: developing an instrumentation tool capable of in-field data measurement of wheelchair racing performance. Based on their practical viability, the use of IMUs were explored for measuring the interactions between the hand and the pushrim.

In this chapter, the robustness of the use of IMUs was analysed across three experimental studies which investigate the capability of the IMU method, whether this capability is reduced across different athlete equipment and techniques, and how the reliability is affected across different placement locations. These studies were performed to ensure the generalisability of the solution to the greater wheelchair racing population. The final experimental study presented in this chapter contains the first research exploring the capability of IMUs to estimate the kinetic requirements of wheelchair propulsion as a more practically viable method than what is currently available with the SMARTWheel. These four experimental studies are summarised following, highlighting the focal research questions which drove each study, with their relations to overall aim presented in Figure 4.1.

#### **Characteristic response from IMUs measuring wheelchair propulsion at various placement locations (Section 4.1)**

*Research Questions:*

- Are IMUs capable of identifying wheelchair propulsion data?
- How does this compare with video data, which is the current gold standard measurement?

This study was a proof of concept study, performed using able-bodied participants to identify whether the IMU was a suitable method before involving elite athletes. Consequently, the methods differ from the remaining studies.

#### **Intra stroke profiling of wheelchair propulsion using IMUs, and the influence of equipment (Section 4.3)**

*Research Questions:*

- Can IMUs identify both the contact and release points of propulsion?
- Does the characteristic response of IMUs differ when using different equipment and at varying speeds of propulsion?

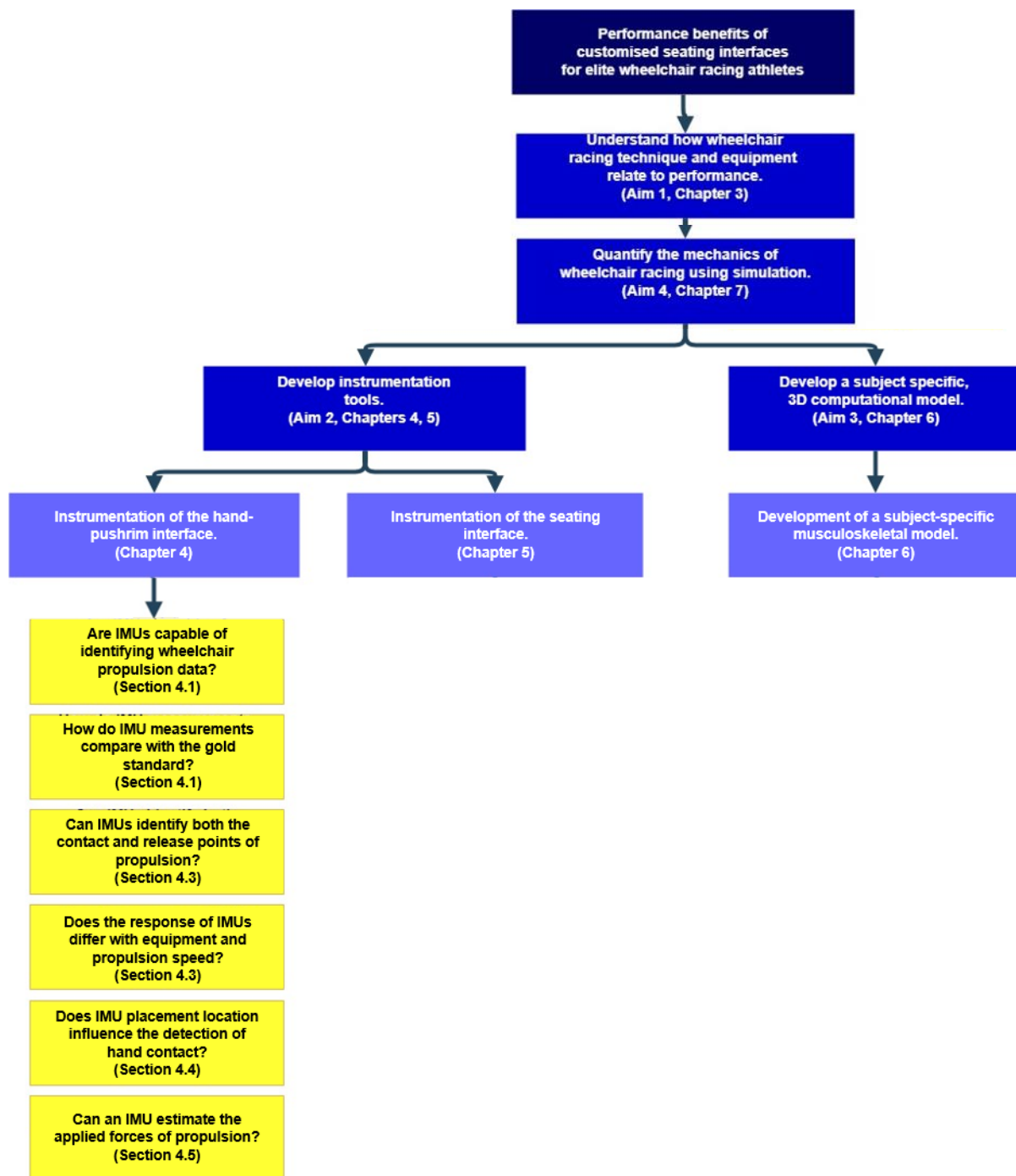


Figure 4.1 Relevance of the Chapter 4 (Wheelchair instrumentation using IMUs) to the fundamental research question; what is the performance impact of customised seating interfaces on wheelchair racing propulsion?

---

## **Does the placement of IMUs affect the macroscopic measurement of acceleration in wheelchair sports? (Section 4.4)**

*Research Question:*

- Is there a placement location which increases the reliability of the IMU for detecting hand-contact reliably?

## **The validation of IMUs on estimating torque production of wheelchair racing athletes (Section 4.5)**

*Research Question:*

- Can an IMU estimate the applied forces of propulsion?

The development of practically-viable instrumentation is beneficial not only for collecting relevant performance data for use in the computational model but also for regular biomechanical assessment. The margin of victory in wheelchair racing can be a few hundredths of a second, with medals decided within 0.5% of the winning time.<sup>200</sup> The optimisation of technique can hence have a substantial impact on performance outcome. Tools which can be integrated in the daily training environment for regular performance feedback could considerably improve performance preparation.

## **4.1 CHARACTERISTIC RESPONSE FROM IMUs MEASURING WHEELCHAIR PROPULSION AT VARIOUS PLACEMENT LOCATIONS**

### **4.1.1 INTRODUCTION**

The key propulsion characteristics for wheelchair racing have been identified as stroke speed, stroke length (time between successive contacts), push times (the time when the hand is in contact with pushrim) and recovery times. These parameters diagnose the efficiency of the interaction between the hand and wheel. Understanding the relative timing between the hands is also beneficial to performance, as kinematic asymmetries can negatively impact performance by introducing steering difficulty.<sup>70, 94</sup>

The importance of obtaining the temporal kinematics of propulsion are highlighted through the use of the strain gauge force transducer used by Newsam et al. <sup>207</sup> and Kulig et al. <sup>208</sup>. As wheelchair propulsion is a highly ballistic motion, it can be hypothesised that these points of contact will be accompanied by large acceleration peaks occurring at the points of contact and release.

IMUs have recently been used to measure wheelchair propulsion kinematics. However, there has been no consistent methodology used. Previously, there have been three key placement locations used; the frame,<sup>180,216,218</sup> wheels,<sup>180,216,217</sup> and the wrist.<sup>218</sup> These studies have not detailed the placement location on the wheel (radius from axle), and whether signal characteristics change with placement radius on the wheel. The different placement locations have enabled measurement of various parameters, with propulsion and coordination measured from the wheelchair and wrist, while push detection has been quantified from placement on the frame and wheels.<sup>180</sup> As no literature has currently explored the use of IMUs for kinetic profiling; it is uncertain as to which of these placements provides the cleanest and most reliable data.

This study aimed to investigate the effects associated with IMU placement on the quality of the acceleration signal, with specific consideration into identifying separate left and right contacts, and ease of signal processing. This was a preliminary study performed to confirm the methods presented in literature, and ensure the capability of the IMU to ensure it is a valid tool for the instrumentation required to satisfy the first aim of this research, to ultimately provide kinetic input into a musculoskeletal model for the comprehensive analysis of wheelchair racing performance. It was hypothesised that the hand will provide the best contact location, as this location minimised the distance between the acceleration phase and the contact event.

##### 4.1.2 METHODS

This was a proof of concept study which was performed in the laboratory using non-athletic participants and available equipment (rugby wheelchair). It is acknowledged that the signal characteristics of the accelerometer may differ between racing and rugby wheelchairs.

Triaxial acceleration data were collected using three synchronised IMUs (Figure 4.2: IMeasureU, New Zealand; Accelerometer:  $\pm 16$  g; Gyroscope:  $\pm 2000$  °/s; Compass:  $\pm 1200$   $\mu$ T),<sup>219</sup> sampling at 500 Hz. Rigid fasteners coupled the three IMUs at varying radii (2.8 cm, 10.4 cm and 24.3 cm) onto a rotating wheel pedalling at a constant rate (as driven through cranks) for two minutes continuously, to assess whether the units were susceptible to the effects of drift and centripetal acceleration. Figure 4.2 demonstrates the experimental set-up for this investigation.

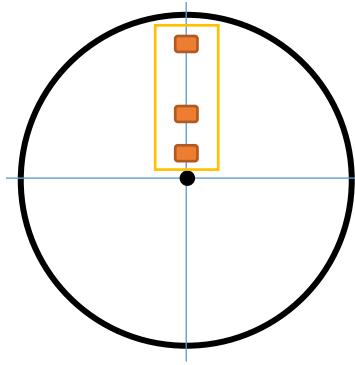


Figure 4.2: Schematic demonstrating how IMUs were coupled to the wheel. Solid rectangles represent IMU placements, with the surrounding box indicating the size of the coupling mechanism.

Three placement configurations were tested; Hand (L) versus Wheel (L) versus Frame (L); Frame (L) versus Frame (R) versus Frame (C); Wheel (L) versus Wheel (R) versus Frame (C). L and R denote left, and right sides and C indicates the central axis of the wheelchair frame. The IMUs were synchronised automatically within the IMeasureU Research iPad App and Lightning software. Three distinct synchronisation contacts between the hand and wheelchair frame, followed by 10 s of being stationary were performed prior to movement to confirm synchronisation between sensors (Figure 4.3). Initial contact timings (identified by clear acceleration peaks) were validated against a ‘gold standard’ video observation method.<sup>180</sup>

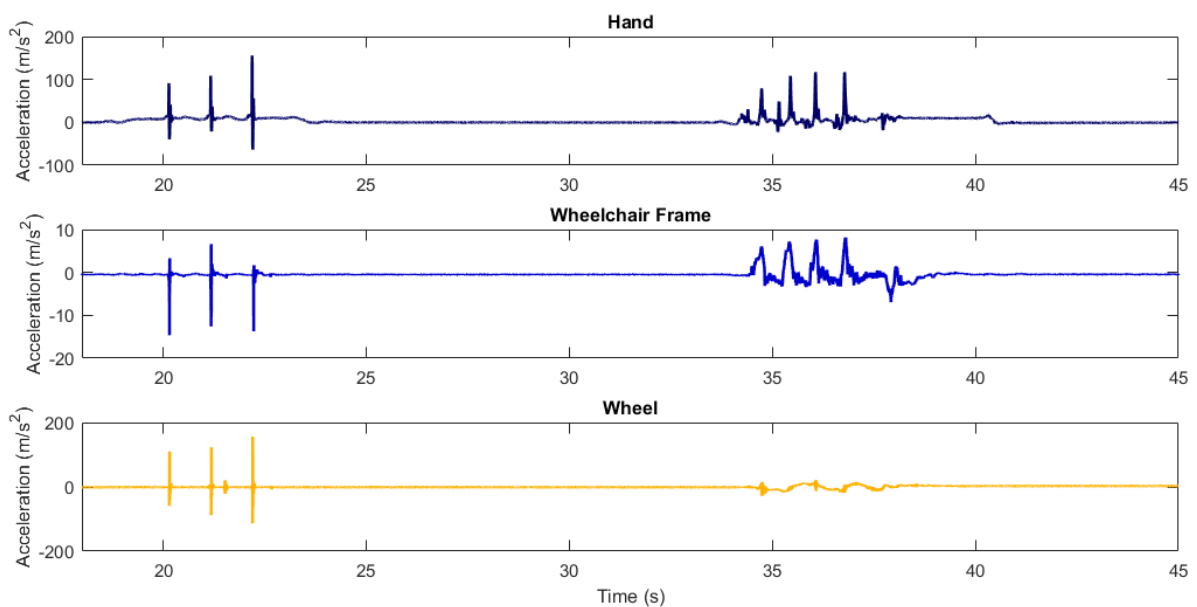


Figure 4.3: Example of IMU synchronisation as performed through comparing impact peaks.

Temporal differences less than the *a-priori* threshold of  $\pm 0.08$  s were required for acceptable agreement between methods. The propulsion task consisted of four consecutive pushes, a stationary  $180^\circ$  turn, and five successive pushes back to the start. A single camera located in line with the direction of travel allowed digitisation of both hands in the same footage, preventing synchronisation errors resulting from a two camera placement method. IMU data (500 Hz) were down-sampled for synchronisation with the video camera (100 Hz).

Intra and inter-rater reliability (R1 and R2) were assessed through ICCs, with an *a-priori* threshold of  $\text{ICC} > 0.9$  established to ensure sufficient accuracy of results.<sup>250</sup> R1 and R2 represent independent raters experienced with the analysis of wheelchair propulsion motions. Systematic differences between the video-based methods were assessed through Bland-Altman analyses, and ICCs were used to observe agreement between left and right signals.

#### 4.1.3 RESULTS

Exemplar data (in the propulsive direction) from IMUs located on the wheelchair and wheel are presented in Figure 4.4. IMU placement on the hand was inadequate as the resulting acceleration signals were ambiguous, as peak accelerations correlate with both impact, and movement back to the start of the rim, for the beginning of each propulsion phase, as visualised in Figure 4.5.

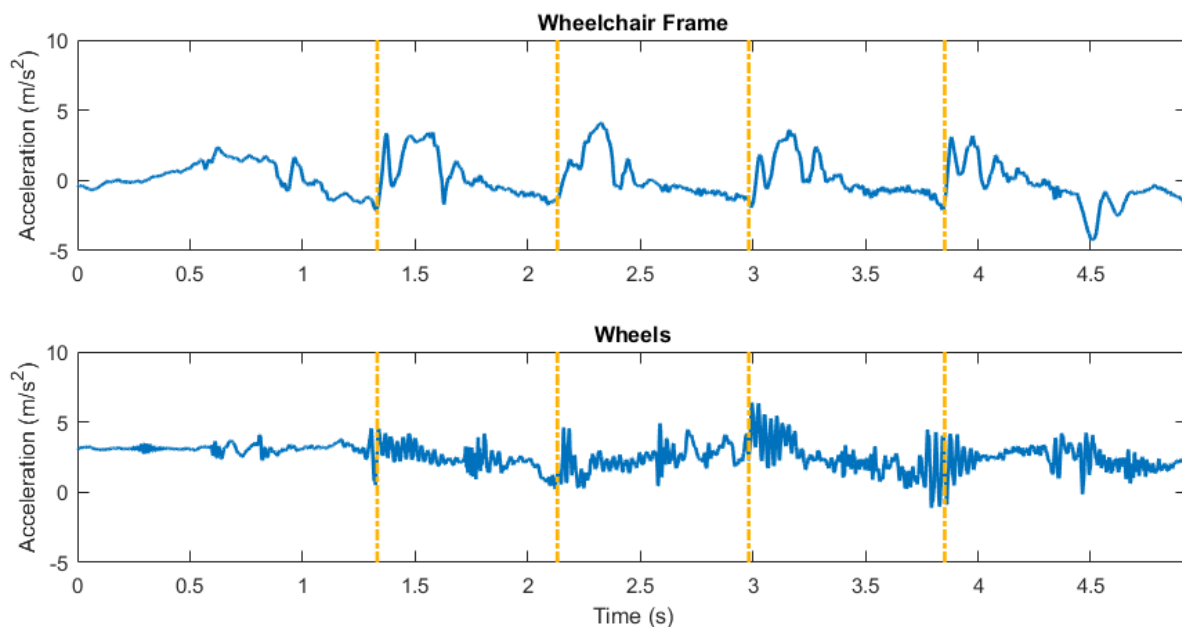


Figure 4.4: Exemplar data from the IMU at different placement locations on the wheelchair. Contacts indicated by vertical dashed lines.

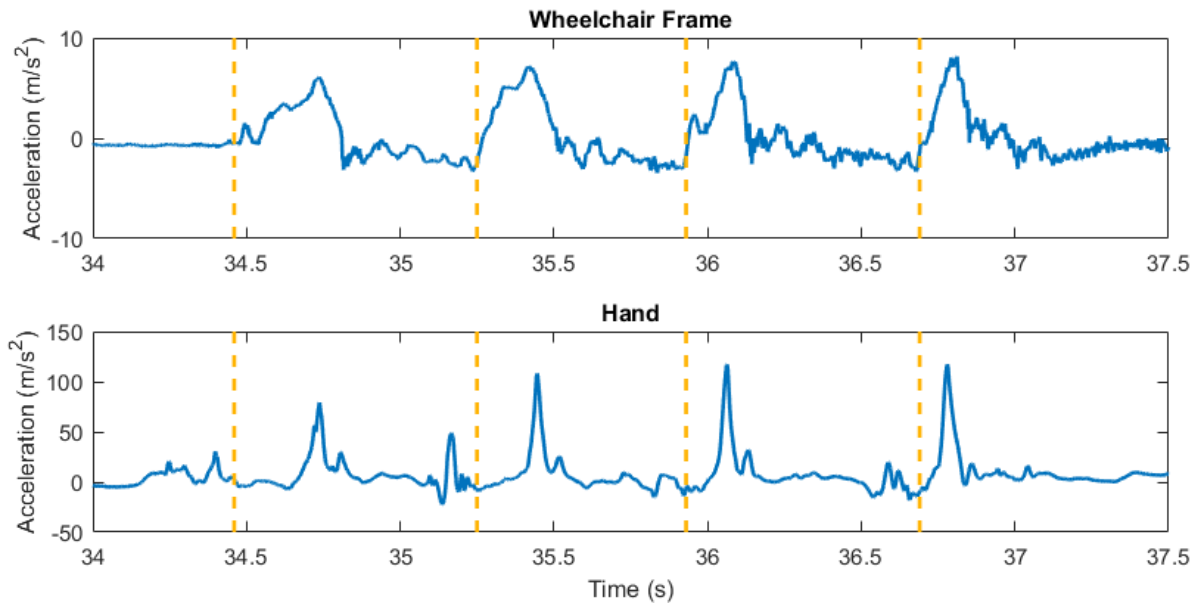


Figure 4.5: Characteristic acceleration data from IMU located on the wheelchair frame and hand.

The differences in contact timings between video observation and wheel and frame measurements were within predefined bounds (0.00-0.02 s and 0.00-0.04 s). A high degree of both intra- and inter-rater reliability was obtained (Table 4.1). Additionally, a strong positive correlation ICC ( $> 0.95$ ) was found between temporal parameters for both the right and left sides when IMUs were placed on either the frame or wheels, suggesting both locations are equally useful for identifying the contact.

Table 4.1 Reliability of IMUs in contact timings, data presented as mean time  $\pm$ SD.

IMU		High-Speed Video	
R1 v R2	R1 v R1	R1 v R2	R1 v R1
0.01 $\pm$ 0.03 s	0.00 $\pm$ 0.06 s	0.05 $\pm$ 0.07 s	0.02 $\pm$ 0.04 s

R1 and R2 represent independent raters experienced with the analysis of wheelchair propulsion motions.

When comparing the differences in push time, intra-rater differences are normalised around zero, while inter-rater differences are negatively skewed around one or two frames different (Figure 4.6). The three pushes shown in Figure 4.4 have durations of 0.80 s, 0.85 s, and 0.87 s, respectively. Therefore, this difference in two frames (which are equivalent to a duration of 0.04 s), is relative to push time.

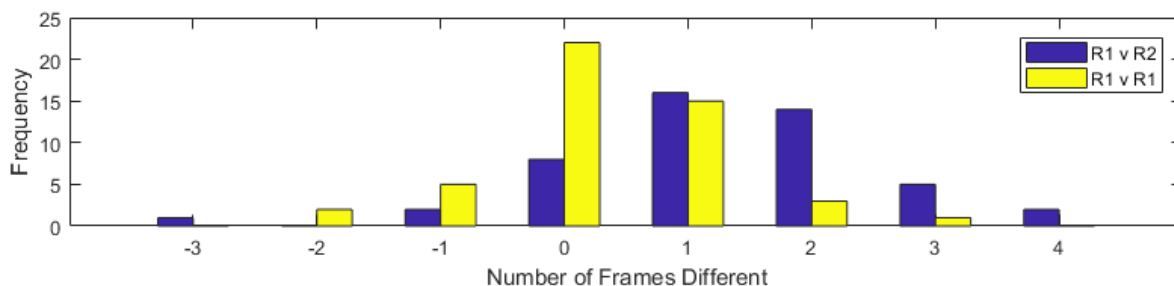


Figure 4.6: Inter- and intra- rater reliability of contact identification between two experienced raters. IMU data obtained from wheelchair wheel.

Video observation was found to be reliant on the direction of travel of the wheelchair (Figure 4.7). When the participant travelled towards the camera, IMU detection preceded that of video observation, whereas video observation preceded IMU detection when the participant moved away from the camera. Additionally, manual identification of specific timings of hand contact was faster and more reliable using acceleration signals, further suggesting its superiority over video observation.

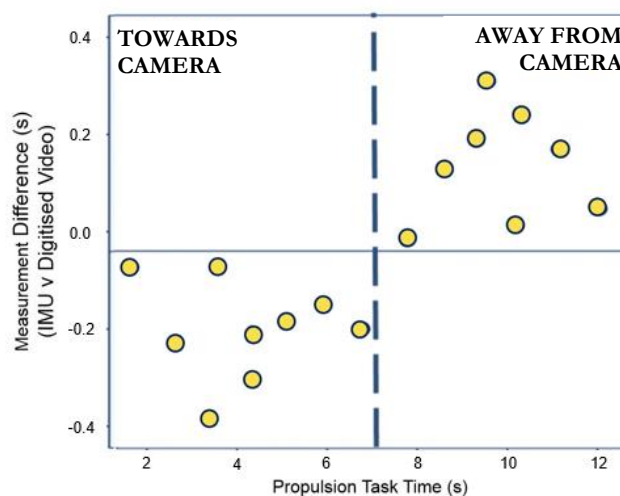


Figure 4.7: Directional bias in video digitisation approaches, based on IMU located on the wheelchair wheel.

Accelerometer data from wheel-mounted IMUs were subject to radial effects (Figure 4.8) and sensor noise. Distal placements were more affected by radial acceleration. Conversely, the acceleration signals resulting from more distally located IMUs were higher in amplitude, and more clearly defined. The increased signal magnitude was likely a consequence of being closer to the point of force application than the axially located sensor. Thus, a fusion of both sensors may most effectively ascertain all performance variables of interest.



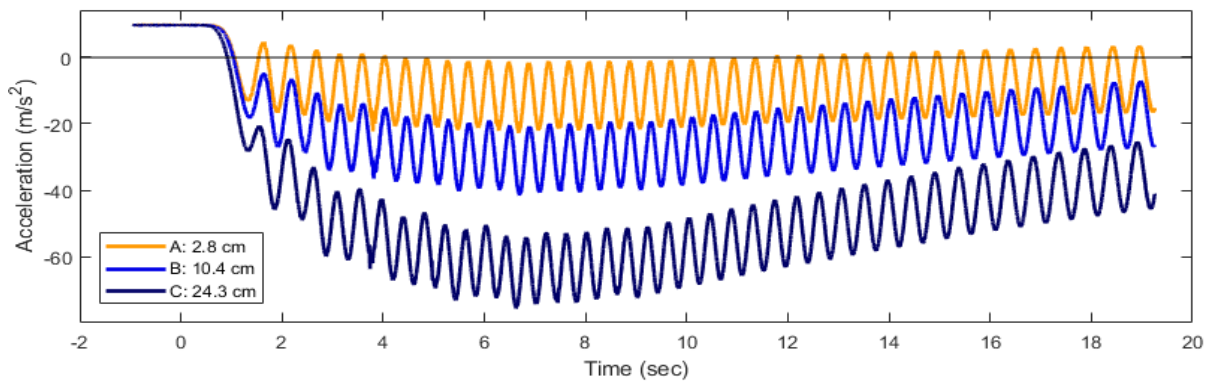


Figure 4.8: Influence of centripetal acceleration in IMU measurements located at different radii (2.8 cm, 10.4 cm, and 24.3 cm) on a wheel.

Root mean square (RMS) values demonstrated tri-axial consistency for the gyroscope measurements throughout the two-minute test duration, indicating that these units are not susceptible to drift over short durations, suggesting the appropriateness for in-field measurements.

#### 4.1.4 DISCUSSION

This study investigated the characteristic response of wheelchair propulsion as measured using IMUs, and how this varies across different placement locations on the athlete-wheelchair system and the wheels. The IMUs were demonstrated to be effective at identifying contact between the athlete's hand and the wheelchair. Additionally, IMUs may also offer a more accurate representation of contact identification, which is less susceptible to subjective assessment than the current gold standard method of video digitisation. This suggests that further exploration is warranted into the use of IMUs as an instrumentation tool for the analysis of wheelchair racing propulsion.

A notable finding from this study was the presence of bias in the manual identification of wheelchair contact when analysed using video digitisation. A more conventional grab-push motion was employed for this study. Initially, the palm contacted the wheel before the fingers made contact. When the camera was placed in front of the participant, the contact of the palm on the wheel was partially occluded by the fingers, making it difficult to identify the start of contact visually. Conversely, when the camera was placed behind the athlete, the palm is the most prominent feature.

It is presumed that these effects will not be present for a camera located perpendicularly to the athlete which was able to capture the movement in the sagittal plane. However, this is not practically viable for in-field analysis. This is due to the cost of multiple-camera systems and the reliance on effective synchronisation approaches.

Placement effects were identified. Rotational effects were observed on the wheels at varying placement radii, with noise increasing with sensor placement radius. Further work is required to determine the impact of this on both the reliability and capability of processing the data. As well as the difficulties in interpreting the data from the IMU located on the hand, it may not be revered by the athlete, as it requires strong adhesion to either the athlete skin or glove. Placement locations for the remainder of the research were hence restricted to being on the athlete's equipment.

Due to a high degree of symmetry (asymmetry index = 0.01), negligible differences were observed for left, and right contact (ICC > 0.95) for IMUs mounted on both the frame and wheel. Although the welded nature of the frame prevented distinguishing left and right contact timings, non-significant differences were detected between wheel-mounted IMUs, demonstrating the capacity for identifying temporal asymmetries.

Interpretation of data collected by the IMU located on the hand was limited by the difficulty in distinguishing peaks associated with a contact from those associated with hand motion. It is important to acknowledge that this finding may be a consequence of the testing protocol used for this preliminary investigation. This changes the propulsion style, as well as differences across the frame. It is anticipated the same bias will be present across wheelchair racing propulsion, as neither technique has a synchronised hand contact on the wheel, with both requiring rotation of the wrist during the propulsion phase. It is anticipated that impact peaks (at contact) of larger magnitude will be observed from elite athletes, based on the striking nature of wheelchair racing propulsion. However, there is also a higher cadence of propulsion, and so the movement artefacts will also be greater during the recovery phases. Additionally, wheelchair rugby frames are far stiffer than that of wheelchair racing chairs to withstand the impacts common in that sport. As the plausibility of IMUs has been demonstrated from this study, the use of racing wheelchairs and elite athletes were used the remainder of the research.

##### 4.1.5 CONCLUSION

IMUs are a reliable measurement tool for monitoring the timings of wheelchair contact, with the objective measurements provided by the technology superior to the video digitisation methods currently used. This suggests that IMUs are an appropriate tool for instrumenting a racing wheelchair and were worthy of further investigation to satisfy the first aim of this thesis. The response of the IMUs changes with placement locations, warranting ongoing research into identifying the optimal placement locations to ensure highly reliable data.

---

## 4.2 METHODS OF COLLECTING WHEELCHAIR RACING PERFORMANCE DATA USING IMUs

A common methodology was used to collect the data for the remaining experimental studies presented in this chapter using elite wheelchair racing athletes. Athletes provided written, informed consent, with ethical approval obtained by the University of Adelaide and the Australian Institute of Sport. The methods which are common to these remaining studies are presented within this section. Any methodologies in the following studies which differ to this are elaborated on later.

### 4.2.1 EXPERIMENTAL PROPULSION TASK

Athletes completed trials at a constant velocity on a single-belted treadmill (H/P/Cosmos® Saturn, Traunstein, Germany) inclined to 1%, as this has been demonstrated as being most physiologically and biomechanically representative of overground propulsion.<sup>183</sup> Treadmill (belt) velocity was comparable to individual regular race training velocity ( $92.1 \pm 2.4\%$  of mean race velocity at an international competition held within six months of data collection).<sup>251, 252</sup> Athletes who were new to treadmill propulsion completed a familiarisation protocol, whereby treadmill velocity was incrementally increased until testing velocity was reached. A 5 min active recovery period was provided between trials to minimise the effects of fatigue. All athletes participated in their own racing wheelchairs (Invacare and Top End).

The front fork of the wheelchair was fastened to the treadmill using a custom designed clamp, which prevented lateral translations of the wheelchair but allowed normal fore-aft movement of the wheelchair within a safe operating range (Figure 4.9). Any potential detriments to athlete performance from treadmill based propulsion did not impede the recording capabilities of the IMU.



Figure 4.9: Testing set up. A) Custom clamp (circled) keeping wheelchair on the treadmill; B) IMU locations (circled).

Senior athletes completed three trials (each 1 minute in duration) of constant velocity propulsion at three speeds (Table 3.1). A modified testing protocol was applied for the junior athletes to ensure that effects of fatigue did not deter results. For the junior athletes, belt speed was in line with regular training speeds, with athletes only completing trials at two speeds. An additional 30 s trial was performed by Athlete F to replicate expected finishing conditions of a male T54 athlete, which places greater emphasis on sprinting, and far higher than the speeds demonstrated by the female and junior athletes. For each trial, three discrete data capture periods, 10 s in duration were obtained (however, only one was collected for the sprint speed performed by Athlete F). Motion capture data could only be analysed for one trial at 20 km/hr for Athlete A.

#### 4.2.2 MEASUREMENT SYSTEM

Triaxial acceleration data were collected using eight synchronised IMUs (Figure 4.10: IMeasureU, New Zealand; Accelerometer:  $\pm 16$  g; Gyroscope:  $\pm 2000$  °/s; Compass:  $\pm 1200$   $\mu$ T),<sup>219</sup> sampling at 500 Hz. The IMUs were synchronised automatically within the IMeasureU Research iPad App and Lightning software. Units were located on the left and right axle housings of the wheelchair frame (FL, FR), the wheel axis (WLA, WRA), at the radius of the pushrim, which is located at the midpoint of the wheel, (WLM, WRM) and at the outer rim (WLR, WRR). All units were carefully fastened using double-sided adhesive tape and secured using fabric tape to rigidly couple all units on each disc wheel, preventing unwanted lateral translations and vibrations. Each of the ensuing research studies used a subset of these eight IMUs. The IMUs used in each study are documented for each case in the following sections.

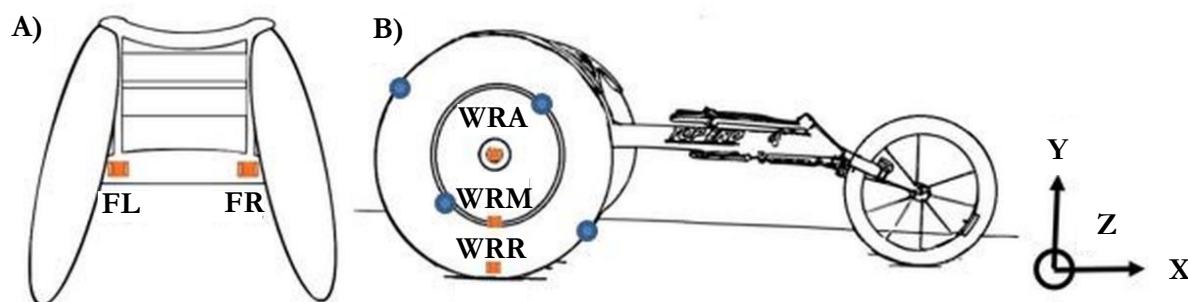


Figure 4.10: IMU (square) mounting locations and reflective marker (circle) positioning. An additional marker was located atop the WRA IMU. A) Rear view: demonstrates frame (axle housing) placements (FL, FR). B) Right side view: highlights where IMUs were located on the wheel axle (WLA, WRA), pushrim (WLM, WRM), and outer rim (WLR, WRR). The left wheel was instrumented identically.

---

Minor variation existed between WRR and WLR placement location, to accommodate differences in wheelchair frame size. IMUs were moved marginally closer to the axle to ensure the wheel could rotate freely and not damage the IMU. Consequently, units located at WLM, WRM, WLR, and WRR were all located on the inside of the wheel. WLM and WRM units were not present for Athlete I.

Careful consideration was required to ensure FL and FR placements were not fastened to the frame itself, but just the axle housing (connection between wheel and frame). This ensured that the two IMUs were not coupled via the rigid frame, which if not accounted for would have resulted in compromised accuracy in athletes with pronounced temporal asymmetries.

#### 4.2.3 DATA PROCESSING

Cut off frequencies have been demonstrated as having a significant influence on kinematic waveforms.<sup>253</sup> Resultant accelerometer data were all low pass filtered with a bidirectional low-pass filter using a -6 dB cut off frequency of 100 Hz, which was determined through performing independent residual analyses for each IMU, athlete, and speed. 100 Hz represented the highest recommended cut off frequency and was nominated due to the low likelihood of distorting the temporal data to identify the contact point. Although a high value, this is an appropriate cut off measure, similar to literature by Andena et al.,<sup>254</sup> who used a cut-off frequency of 120 Hz when investigating impacts between the feet and ground for running motions. The resultant acceleration vector was used to account for orientation discrepancies during placement.

Contact and release points were automatically detected using a custom peak-detection algorithm developed using MATLAB which located local maxima, with push time calculated as the time between successive contacts. The algorithm specified the minimum distance between corresponding points (contact or release), 0.45 s based on previous literature,<sup>115</sup> with athlete-specific minimum peak thresholds manually defined based on visual inspection (0.3 – 17 m/s<sup>2</sup>). Temporal parameters were validated against the video data, which served as the gold standard measurement.<sup>180</sup> Video data was manually digitised (Kinovea v0.8.15 [www.kinovea.org](http://www.kinovea.org)) with hand contact and release identified as the first and last frame where any part of the athlete's hand or glove was touching the pushrim, respectively.

#### 4.2.4 DATA VALIDATION AND VERIFICATION

Although this research is examining the practical plausibility of IMUs, motion capture is used as the primary method of comparison in this research. Through understanding the capabilities of the IMU

under controlled environments, it is plausible to extrapolate the practical usability of the solution with greater precision than is available from video analysis alone.

Push contact durations were validated through either motion capture or video. Kinematics of the upper extremity and trunk were recorded at 250 Hz using a twenty camera motion capture system (VICON Bonita V16, Oxford Metrics, Oxford, United Kingdom). A whole body marker model (based on the UWA model) was used.<sup>255</sup> A cluster-based model was used due to its improved reliability in measuring non-sagittal plane kinematic data.<sup>256</sup> More details on cluster-based models can be found in Appendix A.2. For the musculoskeletal modelling component (Chapter Six and Chapter Seven), only the markers on the upper extremity and torso were used. Nineteen retro-reflective markers were located on the upper extremity using a cluster-based marker configuration, with calibration accurate to 0.02 mm. Two marker clusters (cuff) of three markers each were fixed on the acromion, and at the distal humerus (in line with the medial epicondyle). Two T-bar clusters of three markers each located on the distal forearm, and at the hand (between the lateral epicondyle, ulnar styloid and at the base of the second digit). Four markers were located on the head (left and right, front and rear), and three markers on the trunk, at C7, T10 and the sternum (however, this was rarely visible during motion). An additional six static markers were used for model scaling but were removed before data collection. Two markers were each located at the shoulder, elbow and wrist, which were converted into virtual markers acting at the joint centres to scale limb length (Figure 4.11).

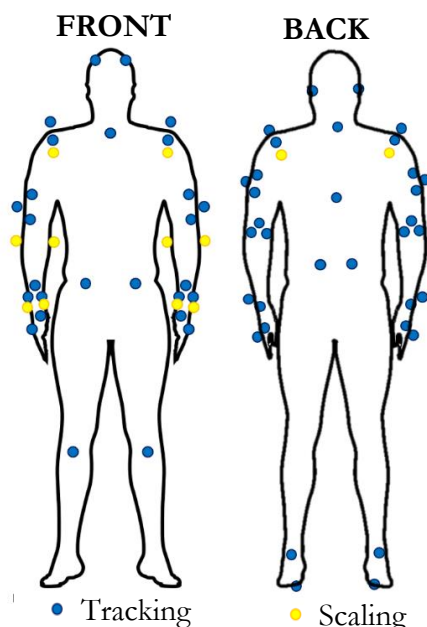


Figure 4.11: Tracking and Scaling marker placements used to actuate a musculoskeletal model with the Inverse Kinematics tool in the OpenSim environment.

Gaps in kinematic data ( $<25$  ms) were interpolated using a cubic-spline interpolation, with all kinematic data filtered using a bidirectional 6 Hz low-pass Butterworth filter with -6 dB cut-off frequency.<sup>113</sup> Coordinates of the kinematic data were converted into the global coordinate system of OpenSim using a rotation matrix.

No gold standard has been reported in the literature for the definition of contact between the hand and pushrim from motion capture data. Kinematic data (position, velocity and acceleration) from multiple configurations of markers on the hand of multiple athletes were compared against IMU data to determine whether key phenomena correlated between the two measurement systems. Figure 4.12 represents kinematic data from Athlete E. Correlation between data sets are observed for  $P_{ML}$ ,  $V_{AP}$ ,  $A_{ML}$ , and  $A_V$ . Similar trends were observed for other athletes, which justified the use of acceleration data for comparison purposes.

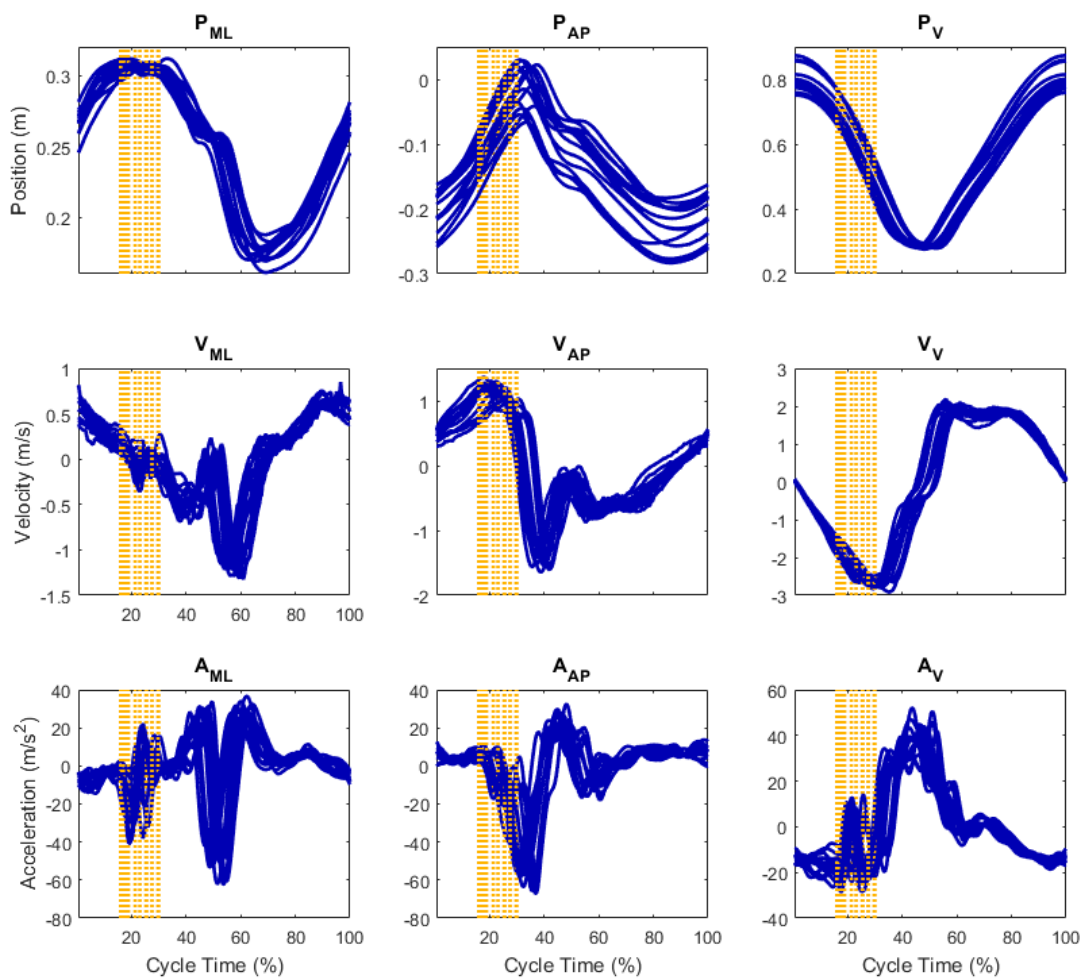


Figure 4.12: Comparison of motion capture data and its derivatives over 15 push cycles, for the marker at the base of 2<sup>nd</sup> metacarpal joint on the left hand for athlete E at 22 km/hr. Dashed lines represent contact (minimum  $A_V$ ) as determined from visual inspection of motion capture data.

In addition to motion capture, three high-speed Sony PXW-FS7 video cameras (located at the rear and perpendicularly left and right of the athlete-treadmill system) were used to collect data to validate the push durations calculated by the IMUs. Cameras operated at a sampling frequency of 100 Hz and a shutter speed of 1/1000 s. Three distinct contacts were made between the hands and wheels followed by a period of 20 s where no movement occurred to synchronise IMU and video data. Video data were only used as a visual point of reference for post-processing.

### 4.3 DOES THE PLACEMENT OF IMUs AFFECT THE MACROSCOPIC MEASUREMENT OF ACCELERATION IN WHEELCHAIR SPORTS?

#### 4.3.1 INTRODUCTION

In Section 4.1, it was demonstrated that IMUs were capable of identifying contact between the hand and the pushrim of an able-bodied participant in a wheelchair rugby chair more reliably than the previous gold-standard method (video digitisation). This suggested the plausibility of investigating the capabilities of the IMU for use within an elite wheelchair racing population. Limitations of the preliminary study in Section 4.1 included the use of non-wheelchair racing athletes or equipment, with the analysis also limited to only identifying the contact phase.

This study aimed to explore the effect of IMU placement on the qualities of the acceleration signal, with a specific focus on accurately identifying individual propulsion characteristics such as contact time. It was hypothesised that IMU sensors would detect contact at all points on the frame and wheels; with wheel placements being more reliable due to proximity to the contact point and hence vibration source.

#### 4.3.2 METHODS

##### *Athlete Selection*

To ensure that any observed differences in the signal were attributed only to placement location and not athlete or equipment characteristics, athletes were separated into two groups. The first group of athletes ( $n = 3$ , Athletes E, F and I) were senior athletes who all utilised disc wheels at the rear of the chair (Corima, Lorient-sur-Drome, France), and custom gloves using a rigid thermoplastic material. The resulting sample of elite athletes ( $8.7 \pm 5.9$  years of international experience) demonstrated comparable wheelchair set up, despite varied physical characteristics, propulsion styles, and speeds. Athletes include both male ( $n = 1$ ) and female ( $n = 2$ ), with full function of the upper extremities, and either full to



partial trunk control ( $n = 2$ , T54 classification), or no trunk control ( $n = 1$ , T53 classification). Athlete information is summarised in Table 4.2. The second group of athletes ( $n = 2$ , Athletes A and B) consisted of junior athletes having a coordination impairment, and utilised soft gloves and either disc wheels or aero spoke wheels. Athletes were classified as T34, having good functional strength with minimal limitation to the control of the upper limbs and back.<sup>22</sup> Motion capture data could only be analysed for one trial at 20 km/hr for A4, as reflected in Table 4.2.

Table 4.2: Relevant athlete demographics for the five athletes in this study. Further characteristics were presented previously in Table 3.1.

	Athlete A		Athlete B		Athlete E			Athlete F				Athlete I		
Gender	M		M		F			M				F		
Age (Years)	16		16		26			24				35		
Classification	T34		T34		T54			T54				T53		
Speed (km/hr)	19	20	21	22	22	23	24	28	29	30	37	26	27	28
# Contacts Analysed	33	0	34	34	48	59	48	51	60	79	21	52	50	55

Pilot testing revealed differences in individual acceleration signals based on equipment stiffness (i.e., spoked wheels: low stiffness, disc wheels: high stiffness). Lower stiffness equipment reduced the magnitude of the impact spikes, making these of comparable size to the underlying noise (i.e., low signal to noise ratio, SNR). Low SNR values limited accuracy and reliability throughout the analysis. The characteristic acceleration signal depicting a high and low SNR are presented in Figure 4.13.

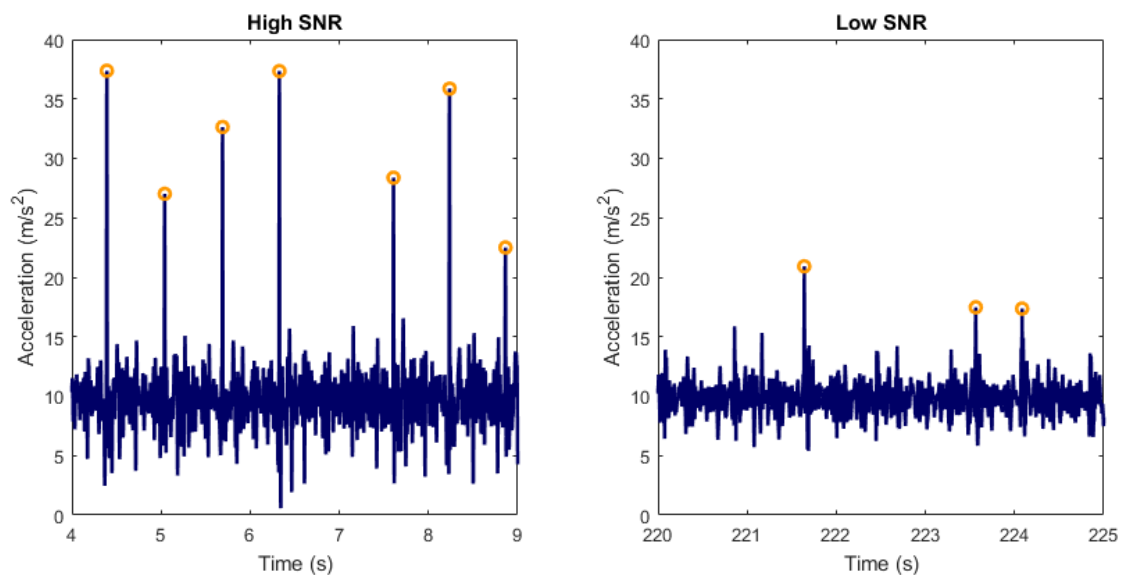


Figure 4.13: Comparison of data from High SNR (Athlete F, 28 km/hr) and Low SNR signals (Athlete C, 22 km/hr).

As such, athletes having spoked wheels were excluded from analysis. At the previous Paralympic Games (Rio, 2016), less than 4% of competitors in the finals used spoked wheels, demonstrating that this exclusion criterion does not limit the significance and applicability of the research. An even distribution of thermoplastic and leather glove use was observed amongst these finalists.

### Data Processing

For both measurement systems, contact times were located using a custom peak detection algorithm, as discussed in Section 4.2. Peaks in resultant acceleration were assumed to correspond to the impact between the hand and the pushrim (Figure 4.14). Two data points were established for each push; one each for the left and right hands. In the event the algorithm detected noise as a contact (false positive,  $F_P$ ), the event was gathered. Similarly, missed contacts (false negative,  $F_N$ ) were accounted for in post-processing. The number of these events, compared with the actual number of contacts was used as a measure of placement robustness and demonstrated the plausibility for automated detections. An individual analysis approach was employed due to the unique interaction between these constraints.

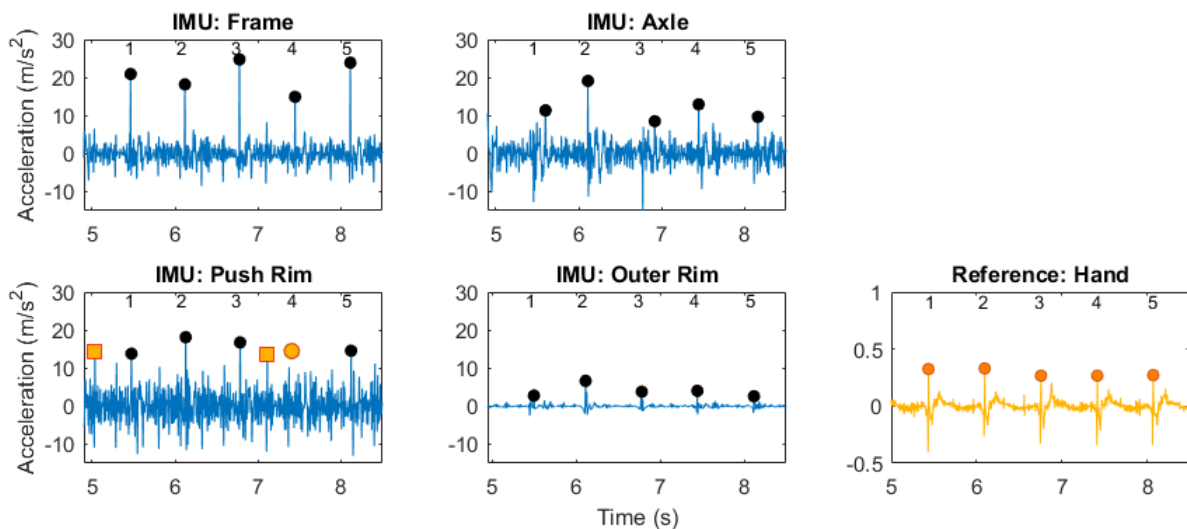


Figure 4.14: Typical resultant acceleration patterns from Athlete F (29 km/hr) for verifying the four IMU placement locations (Frame, Axle, Pushrim and Outer Rim) against the reference data (motion capture), which was used to determine the acceleration of the hand. Peak accelerations are represented by solid circles, with contacts being annotated on each plot with labels 1–5. Squares demonstrate false positive contacts, while an open circle represents a false negative contact.

---

### Statistical Analysis

The effectiveness of placement locations was objectively measured using two metrics: linear correlation with reference measurement (motion capture) and through the use of an  $F_1$  score, which is the harmonic mean of precision and recall. This metric incorporates both the recall (defined as the ability of the system to identify contacts correctly) and precision, (defined as the ability of the system not to generate false detection). These require the measurement of true positives ( $T_P$ : actual contacts), false positives ( $F_P$ : impact peak not corresponding to contact between the hand and pushrim), and false negatives ( $F_N$ : no impact peak at the time of contact between hand and pushrim). An  $F_1$  score ranges between 0 and 1, with a value of 1 indicating perfect accuracy, and was calculated as follows:

$$F_1 = 2 \cdot \frac{\text{precision} \cdot \text{recall}}{\text{precision} + \text{recall}} \quad \text{Equation 4.1}$$

Where: precision  $P = \frac{T_P}{T_P + F_P}$  Equation 4.2

recall  $R = \frac{T_P}{T_P + F_N}$  Equation 4.3

Reliability and repeatability of contact identification for both measurement approaches were obtained using inter-rater reliability assessments using ICCs. *A-priori* thresholds of ICC > 0.9 were desired, as this suggested excellent levels of reliability and repeatability.<sup>250</sup> The between-method agreement was obtained for each placement location using the method-comparison approach of Hanneman<sup>257</sup> which is based on the analysis of Bland-Altman plots. Cycle times obtained from both the IMU (at each placement location) and motion capture was subjected to a Spearman's correlation analysis to obtain a mathematical relationship to quantify the agreement between both methodologies. Spearman's correlations were used as all sample distributions were not normally distributed, as indicated by the Kolmogorov-Smirnov test for normal distribution ( $p < .001$ ). To facilitate objective comparison between placement conditions, a Likert-scale approach was adopted, whereby a Spearman's  $r > 0.9$  was considered to have nearly perfect goodness of fit,  $0.7 < r < 0.9$  was very high,  $0.5 < r < 0.7$  was high,  $0.3 < r < 0.5$  considered moderate, and  $0.1 < r < 0.3$  considered low.<sup>258</sup> Precision, bias, and percentage error between measurements were then obtained using Bland-Altman plots, using the methods described in Hanneman.<sup>257</sup> To be established as a robust solution, each placement location had to be less than the *a-priori* thresholds of absolute measures of bias and precision <0.03 s ( $\pm 4$  motion capture frames) and %Error <14.8% ( $\pm 0.05$  s,  $\pm 6$  motion capture frames), respectively. All statistical calculations were performed using IBM SPSS Statistics 24 Software for Windows.

## 4.3.3 RESULTS

Acceleration data were collected for a total of 624 contacts in each of the eight IMUs. Excellent inter-rater reliability were obtained for the identification of contact locations from both the IMU detection approach ( $R = .990, p < .001$ ) and motion capture ( $R = 0.997, p < .001$ ). A high level of agreement was found between the motion capture and IMU measurement approaches. Reported correlations for all athletes and placement locations were statistically significant ( $p < .001$ ).

IMUs located on the frame demonstrated the greatest  $F_1$  score, as would be anticipated by the reduced incidence of detection of both  $F_P$  and  $F_N$  pushes (Figure 4.15).  $F_1$  scores of  $0.99 \pm 0.03$ ,  $0.92 \pm 0.09$ ,  $0.94 \pm 0.07$  and  $0.92 \pm 0.09$  for the frame, axle, pushrim, and outer rim placements, respectively for all athletes. The frame demonstrated the most trials with no  $F_P$  or  $F_N$  ( $n = 62$  and  $n = 64$ , respectively, out of a possible 72). Other location placements demonstrated an error in at least half of the recorded trials (Axle:  $F_P = 0, n = 36$ ;  $F_N = 0, n = 31$ , Pushrim:  $F_P = 0, n = 47$ ;  $F_N = 0, n = 34$ , Outer rim:  $F_P = 0, n = 26$ ;  $F_N = 0, n = 30$ ). Higher values indicate fewer errors (either  $F_P$  or  $F_N$ ).

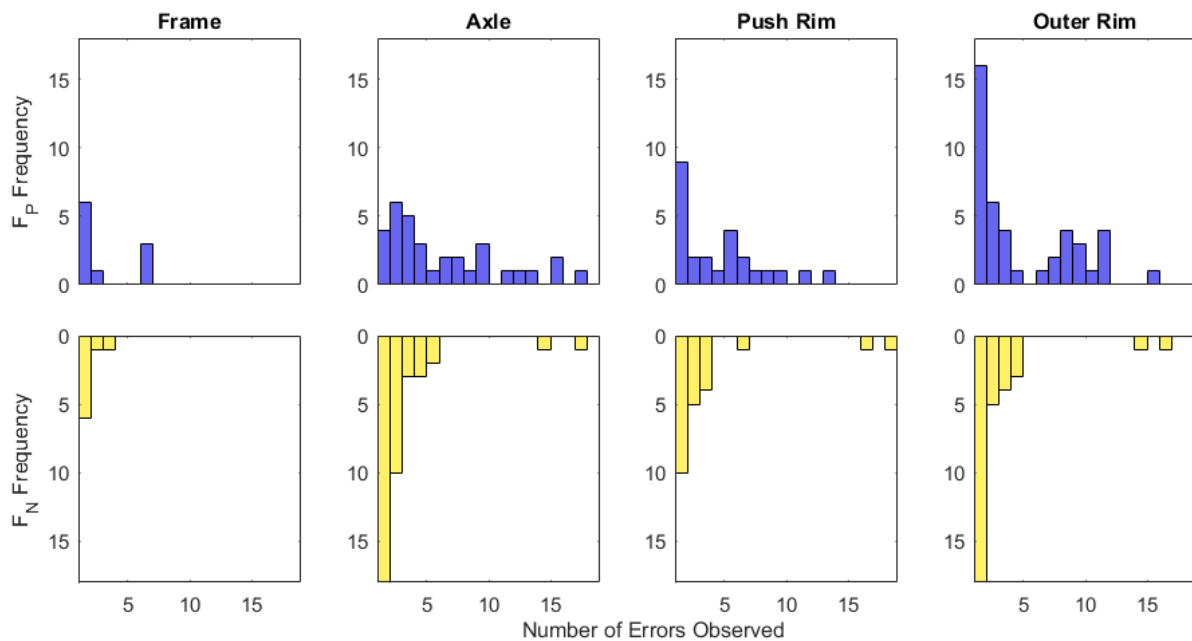


Figure 4.15: Detection rate of false positive ( $F_P$ ) and false negative ( $F_N$ ) contact recordings across the four main placement locations. Frequency is indicative of the sensitivity or specificity value for each side (L or R), and each trial ( $n = 3$ ) at each speed ( $n = 3$  or 4) for each athlete ( $n = 3$ ). A maximum value of frequency is therefore 72.

For athletes using thermoplastic gloves, high to nearly perfect between-method agreement was observed when IMUs were located on the frame (Figure 4.16, Athlete E:  $r = 0.521, p < .001$ ; Athlete I:  $r = .919, p < .001$ ; Athlete F:  $r = 0.848, p < .001$ ). The increased agreement was associated with the

increased signal to noise ratio (SNR) when units were located on the frame, at the axle, or pushrim radius ( $SNR > 6.328 \pm 2.411$ ). Lowest between-method agreement was observed at either the outer rim (Athlete E:  $r = 0.211, p = .001$ ; Athlete I:  $r = 0.833, p < .001$ ) or at the axle (Athlete F:  $r = 0.515, p < .001$ ). For IMUs located on the wheels, both Athlete E and Athlete F demonstrate a larger variability of IMU defined cycle times compared to those measured by motion capture.

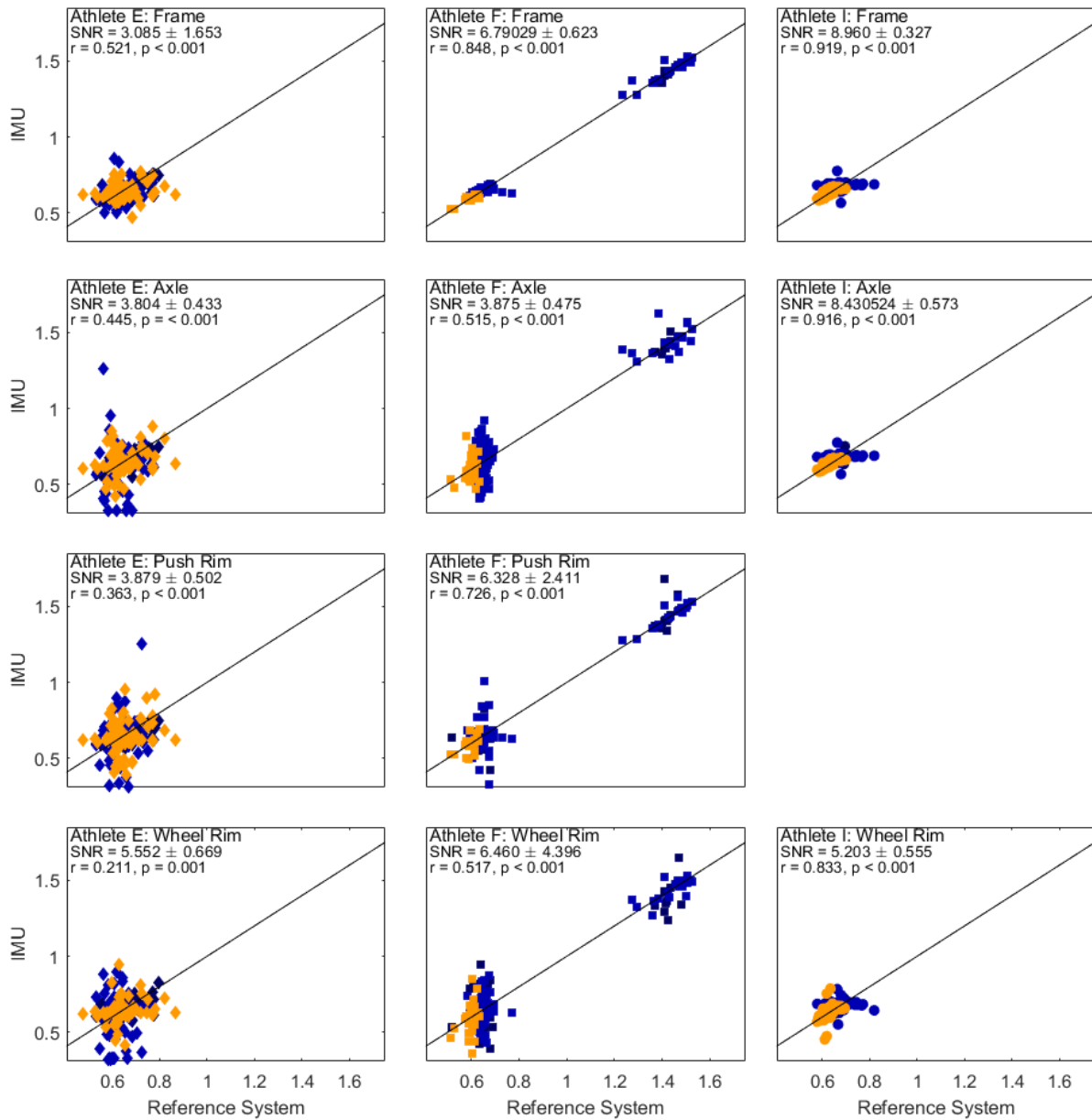


Figure 4.16: Comparison of cycle times (s) estimated by IMUs against reference system (motion capture) for 523 push cycles. Signal to noise ratio (SNR) and correlation values ( $r$ ) from all trials and conditions for each athlete are labelled on each graph. IMUs were not located on the Pushrim for Athlete I. Shading of each measurement corresponds with the speed with darker markers representing slower speeds.

Lower agreement was observed for the second (junior athletes) group (Figure 4.17), demonstrating a moderate agreement for all placement locations (Frame:  $r = 0.372$ ,  $p < .001$ , Axle:  $r = 0.300$ ,  $p = .001$ , Pushrim:  $r = 0.406$ ,  $p < .001$  and Outer Rim:  $r = 0.464$ ,  $p < .001$ ). Results were of comparable magnitude to Athlete E, who also had comparable SNR to Athlete A and Athlete B. Interestingly, SNR was more consistent across this second group than for Athletes E, I and F.

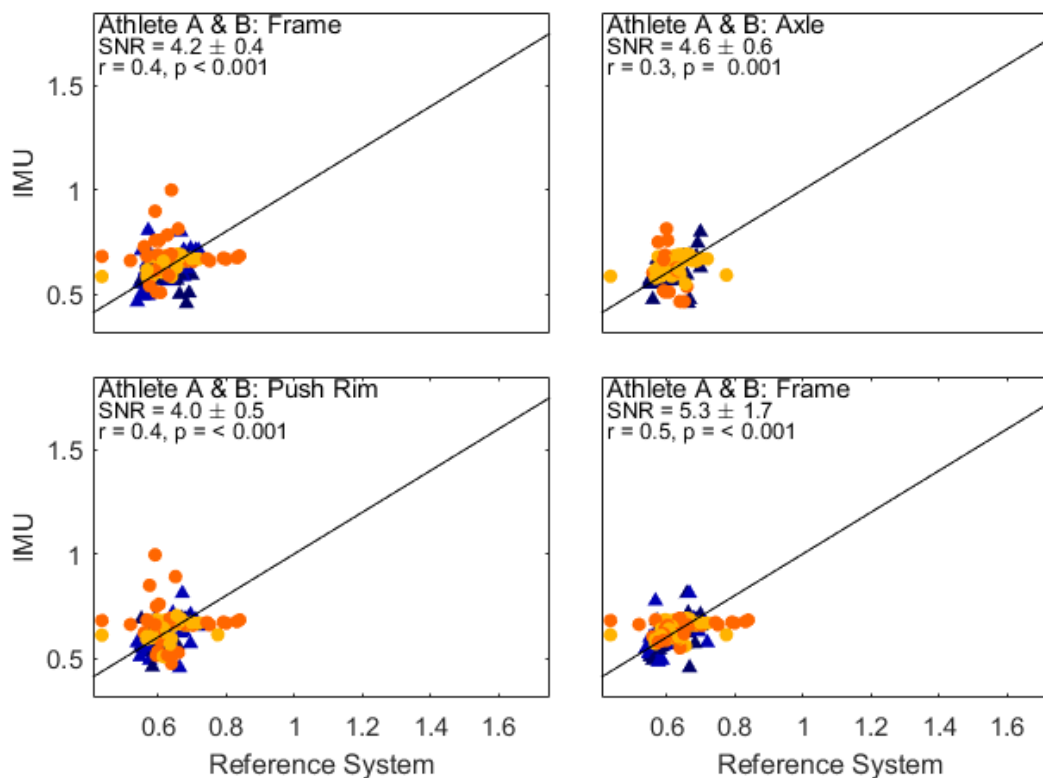


Figure 4.17: Comparison of cycle times (s) estimated by IMUs against reference system (motion capture) for 127 push cycles for athletes with a coordination impairment. Signal to noise ratio (SNR) and correlation values ( $r$ ) from all trials and conditions for each athlete are labelled on each graph. IMUs were not located on the Pushrim for Athlete A. Axle data was not recorded on one side for one speed for Athlete A, and both speeds of Athlete B.

A systematic error (bias) was observed in the IMUs used for the analysis of Athlete E, which demonstrated the IMU methodology consistently underestimated cycle time, as compared with the conventional motion capture methodology (Table 4.3). However, as these values were all less than the *a-priori* threshold of 0.03 s, it can be considered that the IMU method was equivalent to the motion capture method for all placement locations, excluding at the axle for Athlete E and Athlete B. Additionally precision values were within the *a-priori* thresholds for Athlete E (outer rim), Athlete I (frame), Athlete F (frame), however not for Athlete A and Athlete B.

Table 4.3: Summary statistics demonstrating the quality of agreement between methods (conventional versus IMU) for each IMU placement location. Quality of agreement is shown visually through shading, yellow (good) through blue (poor). High SD values of Athlete F are attributed to the different propulsion strategy, including swing throughs (cycle time  $\sim 1.3$  s), which the athlete used for efficiency. No IMUs were located on the pushrim for Athlete I.

	Frame	Axle	Pushrim	Outer Rim	Frame	Axle	Pushrim	Outer Rim
	<b>Athlete A</b>				<b>Athlete B</b>			
Mean (s)	0.6	0.6	0.6	0.6	0.6	0.6	0.6	0.6
SNR	4.1	4.2	4.0	4.5	4.3	4.9	4.1	5.9
SD (s)	0.0	0.1	0.1	0.0	0.1	0.1	0.1	0.1
Bias (s)	0	0	0	0	0	-0.3	0	-0.0
Precision (s)	0.0	0.1	0.1	0.1	0.1	0.3	0.1	0.2
% Error	38.6	49.7	49.4	42.1	54.8	105.9	39.9	48.8
	<b>Athlete E</b>				<b>Athlete F</b>			
Mean (s)	0.6	0.6	0.6	0.6	0.7	0.7	0.7	0.7
SNR	3.1	3.8	3.9	5.6	6.8	3.9	6.3	6.5
SD (s)	0.1	0.1	0.1	0.1	0.3	0.3	0.3	0.3
Bias (s)	-0.0	-0.0	-0.0	-0.0	0	0	0	0
Precision (s)	0.1	0.1	0.1	0.1	0.0	0.1	0.0	0.1
% Error	19.3	74.9	56.7	63.3	5.1	46.0	24.8	41.2
	<b>Athlete I</b>				<b>ALL</b>			
Mean (s)	0.7	0.7		0.7	0.7	0.7	0.7	0.7
SNR	9.0	8.4		5.2	5.5	5.1	4.6	5.5
SD (s)	0.0	0.0		0.0	0.1	0.1	0.1	0.1
Bias (s)	0	0		0	0	-0.1	0	-0.0
Precision (s)	0.0	0.2		0.3	0.1	0.2	0.1	0.1
% Error	10.7	11.0		16.4	25.7	57.5	42.7	42.4
	Excellent				Poor			
	[Yellow]				[Blue]			

Errors were smallest for the units located on the frame, with %Error values within *a-priori* limits of  $< 14.84\%$  ( $\pm 0.05$  s,  $\pm 6$  motion capture frames) for two athletes (Athlete I and Athlete F). As both error and precision values obtained from IMUs located on the frame in this research satisfied the *a-priori* accuracy requirements, it can be concluded that the IMU method was able to identify contact across the sample population. This conclusion, however, does not hold for IMUs located on the wheels, at the axle, pushrim or outer rim, as average precision values  $> 0.07$  s, and % error  $> 40\%$ .

### 4.3.4 DISCUSSION

This study demonstrates how the efficacy of IMUs in detecting contact between the hand and pushrim during wheelchair racing propulsion varies with placement. This aids in understanding how to maximise the effectiveness of the measurement solution to provide accurate input data into the computational model based on the detrimental propagation of errors highlighted in the Background section (Chapter Two). All placement locations investigated were capable of identifying contact events, supporting the hypothesis. In terms of estimating cycle time, the IMUs located on the frame and pushrim demonstrated the highest accuracy, while the IMUs at the outer rim showed consistently lower accuracy than the other placements. Similarly, when comparing the automated detection of contacts across all placement locations, the units located on the frame demonstrated the lowest error rate of all placements, while the outer rim placement showed the most significant error. This was in contrast to the second part of the hypothesis, which predicted wheel placements being more reliable due to proximity to the contact point and vibration source.

The errors observed by units located on the axle, pushrim, and outer rim may be attributed to rotational effects. Differences in the relative displacement between the hand location at contact and the position of the IMU may introduce small timing delays. These effects are more pronounced in more distally located units on the wheel, such as at the outer rim. Additionally, the variability observed from the data collected from IMUs placed on the axle housings may be a result of the wheelchair. Between brands, this housing can either be rounded or flush. The vibration response and hence underlying signal noise is enhanced for units which are not fastened to flush surfaces, as there is inherent movement within the unit relative to the wheel rotation. Variability in the reliability of units located at the pushrim may be associated with athlete technique. However further study is required to confirm this.

The response was observed to be lower for Athlete A and Athlete B as compared with Athletes E, I and F. As mentioned previously, classification and experience impact kinematic patterns, and the response of the IMU signal was found to be affected by athlete equipment. The compromised capabilities observed from Athlete A and Athlete B can be suggested as being a cumulative effect of all of these factors. As the IMU signal of Athlete E had lower accuracy than Athlete I and Athlete F, it can be suggested that the use of IMUs are better suited to more experienced athletes, having cleaner interactions between the hand and pushrim.

SNR was a critical factor in the success of the IMU approach (Figure 4.13). This was influenced both by athlete technique, and equipment. For example, the best results were observed for Athlete I, who was the most experienced athlete and has broken multiple world records. It is possible that a more efficient technique has a higher mean peak response of the acceleration signal at the pushrim as



---

compared to the wheel, thus enhancing the SNR. Furthermore, use of spoked wheels and soft gloves can reduce this SNR, with the soft gloves providing damping at this contact interface, and hence result in impact peaks of lesser amplitude. Therefore, regardless of the placement location, the IMU approach may be less robust. This suggests the use of this solution is a top end solution for elite athletes, as spoked wheels and soft leather gloves are more common across the junior population.

#### 4.3.5 CONCLUSION

Highest accuracy in temporal parameter identification was influenced by the SNR of the resultant acceleration trace. However, reliability should be suitably high regardless of placement as long as the SNR is sufficiently high.

### 4.4 INTRA STROKE PROFILING OF WHEELCHAIR PROPULSION USING IMUS, AND THE INFLUENCE OF EQUIPMENT

#### 4.4.1 INTRODUCTION

To be able to provide relevant performance metrics such as contact duration (time hand is in contact with the wheel) and the relative timing between the propulsion and recovery phases, it is also important to understand whether the release points can also be detected reliably. No studies have been found in the literature to investigate this.

The literature is also yet to report on whether there exists any variation in the resulting acceleration signal corresponding to athlete equipment or technique. While this was likely a consequence of the methodology used (non-impaired participant, at very low propulsion speeds), this may also have been a result of the high stiffness of the frame. As noted in Section 1.2, wheelchair rugby chairs are up to four times as heavy as a wheelchair racing chair. Therefore, it is possible that the vibration response across a wheelchair rugby chair and wheelchair racing chair may differ.

Glove selection has already been demonstrated to alter force transmission (Section 3.2). Additionally, variable reliability in IMU detection was observed across the population sample in Section 4.3. Glove selection, wheel type and propulsion characteristics may also influence the amplitude of the resulting acceleration signal, therefore impacting the ability of the IMU to identify propulsion characteristics. Athletes can opt to use carbon wheels (disc or aero four spoke) and custom, thermoplastic hard gloves (over traditional spoked wheels, and leather gloves) to increase the stiffness of contact, and thus provide a more efficient transfer with smaller transmission losses.

This study in this section builds on the findings from the preliminary investigation to understand whether IMUs are appropriate for use with wheelchair racing chairs. This study aimed to determine the capability of IMUs in automatically identifying both contact and release times (and hence push time) across different athlete and wheelchair configurations. From this, the generalisability of the use of IMUs for instrumentation can be gauged for a broader wheelchair racing population.

### 4.4.2 METHODS

#### *Athlete Selection*

Seven wheelchair racing athletes (Athletes A – F, I) from the national level junior ( $n = 4$ , < 19 years of age,  $4.0 \pm 0.58$  years of experience) and senior ( $n = 3$ , >19 years of age,  $8.3 \pm 3.3$  years of experience) program were recruited for this study.

#### *Measurement System*

Based on the findings in Section 4.3, IMUs were located on the axle housings of the wheelchair frame (FL, FR). Spatiotemporal data were validated using motion capture cameras (Section 4.2). A total of 221 push times were analysed (4 junior athletes  $\times$  13 push times  $\times$  2 speeds + 3 senior athletes  $\times$  13 push times  $\times$  3 speeds) for each hand (442 data points total).

#### *Data Processing*

Contacts were identified using the automated algorithm described previously. When fewer hand contacts were identified using this approach than detected using motion capture ( $F_N$ ), manual contact identification was performed. This was achieved using the most prominent peak around the time stamp identified from the motion capture data. The frequency of ( $F_N$ ) across the sample presentation are presented in Figure 4.15.

#### *Statistical Analysis*

Reliability and repeatability measures were obtained through ICCs. Two independent raters (both familiar with wheelchair acceleration data and video) performed manual digitisation on the same video and analysed IMU data using the custom peak detection algorithm. Both raters performed a repeated

assessment of tasks following a period of two weeks with no exposure to the data. Appropriate reliability and repeatability required ICC > 0.9.<sup>250</sup>

It was defined for this study that an adjusted coefficient of determination ( $R^2$ ) value > 0.97 ( $\pm 1$  video frame (0.01 s)) demonstrated excellent goodness of fit,  $R^2 > 0.91$  ( $\pm 2$  video frames (0.02 s)) was very good,  $R^2 > 0.80$  ( $\pm 3$  video frames (0.03 s)) was good, with  $R^2 < 0.80$  considered average. Results of the above regression were then ranked and compared across athlete demographics using a Mann Whitney U test. Pearson Correlations were used to establish the relationship present between speed and reliability. Effect sizes were established based on the methods reported by Field.<sup>259</sup> All statistical calculations were performed using IBM SPSS Statistics 24 Software for Windows.

#### 4.4.3 RESULTS

Excellent inter- and intra-rater reliability (ICC > 0.95) were obtained for the manual digitisation of high-speed video. For all reliability assessments, mean absolute error in the time for push length was < 0.01 s, with standard deviation being < 0.06 s and < 0.01 s for IMU, and video defined contacts, respectively. To relate this to a push cycle duration, the four push cycles presented in Figure 4.18 have length  $0.65 \pm 0.00$  s, which are example data from Athlete F at 28 km/hr.

IMUs were effectively capable of automatically identifying contact, however, the algorithm located release less reliably, without also detecting noise (Figure 4.18). At this stage, automatic detection of release points is not plausible without the assistance of motion capture data.

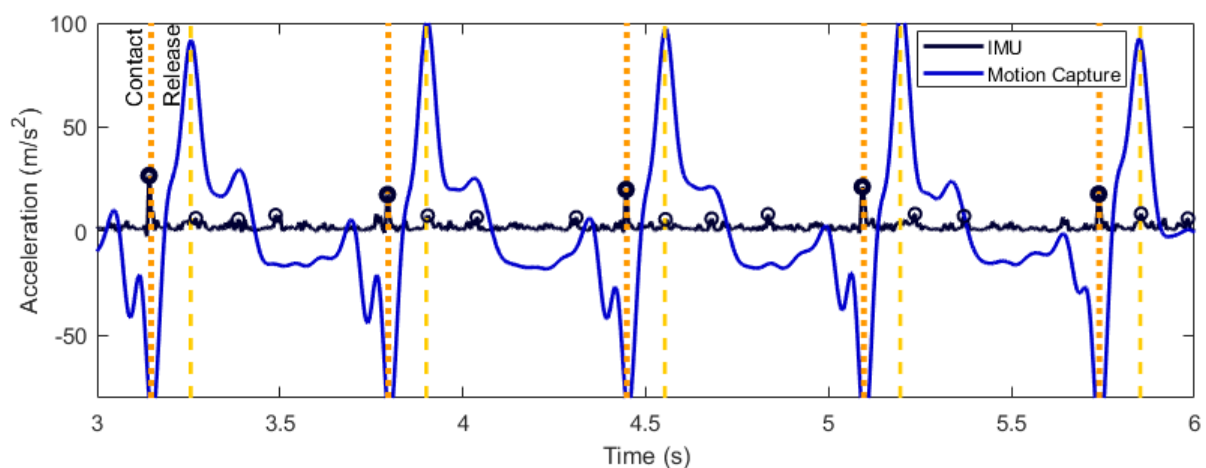


Figure 4.18: Representative example of acceleration trace demonstrating the detection of contact points with an IMU compared to motion capture, however, issues with the identification of release.

Athlete-specific characteristics were observed to influence the robustness of the IMU method, and hence the level of agreement with the video obtained contact timings (Figure 4.19). Results from the Mann U Whitney test revealed that, glove type ( $U = 6$ ;  $W = 34$ ;  $p = .02$ ), and wheel type ( $U = 12$ ;  $W = 22$ ;  $p = .26$ ) were not observed to impede the effectiveness of IMUs in determining contact (Figure 4.19). Statistical affects were identified between the reliability of IMU and video derived push lengths, with speed ( $r = 0.72$ ;  $p < .01$ ), gender  $U = 0$ ;  $W = 55$ ;  $p = .05$ ), athlete classification ( $U = 4$ ;  $W = 14$ ;  $p = .02$ ) and age ( $U = 0$ ;  $W = 36$ ;  $p < .01$ ), or a compounding affect between these. Effect sizes ranged between small (Wheel  $r = .05$ ; Gender  $r = .05$ ), medium (Glove  $r = .11$ ; Age  $r = .15$ ; Classification  $r = .11$ ) and large (Speed  $r = .72$ ).

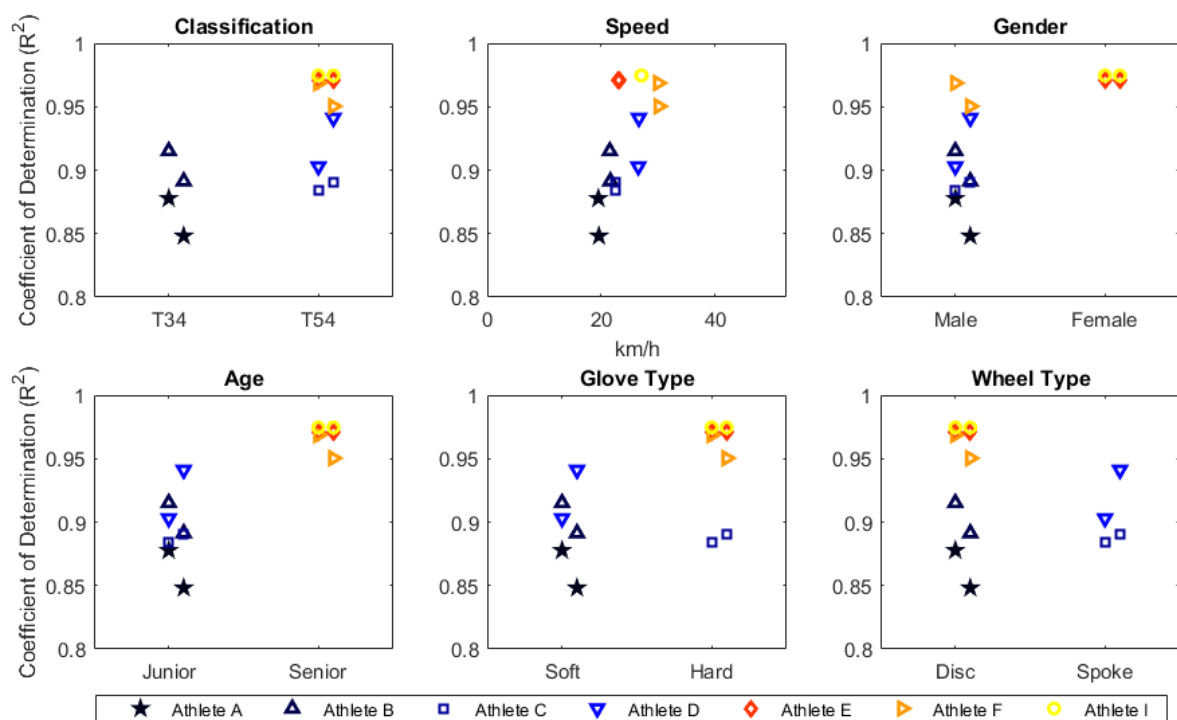


Figure 4.19: Capability assessment of the accuracy of the IMU-based contact detection methodology across varying athlete characteristics. The coefficient of determination ( $R^2$ ) data is presented from the FL (open markers) and FR (solid markers) for each athlete.

#### 4.4.4 DISCUSSION

This study investigated whether IMUs are capable of intra-stroke profiling for wheelchair racing propulsion, and the influence of athlete and wheelchair demographics on this capability. IMUs provided a reliable and repeatable method of identifying the contact, but not the release point. The release was able to be detected, however as acceleration signals at this moment were comparable to the magnitude of signal noise, it precluded entirely automated processing. The accuracy of the IMU

method was influenced both by athlete technique. This suggests that it is plausible to use the IMU approach across the greater wheelchair racing population, however, to also be mindful that the individual response may change between athletes, and so to employ athlete-specific analysis protocols to ensure these variations do not influence reliability.

Contact is a far more ballistic motion than the release of the hand on the pushrim, which can explain the reduced accuracy of its detection. One athlete demonstrated consistent identification of release points. Qualitative assessment of performance suggests this may be likened to a flicking motion of the wrist upon release. Without kinetic validation, it can be hypothesised that this motion does not maximise athlete efficiency. While IMUs may have a limited capacity to quantify the release time; they can still assist in kinematic profiling, by recognising inefficient release techniques.

Additional data processing techniques were explored with the intention of better emphasising the release point. Taking the log of the data did not increase the visibility of the point, however squaring the acceleration data offered a marginal improvement (Figure 4.20). Further research could explore the use of wavelet analyses, which are well suited to detecting small temporally related events and machine learning algorithms based on athlete-specific temporal data.

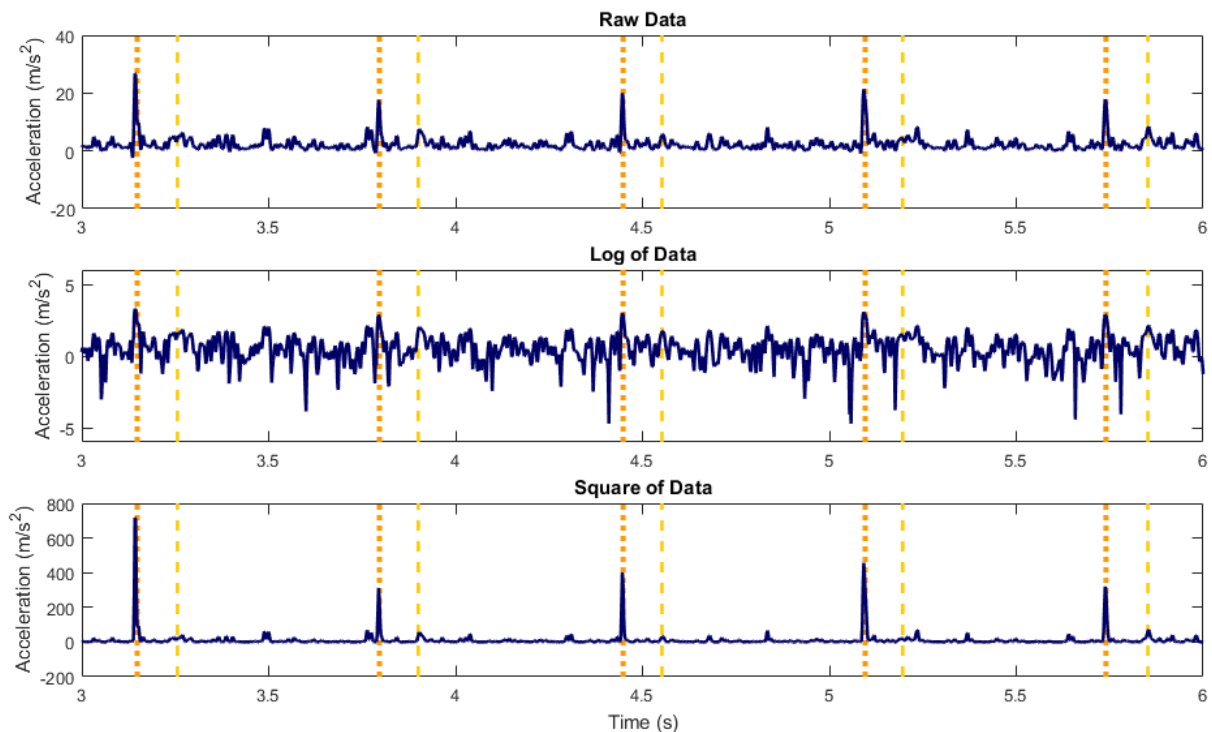


Figure 4.20: Comparison of different processing methods which can be used to improve the detection of release points.

Results suggest that differences in reliability of the IMU are not associated so much with athlete equipment (wheel type or glove type) but are related to individual propulsion techniques. However, notable differences were observed between the characteristic traces of acceleration data between athletes with different equipment type, specifically regarding the magnitude of underlying noise. It was typical that the signals from soft gloves or spoked wheels to have a higher number of false negative detections. Thus, although contacts were able to be retrospectively deduced from the traces with relative accuracy, the ability for automated processing across equipment types may be limited.

Findings from this study suggest that IMUs demonstrate greater agreement with the current gold standard method when used with more experienced, senior athletes, and at higher propulsion speeds. Females demonstrate different propulsion kinematics,<sup>239</sup> which may provide the rationale as to why reliability and gender are correlated, however, this cannot be confirmed from the results of this study. Athlete classification, which influences the kinematic technique, was not demonstrated to influence the reliability of the IMUs in determining contact. However, both the athlete classifications included had full function of their upper extremities. It is expected that level of activity limitation (and therefore classification) would be an influencing factor when concerning athletes with different types of impairment, specifically when reduced muscular function and greater physical asymmetry is present in the upper extremities.

##### 4.4.5 CONCLUSION

Identification of propulsion events from IMU data was found to be reliable for contact and push length, but not for release. The reliability of IMU obtained data was impacted by athlete propulsion technique. The robustness of detecting contact was not influenced by classification, wheel type, or glove type. However, improved reliability may be associated with athlete speed, gender and variability in technique. This suggests that for the population sample of this research, IMUs present a viable solution for the instrumentation of racing wheelchairs. While it is considered that the success of the methodology can be generalised across elite wheelchair racing athletes, further research is required for the extrapolation into other wheelchair sports, manual or daily wheelchair propulsion.

---

## 4.5 THE VALIDATION OF IMUs ON ESTIMATING TORQUE PRODUCTION OF WHEELCHAIR RACING ATHLETES

### 4.5.1 INTRODUCTION

Prior to the use of instrumented wheels, researchers have used a force plate to measure the external propulsion loads.<sup>260</sup> A limitation of this approach, however, is that only a single push can be recorded per force plate and that testing had to be performed under laboratory conditions, meaning speeds were not reflective of competition speed. Additionally, commercially available instrumented wheels are not practically viable for use within wheelchair racing, highlighting the need to explore new methods (Section 2.4).

Wearable technologies (such as IMUs) are an emerging trend in sporting biomechanics due to their unobtrusive measurement. Benefits of IMUs are their low mass (12 gm mass per unit),<sup>219</sup> wireless operation, ease of fastening, and ease of data recording. Although IMUs have been used extensively in the literature for kinematic monitoring, there is no current literature available commenting on the feasibility of the use of IMUs in the kinetic monitoring of wheelchair biomechanics. Kinetic estimation would be the result of the conversion of the acceleration signal into torque estimates.

This study aimed to examine the plausibility of IMUs specifically that of the accelerometer, in estimating reaction forces using Newtonian mechanics. This data can be used to drive computational models with performance-based data, to maximise the relevance and impact of obtained results. It was hypothesised that there will be good agreement between the IMU and force plate data per session, facilitating a practically viable tool for in field athlete monitoring. It was assumed however that a systematic bias would exist between IMU and force plate measurements due to the damping of the tires due to the rubber surface (Mondo track surface) overlaying the force plates.

### 4.5.2 METHODS

#### *Athlete Selection*

Seven athletes (Athletes A – E, Athlete I; gender: males ( $n = 5$ ), females ( $n = 2$ ), age:  $24 \pm 7$  years, body mass:  $62.87 \pm 10.94$  kg, experience: senior ( $n = 3$ ), junior ( $n = 4$ ), classification: T34 ( $n = 2$ ), T53 ( $n = 1$ ), T54 ( $n = 4$ )) participated in this study.

##### *Measurement System*

Three-dimensional acceleration data were captured using three IMUs, which were rigidly fastened to the wheelchair frame at the left and right axle housings (FL and FR, respectively). Force plate and IMU data were synchronised through the use of a thresholding algorithm compared to resting force and acceleration, respectively. Acceleration data were converted to equivalent forces using the relationship:

$$F = ma \quad \text{Equation 4.4}$$

Where  $F$  is the applied propulsion force,

$m$  is the mass of the system (athlete and wheelchair), and

$a$  is the measured acceleration.

It is acknowledged that force can also be estimated considering the apparent mass of the system. At most, the apparent mass of the system was 2.09% and thus a minor contribution to the total estimate of the system, and so was not introduced into the processing methodology.

For the steady-state trials, mean rolling resistance was calculated as being  $7.01 \pm 1.10$  N, with the contribution of these forces per hand being up to 1.02 % of the maximum applied forces. These values were subtracted from the propulsion force estimates. It was assumed that there was a symmetrical distribution of weight across the seat and that even contributions of rolling resistance acted for each hand. Aerodynamic resistance was negligible (calculated as being 0.09 N) based on equations presented by Fuss,<sup>11</sup> and using parameters defined by Barbosa et al.,<sup>9</sup> and were hence not included in this analysis.

##### *Experimental Propulsion Task*

As with the study presented in Section 4.3, while the intention is for in-field data measurement, research was performed under controlled, laboratory conditions to ensure maximum data reliability. Applied forces were analysed under two conditions: acceleration from stationary, and compared to a gold standard force plate measurement; and steady state, and compared to literature reference data. It is acknowledged that for wheelchair racing, an instrumented wheel (SMARTWheel) is the gold standard comparison tool, however, due to their cost, were not able for this research. The force plate was selected as the gold standard measurement tool based on its frequency of use in the collection of ground reaction force data for gait.



For the acceleration condition, athletes propelled their own wheelchairs over a series of force plates (Figure 4.21) sampling at 1000 Hz (Kistler, Kistler Instruments Ltd., Alton, Hampshire) embedded in the floor (Mondo track surface) of a 46 m biomechanics laboratory. Athletes performed four stationary starts (Start) from the force plate and pushed for at least 10 m at a maximal velocity to ensure the starting procedure was well performed. Lane markings and a defined start line were over-laid on the Mondo track surface, and start procedures reflective of race conditions were used to represent race conditions.

For the start trial, each wheel (front, and two rear) was located on a separate force plate (Figure 4.21). As there is a gap between the front and rear force plates, a full cycle data was not always captured. Mass was calculated for the athlete-wheelchair system (with instrumentation attached) using static measurements on the force plates. The mean value over fifty data points (representing 0.05 s) was used as the mass value. Wheel camber was accounted for in data processing for the mediolateral data. A shear force was present in the mediolateral direction, which was equal and opposite for each wheel. As effects of camber were not present in the IMU data, this shear force was removed.

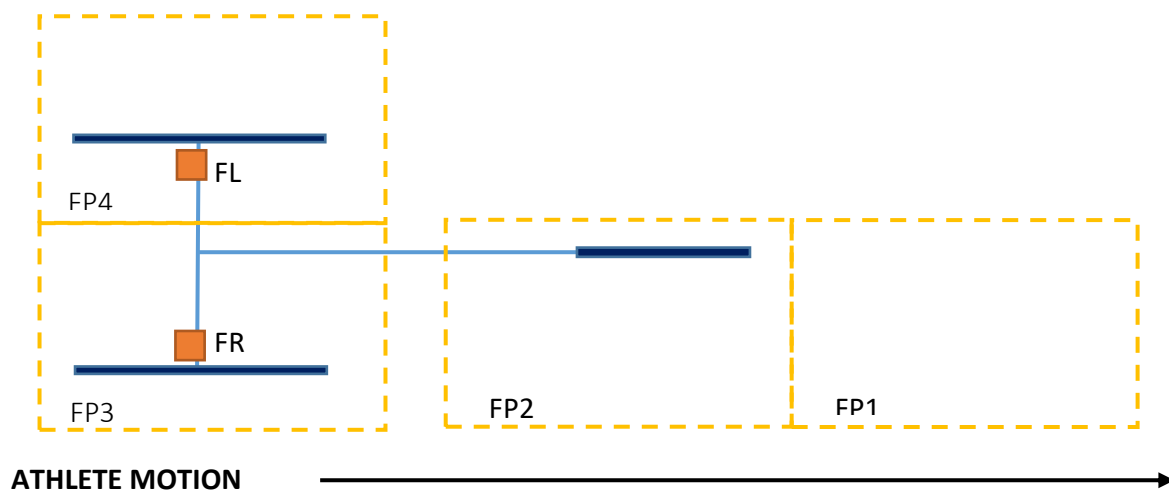


Figure 4.21: Instrumentation configuration, demonstrating the placement locations of each of the three IMUs, and the chair on top of the force plates, demonstrating the wheels each starting on a different force plate.

Steady-state trials were performed on a non-instrumented treadmill (as described in Section 4.2), at a range of speeds ranging from warm up through to competition pace; IMU data was collected throughout. Total test duration and speed were customised for each athlete in accordance with race speeds and age (i.e. junior athletes test protocols were scaled down appropriately). Data were collected

for one-minute trials once athletes reached steady state propulsion (as controlled by the treadmill). Data were analysed for 10 s trials within this data capture period. Measurements were verified against results of a comprehensive, but non-exhaustive literature review on resultant force application in wheelchair propulsion.<sup>41, 55, 56, 62, 188, 220, 261-265</sup> It is acknowledged that these sources all depict manual wheelchair propulsion and that there are distinct differences between racing and manual propulsion.

#### *Data Processing*

Triaxial components of acceleration were re-oriented to the global coordinate system. The power spectral density of resultant acceleration signals from all athletes for both the acceleration and steady-state conditions demonstrates a decline between 9 Hz and 10 Hz (Figure 4.22). As filtering data reduced the magnitude of impact (see Figure 4.23), following filtering, data were scaled by mean peak magnitude, ensuring this mean peak value was consistent with the raw data, and filtered data. Consequently, a Butterworth low-pass filter, with a 9 Hz, -6 dB cut off frequency was selected.

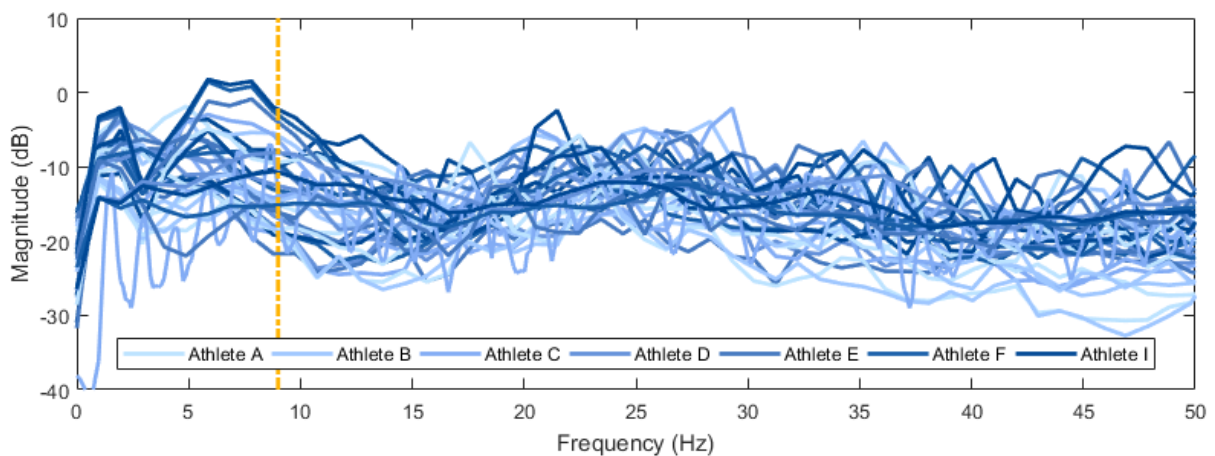


Figure 4.22: Power spectral density of resultant acceleration signals from all athletes for both the acceleration and steady-state conditions for determining appropriate cut-off frequencies for the filtering of IMU data. The dashed line shows the selected low pass filter.

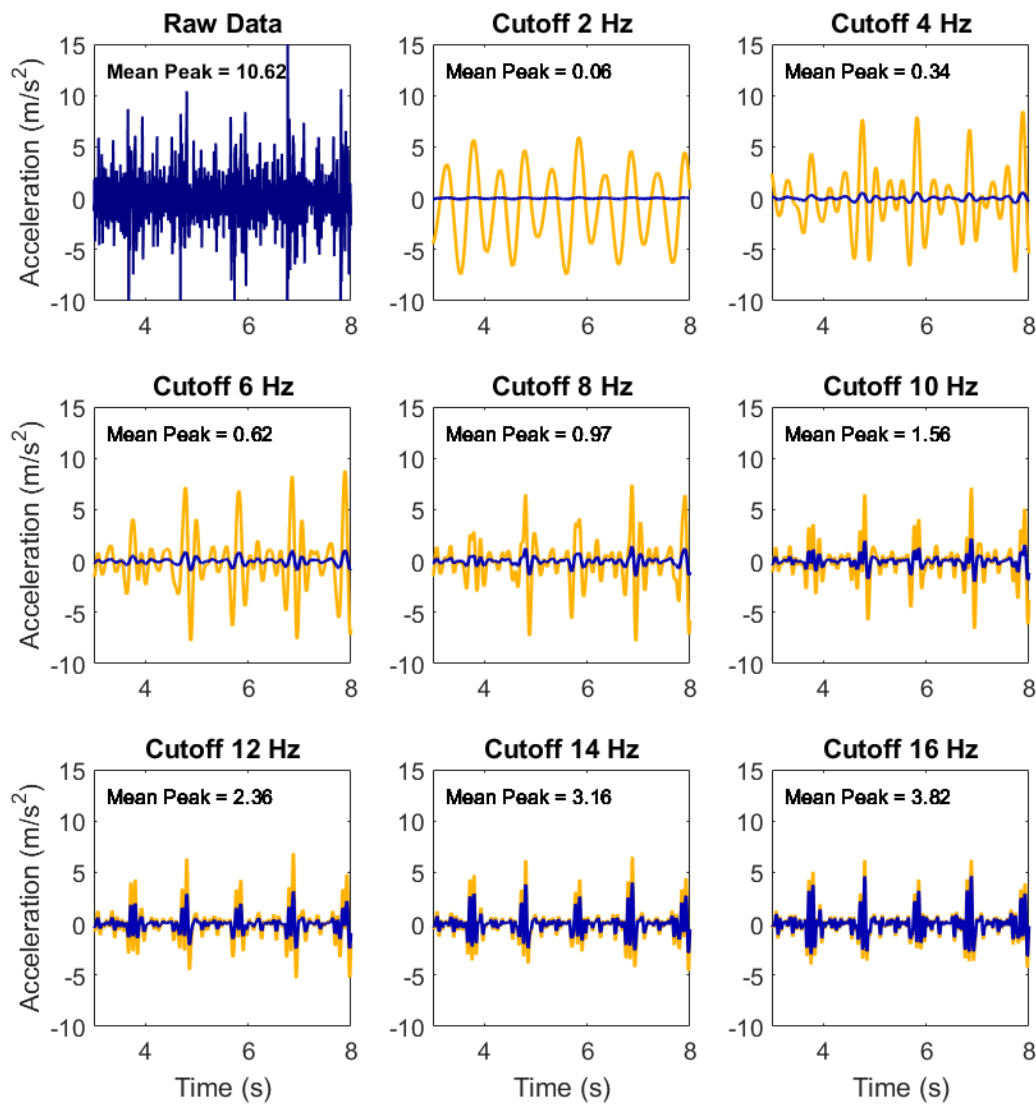


Figure 4.23: Selection of most appropriate cut-off frequency. The blue line represents filtered data (at the specified cut off frequency). The yellow line represents a proportional increase to maintain consistent mean peak data as the raw data. Higher cut off frequencies demonstrates a closer fit between data sets.

### Statistical Analysis

Kinetic measures from IMU and force plate data which were extracted for statistical analysis included rate of force development ( $RFD_{ML}$ ,  $RFD_V$ ,  $RFD_{AP}$ ), the magnitude of peak forces ( $PF_{ML}$ ,  $PF_V$ , and  $PF_{AP}$ ), mean force ( $MF_{ML}$ ,  $MF_V$ ,  $MF_{AP}$ ), signal RMS ( $RMS_{ML}$ ,  $RMS_V$ ,  $RMS_{AP}$ ), and impulse ( $I_{ML}$ ,  $I_V$ ,  $I_{AP}$ ). Push time ( $T_{ML}$ ,  $T_V$ ,  $T_{AP}$ ) was also calculated for both IMU and force plate measurements.

Statistical differences in force parameters between force plate and IMU methods were compared using Bland Altman analysis, as performed by Hanneman.<sup>257</sup> Significance was accepted at the ( $p \leq .05$ ) level. Bias and precision estimates of  $\pm 10$  N and  $\pm 5$  N, respectively, were established *a-priori* as the

maximum parameters indicating acceptable agreement between methods and precision of difference. All statistical analyses were completed using IBM SPSS Statistics 24 Software for Windows.

### 4.5.3 RESULTS

Visually, there was an apparent variation in the agreement between IMU and force plate data. Figure 4.24 demonstrates data with strong between method agreement (Athlete A; Left), and an example where the IMU data substantially underestimated the forward's acceleration data (Athlete C; Right). The between-method agreement was variable between athletes, with Athletes A, B, F and I consistently demonstrating greater performance as compared with Athlete C and D. Directionally, best between-method agreement was demonstrated in the anterior-posterior direction.

Statistical analysis reveals that apart from RFD, the IMU was most accurate in the AP (forwards) direction (Table 4.4). Impulse, peak and RMS values were all under the a-priori threshold of 10%, with mean values very close to this threshold (10.3%). It can be seen that this is accompanied by low bias (systematic error), but considerable precision (measurement error) in the AP direction measurements. Such a large precision value can be attributed to the aforementioned equipment limitations, such as Athlete C, who used spoked wheels.

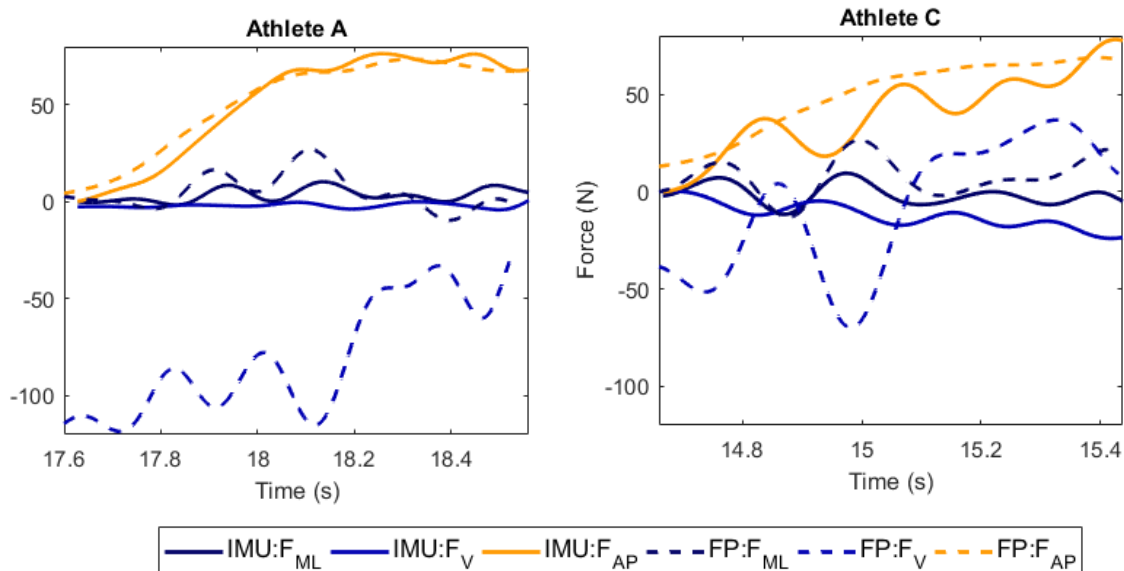


Figure 4.24: Example of two athlete data in three dimensions (IMU data: solid lines; force plate data: dotted line) for a good (right) and poor (left) comparison of data in the AP direction. Body mass has been removed in the vertical ( $F_v$ ) direction. N.B. starting time on the x-axis included calibration of the force plates and the audible three-command cue for start of motion.

Bland-Altman analysis revealed a negative bias (force plate > IMU) for RMS (RMS<sub>V</sub>), Peak (PF<sub>ML</sub>), Mean (MF<sub>ML</sub>, MF<sub>V</sub>), Impulse (I<sub>ML</sub>, I<sub>V</sub>) and RFD measurements (RFD<sub>ML</sub>, RFD<sub>AP</sub>, Figure 4.25). The magnitude of this bias was also demonstrated in Table 4.4. However, there was a positive bias for the majority of the AP measurements peak, mean, RMS, as well as in the vertical direction for RFD and RMS.

Table 4.4: Precision and bias between IMU estimates and force plate data. RFD data were not presented as % mean due to the small denominator.

	Precision			Bias		
	ML	V	AP	ML	V	AP
RMS (N)	24.3	43.6	13.9	11.3	-52.4	-3.7
Peak (N)	39.5	259.6	20.6	-7.5	18.0	0.7
Mean (N)	23.5	51.2	14.1	-8.7	38.6	-3.4
Impulse (N/s)	30.3	37.5	24.5	9.0	21.7	2.6
RFD (N/s)	0.3	0.5	0.4	0.3	-0.6	0.4
Length (s)	<0.01	<0.01	<0.01	<0.01	<0.01	<0.01
	Precision (% Mean)			Bias (% Mean)		
	ML	V	AP	ML	V	AP
RMS (%Mean)	237.0	69.9	35.0	28.3	83.9	9.2
Peak (%Mean)	387.8	376.9	38.0	74.0	26.1	1.3
Mean (%Mean)	245.5	94.5	42.7	90.8	71.2	10.3
Impulse (%Mean)	176.7	348.9	78.1	52.5	206.9	8.3

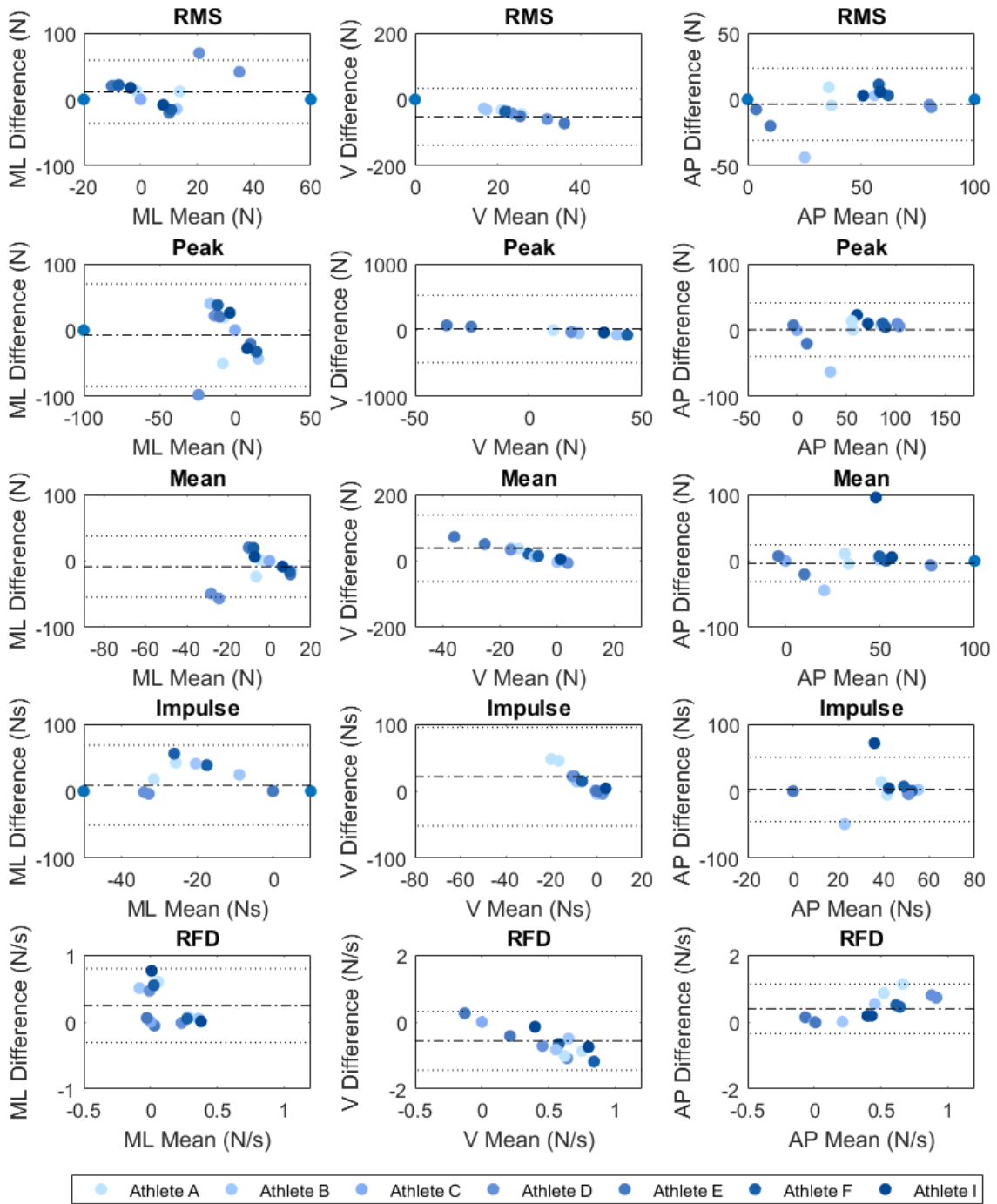


Figure 4.25: Bland Altman Plots of Agreement for a Start trial for each of the kinetic parameters for each athlete in each primary direction.

Mean peak resultant force data, as measured by the IMU, for each athlete was plotted against speed, for both the athlete-measured values and literature-defined values (Figure 4.26). A line of best fit ( $R^2 = 0.92$ ) was placed between the literature-defined values. Each experimental data point is representative of the mean of at least 10 s of consecutive propulsion.

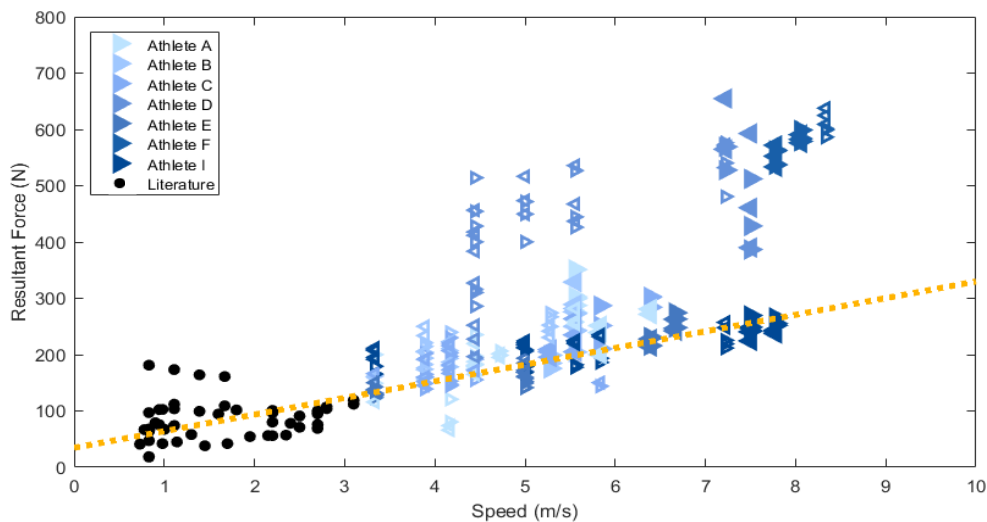


Figure 4.26: Comparison of steady-state data as recorded by IMUs to literature. Data from the literature is below 3 m/s are representative of manual wheelchair propulsion, while athlete data is above.

#### 4.5.4 DISCUSSION

This study aimed to examine whether an accelerometer (IMU) served as an appropriate method for the estimation of the applied forces to the athlete-wheelchair system (including trunk motion) applied by the athlete. Data showed that for specific athletes, the IMUs were very competent in measuring the forwards applied forces. However, the effectiveness of this solution varied and was inappropriate for two of the seven athletes analysed in this research. Consequently, the use of IMUs may not always be appropriate for the use within a computational model based on the propagation of errors. However, there does still exist merit for the use of these from a performance perspective.

This phenomenon can perhaps be explained due to the differences in athlete equipment. For the conditions when the IMU performed worst (Athlete C and D), athletes were using spoked wheels. The energy response between wheel types is anticipated to differ, with higher energy loss expected for the spoked case. The loss in energy across the spoked wheels may contribute to the underestimation of force estimations from the IMU as compared to the force plates. As Athlete C was using spoked wheels like Athletes A, E and F, who demonstrated the best between method agreement, it can be considered that equipment is not the sole contributor to the performance of IMUs. However, from the results of Athletes C and D, it can be recommended that this analysis is not performed using spoked wheels, which may mean this solution is better suited to elite populations. Less than 2% of the athletes in the previous Paralympics (Rio 2016) used spoked wheels, demonstrating that this limitation does not restrict the significance of this research. The loss of energy across spoked wheels was not quantified in this research, however, should be investigated in the future. The amount of energy lost through vibration may be demonstrated through high-speed video analysis.

Although the study did not show perfect between-method agreement, particularly for athletes with spoked wheels, it did substantiate the merit in the further refinement of data processing to fill the void of practically viable instrumentation solutions available for wheelchair racing. For example, this tool allows the correlation of force application to performance, and can also look at how much forwards directed force is applied, and whether modifications to technique improve or reduce this component. It is acknowledged that there are discrepancies to the gold standard measurement, and so the use in computational modelling should be limited to prevent the compounding of these errors throughout the successive processing. However, there is still merit in the solution from a practical perspective. Differences between IMU and force plate data suggest it is not apt to compare multiple athlete's data. However the use of an IMU can still provide a good relative measure of an athlete over time.

For the out-of-plane directions ( $F_{ML}$  and  $F_V$ ), no parameter was under the defined thresholds. Once again, some of this can be attributed to athlete equipment (spoked wheels), damping on the floor ( $F_V$  measurements), and cambered wheels ( $F_{ML}$  measurements). Additionally, some of the disagreement in  $F_V$  measures may be due to trunk motion, and changes to CoM, which were able to be recorded by the force plate, however not by the IMU. Precision and bias measures (in all three directions) for length were all  $< 0.01$ , validating the appropriate calculation of Impulse.

Literature has demonstrated that for manual wheelchair propulsion, absolute peak force magnitudes in the anteroposterior direction are far greater than the out-of-plane forces. In-plane forces (in the direction of travel) are approximately 3.0 times greater than the forces in the vertical direction, and 3.2 times greater than in the mediolateral direction across a population with varying spinal cord lesion levels.<sup>266</sup> Additionally, Goosey-Tolfrey et al.<sup>195</sup> have stated that the tangential (or propulsive) component as the most significant. Hence, the anteroposterior direction is the most relevant for the evaluation of wheelchair performance, as it best provides the propulsive component. Ensuring the interpretation of data (and its precision) is treated carefully, this approach presented provides a vast potential for the large scale performance assessment of wheelchair racing during competition.

The capacity for estimating propulsion forces from IMUs has been demonstrated, however further refinement of the data processing methodology is required to increase the reliability of the data such that it can be incorporated in computational modelling. For example, rolling resistance was neglected in this research, however, may have an impact on road surfaces. Additionally, considering the acceleration during a starting motion, and the inertia of the non-spoke wheels, future data analysis could consider the apparent mass rather than simply the mass. This could be performed using the relation described in Equation 4.5.



---


$$F = \left(m + \frac{I_R}{R_R^2} + \frac{I_F}{R_F^2}\right)a \quad \text{Equation 4.5}$$

Where  $F$  = the forward external force,

$m$  = system mass (athlete + wheelchair),

$I_R, I_F$  = mass moment of inertia of the rear and front wheels along their rotation axes,

$R_R, R_F$  = rear and front wheel radii, respectively, and

$a$  = measured accelerations

At faster propulsion, peak force followed the line of best fit for the literature values. The observed trend is consistent with the literature of walking and running whereby vertical reaction forces increased linearly with gait speed up to 60% of maximum speed.<sup>267</sup> This suggests the appropriate extension of the IMU at speeds more reflective of performance. Two athletes demonstrated consistently greater force than the rest. This may be explained due to technique (including experience and skill level), with results possibly suggesting an inefficient technique for Athletes F and D, both of whom are male.

It is possible that damping occurred in the force plate measurements, as the force plates were embedded beneath a Mondo track surface, which is made from a synthetic rubber material. An attenuation in peak forces has been demonstrated for impacts occurring on lower stiffness floors.<sup>268</sup> For example, firm foam (density 32 kg/m<sup>3</sup>) can attenuate peak forces by up to 76.6%. A material with comparable density to the Mondo track surface (SmartCell (SATech, Chehalis, WA, USA) 1120 kg/m<sup>3</sup>, Mondosport 911.1 kg/m<sup>3</sup>)<sup>269</sup> can attenuate peak forces by between 17.3% to 33.7%.<sup>268</sup> As damping is only demonstrated in the force plate measurements; this can explain the observed offset for the IMU obtained data as compared with force plate measurements. Based on the maximum values of AP data presented in Figure 4.24 (~60 N) and the corresponding mean bias value (AP) presented in Table 4.4 (8.97 N), the bias is approximately 15% of the maximum value. This is in line with the level of damping which would be expected from the Mondo track surface.

Acceleration and steady-state data were analysed separately on account of the kinematic variations between motions. For a start, athletes demonstrate greater cycle time with a shorter contact duration, as compared to steady-state propulsion. The motion is very much a pushing motion. However, for steady-state propulsion, athletes employ more of a striking motion, meaning substantially greater impact peaks are present for steady-state data as compared with starting data, unless removed through filtering, (Figure 4.27). The large impact peak upon contact may not be observed in starting motions

based on athletes applying pre-tension to the wheels. For the data analysed, impact peaks (for Athlete A) were in the magnitude of  $1.21 \pm 0.2$  g for steady-state propulsion, with peaks from the starting motions being just 8.6% of this value ( $0.1 \pm 0.1$  g). The operating range of the IMUs in this research was  $\pm 16$  g, meaning the observed propulsion, specifically that at the start were very small with regards to the operating range of the sensor. It can hence be assumed that there was a reduced capacity for the IMU during the starting motion. It is anticipated, that use of accelerometers with a variable operating range, more representative of wheelchair propulsion would result in higher accuracy.

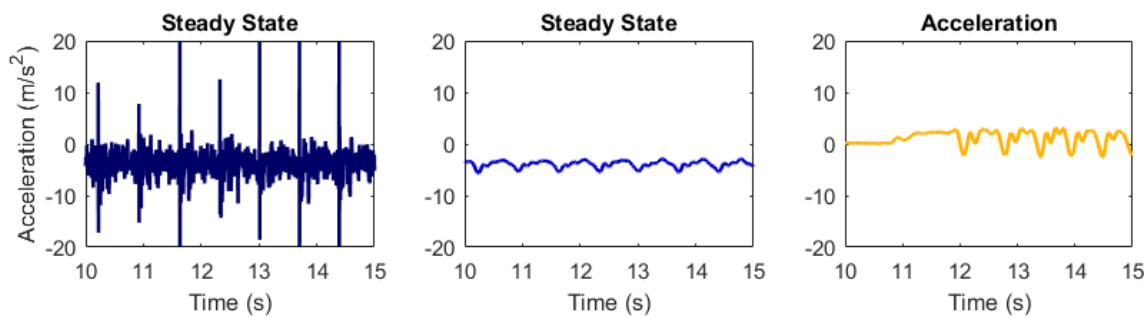


Figure 4.27: Comparison of raw and filtered steady state and acceleration data demonstrating a clear difference in magnitude of acceleration data with movement speed, and how the impact peaks used in Sections 4.1 through 4.4 relate to the force profile.

Previous literature has demonstrated that a three-axis piezoelectric accelerometer has a transverse sensitivity below 3%.<sup>270</sup> This means very low cross-talk between the components of acceleration exists within each IMU, and that data obtained can be considered as being reliable. I Measure U branded IMU sensors, as used in this research, utilise a PCB accelerometer,<sup>271</sup> which contains piezoelectric crystals,<sup>272</sup> while the force plate also contains piezoelectric force sensors.<sup>273</sup> Therefore, both sensors used are operating on the same working principle.

#### 4.5.5 CONCLUSION

This study investigated the plausibility of the use of IMUs for the estimation of applied forces for wheelchair racing propulsion. Although perfect agreement was not attained between IMU and force plate measurements for mean force, max force and rate of force development over a starting motion, sufficient accuracy was obtained, particularly in the forward's direction, with results showing more reliability at steady state speeds. Caution must be used in data interpretation. Data from IMUs can facilitate in-field kinetic assessment of performance, however, should not be used within computational modelling environments based on the propagation of out-of-plane errors.

---

## 4.6 DISCUSSION

This chapter investigated the credibility of IMUs in detecting wheelchair propulsion kinetics. The IMUs may provide an advancement to current technologies, through providing a more objective measure of performance, as it is not subject to perspective or parallax errors. The practical use of IMUs can provide near real-time feedback to coaches and athletes as part of targeted training or competition. Although the use of IMUs is intended for practical settings; a controlled laboratory-based environment was utilised to assess the accuracy of IMUs to determine hand contact times in wheelchair athletes. Motion capture served as a gold standard measure for kinematic assessment, while force platforms were the gold standard measure for kinetic assessment. Marker positions and their derivatives were compared against IMU acceleration data to determine the most reliable method of identifying contact from motion capture data. Both data series presented impact spikes, with similar timings, depending on the placement location of the IMU. Hence, for placement locations where good agreement was observed between IMU and motion capture data, there exists an improvement on the current practical approach of video digitisation. IMUs can plausibly estimate the kinetic contributions of propulsion, however, processing requires further refinement before reliably being used in computational analyses.

From an engineering perspective, validation of the IMU would have benefitted from comparisons made against instrumented wheels (such as a SMARTWheel), despite aforementioned criticisms on performance impact. Due to the financial cost of obtaining a SMARTWheel, and its lack of anticipated future use, it was not deemed practical to procure one. Another advantage of the IMU system is, therefore, the greater accessibility of the device, as compared to commercially available, pre-existing solutions. A standard tool used for measuring applied power in cycling is the PowerTap. Pilot testing was performed using a PowerTap to assess suitability and the potential for its use. However, as wheelchair propulsion is not crank driven like cycling is, this tool was not viable.

Visual inspection of the IMU data revealed the capacity to differentiate timings between discrete contacts of the left and right hands. This would be beneficial in the monitoring and assessment of temporal asymmetries, which are common amongst athletes and can negatively impact athlete steering or promote athlete injury<sup>70, 94, 194</sup> and are difficult to observe through video. Propulsion asymmetries may have been underestimated in this research as a consequence of the constrained, treadmill-based motion. Although kinematic adaptation to treadmill propulsion (particularly regarding athlete symmetry)<sup>184</sup> is expected, a motor-driven treadmill is suitable for investigating manual wheelchair propulsion.<sup>274</sup> The primary focus was concerned more with signal detection than performance assessment. Despite this, the IMUs still demonstrated the capacity for discerning participant

asymmetries. This highlights the precision of this measurement tool, as well as the potential capabilities of this technology in a practical environment.

The sample population was controlled to ensure homogeneous wheelchair configurations, such that observed differences were only attributable to IMU placement, and not external factors, such as wheel and glove type, which were observed to be influential. Due to the unique impairments and experience of each athlete, data were compared on an individual level. The unique kinematic strategies employed by each athlete was reflected in the IMU response (Figure 4.16), as well as the amplitude of the signal. For example, Athlete F demonstrated a different technique to the remaining four athletes. The athlete maintained the cyclic upper extremity motion, however, did not always need to contact the wheel (push through action) to maintain speed. Because of this, the cycle time is approximately doubled, which is reflected in Figure 4.16.

As mentioned already, the reliability of the IMU methodology increased with SNR. This can be influenced through the use of disc wheels, thermoplastic gloves, and strong impact peaks. These characteristics are all relevant to the elite wheelchair racing population. Therefore, the generalisation of this method may be limited to some applications of manual wheelchair propulsion analysis, as well as within other sports. For example, the contacts of wheelchair rugby may result in false positive detections using the developed algorithm.

#### 4.7 IMPLICATIONS AND CONCLUSION

This chapter demonstrated that IMUs provide a more objective measure of contact, which is less susceptible to perspective and parallax error than the current gold standard method of video digitisation (Section 4.1). Therefore, IMUs serve as an improvement to the currently available technology for wheelchair racing athletes. Although the solution does come with some flaws, it optimises the requirements of both high engineering rigour, and practical usability. It was established that the method is more reliable in determining contact than release (Section 4.3). The reliability of the IMUs approach was subject to both athlete and wheelchair characteristics (Section 4.3), as well as placement locations (Section 4.4). Finally, it was established that the IMU could estimate propulsive forces of a wheelchair athlete. However, this is only achieved in the AP direction (Section 4.5). While this serves as the primary component of propulsive force, and hence an appropriate tool for measuring performance, it is not accurate enough for use within the computational modelling environment. As such, alternate methods of estimating the reaction forces at the pushrim are required. In this research,

---

estimations using kinematic data were used (and discussed in more detail in Section 6.1). However, the problem of instrumenting wheelchair racing chairs warrants further investigation.

*Key Findings:*

- IMUs are equally useful in identifying contact as compared to the ‘gold standard’ high-speed video observation method, and they provide an advancement due to greater objectivity of data analysis which is less subject to parallax and perspective errors.
- Acceleration response differs between the wheel and frame, with further differences noted based on specific placement on the wheel.
- Release points were not always detected as they were of comparable magnitude to the underlying noise of the signal.
- The reliability of the IMU methodology is reliant on the inherent SNR and was shown to vary significantly with speed, gender, athlete classification and age.
- IMUs can reliably estimate propulsive forces in the AP direction, but are less reliable in estimating out of plane forces in both the mediolateral (due to wheel camber) and vertical directions.

*Implications:*

- Athlete-specific processing algorithms are required to accommodate differences in signal characteristics across different propulsion styles.
- Poor placement of IMUs can result in large differences in performance metrics, which has the potential for creating large errors if used to drive a computational model.
- Frame placements are accessible for use by coaches and biomechanists to ensure compliance with the solution for long-term gain in performance preparation.
- Inaccuracies in out-of-plane estimates question the validity of the approach for use in computational modelling approaches.
- IMUs provide a useful tool for in-field monitoring of the kinetic and kinematic requirements of wheelchair propulsion.

---

## CHAPTER FIVE:

# WHEELCHAIR INSTRUMENTATION USING A PRESSURE MAT

---

Despite the influence of the seating interface on propulsion being recognised repeatedly in the literature,<sup>1, 106, 230</sup> little literature exists for wheelchair athletes, detailing the transient variation of pressure throughout a stroke.<sup>227</sup> Pressure mats have demonstrated success in measuring reaction forces of running,<sup>230</sup> and they have provided an indication of the quality of athlete-wheelchair interaction, which is a crucial aspect of wheelchair performance.<sup>119</sup> Pressure mapping technology has demonstrated success for clinical based load monitoring literature<sup>233</sup> and measuring reaction forces,<sup>231</sup> but is yet to be applied in sport-based wheelchair propulsion.

The most relevant pressure mapping literature for wheelchair use is predominantly clinical and performed using a pressure mat. Although the interactions at the seating interface are presumed to be more quasi-static than the dynamic hand contacts, the transient force data are unknown and are required as an input into the computational biomechanical analysis of wheelchair propulsion.

---

The content in this chapter completes the first aim of this research in developing an instrumentation tool capable of in-field data measurement of wheelchair racing performance (at the seating interface). Within this chapter, the efficacy of a pressure mat in measuring interface parameters at the seating interface is investigated and is split into three experimental studies. The first two studies investigate the applicability of the pressure mat, and whether its reliability is affected by the use of a foam cushion. The chapter concludes with an investigation into how well the lower extremity motion of track-based propulsion is replicated during the more controlled, treadmill-based propulsion. These three studies and their research questions are summarised following, with their connection to the primary research aim demonstrated in Figure 5.1.

**Can a commercially available pressure mat effectively measure interactions acting at the seating interface? (Section 5.2)**

*Research Question:*

- Can a commercially available pressure mat measure interactions at the seating interface?

**Effect of seating cushions on pressure distribution (Section 5.3)**

*Research Question:*

- Does a foam cushion at the seating interface impede the ability of the pressure mat to record valid data?

**Changes in leg pressure during modes of wheelchair propulsion (Section 5.4)**

*Research Questions:*

- Does treadmill-based propulsion accurately represent track based propulsion?
- Is data collected on a treadmill appropriate to analyse the influence of customised seating interfaces on elite wheelchair racing performance?

The findings from this chapter have additional practical implications. Use of the pressure mapping technology can extend to the analysis of performance in the daily training environments, demonstrating the practical significance of this research. For example, understanding the transient pressure profile at the seating interface can assist in the assessment of sustaining a pressure-related injury and for its role in performance-enhancing strategies. It is vital to understand whether athletes can gain a mechanical advantage during propulsion through the application of well-directed counter-forces at the seating interface.

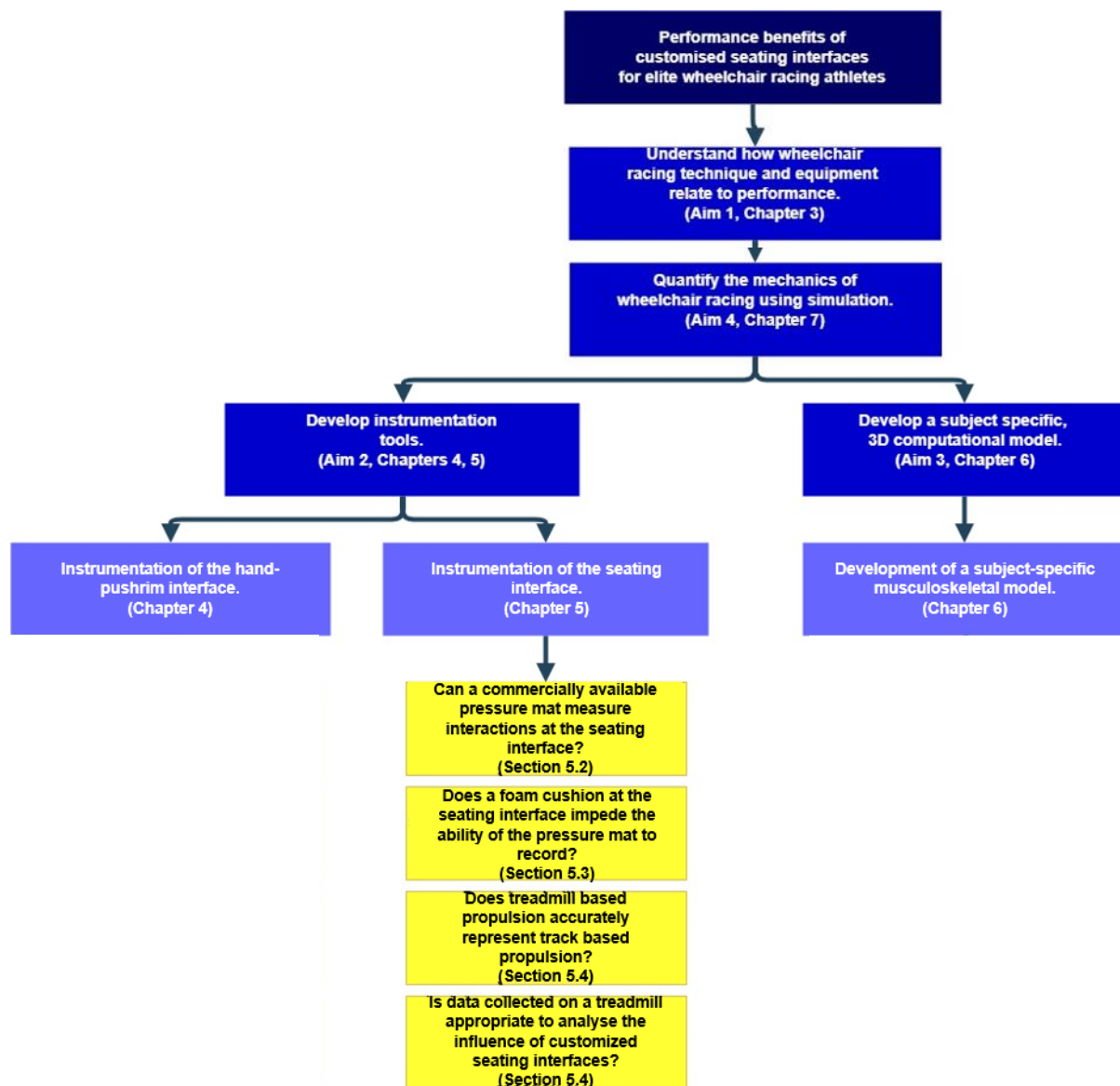


Figure 5.1: Relevance of the Chapter 5 (Wheelchair instrumentation using a pressure mat) to the fundamental research question; what is the performance impact of customised seating interfaces on wheelchair racing propulsion?

## 5.1 METHODS OF COLLECTING WHEELCHAIR RACING PERFORMANCE DATA USING A PRESSURE MAT

The same pressure mat data was utilised in each of the three experimental studies within this chapter. The common methodology is summarised following. Study-specific details are elaborated on within each specific experiment.



---

### 5.1.1 MEASUREMENT SYSTEM

Pressure was measured at the athlete-wheelchair seating interface during propulsion using a pressure mat (XSensor LX100; Calgary, Alberta, Canada) at a sampling frequency of 4 Hz (Figure 5.2). It is acknowledged that this sampling rate is low. However the procurement of a pressure mat with higher sampling rate was outside the scope of this research. This device has been cited as having an accuracy of 5 mmHg, less than 1.3% hysteresis and less than 5% creep over 1 hr usage.<sup>275</sup> Pressure measurements were obtained through a measured change in voltage across the 0.46 m × 0.46 m (18 × 18 inches) sensing area of the pressure mat, which was measured through 1,296 sensor points (sensels) with a spatial resolution of 12.7 mm. Throughout the remainder of the thesis, the term pressure mat relates to the measurement technology, while the term pressure map refers to the resulting image. Pressure mat placement facilitated the measurement of pressures applied normally (directly below shins), laterally (towards the seating bucket), and propulsively (in front of knees). No visible shear or crinkling of the mat was present during the 30 min settling time, which was required to ensure appropriate calibration and equilibration (accounting for creep in sensors).



Figure 5.2: Placement of a pressure mat in two different wheelchairs (A and B). Tablet demonstrates no apparent singularities from placement.

Video was collected using two SONY PXW-FS7 digital video cameras positioned perpendicularly to the right, and at the rear of the athlete. Video data were only used as a visual point of reference for post-processing. Data were captured for two independent 10 s periods for each athlete and corresponding motions. As each athlete has a unique technique, athletes were analysed independently, with no averaging performed across multiple athletes.

### 5.1.2 DATA PROCESSING

Pressure parameters at the seating interface were calculated using specialised software (ForeSite SS), accompanying the pressure mat. Pressure parameters included; peak pressure, average pressure (which is the average of all non-zero pressure sensing cells), and contact area (which is calculated by the number of pressure sensing cells under load).<sup>276</sup> Data were averaged over three separate trials for each athlete. Data processing was performed using MATLAB.

### 5.1.3 EXPERIMENTAL PROPULSION TASK

All athletes completed the testing protocol, in their regular racing wheelchairs, on either a Mondo track surface, athletics track surface or on the treadmill inclined to 1%.<sup>183</sup> Treadmill speeds were selected based on individual training speeds, based on whether athletes were either sprinters, or endurance based athletes, to ensure technique was representative, and to minimise effects of fatigue. These speeds ranged from 20 km/hr through 37 km/hr (Table 3.1). Trials were one minute in duration, allowing three periods of 10 s data capture at steady state speed. Before testing, a period of acclimatisation both at steady state (including at the speed of testing), and acceleration were provided to all athletes, to provide confidence in the use of the treadmill during the test protocol.

Ethical approval for this research was granted by the University of Adelaide Human Research Ethics Committee, and by the Australian Institute of Sport, with each athlete providing written, informed consent before participation.

## **5.2 CAN A COMMERCIALY AVAILABLE PRESSURE MAT EFFECTIVELY MEASURE INTERACTIONS ACTING AT THE SEATING INTERFACE?**

### 5.2.1 INTRODUCTION

Pressure mapping technology has been demonstrated to be an effective tool for understanding athlete-wheelchair interactions for manual wheelchair users in clinical environments. The translation of the technology from clinical to sporting applications, however, may be limited as a consequence of the additional complexities of sporting propulsion. Issues may pertain to the variation in seating geometry between sporting and manual wheelchairs and how the pressure mat (and corresponding data logger) is mounted.

---

Athletes in sports such as wheelchair rugby, wheelchair basketball and wheelchair tennis assume a conventional upright seated posture. From a geometric perspective, there are many similarities between the seating interfaces of manual wheelchairs with wheelchairs for these sports. However, as already stated (Section 1.1), wheelchair racing athletes adopt a kneeling posture, meaning the interactions with the wheelchair are acting at the shins. Wheelchair racing manufacturers produce seating buckets having various shapes (i.e. U or V-shaped openings). These are much smaller than the conventional seating interface. Therefore it can be considered that translation of pressure mapping research into practice could be readily achieved for the sports assuming conventional seating postures, but may be limited for wheelchair racing.

A second consideration relates to whether athletes maintain the capacity to perform while using the pressure mat. For example, the pressure mat used in this research has a water resistant outer, meaning it has a low coefficient of friction surface, which may promote athlete movement at the seating interface. Also, although systems are wireless, there are still considerations regarding both weight and placement for the data logger and wireless transmitter.

This study aimed to investigate whether a pressure mat is capable of measuring the distribution of pressure across the athlete-wheelchair interface, and its variation under the following dynamic conditions: steady state (constant velocity) propulsion, acceleration from a standstill, and agility. It is hypothesised that considerable variation in both the magnitude and distribution of seating pressure will be present during acceleration and agility modalities for athletes in both wheelchair racing and wheelchair rugby, where trunk movements are more dynamic.

## 5.2.2 METHODS

### *Athlete Selection*

This study compared pressure distribution at the seating interface from two sample populations; one used a modified kneeling posture (wheelchair racing), and the other a conventional upright seating posture (wheelchair rugby). Athletes from the National wheelchair racing ( $n = 6$ , Athletes A-F) and wheelchair rugby ( $n = 2$ , Athletes G and H) teams were assessed independently, in regular, sport-specific training environments.

### *Experimental Propulsion Task*

Testing was performed in the regular training environment of athletes, and as such minor variations in obtaining athlete testing protocol were present due to equipment availability in each venue. Wheelchair racing athlete masses were obtained through averaging 0.05 s of force plate output (taken as the summation of the forces from the three force plates located under each of the three wheels) from a static trial and taking the difference in measurements between the athlete-wheelchair system and the wheelchair itself. Wheelchair rugby athlete masses were determined using calibrated scales, as no force plates were available at the venue of data collection.

Pressure was measured at the athlete-wheelchair seating interface (wheelchair racing: interface at shank; wheelchair rugby: interface at buttocks). Three modes of propulsion were performed by athletes which were representative of regular performance: steady state (wheelchair racing only); acceleration from stationary (wheelchair racing and wheelchair rugby); and agility (wheelchair rugby only). The experimental tasks were selected to meet sporting requirements, where agility is not required in wheelchair racing, and constant velocity is rare in wheelchair rugby. The steady-state propulsion trials for wheelchair racing athletes were performed on a treadmill, as outlined previously.

Both wheelchair racing and wheelchair rugby athletes performed an acceleration from a stationary position. Wheelchair racing athletes performed the task on a Mondo track surface, with an audible, three command start, during which time athletes were allowed to pre-tension wheels (wheelchair racing start) to ensure motions were typical of performance. Conversely, wheelchair rugby athletes completed the task on a regular court surface and were allowed to begin the sprint in their own time (wheelchair rugby start).

As sustained, linear propulsion is atypical of wheelchair rugby athletes, an agility test (wheelchair rugby agility), which consisted of wheelchair rugby athletes completing the standardised Illinois Agility Test (Figure 5.3) was performed instead. Athletes completed the entire test, however, only a portion of this was analysed within this study. The focus was placed on the weaving section in the middle of the test where the most considerable amount of chair manoeuvrability is required, and consequently where the most significant variation in pressures would be observed.

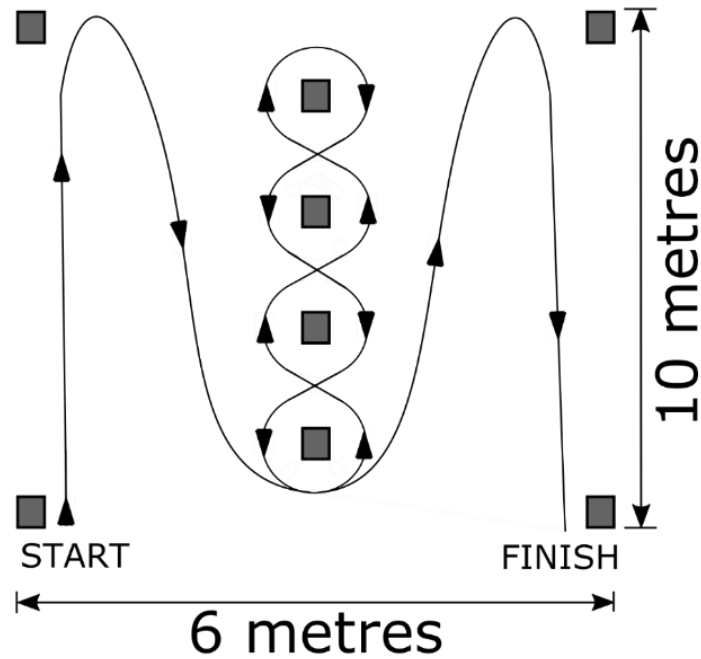


Figure 5.3: Illinois Agility Test used in wheelchair rugby agility trials, with specific data analysed from the weaving section, as evident in the middle of the Figure.

### *Data Processing*

Within-trial seating pressure was quantified using descriptive statistics for each propulsion mode (min, max, mean, and standard deviation) for average pressure, peak pressure, and contact area for each of the tested modes of propulsion: steady state; stationary start; and agility, as a whole, as well as for sport-specific classifications (wheelchair racing: T34 and T54; wheelchair rugby: 2.0 and 3.0). The coefficient of variation (CoV) was calculated for each of average pressure, peak pressure and contact area throughout a single push, to quantify the variability in these parameters.

Paired t-tests were used to determine the influence of the seating cushion on resultant seating pressure and contact area. Statistical analysis was performed using IBM SPSS Statistics 24 Software for Windows, with a significance set at  $\alpha = 0.05$ .

### 5.2.3 RESULTS

Substantial inter- and intra-sport variation of resultant pressure maps were observed, as presented in Figure 5.4. Each sub-figure represents the static posture of each athlete during the pre-tension period at the commencement of the acceleration trials. A static comparison (one frame, before the test was initiated) was selected to minimise the influence of athlete technique and the corresponding influences

on pressure distribution. For wheelchair racing athletes, static postures required them to assume their natural kneeling posture, with hands resting on the wheelchair pushrim where contact occurs. Similarly, wheelchair rugby images were obtained when the athlete was preparing to start. However, this was before any motion (including the upper extremity) had been initiated.

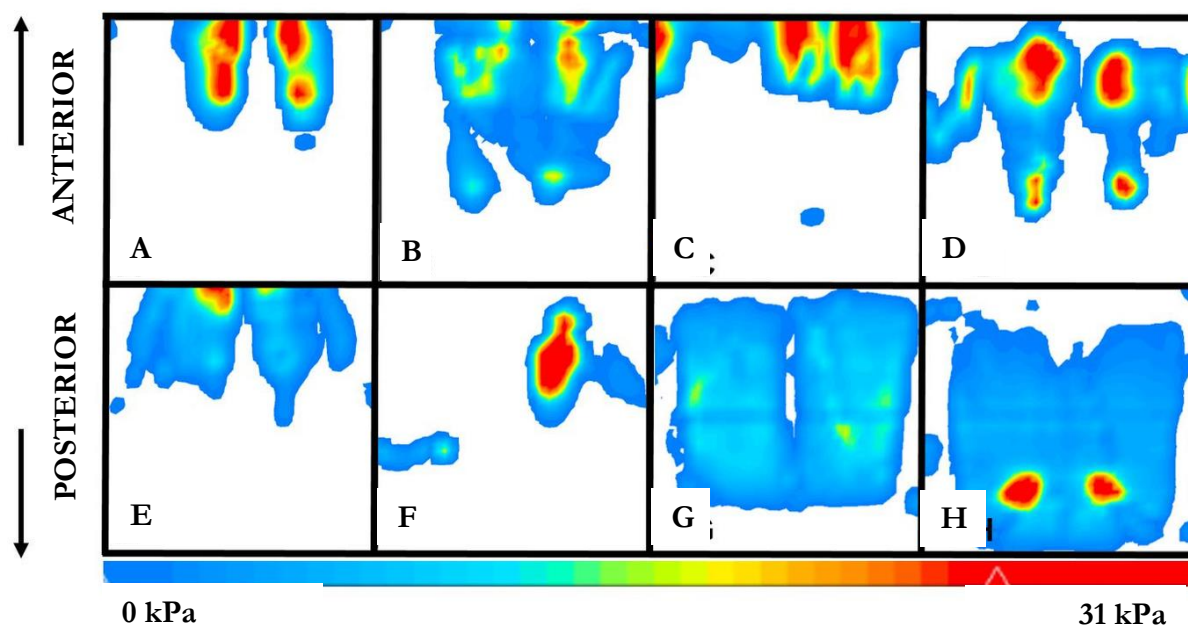


Figure 5.4: Inter-individual variation of seating pressure while stationary for a single timestamp. Sub-figures are labelled alphabetically A-H, which correlates to athlete characteristics presented in Table 3.1, with subfigures A-F and G-H representing wheelchair racing and wheelchair rugby athletes, respectively.

For the wheelchair racing athletes, the average pressure during the static measurement, presented in Figure 5.4, ranged between 7.3 kPa and 16.1 kPa (a factor of 2.2 times), while contact area varied between 0.0 m<sup>2</sup> and 0.1 m<sup>2</sup> (a factor of 3.1 times). It was observed that athletes exerted more peak pressure than the pressure mat had the capacity for (34.7 kPa). Consequently, at pressures greater than 34.7 kPa, there was sensor saturation, which prevented the calculation of variability within a trial. As average pressure calculations take into consideration all sensels, including the saturated ones, it is possible this saturation would also impact average pressure measurements. However, as is visualised in Figure 5.4, these regions of high pressure occur over a relatively small area compared with the total contact area of the athlete. Wheelchair rugby athletes demonstrated greater consistency in these parameters, with the variation being 5.7 kPa and 7.2 kPa (a factor of 1.3) for average pressure, 20.0 kPa and 34.1 kPa (a factor of 1.7) for peak pressure, but did not vary for contact area (0.1 m<sup>2</sup> and 0.1 m<sup>2</sup>).

A representative example of a within-trial variation of individual athletes is presented in Figure 5.5. Peak pressure measurements for wheelchair racing athletes were not obtained, as sensor saturation occurred, which is demonstrated through the horizontal line at 34.7 kPa in the peak pressure component of Figure 5.5, and subsequent value of 0.0% CoV in Table 5.1.

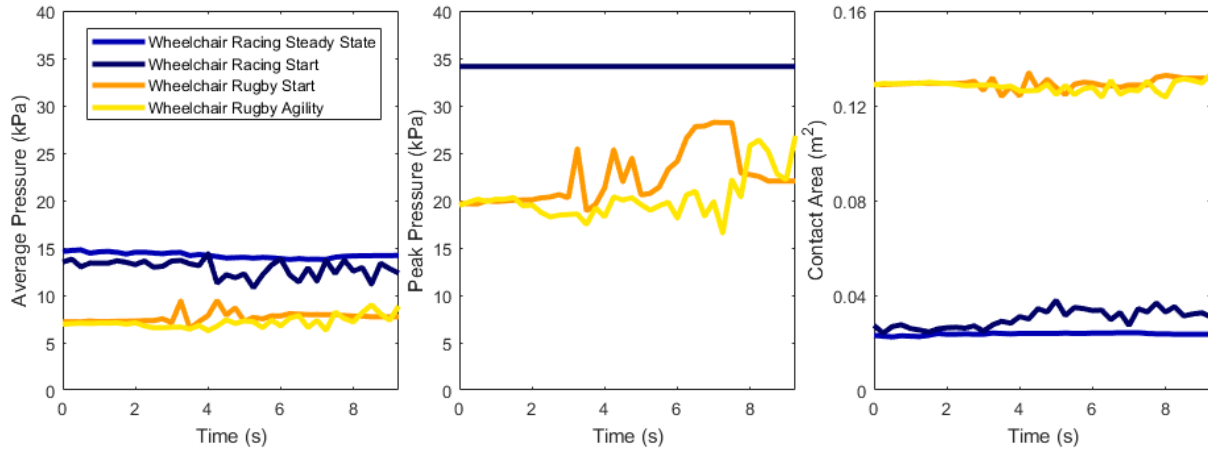


Figure 5.5: Comparison of average pressure, peak pressure and contact area for a single wheelchair racing and a single wheelchair rugby athlete.

A low CoV of average pressure (2.03%) and contact area (1.91%) were observed for the wheelchair racing steady state trials. While contact area remained relatively consistent for both the wheelchair rugby trials, there was a considerable variation in both average pressure and peak pressure, which was similar to all parameters for wheelchair racing start, with all CoV values quantified in Table 5.1.

Table 5.1: Coefficient of variation measures in average pressure, peak pressure and contact area, and demonstrating inter-individual variation between modes of propulsion.

	<b>Average Pressure (%)</b>	<b>Peak Pressure (%)</b>	<b>Contact Area (%)</b>
Wheelchair Racing Steady State	2.0	N/A	1.9
Wheelchair Racing Start	6.6	N/A	12.4
Wheelchair Rugby Start	7.4	12.7	1.7
Wheelchair Rugby Agility	8.8	11.5	1.7

For athlete F, a variation in contact area during propulsive and recovery phases was observed for a wheelchair racing acceleration trial (Figure 5.6, bottom), but not steady-state trial (Figure 5.6, top). This athlete has a congenital limb deficiency, meaning the pressure map is of a stump (left), and full leg (right). It is clear that the contact area for the right leg is substantially increased during the propulsive phase of the acceleration trial ( $0.04 \text{ m}^2$ ), as compared to the recovery phase ( $0.02 \text{ m}^2$ ).

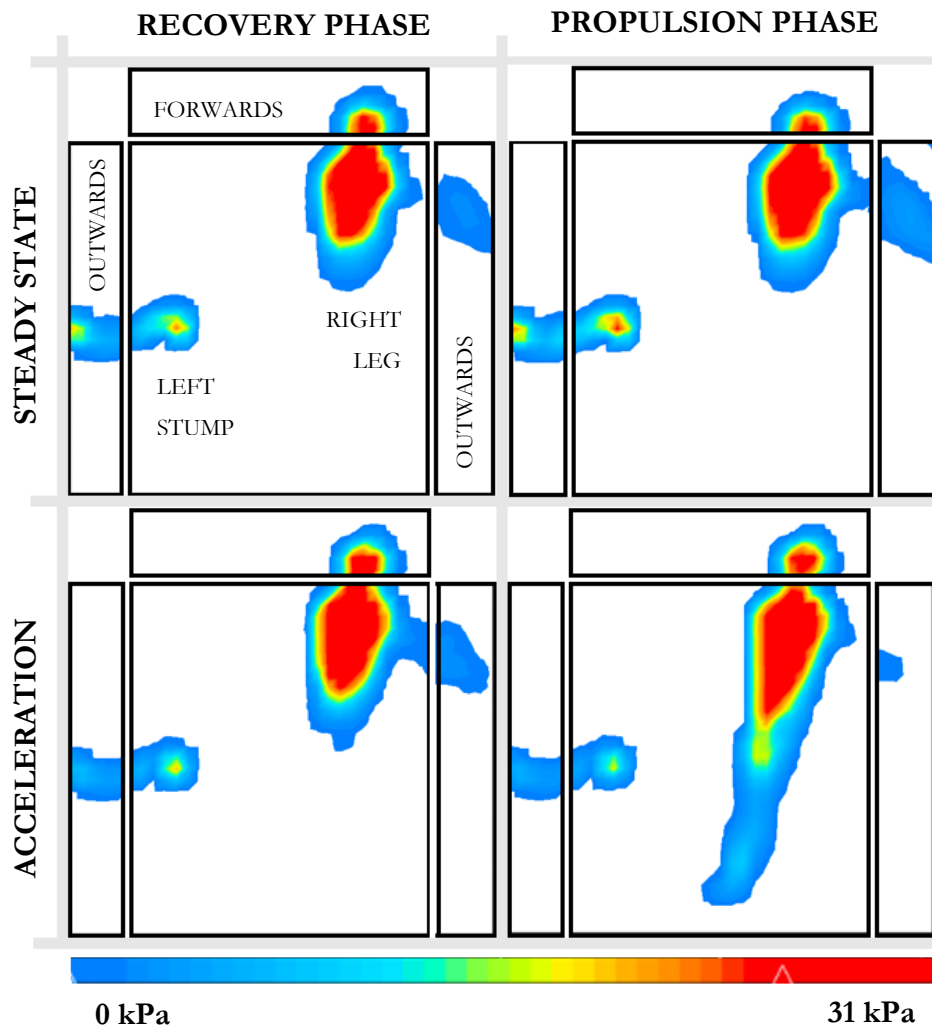


Figure 5.6: Variation of magnitude and location of pressure for Athlete F (wheelchair racing) during steady-state propulsion (Top), and acceleration (Bottom) demonstrating that under non-constant velocity propulsion, the pressure at the athlete interface is not consistent between the recovery phase (left) and propulsion phase (right).

Apparent variations in both location and magnitude of peak pressure were observed in the pressure maps from wheelchair rugby athletes throughout the agility trial, where the athlete was weaving through relatively sharp corners. Figure 5.7 shows evident increases in pressure to the side of the turn compared with the straight-line motion.



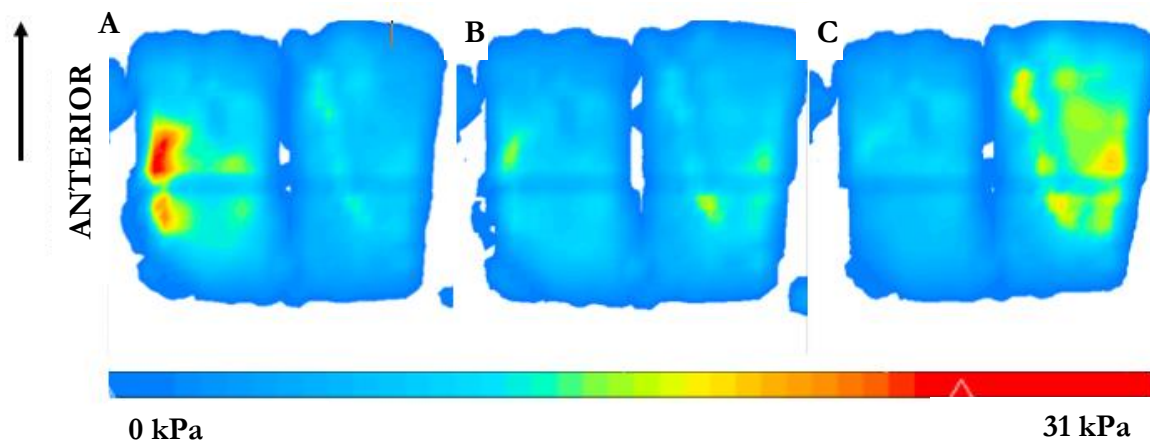


Figure 5.7: Variation in magnitude and location of peak pressures during agility tasks for a single wheelchair rugby athlete at a single time instant demonstrating seating pressure is not constant under non-linear conditions (A; Left turn, B; Straight propulsion, C; Right turn).

#### 5.2.4 DISCUSSION

This study evaluated the efficacy of a commercially available pressure mat in determining the pressure distribution across the seating interface of wheelchair athletes, and its variation throughout various wheelchair sports activities. Clear between-athlete and within-stroke differences in pressure distribution were observed, suggesting the adequacy of the measurement approach. This formed the first study conducted to measure the transient behaviour of pressure throughout wheelchair propulsion across sports.

Average pressure across a trial can be converted to force estimates for use in biomechanical modelling through multiplying obtained values by the spatial resolution of a sensor and normalising against total body mass. The consistency demonstrated during constant velocity suggest the plausibility for an appropriate simplification to modelling, using a constant force input proportional to a percentage body weight. This simplification was applied in the computational model in Chapter Seven. However, from the findings of this research, due to the dynamic nature of the seating interface, the assumption of constant mass at the seating interface is only valid under linear propulsion at a constant velocity. Consequently, for whole body biomechanical modelling of linear propulsion, kinetic measurements at the seating interface are required for acceleration conditions, as well as non-linear propulsion to provide a more comprehensive analysis.

Variability in pressure at the seating interface can be influenced by trunk motion, the interaction between the hands and pushrim at contact, wheelchair set up parameters (e.g. bucket angle, position in relation to wheels, use of foam cushion), as well as the aforementioned spatiotemporal parameters.

Further research into these characteristics, with the inclusion of instrumented wheels, is warranted to optimise the seating interface for both performance and health reasons. It is plausible that differences in leg pressure would be reflective of greater applied hand pressures, suggesting the pressure mat alone may facilitate in-field kinetic measurements during propulsion.

One of the most clinically relevant outcomes of this study was the potential for reduced risk of pressure sore ulceration in athletes, through identifying when large loadings occur. The technology utilised demonstrated sensor saturation at 34.70 kPa, whilst the limit of tissue viability has been reported as 8 kPa.<sup>81</sup> Although the saturation level, and hence the magnitude of peak pressures exemplified by the athletes in this study were higher than the clinically relevant pressure of 4.3 kPa,<sup>80, 81</sup> the duration over which such high peak pressures are applied is much shorter than what is observed in clinical applications. Therefore, the occurrence of sensor saturation does not indicate the athlete will obtain a pressure related injury; however, it is of importance to monitor this over extended durations. Based on the aforementioned cell break down after sustained compression, it can be recommended that a duration dependent injury criterion is imposed in athletic practice to minimise the risk of injury. This should be established in line with athlete-specific peak pressure magnitudes. However, it is recommended that extended periods of sustained compression should be avoided.

Currently, wheelchair design incorporates rigid materials at the seating interface to improve performance. However this study has demonstrated the necessity to implement cushioned interfaces to reduce the peak pressure present for injury prevention purposes. Further exploration is required to understand the implications of cushioned interfaces on the performance of both the pressure mat as a recording system and the athlete, as it is likely that low-density foams which are highly compressible may act as a damper, and thus reduce overall power transmission.

### 5.2.5 CONCLUSION

A commercially available pressure mat was capable of identifying between-athlete, and within-stroke variation in pressure distribution at the seating interface. Variation in pressure (peak and average) and contact area were identified between the propulsion and recovery phases during acceleration tasks for both wheelchair racing and wheelchair rugby athletes, as well as during agility tasks for wheelchair rugby athletes. This study demonstrated the importance of quantifying seating interactions for implementation in biomechanical modelling, as well as exposed that athletes, specifically wheelchair racing athletes, are at potentially unsafe levels of pressure at the seating interface.

---

## 5.3 EFFECT OF SEATING CUSHIONS ON PRESSURE DISTRIBUTION

### 5.3.1 INTRODUCTION

Seating cushions can be used by athletes to increase the contact area with their chair to increase stability and reduce peak pressures. They can be used to increase comfort at the seating interface, and can also be used to elevate the athlete to increase their purchase on the pushrim, and hence elongate the force delivery to the wheelchair during the propulsion phase, hopefully leading to improved performance.

It is possible that a pressure mat beneath a custom-contoured cushion may not be able to record as accurately as on a flat, rigid surface. As the fundamental goal of this research is to understand the impact on customised seating interfaces on performance, the ability for a device to be capable of recording beneath a foam cushion is necessary. Placement of the pressure mat on top of the cushion may not always be plausible, as they may have a highly organic shape based on the anthropometry of the individual.

This study aimed to address the appropriateness of the pressure mat in measuring racing athlete-wheelchair interaction at the seating interface during propulsion and assess how this varies when seating cushions are used. It was hypothesised that the seating cushion would not prevent the ability of the pressure mat to record data at the seating interface.

### 5.3.2 METHODS

#### *Athlete Selection*

Six athletes provided the population sample for this study (Athletes A – F), with a seating cushion used by Athlete B.

### 5.3.3 RESULTS

Substantial inter-individual variation in both average pressure and contact area was present between athletes (Figure 5.8). Variation in peak pressure measurements was not obtained due to sensor saturation. A reduction in peak pressure and larger contact area can be observed when a foam insert was used (Figure 5.8 C and F). Contact area varied from 0.2 m<sup>2</sup> through 0.7 m<sup>2</sup> (where laterally applied pressures were present), highlighting a between-athlete increase of 3.1 times was present.

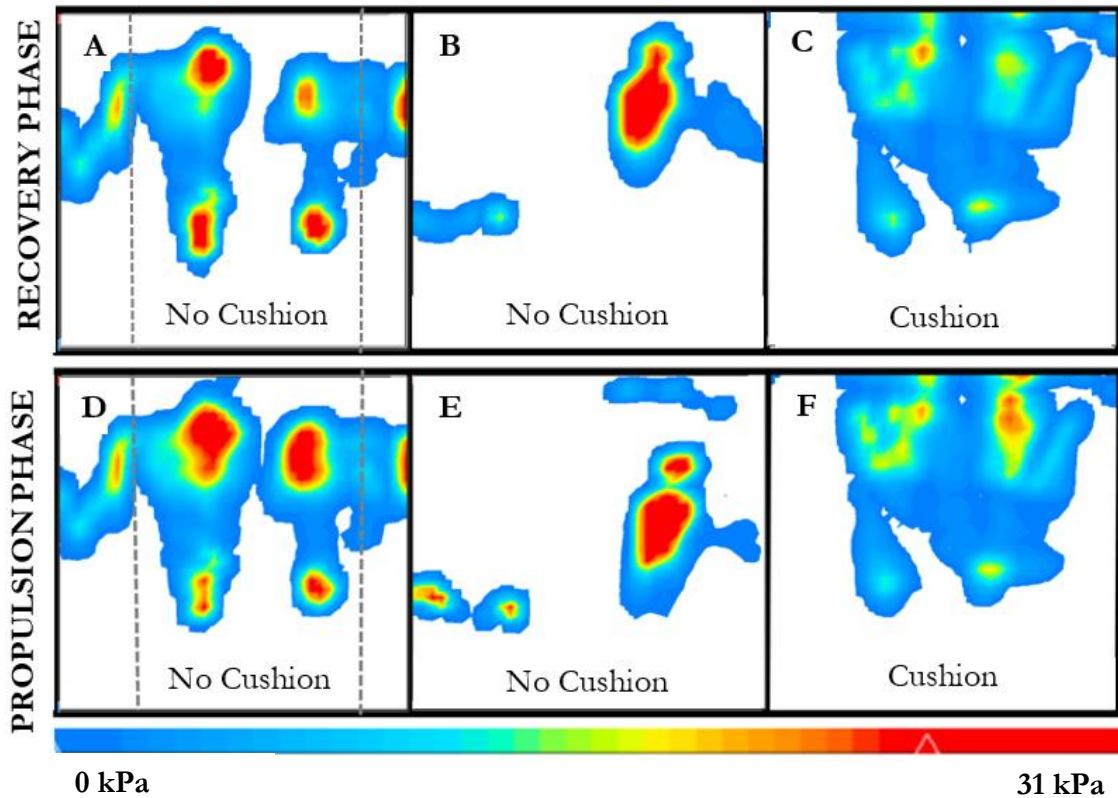


Figure 5.8: Exemplar data of seating pressure across three athletes, obtained as a static measure before data collection. Dashed lines are representative of laterally applied pressures.

A significant decrease in average pressure and significant increases in contact area ( $p < .01$ ) occurred when seating cushions were used. The magnitude of differences is shown in Figure 5.9, for a single 10 s trial. Foam cushions can effectively reduce peak pressure, such that they are below the threshold of sensor saturation. Average pressures were also more consistent (smaller variance) when foam cushions were used.

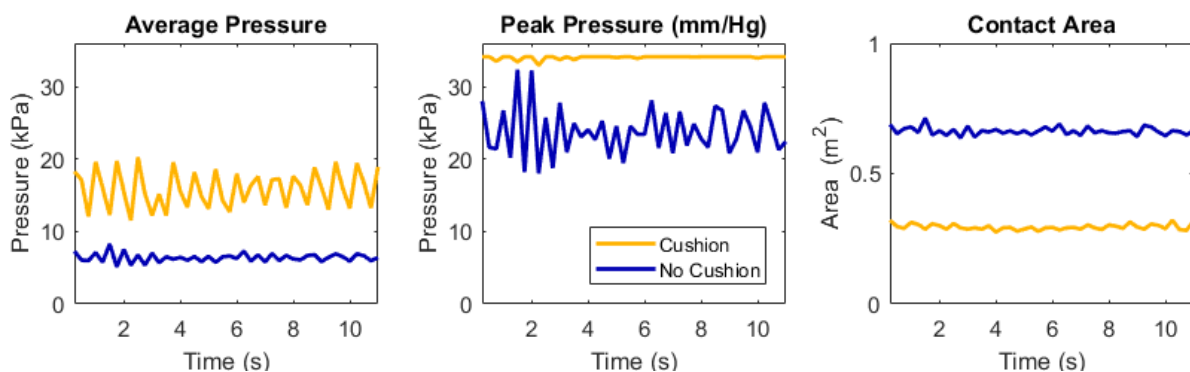


Figure 5.9: Exemplar data from two athletes demonstrating the influence of foam cushions on average pressure, peak pressure and contact area. Data are presented as a mean of all athletes who use or do not use foam seating cushions.

Statistically significant differences were present between propulsion and recovery phases (no cushion and with cushion) as well as between the propulsion phase data and recovery phase data of the no cushion and with cushion conditions (Table 5.2).

Table 5.2: Comparison of average pressure, peak pressure and contact area (mean  $\pm$  SD) during the propulsion and recovery phase when a seating cushion was not, and was used. Data are presented as the average of all athletes.

	No Cushion		With Cushion	
	Propulsion Phase	Recovery Phase	Propulsion Phase	Recovery Phase
Average Pressure (kPa)	131.9 $\pm$ 11.8	98.3 $\pm$ 6.5	51.3 $\pm$ 3.2	43.9 $\pm$ 2.2
Peak Pressure (kPa)	256.0 $\pm$ 0.0	254.3 $\pm$ 2.5	196.4 $\pm$ 18.7	157.4 $\pm$ 11.4
Contact Area (m <sup>2</sup> )	0.3 $\pm$ 0.0	0.3 $\pm$ 0.0	0.7 $\pm$ 0.0	0.7 $\pm$ 0.1

#### 5.3.4 DISCUSSION

This study evaluated whether the recording capabilities of a pressure mat were impeded as a consequence of being beneath a foam cushion. Use of foam seating cushions did not interfere with the capability of the pressure map to record, suggesting that the use of a pressure mat as the instrumentation tool is valid for measuring the reaction forces at the seating interface, to ultimately analyse the effect of customised seating interfaces on athlete performance.

Implementation of customised seating cushions effectively increases the contact area of athletes, while minimising both average pressure and peak pressure. Aside from the benefits of decreased likelihood of injury, increasing contact area may improve the athlete–wheelchair interface. By having a more stable base of motion, athletes are more likely to be able to more consistently contact the wheel symmetrically, and over an optimal push range. Furthermore, these interfaces may promote consistency at the seating interfaces of wheelchair athletes, which may benefit athletes who have a more significant physical impairment and greater muscle atrophy in the lower extremities.

Assessment of the use of pressure mapping technology in a performance capacity is still required, to determine the impact of these reductions in pressure. It can be observed in Figure 5.8 A that athletes sometimes push outwards on the seat. A seating cushion may not be able to cover these surfaces to lower the loading in these regions, however, if athletes have a larger contact area under their legs, they may be less inclined to push outwards, but instead, direct their momentum forwards.

### 5.3.5 CONCLUSION

Cushions at the seating interface effectively increase the total contact area of an athlete, which can hence be correlated with lower peak pressures. As these do not impede regular athlete motion, implementation of seating cushions can be considered as a beneficial tool for the real-time assessment of athlete seating performance. Additionally, use of a cushion can decrease peak pressures, reducing the risk of obtaining pressure sore related injuries, and promote greater stability at the seating interface. Based on these results, it can be established that both pressure mapping technology, as well as customised cushions, would benefit wheelchair racing athletes, and that future research is warranted.

## 5.4 CHANGES IN LEG PRESSURE DURING MODES OF RACING WHEELCHAIR PROPULSION

### 5.4.1 INTRODUCTION

The movement of the lower extremity during non-steady-state and non-linear propulsion has been demonstrated earlier in this chapter (Section 5.2). However, these findings only provided a simple comparison between steady-state and non-steady state or non-linear propulsion. Literature has established that laboratory conditions are unable to depict the physiological and biomechanical requirements of performance accurately.<sup>185</sup> For example, neither roller-based ergometers nor treadmills can holistically replicate acceleration, due to the omission of air resistance, rolling friction and balance, or the fixed speed of the treadmill belt.<sup>119</sup> Although literature already demonstrates how the upper extremity kinematics differ between conditions, to the author's knowledge, no literature currently exists which demonstrates how the interactions at the athlete-wheelchair interface differ between laboratory-based and in-field testing. Consequently, it is possible that there exist differences in both steady-state and acceleration motions between a simulated laboratory environment and on-track conditions.

This study aimed to assess the efficacy of the pressure mat as a measure of seating interface movement, under both training and simulated race conditions. It was hypothesised that the pressure profile would be similar between treadmill-based and track-based propulsion under steady-state conditions. It was also hypothesised that differences might be noted across acceleration techniques, based on an increased stimulus in reaching higher speeds.

---

## 5.4.2 METHODS

### *Athlete Selection*

A single elite athlete (Athlete F; age: 24 years, international experience: 6 years, body mass: 54.2 kg) provided the sample population for this study.

### *Experimental Propulsion Task*

The athlete completed four protocols of wheelchair propulsion; two at steady state (treadmill and track) and two accelerations (stationary start and 150 m acceleration). Steady-state propulsion was performed on both a treadmill and a track surface. Treadmill speed was determined based on preferred speed in regular training and was kept consistent with track speed.

### *Statistical Analysis*

Three sets of 10 s trials were collected for each condition and averaged. Significant differences between propulsion tasks were characterised by performing a repeated measures One-Way ANOVA with Bonferroni Adjustments. Statistical analysis was performed using IBM SPSS Statistics 24 Software for Windows.

## 5.4.3 RESULTS

The transient progression of both average pressure (lower) and contact area (upper) is demonstrated in Figure 5.10. A minor cyclic variation occurred in the contact area for all modes of propulsion indicating propulsion and recovery phases. Acceleration on track surfaces demonstrated the lowest contact area. Although this motion appears to have the largest contact area in Figure 5.10, it can be suggested that pressure is applied in different directions with propulsion style.

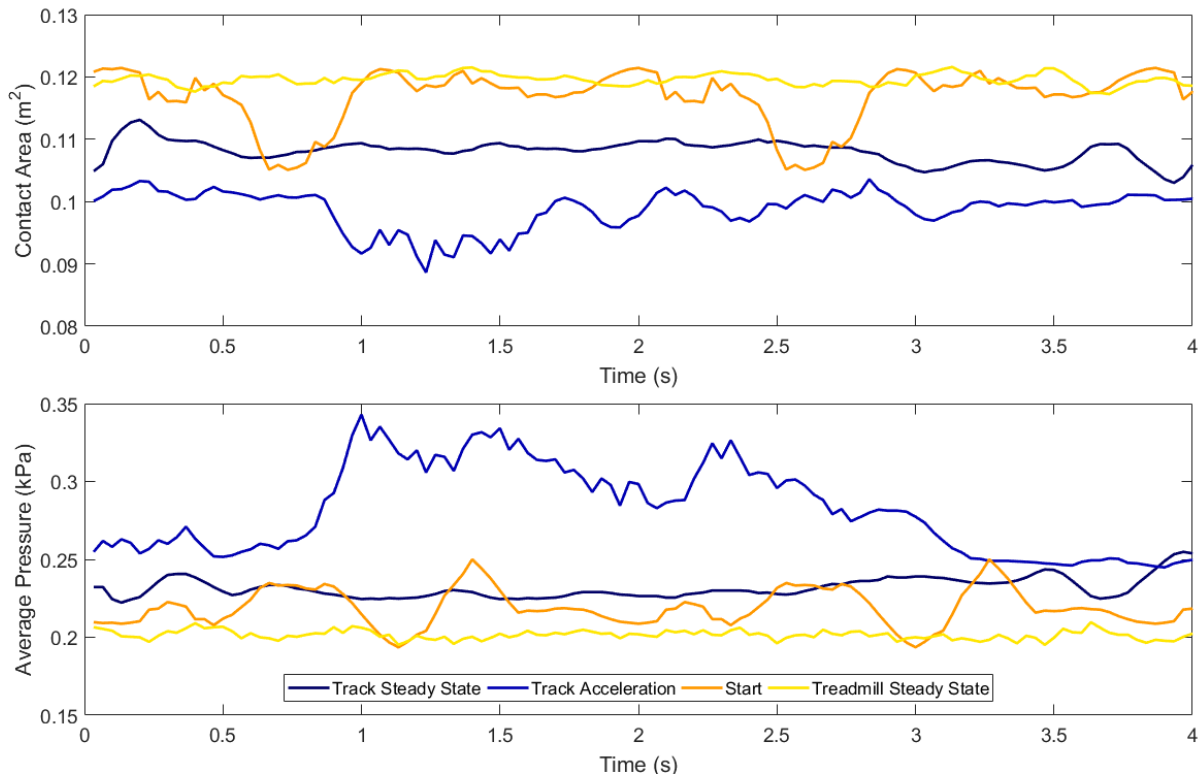


Figure 5.10: Transient behaviour of average pressure and contact area for a single athlete (Athlete F) during steady state propulsion on a track and treadmill, acceleration on the track, and a starting motion.

Similarities were observed for all pressure parameters during the recovery phase of all modes of propulsion. However the most forward point of contact was translated forwards for laboratory-based propulsion (Figure 5.11: Treadmill steady-state, start). More distinct differences were observed between the propulsion and recovery phases of acceleration based trials, where the pressure placed across the athlete's entire leg increased substantially. Further assessment revealed these pressures were predominantly applied vertically downwards, with greater lateral pressures (greater peak pressure in left leg) under steady-state propulsion than was observed during acceleration.

Between-conditions differences between the three key performance parameters are compared visually in Figure 5.11. Consistency in average pressure and contact area was demonstrated for steady-state motions, with substantially greater variation demonstrated for the acceleration trials.



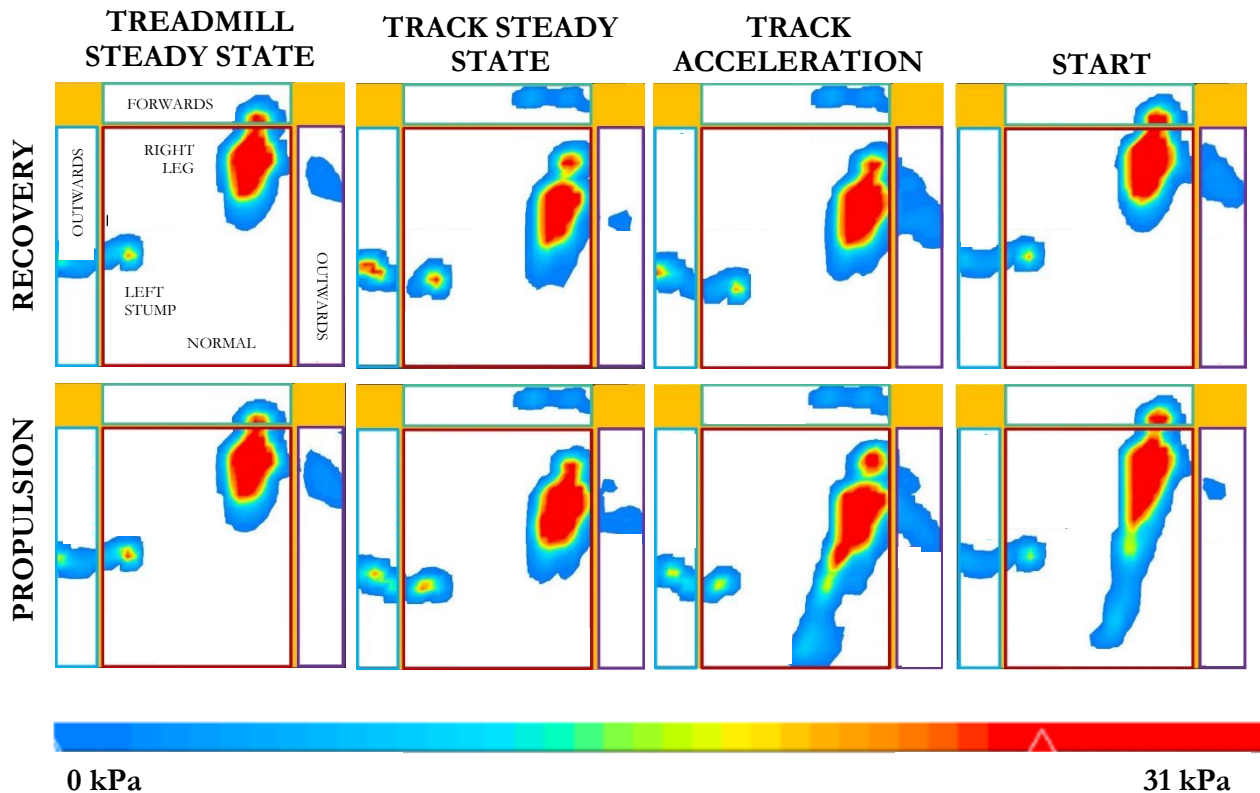


Figure 5.11: Variation in pressure for a single timestamp across different modes of propulsion. Panels represent the different directions of pressure measured by the pressure mat.

Increased forwards leg drive was associated with an increased contact area in both acceleration trials, with negligible applied knee force demonstrated in both of the steady state conditions. Despite athlete velocity being controlled across all condition, it is clear that these acceleration trials demonstrate a much more dynamic, and less controlled motion. This can be attributed to the greater bioenergetics requirements of acceleration. Steady-state propulsion on a treadmill demonstrated greater consistency than on track surfaces, with a systematic difference observed, suggesting that propulsion does differ between lab-based and track-based environments. No relationship was established between average pressure and contact area for acceleration and start motions (Figure 5.12). Data are presented as variability, whereby a value of 1 represents the minimum value to prevent the influence of different seating configuration from masking trends in the results. The greater spread of data is indicative of greater variability in technique.

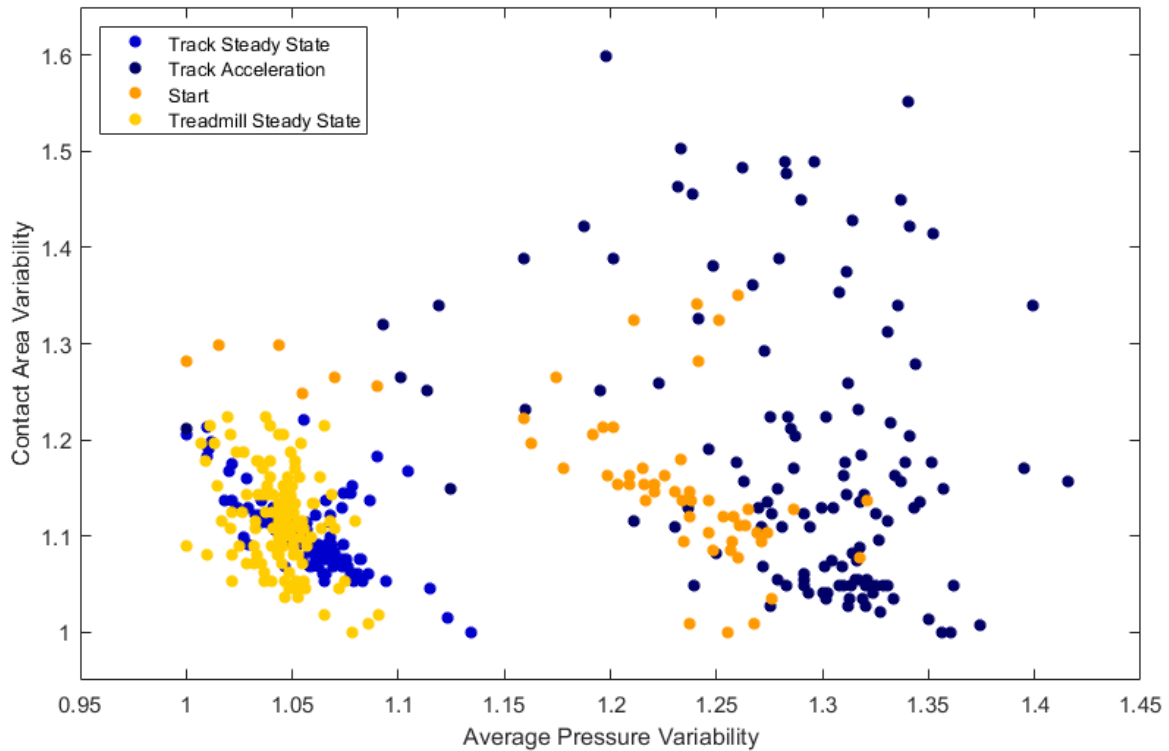


Figure 5.12: Variability of average pressure and contact area during different modes of propulsion (track steady-state, track acceleration, start, treadmill steady-state), compared to the minimum value for a single athlete (Athlete F).

Observed differences in pressure parameters across modes of propulsion were supported from the repeated measures One-Way ANOVA (Table 5.3). Significant differences at the  $\alpha = 0.05$  level were revealed between most conditions for measures of average pressure and contact area. Apart from track steady-state versus start, both average pressure and contact area demonstrated significant differences between all modes of propulsion. Similarities in the contact area for track steady-state versus start may be a consequence of taking the average of the cyclic data.

Table 5.3: Differences in average pressure and contact area between modes of propulsion (track steady-state, track acceleration, start, and treadmill steady-state).

	Average Pressure	Contact Area
Track Steady-State v Track Acceleration	** $p < .010$	** $p < .010$
Track Steady-State v Start	** $p < .010$	$p = .14$
Track Steady-State v Treadmill Steady-State	** $p < .010$	** $p < .010$
Track Acceleration v Start	** $p < .010$	** $p < .010$
Track Acceleration v Treadmill Steady-State	** $p < .010$	** $p < .010$
Start v Treadmill Steady-State	** $p < .010$	** $p < .010$

\*\* indicates statistical significance at the  $p < .01$  level.

---

#### 5.4.4 DISCUSSION

This study evaluated the practical significance of the use of a pressure mat in an applied setting to understand the similarities in the interactions between the athlete-wheelchair at the seating interface across laboratory-based and in-field testing. The pressure mat was a useful tool in monitoring athlete-wheelchair interactions, with potential performance gains obtained through insights of where and the direction forces are being applied. For example, low contact area may be due to the athlete applying too much of a vertical component of force at the pushrim, which may contribute more towards athlete elevation than forwards movement. The consistency in leg drive data obtained from the pressure mat under both steady state conditions suggests the treadmill does not simulate non-steady-state conditions completely.

Due to the relative importance of measuring the athlete-wheelchair interaction for this research, other testing protocols need consideration for the assessment of customised seating interfaces. Treadmills are limited by their controlled speeds, which prevent the acceleration phase of wheelchair propulsion motion. As the kinematics of multiple successive trials are required for use within the computational model, testing is restricted to laboratory environments. At the time of data collection, outdoor motion capture systems were not available. As such, despite the biomechanical and physiological dissimilarities identified by Mason et al.,<sup>183</sup> an ergometer based protocol will be used in ensuing testing protocols to assess the influence of the customised seating interface better.

Generally, average pressure and contact area were inversely proportional, however, under track acceleration conditions, these were directly proportional, and suggesting increased force application from the leg. The qualitative assessment revealed that increased contact area was applied predominantly in the lateral and normal (downwards) directions of the functional leg. This suggests that although the leg is increasing its contribution, this contribution is not currently being directed optimally. As all athletes are unique in both functionality and anthropometry, it can be assumed that this level of contribution will vary significantly between athletes, concerning both magnitudes and applied directions.

The minimal variation in contact area under steady-state trials may be indicative that at the applied propulsion speed, the athlete is not at maximum exertion, suggesting the pressure mat may assist in quantifying effort to refine athlete development strategies. Furthermore, the observed similarities between steady-state conditions on both the track and treadmill surfaces suggest the adequacy of treadmill-based training under steady-state conditions only. Use of a treadmill can be seen to be inadequate at replicating all required kinematics of acceleration.

### 5.4.5 CONCLUSION

The efficacy of pressure maps in quantifying leg pressure was assessed on varying track surfaces and tasks. Although limited by recording frequency and sensor saturation, the pressure map was a suitable method of quantifying leg contribution to acceleration, and easily applied to in-field measurements. When function is present, athletes use their legs during the acceleration phase of propulsion. The level and direction of this applied pressure, and hence force is variable between different modes of propulsion, and hence should be assessed under performance conditions.

### 5.5 DISCUSSION

This chapter investigated the effectiveness of a pressure mat in monitoring seating interface, and how these interactions change between athletes, and across different terrains. The pliable surface of the pressure mat allowed ease of application across a number ( $n = 6$ ) of differently shaped seating interfaces. Collected data revealed that as the literature suggests, interactions at the seating interface can benefit performance.

It is plausible that variation in centre of mass location across the seating interface may be related to the altered kinematics resulting from both spatial and temporal propulsion asymmetries. Use of a pressure mat may provide a more practically viable solution for kinematic measurement than motion capture, with potential for in-field measurements. Practical limitations of this pressure mapping technology, however, include the limited Bluetooth transmission range (10 m), and the reduced coefficient of friction of the pressure mat surface, than that present for normal seating conditions. However, athlete feedback suggested that the pressure mat would not be an encumbrance during regular training.

This chapter confirmed that athletes could move relative to the seat (based on the changes in contact area). Further research into quantifying the performance impact of this is required, as such movement of the athlete relative to their wheelchair may be undesirable, with applied energy not completely translating to forwards propulsion. This, however, may assist some athletes in generating a rhythmical movement, or act as a source of leverage for greater range of motion or applied power. It is considered that optimal stiffness at the seating interface may be motion dependent, with linear tasks favouring a stable base, while it may be advantageous for movement at the seat to be present for agility motions.

While the system utilised in this research adequately demonstrated movement present at the seating interface, restrictions in data analysis were evident due to the recording frequency and maximum pressure of the system. Wheelchair propulsion is approximately a 2 Hz motion, with literature reporting steady state push durations of 0.45 s.<sup>116</sup> Of this, the propulsion phase occurs for 0.21 s,<sup>116</sup> meaning that

---

at least one data point can reliably detect each of the propulsion and recovery phases. Other systems have recording frequencies up to 20 kHz, and pressure ranges up to 207 MPa (I-Scan VersaTek system: Tekscan Inc., Boston, MA),<sup>277</sup> facilitating the quantification of the transient nature of propulsion between the propulsion and recovery phases. These systems were not available for this research, however. As limited processing capabilities were inherent with the system used, the effects of sensor saturation impacted the calculation of average pressure and the variation in peak pressure. Although obtaining the actual peak values would be relevant, as sensor saturation is approximately the same as the limits of tissue viability, the presence of any saturation is indicative of injury risk. Although outside the capabilities of the pressure mat utilised in this research, future research may benefit from fragmenting the seating area into sub-sections, such as the left and right sides to better measure athlete symmetry, or understand the direction of pressure application and centre of pressure location. Ultimately, the limitations of the pressure mat used did not hinder this research, as the efficacy of pressure mapping technology, and the dynamic response of the lower extremity during propulsion was still identified.

Although the inclusion of cushioned interfaces may benefit athletes through a reduced risk of injury, it is uncertain whether these cushioning tools may be detrimental to performance. For example, the compressibility of a cushion may absorb applied energy from the lower extremity during propulsion and hence reduce the rate of force transfer to the chair. Similarly, if the seat is compressing, and hence moving underneath the athlete, it is possible that inclusion of these devices may effectively reduce the level of stability an athlete has at the seating interface. Further research is required to understand the performance impact of customised seating interfaces, and how performance varies with cushion manufacture.

## **5.6 IMPLICATIONS AND CONCLUSIONS**

This series of studies were the first to demonstrate the propulsive advantage that can be achieved through the practical use of the seating interface (Section 5.2). It was shown that these interactions vary substantially across athletes, in line with physical impairment and functionality. Seating interfaces were demonstrated to be sport-specific, meaning the construction and optimisation of this interface must be performed on an athlete based approach. Seating cushions have been demonstrated to reduce the load acting at the seating interface, which is beneficial for the competitive longevity (Section 5.3). Treadmills were also demonstrated to not fully replicate the seated dynamics of overground propulsion (Section 5.4), suggesting that future evaluation of the performance impact of a seating cushion should be performed using an alternative methodology.

### *Key Findings:*

- A commercially available pressure mat was capable of measuring the reaction forces at the wheelchair seat, while not being an encumbrance to athletes.
- Implementation of a foam insert at the seating interface did not impede the recording capability of a pressure mat.
- The assumption of constant mass at the seating interface is only valid under linear, steady-state propulsion, with athletes possibly able to gain a mechanical advantage from the dynamic interactions at the seating interface during acceleration or non-linear movements.
- The inclusion of a foam insert at the seating interface altered athlete-wheelchair interaction, through a reduction in seating pressure (average and peak), and an increase in contact area.
- Treadmill based propulsion does not entirely represent the dynamic interactions at the seating interface compared to on-track performance.

### *Implications:*

- Biomechanical analysis incorporating a pressure mat can provide insight as to how to optimise the seating interface to provide a stable support for the most powerful and efficient technique.
- Wheelchair racing athletes require cushioning at the seating interface based on the high stresses applied, to reduce the chance of obtaining a pressure sore injury.
- Use of a seating interface may promote greater stability at the wheelchair-athlete seating interface due to the enhanced contact area.
- Pressure mat technology can measure whether athletes are utilising their lower extremity.
- When analysing the performance of the seating interface, the analysis should not be performed using the treadmill.

---

## CHAPTER SIX:

# DEVELOPMENT OF A SUBJECT-SPECIFIC, 3D MUSCULOSKELETAL MODEL

---

Gross performance of wheelchair racing can be analysed merely through a time metric (which can be adjusted to take into consideration air density and wind conditions). However, this only measures performance outcome and not how it was achieved. Alternatively, computational biomechanical simulations can analyse performance more holistically through estimating the intersegmental joint loads and muscular contributions (activations, coordination and forces) of movement,<sup>129, 153</sup> including when functional asymmetries are present.<sup>278</sup> Modelling error results from the poor estimation of physical parameters,<sup>107, 158</sup> specifically when they differ from the norm as a result of age, size or physical deformation.<sup>124, 130</sup>

This chapter addresses the second aim of this research in developing a subject-specific musculoskeletal model of wheelchair racing athletes. The sensitivity of the simulation protocol to the anthropometric adaptations associated with impairment and whether the use of subject-specific parameters derived from the analysis of DXA scans improves reliability was explored. Three experimental studies were performed. The first investigated the sensitivity of the simulation to the processing of DXA scans. Body mass distribution of elite wheelchair racing athletes was compared to other populations (including those which musculoskeletal models are currently derived from) to see whether subject-specific parameters were required, or whether generic inertial parameters would suffice. Finally, another sensitivity analysis was performed to understand how to modify maximum isometric force generating capacity in the musculoskeletal model of wheelchair athletes, and whether this could be estimated using data obtained from the analysis of DXA scans. These three studies and their research questions are summarised following, with their relation to the main aim of this research demonstrated in Figure 6.1.

### **The effect of altering intensity thresholds in DXA scans for the calculation of body segment inertial parameters (Section 6.2)**

#### *Research Question:*

- How sensitive are segment mass estimates (derived from DXA scans) to the processing methodology used?

### **Mass distribution of wheelchair athletes assessed using DXA scans (Section 6.3)**

#### *Research Question:*

- Is the body mass distribution of wheelchair racing athletes significantly different from an able-bodied population?
- What magnitude of errors will be present if a simulation uses body segment inertial parameters from an able-bodied distribution, and is it appropriate to make simplifications?



---

**A strategy for estimating maximum isometric force-generating capacity of wheelchair racing athletes. (Section 6.4)**

*Research Questions:*

- Does the maximum isometric force-generating capacity of a model need to be altered to reflect the muscular hypertrophy following athletic training?

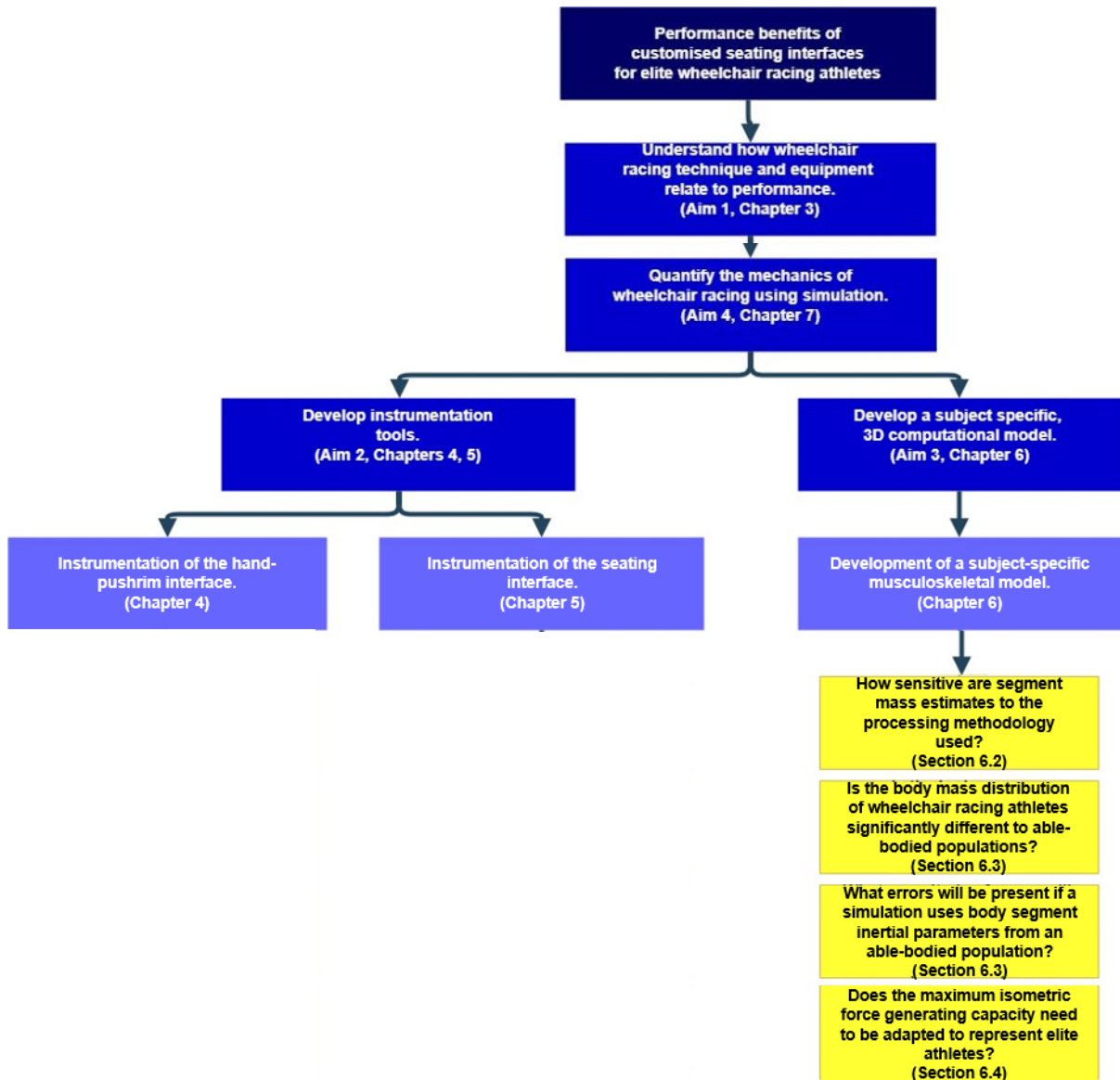


Figure 6.1: Relevance of the Chapter 6 (Development of a subject-specific, 3D musculoskeletal model) to the fundamental research question; what is the performance impact of customised seating interfaces on wheelchair racing propulsion?

## 6.1 PROCESSING OF DXA SCANS FOR THE CALCULATION OF BODY SEGMENT INERTIAL PARAMETERS

### *Athlete Selection*

DXA scan data were obtained for five internationally ranked Australian wheelchair athletes (Table 6.1) competing in wheelchair racing ( $n = 3$ , Athletes I, L and M) and triathlon ( $n = 2$ , Athletes E and K) from a prospectively maintained database at the Australian Institute of Sport (Canberra, ACT, Australia). The population for this study was a convenience sample, based on what data was available at the time of testing. The mass of Athlete E and I varies in section 6.3 compared with the remainder of the thesis, in line with the collection of DXA scans and kinematic data collection at different times. Additionally, values presented in Table 6.1 are representative of system mass (athlete + wheelchair), while DXA data is purely athlete mass.

Table 6.1: Relevant athlete characteristics. Further elaboration can be found in Table 3.1.

	<b>Gender</b>	<b>Mass (kg)</b>	<b>Impairment</b>
Athlete E	F	52.9	Spinal Cord Injury (acquired)
Athlete I	F	48.0	Paraplegia
Athlete K	M	72.3	Incomplete Paraplegia
Athlete L	M	56.2	Spina Bifida
Athlete M	M	62.0	Paraplegia

### *Measurement System*

DXA scan data were previously obtained using contemporary methodologies,<sup>279</sup> with ethical approval obtained from the Australian Institute of Sport. All scans were taken since 2015, using the same densitometer. The physical collection of the DXA scans did not form part of this research. DXA scan data were exported into the raw DICOM format using enCORE version 16 software (GE, Medical Systems Ultrasound and Primary Care Diagnostics, USA). Limb segments were manually delineated using the low attenuation image (with more clearly defined anatomical landmarks) using custom code developed in MATLAB. A standard fourteen segment configuration was defined<sup>280-285</sup> which included: Head and Neck; Torso; Upper Arm; Forearm; Hand; Thigh; Shank; and, Foot for both the left and right limbs (Figure 6.2). Segment boundaries identified during the delineation process were transferred to the high intensity (soft tissue) image, for the calculation of segment masses.

The intensity of a pixel and the density of the region represented by the pixel were related using linear regression. The mass of each pixel was calibrated using coefficients of attenuation, which were

---

explicitly derived for each athlete. Segment masses were calculated through summing all segment intensities within a specified limb segment boundary and scaled with an areal density calibration factor to determine specific segment masses. This method was validated by comparing total body mass (as a sum of all pixel elements for the fourteen segments for the five athletes) with measured total body mass (calibrated scale measurement) based on the methods presented by Rossi et al. <sup>284</sup>

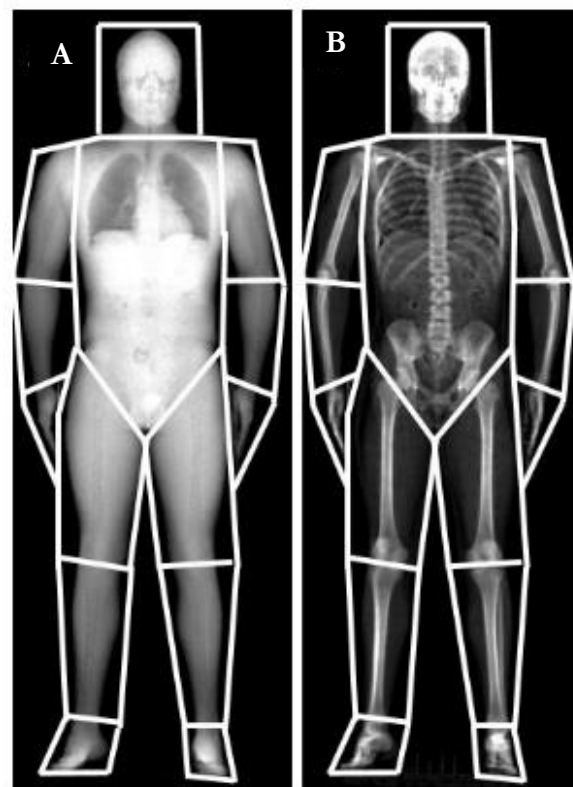


Figure 6.2: Example of DXA scan images delineated into the fourteen segments used in this research. A) provides an example of a high attenuation image which is inclusive of soft tissue mass. B) provides an example of the low attenuation image which shows the skeletal structure.

All fourteen appendicular segments for each athlete scan were analysed by the same investigator over five separate days (with at least 24 hours between analyses) and re-analysed by four independent investigators following the initial analysis. This was performed to ensure consistency in the assessment of body segment masses using DXA scans. All investigators were required to follow the delineation protocol of Rossi et al. <sup>284</sup> to ensure consistency across investigators. Reliability of segment masses obtained from the same rater and independent raters was assessed through the use of ICCs and coefficients of variation (CV), which were calculated using statistical analysis software (IBM SPSS Statistics 24 Software for Windows). The strength of reliability for the ICC coefficients was classified by Hopkins <sup>258</sup> ( $R \geq 0.3$ : moderate;  $R \geq 0.5$ : strong;  $R \geq 0.7$ : very strong;  $R \geq 0.9$ : nearly perfect; and  $R = 1.0$  is perfect).

Some athletes were unable to maintain the standard anatomical position recommended for a DXA scan,<sup>279</sup> meaning their limbs were overlapping in the DXA scan. A limitation of the use of pre-existing scans meant that under such circumstances the overlapping limbs were excluded from the analysis, and mass could not be estimated for these segments. Bilateral symmetry was assumed for affected limbs only to provide an estimate of total body mass to facilitate the verification of the segmentation processes. The asymmetry between masses of left and right limbs ( $m_L$  and  $m_R$ , respectively) was quantified using the asymmetry index (AI) presented by Bell et al.<sup>286</sup>

$$\text{AI: } 100\% \times 2(m_R - m_L)/(m_R + m_L) \quad \text{Equation 6.1}$$

### *Musculoskeletal Model*

The Upper Extremity Dynamic Model<sup>287</sup> was used to calculate the muscle forces required for wheelchair propulsion using OpenSim software.<sup>133</sup> This model was designed to represent the anthropometry and muscle force-generating characteristics of a 50<sup>th</sup> percentile adult male. The model and marker placements can be observed in Figure 6.3. In the generic model, bone length data and inertial parameters were obtained from anatomical studies presented in the literature, including cadaver specimen, while peak isometric force was determined from published muscle volume and isometric joint strength data from healthy young adults.

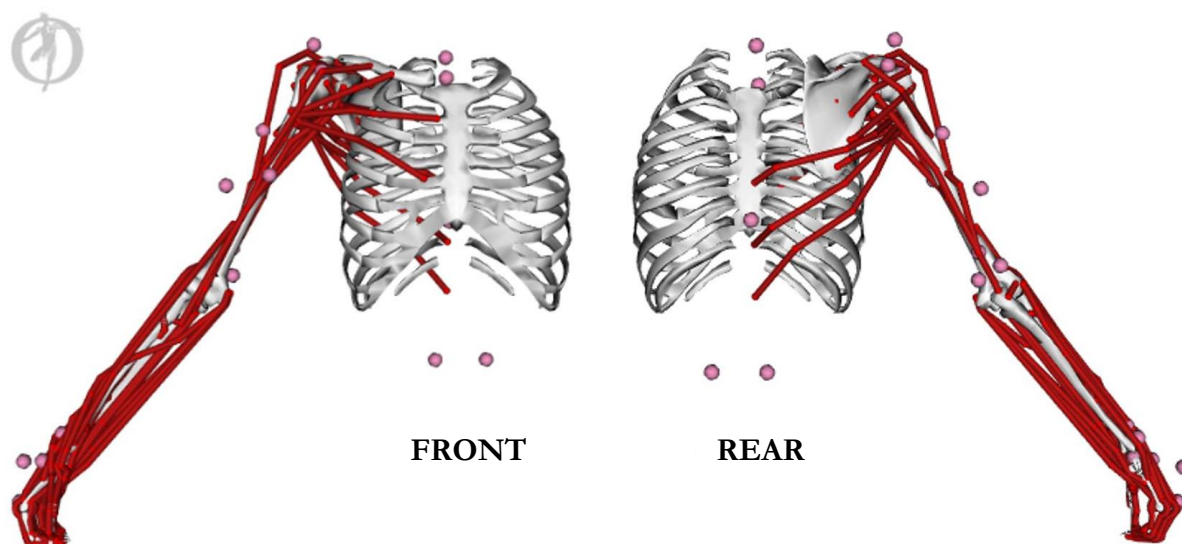


Figure 6.3: Musculoskeletal model used in research, highlighting the muscles modelled and marker placements used to actuate the model.

---

Output joint torques included:

- thorax (tilt; list (increase/decrease trunk relative to horizontal); rotation);
- sterno-clavicular (rotation; elevation; protraction);
- acromio-clavicular (flexion; rotation; abduction);
- glenohumeral (rotation, elevation, plane (adduction/abduction));
- humero-ulnar (flexion/extension); and,
- radio-ulnar (pronation/supination).

An additional three reaction forces were reported:

- thorax (mediolateral ( $F_x$ ); anteroposterior ( $F_y$ ); elevation/depression ( $F_z$ ))

Generalised forces at the joint are calculated as follows:

$$\sum_{m=1}^n [(a_m f(F_m^0, l_m, v_m))] r_{mj} = \tau_j \quad \text{Equation 6.2}$$

Where  $n$  is the number of muscles in the model,

$a_m$  is the activation of the muscle (value between 0 and 1),

$F_m^0$  is the maximum isometric force generating capacity,

$l_m$  is muscle length,  $v_m$  is the shortening velocity of the muscle,

$r_{mj}$  is the muscle moment arm about the  $j^{\text{th}}$  joint axis, and

$\tau_j$  is the generalised force acting about the  $j^{\text{th}}$  joint axis.

This was used to solve a minimum stress cost function (Equation 6.3) which calculated the muscle forces during propulsion.

$$J = \sum_{m=1}^n (a_m)^p \quad \text{Equation 6.3}$$

In this study,  $p$  was set at 2. The solver is constrained by force-length-velocity properties of the muscles, which are all defined during the development of the musculoskeletal model. The muscle forces required to reproduce measured kinetics and kinematics using the default cost function in OpenSim, which minimises the sum of activations squared.<sup>133</sup> Despite relative insensitivity for the user-defined constant  $p$  for values higher than 2,<sup>288</sup> discrepancies may have been introduced by incorrect objective function selection. For example, research by Laschowski et al.<sup>289</sup> has suggested that for wheelchair motion, minimising angular joint accelerations is the most effective. However, these capabilities are not available within the OpenSim environment, with only the single cost-function available for use.

From Equation 6.2 and Equation 6.3, as the maximum isometric force-generating capacity of the muscles spanning the joint increases, the activation of each of the muscles is decreased. This alters the relative contribution of the muscle in the overall cost function  $J$ . Therefore, the calculation of individual muscle forces can be sensitive to the maximum isometric force generating capacity.

Total muscle force was obtained by summing the forces of the muscle elements within the model used. Forces were expressed as absolute values, as well as the percentage of the maximum defined in the generic model to highlight the influence of the maximum force generating capacity parameter.

It is acknowledged that the Upper Extremity Dynamic Model is a single limb (right) model, and hence unable to measure the asymmetries which may be present. As no pathological conditions (or physical impairment) were present in the upper extremity of the analysed athletes, it can be assumed that these asymmetries would be minor. Thus it can be concluded that this approach will introduce fewer uncertainties than through the development of a custom, full body musculoskeletal model. Hence, the use of a pre-verified musculoskeletal model of a single limb is justified, and representative for concluding from this work.

Adaptations were made to this model to reflect the subject-specific inertial and anthropometric parameters. Subject-specific segment masses were obtained from the analysis of DXA scans, in a similar procedure to what is reported in the literature.<sup>282-284</sup> Moments of inertia were scaled to match the subject-specific segment masses. Segment dimensions were obtained through marker based scaling approaches, following best practice guidelines. Although skeletal ratios can be precisely measured from DXA data, it has been shown that each pixel within an image has a precision of 1.3cm.<sup>290</sup> Bone lengths were not measured through DXA data, due to the probable introduction of random errors, with concerns specifically regarding the location of joint centres which are established based on marker placement.

---

In the standard OpenSim methodology, fictitious sets of actuators (reserve actuators) are introduced into the simulation to accommodate for the dynamic inconsistencies between kinematic and kinetic data. The reserve actuators intend to supplement the forces which the muscle actuators cannot resolve alone.<sup>291</sup> Within the computational framework, if a muscle actuator (muscle forces spanning a joint) cannot produce the force required for motion, reserve actuators are recruited. Reserve actuators were applied for each degree of freedom within the model with each optimal force value set at 200 N. The value of optimal force chosen in this study was established by performing a sensitivity analysis on the influence of the optimal force value on outputs (using values of 10 N, 50 N, 75 N, 100 N, 150 N, 200 N and 1000 N). Details of this study can be found in Appendix C.1.

The musculoskeletal model utilised within this research was designed to represent the 50<sup>th</sup> percentile male. However, this model was being used for both male and female athletes. Only the Thoracolumbar Spine Model<sup>292</sup> in OpenSim software contains both a male and female model. Both of these are representative of the 50<sup>th</sup> percentile. For the female model, limb segment sizes are scaled down from the male equivalent, with updated body mass distribution and centre of position. Although a female model was not used in this research, subject-specific inertial parameters and marker-based scaling were used to minimise the impact of these errors. Although some dissimilarities may still result, it was outside the scope of this research to validate a female musculoskeletal model.

### *Experimental Propulsion Task*

After familiarisation with the experimental setup, subjects propelled their own racing wheelchair on a treadmill at self-directed speeds (Athlete I: 26 km/hr, 27 km/hr, 28 km/hr, Athlete E: 22 km/hr, 23 km/hr, 24 km/hr), which were reflective of typical race speeds. Athletes performed conventional propulsion for one minute at the targeted speeds, with three periods of 10s data capture collected at steady state (Section 4.2). Kinematic data were only collected for two of the athletes, as they were the only participants who integrate treadmill-based propulsion into regular training. Kinematics were not modelled using the inertial parameters obtained from the remaining three athletes to ensure biomechanical integrity and relevance of modelling results.

### *Data Processing*

As no practically viable and validated method for the collection of reaction forces at the pushrim is currently available for use in wheelchair racing (as emphasised in Chapter Two:), external loads at the hands were estimated. It was established in Chapter Five that the IMU provided a beneficial tool for

the estimation of applied kinetics in the forwards direction, however out of plane forces were less reliable. An alternative approach is the estimation of reaction forces through kinematic data. This methodology is restricted to laboratory-based testing only, however, places no impediment on athlete motion, and makes use of pre-existing data. Additionally, this method has demonstrated a reliability of 6% for vertical force, 10% for anterior force and 13% for sagittal moment during gait.<sup>293</sup>

As joint reaction forces are all equal and opposite, the sum of external (joint reaction) moments can be derived by taking the sum of translational acceleration vector of each segments mass centre ( $\ddot{r}$ ), multiplied by its mass ( $m$ ), as presented in Ren et al.<sup>293</sup> The translational acceleration vector of each limb segment was obtained through Inverse Kinematics analysis. It was assumed that the left and right sides of the trunk contributed equally to propulsion, meaning half of the total head and torso mass estimated from DXA was incorporated into the external load calculations. Therefore, the external loads on the hands were estimated as follows, assuming a standard value of gravity ( $g = 9.81 \text{ m/s}^2$ ):

$$\begin{aligned} \Sigma F_{ext} = & \left( \frac{1}{2} m_{Head \& Neck, Torso} (\ddot{r}_{Head \& Neck, Torso} - g) \right) + m_{Upper Arm} (\ddot{r}_{Upper Arm} - g) + \\ & m_{Forearm} (\ddot{r}_{Forearm} - g) + m_{Hand} (\ddot{r}_{Hand} - g) \end{aligned} \quad \text{Equation 6.4}$$

Output joint torques were normalised against results from the baseline (generic model). As data were cyclic, an RMS value was taken of each output joint torque.

## 6.2 THE EFFECT OF ALTERING INTENSITY THRESHOLDS IN DXA SCANS ON THE CALCULATIONS OF BODY SEGMENT MASSES

### 6.2.1 INTRODUCTION

The analysis of DXA scans provides a practically effective and reliable estimation of body segment masses (Section 2.3). A DXA scan generates a black and white image of the human musculoskeletal system. The whiteness of each pixel within a scan, or its intensity, has a value between 0 (black) and 255 (white: Figure 6.4A). A histogram demonstrating the distribution of all intensities within an image accompanies each DXA scan (Figure 6.4B). DXA software typically uses thresholding to optimise the dynamic range of the intensity distribution. However, the dynamic range thresholds can be manually adjusted prior to the analysis of a scan (Figure 6.4C).



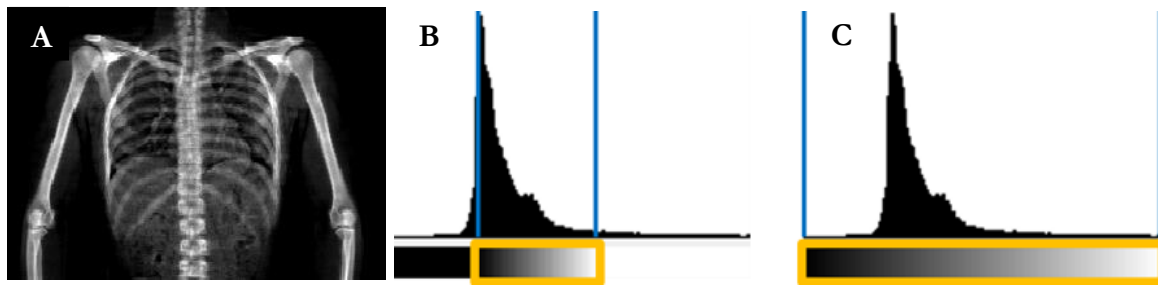


Figure 6.4: A) Example of a DXA scan, B) the histogram with default thresholds and C) the thresholds extended to maximum.

Software to collect DXA data typically uses thresholding to maximise the dynamic range of the images collected. The threshold values used cannot be fixed constant, due to variations in radiofrequency field inhomogeneity, receiver coil sensitivity profile, main magnetic field inhomogeneity, or imperfect properties of the pulse sequences.<sup>294</sup> To the author's best knowledge, no documentation currently exists for a standardised protocol regarding gold standard bounds to ensure the best accuracy. By altering the intensity thresholds of an image, greater emphasis is placed on either the higher (bone) or lower (soft tissue) frequency musculoskeletal elements, potentially altering the total mass distribution.

Greater dynamic ranges may compromise the distinction between pixels due to the fixed intensity range (0-255). This may result in errors, as the impaired ability to differentiate between soft tissue and bone, for example, will affect mass calculations. This can be visually observed in Figure 6.5. It can be seen that when only the lower bound is minimised, the whiteness of the distribution is maintained (Figure 6.5A), however, loses the intensity of the lower end (i.e. black). When all bounds are maximised (Figure 6.5C), the distribution of intensity is lost.

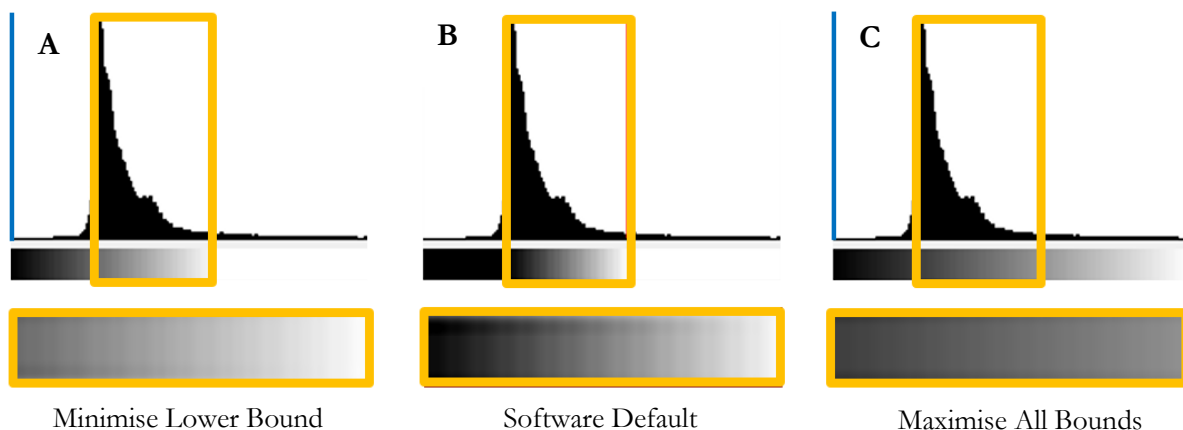


Figure 6.5: Comparison of the distribution of pixels across the majority of DXA scan data.

This research aimed to understand the sensitivity of mass segment calculations obtained using DXA scans with varying intensity thresholds to understand the associated impact of this variation on computational simulations. It was hypothesised that the differences in segment mass values between threshold protocols would significantly impact the accuracy of computational simulation outputs.

## 6.2.2 METHODS

### *Data Processing*

Each athlete's DXA scan was analysed three times, with each one undergoing a different intensity threshold protocol (Figure 6.6). Segment boundaries remained consistent for each of the three analyses of each athlete when intensity thresholds were manipulated. The three intensity threshold protocols can be defined as; the software default (original), minimising the lower threshold value while retaining the software default upper threshold value (standard), and minimising the lower threshold value while maximising the threshold value, and hence including all intensities within an image (maximum). Images were segmented into limb segments using the approach outlined in Section 6.1.

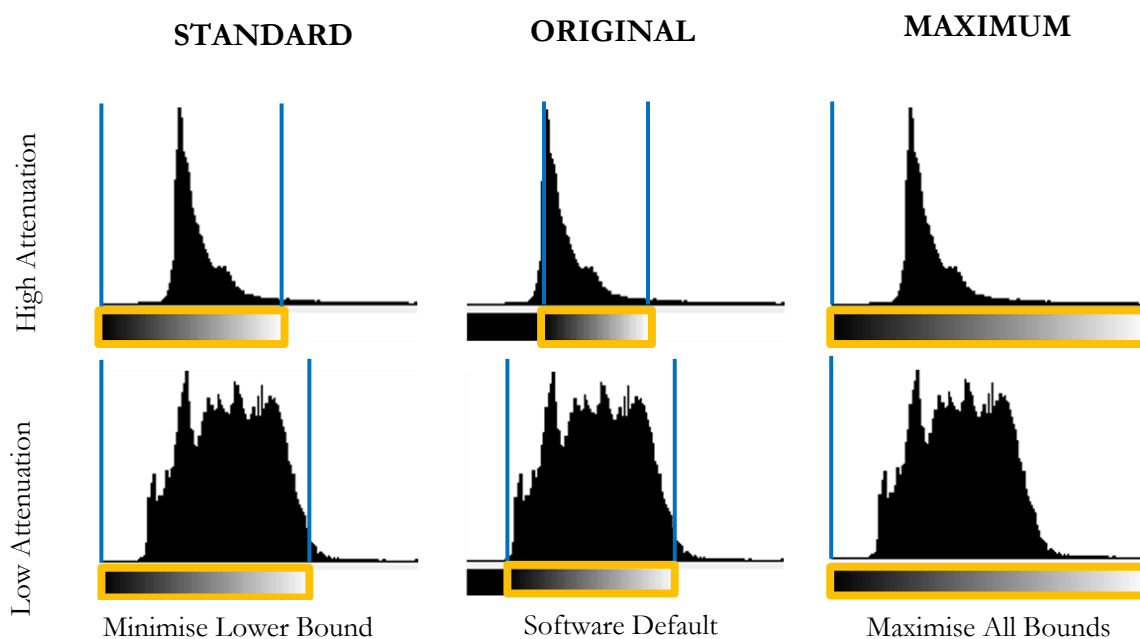


Figure 6.6: Threshold protocols for the high attenuation (soft tissue: top) and low attenuation (bone: bottom).

---

### 6.2.3 RESULTS

Differences between the raw DXA scan, and with adjusted threshold protocols are presented qualitatively in Figure 6.7. There is an evident increase in the presence of soft tissue when the standard and maximum approaches, as compared to the original (default) analysis. Similarly, the contrast and whiteness of bones are visibly reduced in the maximum approach. Similar trends were observed in the comparison of soft tissue scans but to a lesser extent.

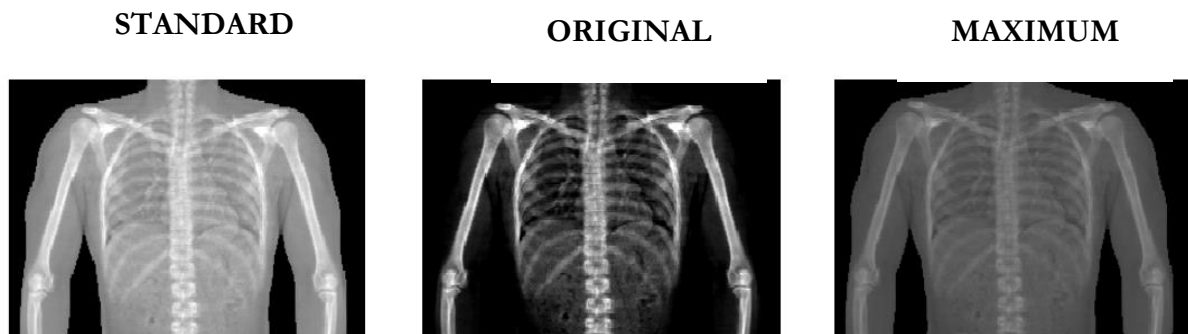


Figure 6.7: Comparison of DXA scan data due to different threshold intensities.

Qualitatively, it is clear that the maximum approach has a more significant impact on the estimation of body segment mass parameters (for a single athlete, Athlete M). Differences of 0.21 % total body mass were observed across all limb segments using the standard approach (Figure 6.8). However, differences of up to 5.57 % total body mass were observed in the torso estimation for Athlete M when using the maximum approach. Although segment masses of the extremities were overestimated, they were unable to balance the substantial underestimation of the trunk, resulting in a net underestimation from the use of the maximum approach (99.6% total body mass). Put simply, altering thresholds artificially altered the distribution of soft tissue and bone within the body.

Trends observed for Athlete M (as presented in Figure 6.8) were consistent across the remaining athletes, with trunk mass consistently underestimated when using the maximum approach ( $91.9 \pm 0.0$  % total body mass, ranging between 89.9% through 93.4 % of the original value). Body mass distribution ranged between 99.9% through 100.3% of total body mass when analysed using the standard thresholding protocol (Figure 6.9), while the maximum approach consistently underestimated total body mass (97.1% through 99.6%). However, bony segments (hands and feet) were significantly impacted segments, being up to 157.1% and 147.0 % greater, respectively than the values obtained using the standard approach. Absolute differences for all athletes are quantified in Table 6.2.

6. DEVELOPMENT OF A SUBJECT-SPECIFIC, 3D MUSCULOSKELETAL MODEL

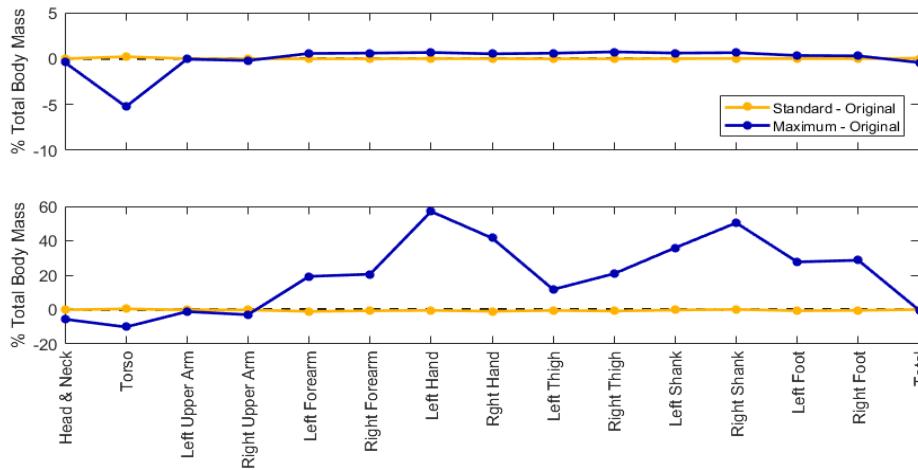


Figure 6.8 Differences in mass segments based on alterations in intensity.

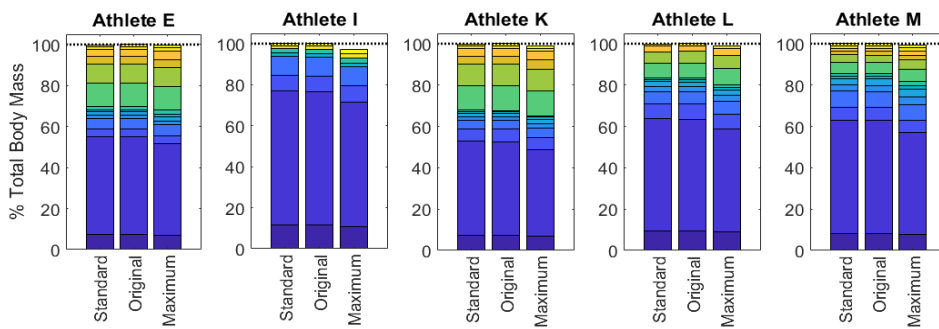


Figure 6.9: Comparison of body mass distribution based on threshold intensity protocol.

Table 6.2: Changes in segment mass based on intensity threshold protocol.

	<b>Standard <math>\Delta</math></b> <b>(% Segment Mass)</b>	<b>Maximum <math>\Delta</math></b> <b>(% Segment Mass)</b>
Head and Neck	$-0.1 \pm 0.4$	$-4.6 \pm 6.3$
Torso	$0.4 \pm 0.4$	$-8.2 \pm 1.4$
Left Upper Arm	$-0.4 \pm 0.4$	$1.7 \pm 2.3$
Right Upper Arm	$-0.4 \pm 0.4$	$1.5 \pm 2.9$
Left Forearm	$-0.8 \pm 0.3$	$22.3 \pm 5.8$
Right Forearm	$-0.6 \pm 0.3$	$22.2 \pm 4.4$
Left Hand	$-0.8 \pm 0.6$	$34.9 \pm 13.7$
Right Hand	$-0.7 \pm 0.3$	$29.9 \pm 12.7$
Left Thigh	$-0.4 \pm 0.2$	$4.2 \pm 6.2$
Right Thigh	$-0.6 \pm 0.2$	$8.2 \pm 10.3$
Left Shank	$-0.3 \pm 0.1$	$23.5 \pm 11.2$
Right Shank	$-0.3 \pm 0.4$	$28.2 \pm 15.8$
Left Foot	$-0.8 \pm 0.6$	$28.7 \pm 12.6$
Right Foot	$-0.8 \pm 0.6$	$24.6 \pm 16.3$

An example of a propulsion cycle can be seen in Figure 6.10. Estimated joint output torques are highly sensitive to the analysis approach of DXA scans (Figure 6.11). Agreement between the standard and original approaches was  $99.2 \pm 0.08\%$  (as calculated by  $\text{Standard/Original} \times 100 \%$  (Equation 6.5) for Athlete E, and  $95.2 \pm 0.2\%$  for Athlete I. The reductions for Athlete I are the direct result of two outputs (sternoclavicular elevation and glenohumeral flexion). However much lower agreement ( $3.6 \pm 4.5\%$ ) can be observed for all joint reaction moment estimates when using the maximum approach. Figure 6.11 also demonstrates the higher range in estimated joint reaction moments using the maximum protocol, as compared with the standard and original protocols. This demonstrates that through the poor estimation of input parameters, there is a change in system dynamics, and hence there is a noticeable impact of the thresholding intensity in biomechanical modelling.

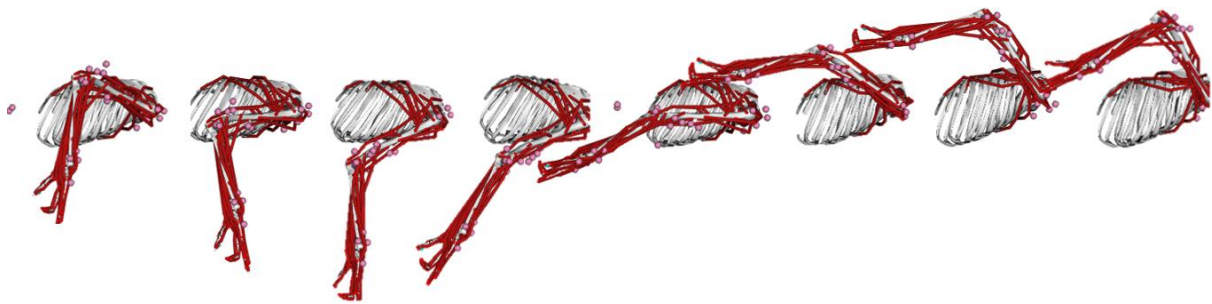


Figure 6.10: Propulsion cycle modelled in OpenSim using the upper extremity dynamic model. Pink dots represent markers.

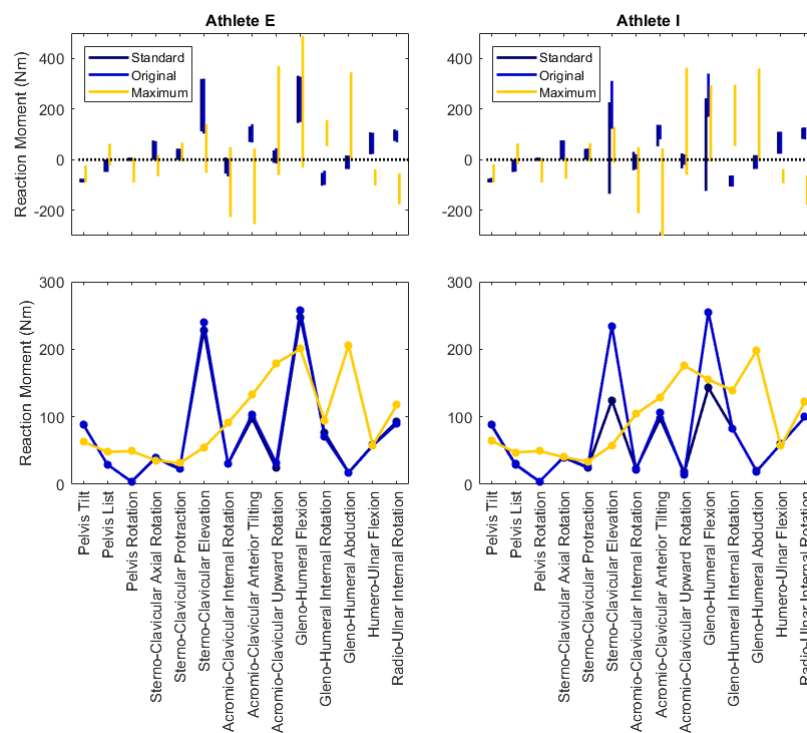


Figure 6.11: Influence of segment mass definition on inverse dynamics results (joint reaction torques).

### 6.2.4 DISCUSSION

The processing of DXA scans is subject to a user-defined intensity threshold. In this study, the reliability of the processing of the DXA scans (based on the definition of threshold intensity) was established. Evident between-method variability was observed for the estimation of body segment mass parameters, which was found to influence system dynamics and the output joint reaction moments dramatically.

While the standard method estimated limb masses consistently with the original approach, it underestimated the trunk segment and correspondingly total body mass. This error may have been a result of poor differentiation between different intensities as a consequence of including too broad a range of intensities within the image. This error was however very minor and had a negligible impact on the joint reaction estimates in this research. Interestingly, the standard method had opposite results to the maximum method, whereby total body mass was calculated the same as the original approach, however substantial variation was demonstrated in the magnitude of each limb. These differences can be assumed as a consequence of the artificially applied high pass threshold from the standard and maximum approaches, which overestimates bony tissue presence, such as the hand which can be seen to differ by approximately 60% (right hand in Figure 6.8). Generally, the denser bony regions were overestimated while the soft tissue regions, predominantly in the trunk, were underestimated. It can be assumed that these differences would have a significant impact on the accuracy of computational simulations. Based on the highly dynamic motion of wheelchair racing propulsion, and hence the high centre of mass accelerations of the upper extremities, the hand segments are also the most susceptible to errors.

Guidelines for defining the ideal threshold intensity were not present within the accompanying user manual of the DXA scans analysed. As such extreme cases were analysed in this study, recommended best practice cannot be identified. Further research to find the ideal values is recommended, with validation to be performed using phantom scans (scans of blocks with known mass and density). The remaining research in this thesis uses data obtained from the original thresholding approach.

### 6.2.5 CONCLUSION

This study demonstrated that the intensity threshold definition influences body segment mass calculations using DXA processes. While no standardised measure currently exists, it appears that the machine default (original) is most reliable and hence least likely to artificially introduce errors into computational simulations, which would be propagated throughout the analysis.

---

## 6.3 MASS DISTRIBUTION OF WHEELCHAIR ATHLETES ASSESSED USING DXA SCANS

### 6.3.1 INTRODUCTION

As a consequence of a physical impairment, such as spinal cord injury, individuals who use wheelchairs demonstrate anthropometric variation to able-bodied counterparts. Such variations are exemplified through a substantial increase in muscle atrophy<sup>30, 295, 296</sup> reduced bone mineral content,<sup>30, 295</sup> and increased presence of adipose tissue.<sup>30</sup> As a result, musculoskeletal geometries and soft tissue composition are dissimilar in the affected limbs of those with spinal cord injuries as compared to their able-bodied counterparts. These dissimilarities, however, are not necessarily observed in unaffected limbs above the level of spinal cord lesion. Additionally, an increased presence of skeletal tissue in the upper extremities may ensue as a consequence of the tissue adaption resulting from the loading during training and competition. It was seen in Section 6.2 that the definition of inertial parameters has an impact on the reliability of the simulation.

This study aimed to first quantify the variation in body segment masses of elite wheelchair racing athletes with those from other populations (able-bodied and non-athletic, able-bodied and athletic, and physically impaired athletes). It was then aimed to understand whether variations from generic and individualised subject-specific models had a significant impact on the estimation of joint reaction moments. It was hypothesised that generic parameters would underestimate segment parameters in the upper extremity (due to muscle hypertrophy), while overestimate them in the lower extremity (due to muscle atrophy). As a consequence, it is anticipated that joint reaction moments at the shoulder would be significantly underestimated when generic body segment mass parameters are utilised.

### 6.3.2 METHODS

#### *Data Processing*

Segmental masses were compared against three populations presented in the literature; commonly referenced anthropometric data of various able-bodied, non-athletic (Generic) populations,<sup>285, 297-305</sup> elite able-bodied athletes (Elite Swimmers),<sup>284</sup> and a para-athlete population (Para Curlers).<sup>282, 283</sup> Generic data were comprised of a comprehensive, but non-exhaustive sample of body segment inertial parameters representing varying ages and ethnicities to develop a broad representation of an able-bodied, and non-athletic population. For the generic model, the scaling of limb lengths was achieved (within OpenSim) through matching the distance between the locations of the virtual markers (which were defined on the musculoskeletal model) with the experimental markers. Mass scaling was either

done through the measured mass values (actual) or through the generic approach used by OpenSim (using the measured mass of the right arm).

Output joint torques were normalised against results from simulations incorporating the generic scaling strategies employed for a mass-matched model. As data were cyclic, a root mean square (RMS) value was taken of each output joint torque.

### *Statistical Analysis:*

Coefficients of variation (CV) less than 5% were considered highly reliable. RMS signal amplitudes of the output joint torques calculated in OpenSim were computed in MATLAB. To establish whether changes in output torques between the actual and generic inertial parameter input were significant, data were compared using an independent-samples Kruskal-Wallis test. The independent variable in this analysis was the RMS difference in joint reaction moments, with three levels corresponding to the limb segments. Additionally, relationships between the magnitude of the difference between output reaction torques, and actual and generic segment masses were determined using Spearman's Correlation.

### 6.3.3 RESULTS

Nearly perfect intra- and inter-rater reliability of estimated masses were observed for all segments, and total body mass ( $R_{\text{INTRA}} > .990$  and  $R_{\text{INTER}} > .990$ ). Furthermore, very high reliability was demonstrated across all appendicular segments and total body mass ( $0.5\% < CV_{\text{INTRA}} < 3.1\%$  and  $0.6\% < CV_{\text{INTER}} < 4.7\%$ ). Verification of limb segment masses (arms, right arm, left arm, legs, right leg, left leg, trunk and total body) were compared between the outputs of this research and the direct measurements from the DXA software. High agreement ( $98.6\% \pm 5.3\%$ ) was observed between the two sets of data for Athletes E, K, L, M and N. Athlete I data was not included in this comparison based on the different posture assumed when taking the scan.

Clear variation in body mass distributions was observed across all five wheelchair racing athletes (Figure 6.12). Due to overlapping thigh and shank segments in the DXA scan of Athlete I, segment masses were not calculated, with total body mass calculated using measured body mass values and not the sum of all segment masses, as was done for Athletes L, M, E and K. Largest between-athlete variation was observed for the torso and thigh segments, and was approximately 10% total body mass for the torso (Athlete E: 46.5%, Athlete K: 56.7%) and 15% total body mass for the thigh (Athlete L: 7.8%, Athlete E: 22.4%), respectively. These differences were supported with large CV values for each



of the segments; head: 20.5%, thorax: 13.6%, upper arm: 27.1%, forearm: 24.6%, hand: 23.7%, thigh: 39.3%, shank: 33.0%, and foot: 12.0%. Consistent measurements were observed (mean  $\pm$  standard deviation) for the following segments within the population sample: foot (1.1%  $\pm$  0.0%), shank (2.2%  $\pm$  0.1%), head and neck (2.2%  $\pm$  0.1%), hand (2.0%  $\pm$  0.1%), and forearm (5.1%  $\pm$  0.3%).

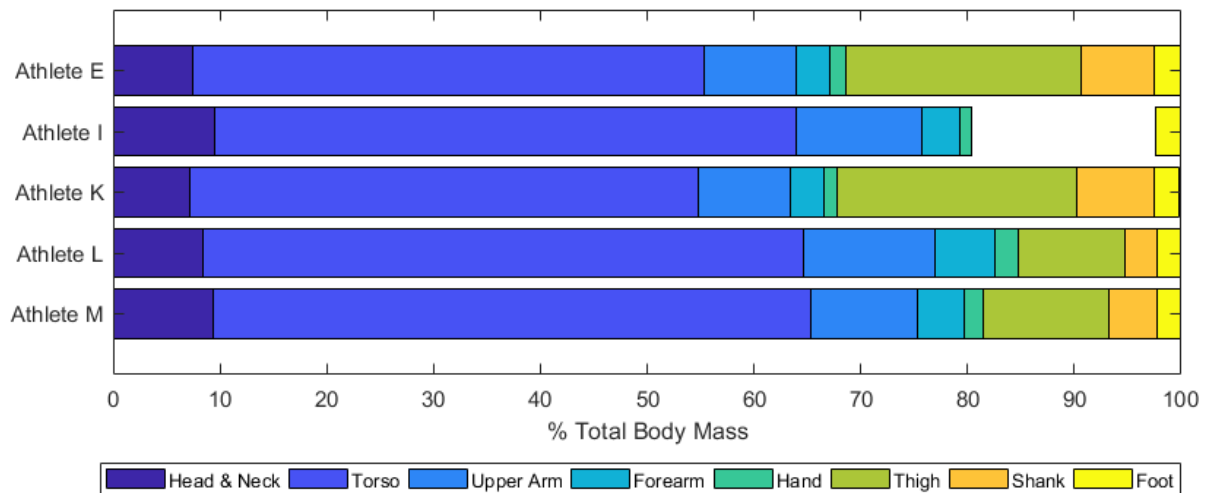


Figure 6.12: Body mass distribution of all athletes. Thigh and shank segments of Athlete I were excluded from analysis due to the presence of overlapping limb segments.

Notable asymmetries were present for some athletes, predominantly in the lower extremities (Figure 6.13). Larger AI values included upper arm (Athlete I: 41.7%, 3.0 kg; Athlete L: 32.97%, 2.0 kg), thigh (Athlete L: 62.4%, 3.1 kg; Athlete M: 22.3%, 1.3 kg) and shank (Athlete L: 24.6%, 0.4 kg).

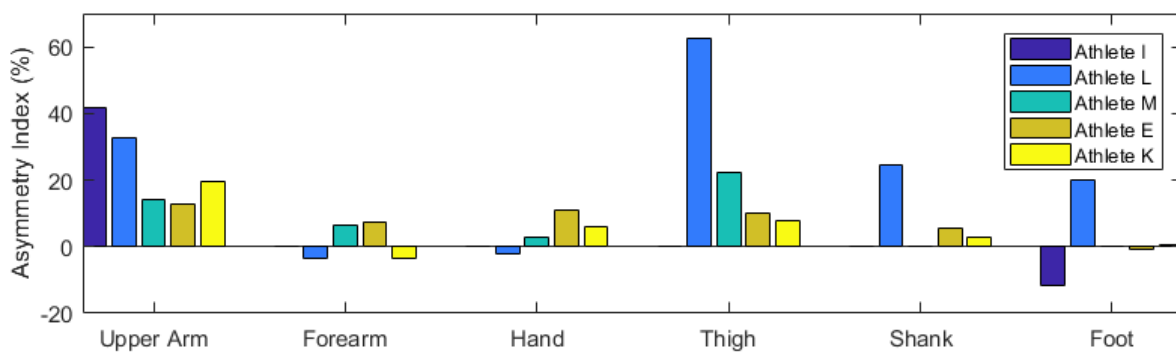


Figure 6.13: Appendicular mass asymmetry indices calculated from DXA data. Positive values indicate right side bias, with larger magnitudes demonstrating larger asymmetry.

Considerable inter-population variation in mean body mass distribution (Figure 6.14) and intra-population variability (Figure 6.15) was also observed. Greatest between-population variance was observed in mean thigh mass (Generic: 24% TBM, Elite Swimmers: 26%, Para Curlers: 17%, Wheelchair Racers: 15%) and torso mass (Generic: 47% TBM, Elite Swimmers: 48%, Para Curlers: 53%, Wheelchair Racers: 52%), with upper arm measurements being twice as large for wheelchair racers, than the able-bodied, non-athletic population analysed (Generic: 6% TBM, Wheelchair Racers: 11%). Maximum differences between methods for individual measurements of each segment ranged between 0.1% TBM (hand) and 13.7% TBM (torso).

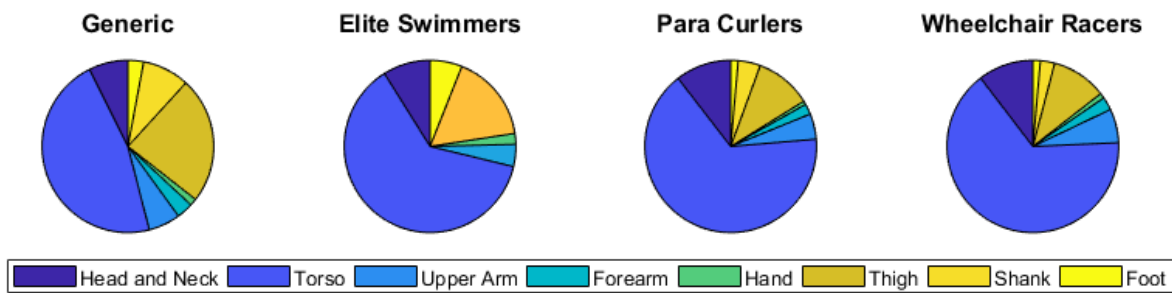


Figure 6.14: Population-based averages for body mass distribution.

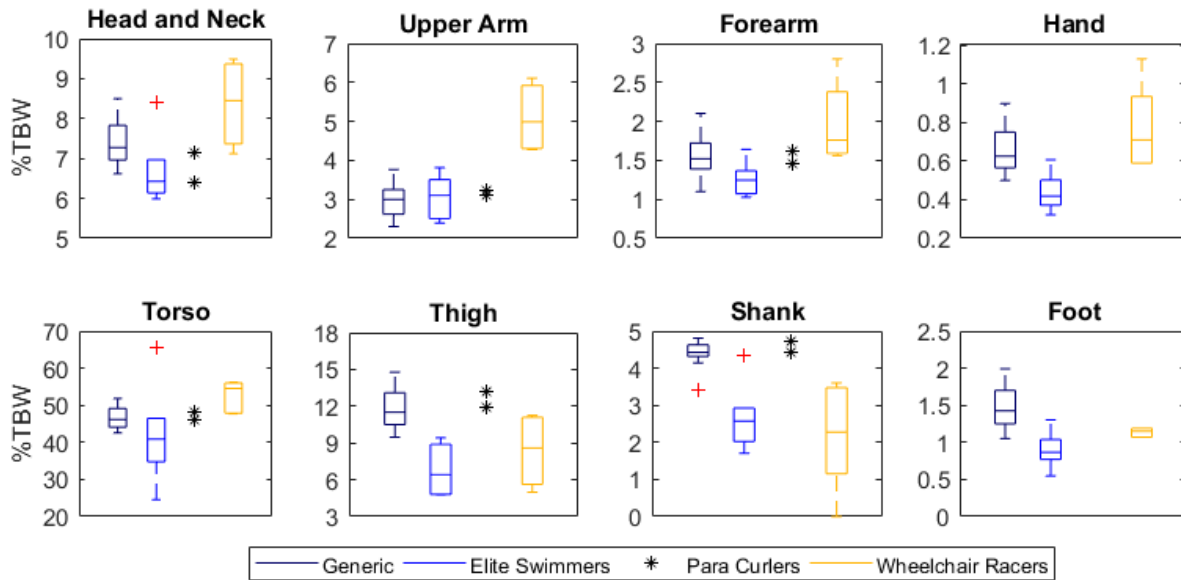


Figure 6.15: Segment masses as presented as a percentage of total body mass (mean of left and right data). Box plots demonstrate mean and range of population sample data, with outliers denoted by a “+”.

Significant differences were observed between all athletes for the estimated segment masses and those of the able-bodied, non-athletic population sample for the torso ( $p < .050$ ), upper arm ( $p < .010$ ), forearm ( $p < .010$ ), thigh ( $p < .010$ ), shank ( $p < .010$ ), and foot ( $p < .010$ ). Significant differences were also observed between segment masses of the wheelchair athletes within this study, and the elite swimming athletes for the head and neck ( $p < .010$ ), torso ( $p < .010$ ), upper arm ( $p < .010$ ) and forearm ( $p < .010$ ) and for the upper arm ( $p < .010$ ), forearm ( $p < .050$ ), and upper arm ( $p < .050$ ) of the para curler athletes.

As stated in Section 6.1, kinematic data was only available for two of the five athletes (Athlete E and I), and so the remainder of the results are presented only for these athletes. Use of generic total body distribution poorly matched the DXA obtained values, with segment masses ranging between 66.7% and 216.7% of the DXA obtained values. For the specific model used, it was observed that the greatest variation between scaling approaches (2.3% total body mass) was observed in the upper arm mass of Athlete E (Table 6.3). Output torques using generic scaling approaches overestimate the torques calculated using measured mass distributions (mean RMS variation Athlete I: 10.2% ( $100 - \text{Actual}/\text{Generic} \times 100\%$ ), Athlete E: 7.0% maximum RMS variation Athlete I: -36.3%, Athlete E: 31.5%, Figure 6.16). Athlete E demonstrated smaller variations between actual and generic parameter use, as would be expected based on the greater agreement between segment masses input to the model.

Table 6.3: Differences in mass distribution of the computational model between scaling approaches (actual and generic).

Segment	Athlete E Actual (%)	Athlete E Generic (%)	Athlete E Difference (%)	Athlete I Actual (%)	Athlete I Generic (%)	Athlete I Difference (%)
Clavicle	0.5	0.3	0.2	0.5	0.4	0.1
Scapula	1.2	1.2	0	1.3	1.6	-0.3
Humerus	4.4	3.5	0.9	6.9	4.6	2.3
Ulna	1.3	1.9	-0.6	1.4	2.6	-1.2
Radius	0.3	0.4	-0.1	0.3	0.5	-0.2
Proximal Row	< 0.1	< 0.1	0	< 0.1	< 0.1	0
Hand	0.8	1	-0.2	0.6	1.3	-0.7

The Kruskal-Wallis test revealed that the difference in output joint torques, as the percentage of the actual value was not significantly associated with limb segment ( $H(2) = 3.0, p = .223$ ). A non-significant correlation was observed between the percentage difference in limb mass between the actual and generic scaled limb masses with the difference in output torques ( $r = -.343, p = .139$ ).

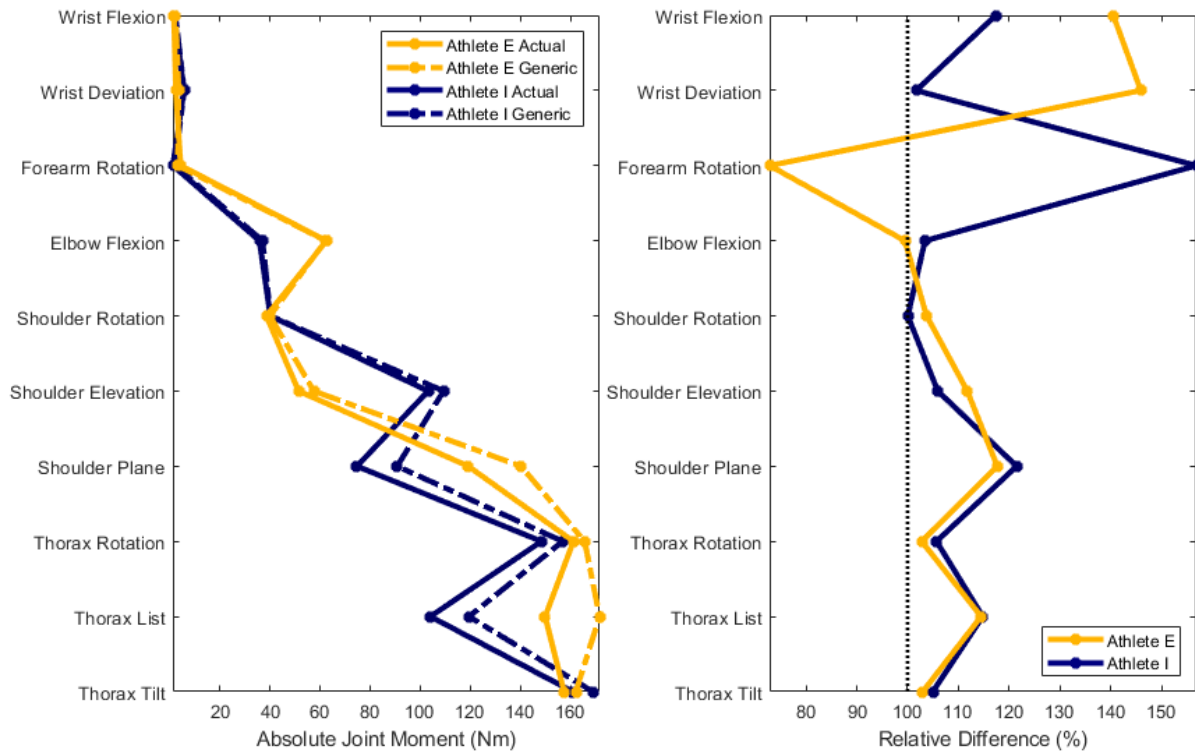


Figure 6.16: Variation in joint reaction moments calculated using inverse dynamics, between athlete-specific and total body mass-matched scaled models.

#### 6.3.4 DISCUSSION

Individual mass segment values were obtained from fourteen manually delineated segments using DXA scans of three elite wheelchair racing athletes and two international-level triathletes. The purpose of this study was to obtain and compare athlete-specific measurements with the generic input parameters currently used in wheelchair literature to ascertain measures of significance of these parameters in the quantitative analysis of wheelchair propulsion for elite athletes. This study addressed the second aim of the thesis, demonstrating methods capable of estimating subject-specific body segment parameters for input into a musculoskeletal model. Results also highlight the importance of the subject-specific modelling approach, and not relying on generic data.

Use of generic mass distribution data in computational modelling was considered inadequate for two reasons; the substantial between-method variation ( $\sim 10\%$ , torso, Figure 6.15), and low relevance to the mass parameters of wheelchair racing athletes. This is in support of previous literature, which has questioned the generalisation of generic body segment inertial parameters, and the necessity of obtaining in-vivo, subject-specific parameters for biomechanical modelling.<sup>140-142</sup> Differences between methods correlate to modelling error, highlighting that the current methods of employing generic body segment inertial parameters and scaling procedures are inadequate. As it was demonstrated that

---

differences in limb segment masses (measured and generic) do not directly correlate with differences in joint reaction moments, it can be suggested that errors in the definition of the model can change the system dynamics. This highlights the necessity of using subject-specific mass parameters for use in the analysis of wheelchair racing propulsion. Additionally, it can be suggested that the increased joint reaction moments at the shoulder for the generic scaled models may be a consequence of increased moment arms due to the mass being more distal from the joint.

This is the first research to report body segment parameter data from a population of wheelchair racing athletes. As hypothesised, substantial differences in segment masses were observed for wheelchair racing athletes as compared with the general population (including cadaver-based data), elite able-bodied athletes,<sup>284</sup> and elite para-curler athletes<sup>282, 283</sup> for the torso, upper arm, forearm, thigh, shank and foot segments. Greatest between-population variance was observed in mean thigh mass (Generic: 24% total body mass, Elite Swimmers: 26%, Para Curlers: 17%, Wheelchair Racers: 15%) and torso mass (Generic: 47% total body mass, Elite Swimmers: 48%, Para Curlers: 53%, Wheelchair Racers: 52%), with upper arm measurements being twice as large for wheelchair racers, than the able-bodied, non-athletic population analysed (Generic: 6% total body mass, Wheelchair Racers: 11%). Maximum differences between methods for individual measurements of each segment ranged between 0.1% total body mass (hand) and 13.7% total body mass (torso). Only the bony segments, such as the head and neck, demonstrated good agreement with the normalised mass segment values of commonly referenced anthropometric data of able-bodied data.<sup>285, 297-305</sup> This can likely be explained due to the higher presence of skeletal tissues in these limbs, and consequently, are less sensitive to the musculoskeletal adaptations resulting from training or atrophy (due to impairment). These findings confirm that generic models are often unsuitable for use within physically impaired populations. The use of subject-specific parameters will allow for more accurate computational biomechanical analysis of sporting wheelchair propulsion. In turn, this can identify whether athletes can gain greater efficiency and power from specific techniques, while also reducing the risk of attaining an overuse injury.

The magnitude of variation between the mass segments of Paralympic athletes and generic approaches is substantially lower than the most comparable literature of elite para curler athletes,<sup>282, 283</sup> despite adopting consistent delineation protocols. These differences result from the use of different normalisation approaches, specifically the denominator used. In the aforementioned literature, the denominator is segment masses, while in this research, the denominator was total body mass. Normalising against relative segment masses demonstrates greater sensitivity to smaller limb segments which have been demonstrated to be influential in this research. However, normalisation against total body mass was preferred in this work as total mass was more efficiently and accurately validated. Additionally, as high reliability was identified for the estimation of segment masses (98.6% of total

body mass), it can be assumed that there will be minimal errors from the conversion of data from an absolute to a relative measure.

Inconsistent boundary definitions of limb segments can overestimate between-method variations.<sup>143</sup> Substantial differences were still noted when comparing data from this study with data presented in the literature which used consistent boundary definitions. For example, thigh mass (as % total body mass) was 10.3 % in Clauser et al.,<sup>280</sup> 10.0% in Dempster<sup>281</sup>, and  $8.3\% \pm 3.4$  in this research. Therefore, although minor discrepancies in boundary definition may exist, there are still clear between-population variations, which are highlighted in this research. These differences highlight the importance of using subject-specific parameters for accurate biomechanical modelling.

The joint torques estimated in this research are of the same order of magnitude as presented in the literature when normalised for speed. Mean absolute elbow flexion torque from this research was approximately 5.1 and 8.9 times higher for Athlete I, and Athlete E, respectively (Athlete I: 35.9 N m, Athlete E: 62.6 N m) than other data presented in the literature ( $7.0 \text{ N m} \pm 0.2 \text{ N m}$ ).<sup>169</sup> This difference can be attributed to both the greater speed of propulsion presented in this research (8.1 m/s here vs 1.4 m/s in literature), with the alteration in wheelchair propulsion mechanics due to speed demonstrated frequently in the literature.<sup>64, 306, 307</sup>

### 6.3.5 CONCLUSION

The use of DXA scans was able to provide a reliable estimation of body segment inertial parameters. Wheelchair racing athletes have substantially different body segment mass properties to the general population currently used in computational modelling approaches. Athlete asymmetries, as well as inter-athlete variation of defined trunk mass by 9.3% total body mass, may impact joint moments, which would limit the reliability of the outputs of computational biomechanical analyses. This study hence revealed the importance of using subject-specific inertial parameters for use within computational modelling of wheelchair racing athletes. Future wheelchair propulsion research should incorporate subject specific in-vivo measurements to ensure confidence in the simulation outputs.

---

## 6.4 A STRATEGY FOR ESTIMATING MAXIMUM ISOMETRIC FORCE GENERATING CAPACITY OF WHEELCHAIR RACING ATHLETES

### 6.4.1 INTRODUCTION

Common musculoskeletal models utilise parameters obtained from cadaver studies, which is a method that has received much scrutiny in the literature for representing a biased sample population (e.g. Milgrom et al.<sup>308</sup>), which has limited generalisability, particularly for wheelchair athletes. Section 6.3 demonstrated the errors associated with this approach. Within a computational simulation, muscle forces are estimated as a distribution of joint loads across the muscle fibres crossing the joint. If maximum isometric force generating capacity is insufficiently defined during the development of the musculoskeletal model, the surrounding muscles will be recruited to complete the movement. However, in the process, muscle co-ordination strategies may be altered, and are hence representative of non-physiologically-plausible movements. As Spinal cord injury (SCI) results in altered skeletal muscle properties,<sup>28</sup> with further musculoskeletal adaption (hypertrophy) resulting from the extensive physical training,<sup>39, 40</sup> and highly dynamic and physically straining propulsion motion (Section 2.1),<sup>309</sup> improving maximum force generating capacity estimates in generic models is warranted.

The maximum force-generating capacity of a muscle can be directly or indirectly estimated through isokinetic dynamometry with muscle activations measured using EMG, respectively, with muscle PCSA estimated using medical scanning technologies. Literature has demonstrated good test-retest-reproducibility of dynamometer data at the shoulder, but, factors such as anatomical postures during testing, software and in particular angular velocity can limit its reliability.<sup>310</sup> While isokinetic dynamometry provides a good representation of the strength of an individual, movements tested are not reflective of the multiple degrees of freedom movement of wheelchair propulsion. Alternatively, EMG can gauge muscle activation. Apart from static or quasi-static activities, it does not directly correlate with muscle force,<sup>311</sup> and so it is better suited to analyses regarding excitation timings, such as in the work of Mulroy et al.<sup>26</sup> and Tries<sup>312</sup>.

The maximum force a muscle can produce is a function of both its specific tension (force generated per unit of cross-sectional area) and its physiological cross-sectional area. Imaging techniques have been used to relate the size of a muscle to its force-generating ability. Volumetric based estimations present a preferred method of evaluating the force-size relationship.<sup>313</sup> For example, O'Brien et al.<sup>314</sup> used MRI scans to obtain muscle volume, which was divided by optimal fascicle length at the angle of peak force, as measured using ultrasound images. Alternatively, this has been achieved using DXA and computed tomography (CT). These methods often do not report individual muscles however.<sup>313</sup>

No literature currently presents recommended values of maximal isometric force generating capacity for use in computational modelling of elite wheelchair racing athletes. The aim of this research was twofold, firstly assessing the sensitivity of a musculoskeletal model to the defined value of maximal isometric force generating capacity. Secondly, this research aimed to compare anthropometric parameters used in the definition of the musculoskeletal model, against subject-specific mass values obtained using DXA. If a close agreement was observed, scaling DXA segment mass values against generic model parameters can provide a simplified method of estimating appropriate input parameters. As athletes commonly present greater strength characteristics than the 50<sup>th</sup> percentile male characteristics currently used in some musculoskeletal models, it is hypothesised that current models (with generic parameters) will underestimate the maximal isometric force-generating capacity of wheelchair racing athletes.

### 6.4.2 METHODS

#### *Athlete Selection*

Data from two female, internationally ranked athletes competing in both wheelchair racing (Athlete I: T53 classification, age: 35 years, mass: 48.2 kg, experience: 13 years) and para-triathlon (Athlete E: PT1 classification; age: 26 years, mass: 52.8 kg, experience: 2 years) for this study. Athletes were classified as having no pathological impairments in the upper extremities. Both athletes had complete spinal cord lesions.

#### *Muscle Scaling*

The maximum isometric force-generating capacities were scaled from 25% to 400% in 25% increments.<sup>315</sup> Throughout the remainder of this manuscript, these are referred to as ‘scaling factors.’ A scaling factor of 1.00 represents the generic musculoskeletal model data, while values of 0.25 and 4.00, for example, represent weakening the model to 25% of its original strength or strengthening the generic parameters by 400%, respectively. A total of 96 simulations (16 variations per three speeds per two athletes) were performed. As athletes were representative of classifications demonstrating no pathological conditions to the upper extremity, all muscles were scaled simultaneously to represent a holistic, proportional increase in limb strength. Due to the many antagonist muscle pairs responsible for motion, it can be assumed there exists no bias to specific muscle groups as a consequence of regular training. This was assumed as no pathological conditions were present in the upper extremity of



---

athletes in this study, however, could not be applied for use with athletes with incomplete lesions, and demonstrating different functional characteristics between left and right limbs.

A review of anthropometric parameters presented in the literature was also performed to demonstrate the morphological similarity between population samples, thus ensuring compliance with the underlying assumptions required for volumetric based estimations. This involved comparing limb circumference measurements of a non-athletic, non-obese population,<sup>316</sup> and against the limb segment masses defined for a generic, musculoskeletal model scaled with athlete-specific total body mass values.<sup>164</sup> This is a similar approach to research by Knarr et al.,<sup>313</sup> who presented the maximum force-generating ability of a muscle or muscle group (between paretic and non-paretic limbs) as the ratio of the volume between the limbs.

### *Data Processing*

A period of 2.8 s (> 5 consecutive strokes) was obtained from the middle of the propulsion task to ensure steady state. Input data were sampled at 250 Hz, and filtered with a bidirectional second-order Butterworth low-pass filter with a -6 dB cut-off frequency of 10 Hz<sup>317</sup> in MATLAB.

A convergence criterion was used to establish the model had sufficient strength. Convergence indicated that the model had reached a balance between the reserve and muscle forces, and despite increasing the scaling factor of muscles, the contribution of the reserve actuators was stable. This method has been performed in the literature previously, with an example by Valente et al.<sup>130</sup> defining the convergence criterion for the variable of interest to have mean and standard deviation over the final 10% of the simulations being less than 5% of the overall mean and standard deviation. The overall mean and standard deviation was taken from all data points.

A similar convergence criterion was established for this study. Data from scaling factors < 1 were excluded from the calculation of overall mean and standard deviation as they were not representative of physiologically viable conditions. Therefore, the overall mean and standard deviation were taken as the mean value of the discrete mean and standard deviation values for scaling factors between 1 and 4. The variable of interest in this study is the difference in muscle or reserve actuation and force compared with the overall mean of muscle force and activation.

The range of convergence was defined to be 10% of the simulations. For each athlete, 16 simulations were performed at each speed, meaning two consecutive data points (based on scaling factor) had to be within the convergence criterion to be considered an appropriate scaling factor.

## 6.4.3 RESULTS

Total muscle force over time for each of the scapulothoracic, scapulohumeral, and upper arm muscles identified as dominant in wheelchair propulsion are presented in Figure 6.17, for each of the scaling values. Figure 6.17 provides a representative example of data from Athlete I, at 26 km/hr. Raw data (for each muscle or reserve actuator), are overlaid on the mean, and 95% confidence interval bounds for each of the scaling factors. With increasing scaling factor, muscle activation, reserve actuation, and reserve force begin to converge. Convergence, however, is not observed for muscle force, which increases with scaling factor, suggesting risks associated with the considerable overestimation of maximum isometric force generating capacity.

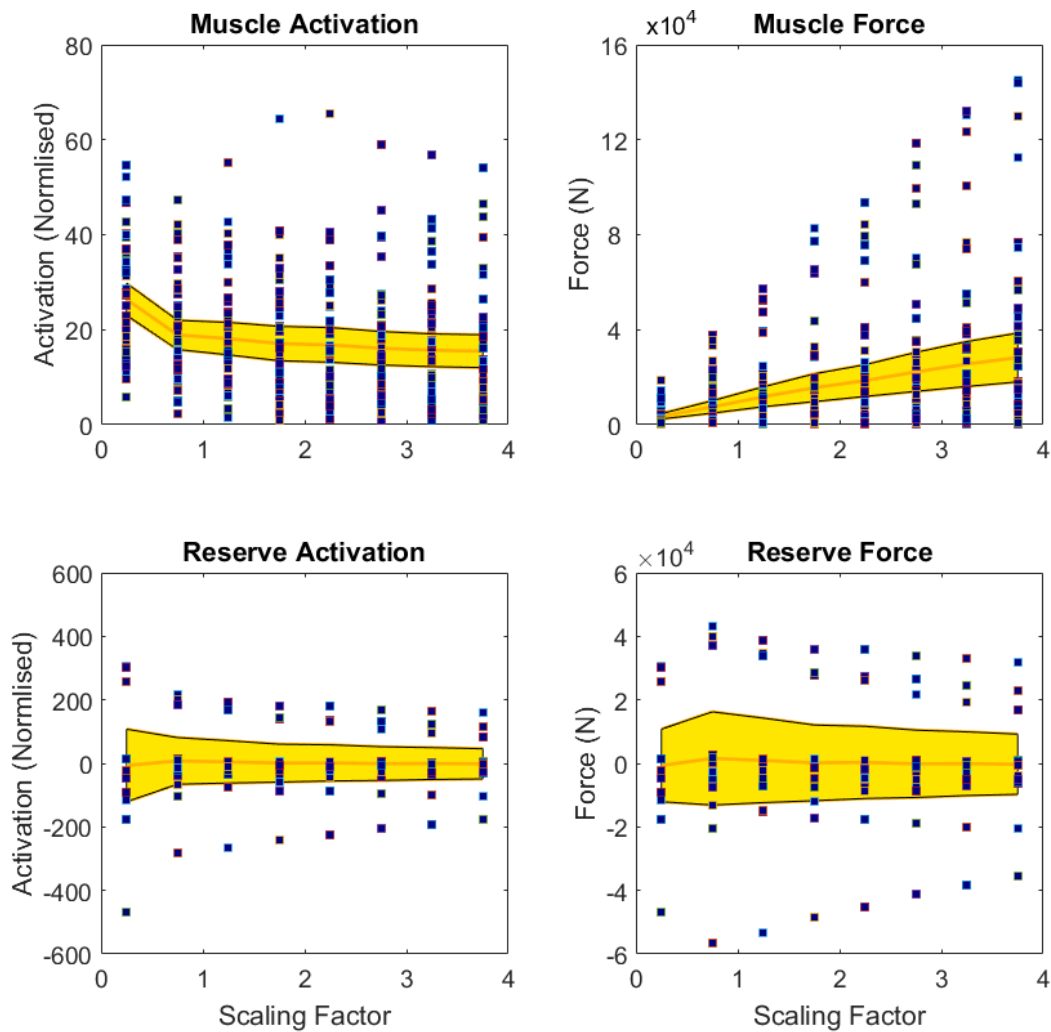


Figure 6.17: Comparison of muscle and reserve actuator contributions to activation and force, for Athlete I at 26 km/hr. Each data point corresponds to the activation or force of each muscle or reserve actuator in the system per time stamp (0.004 s) over the simulation period.

Activation has been normalised against total activation.

As the parameters start to converge, it would be anticipated that the difference between successive scaling factors (e.g. between a scaling factor of 1.25 and 1.5), would decrease. Scaling factors demonstrate the relative value compared to the generic parameters currently present in the musculoskeletal model. When comparing the change in magnitude of muscle activation and muscle force as a percentage of the overall mean (calculated as the mean value from scaling factors 1 – 4) (Figure 6.18), it can be observed that variation decreases in magnitude with increasing scaling factor. For a scaling factor  $> 1$ , it can be seen that between successive trials (e.g., between scaling factor 1.3 and 1.5) there is less than 5% difference (as indicated by the dashed line), indicating convergence in the simulations. The considerable variation observed for scaling factors  $< 1$  demonstrate unsuitable parameter definition.

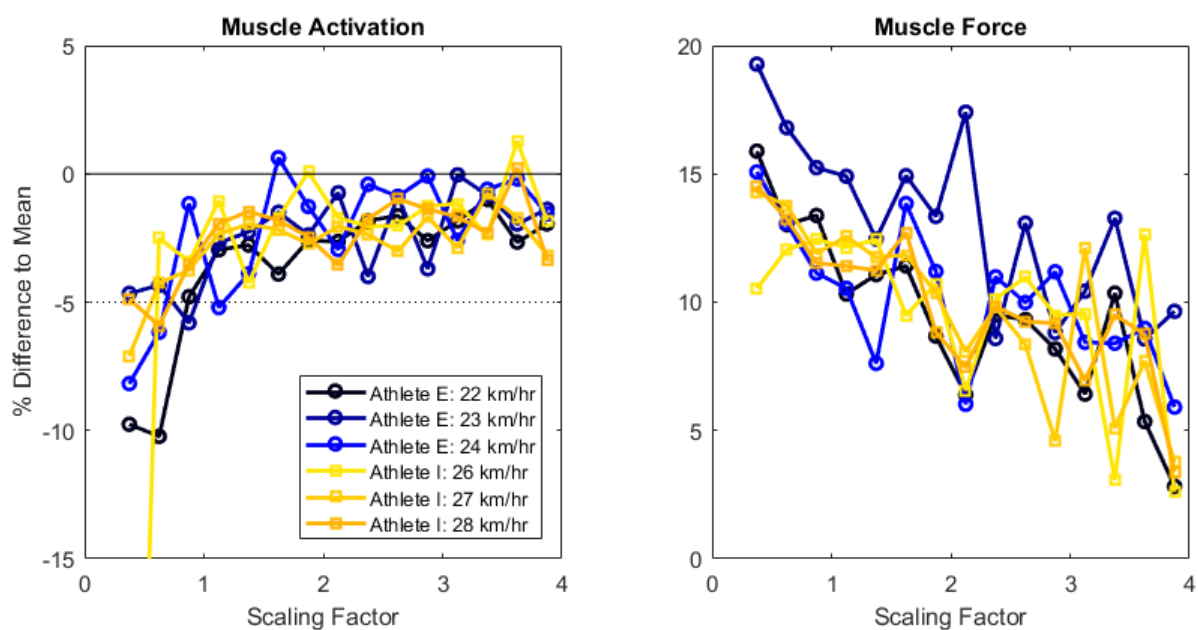


Figure 6.18: Comparison of the difference in muscle activation and force between successive scaling factors. Data are presented as a percentage of the mean value of muscle activation and force for scaling factors 1-4.

Reserve contribution was seen to decrease with an increased scaling factor, as would be expected, as a larger muscle force capacity creates a more substantial solution space. Figure 6.19 demonstrates the percentage of reserve force compared with mean muscle force (top) and the contribution (ratio) of absolute reserve force compared with absolute muscle force. In both absolute plots (left), it can be seen that a contribution of the reserve force is required for higher speeds of propulsion, as would be expected from a musculoskeletal model containing only a subset of all muscles. When investigating the

difference between successive scaling factors, it can be seen that convergence exists at higher scaling factor. Two successive data points must be within the *a-priori* thresholds ( $\pm 5\%$  change in reserve force sensitivity) to satisfy the convergence criteria. As these data points are indicative of the difference between successive scaling factors, the scaling factor was chosen as the higher of the two scaling factors used when calculating the difference in the second data point within the threshold. Athlete I requires a lower scaling factor (1.5) than is required of athlete E (1.75). It can be seen that for athlete E, there is a more variable response for the fastest (24 km/hr) trial, indicative of the maximal nature of propulsion.

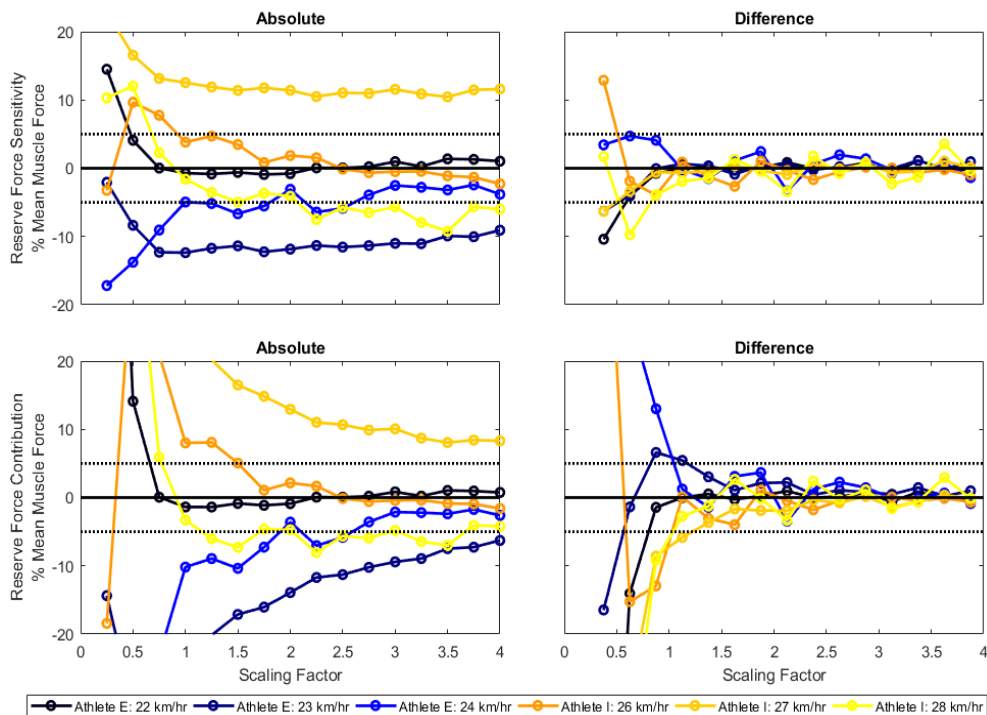


Figure 6.19: The contribution of the reserve actuators varies with increasing scaling factor.

The observed scaling factor of wheelchair athletes to general populations (Athlete I: 1.5, Athlete E: 1.75) was comparable but greater than anthropometric data presented previously by Bulbulian et al.<sup>316</sup> between paraplegic and able-bodied (ectomorph) college athletes. Differences in the chest, flexed and non-flexed bicep and forearm measures were 1.17, 1.24, 1.26 and 1.18, respectively. When comparing athlete-specific segment masses compared to those in the musculoskeletal model used, trunk measurements (as determined by clavicle mass) were 1.45 (Athlete I), and 1.70 (Athlete E), whilst upper arm measurements were 1.49 (Athlete I), and 1.25 (Athlete E).<sup>318</sup> Based on these comparisons, it is possible that the mass of the torso can be used to predict maximum isometric force generating capacity, however, further investigations are required to confirm this.

---

#### 6.4.4 DISCUSSION

This study generated a simulation of wheelchair racing in OpenSim and examined its sensitivity to the defined maximum isometric force-generating capacity of muscles. Higher sensitivity was demonstrated when the musculoskeletal model was artificially weakened for the two female athletes analysed. Sensitivity decreased at higher values of maximum isometric force generation capacity. Muscle activation, reserve (actuator) force and reserve activation all demonstrated a converging trend with an increased scaling factor of isometric force generating capacity (where a scaling factor of 1.5 is equal to 150% of the generic parameters, for example). Muscle activation was observed to vary < 5% between scaling factors when the scaling factor was > 1. At greater scaling factors, the magnitude of this increase reduces, however; an over-estimate of the maximum isometric force-generating capacity of muscles may overestimate the muscle force required to complete the task. Optimal values were observed to be athlete-specific (Athlete I required a scaling factor of 1.5, while Athlete E required a higher scaling factor of 1.75), and partially related to muscular physiology. Thus, the use of DXA or other medical scanning technologies may act as a simplified approach for estimating the required input parameters on a large scale.

Greater disparities in muscle activity were observed when muscles were weakened. This high sensitivity is indicative of the simulation altering muscle recruitment strategies, through the use of compensatory muscles to achieve the desired task. Consequently, it is clear that under-defining the maximum isometric force-generating ability of muscles will result in non-physiologically-representative, or potentially invalid results.

Estimation of muscular force from size is reliant on numerous assumptions with regards to the muscle tissue structure.<sup>313</sup> Volumetric and mass-based comparisons also require morphological similarity, as measurements are also based on bone and adipose tissue. The force to cross-sectional area relationship is complicated, and not all changes in muscle force can be attributed to differences in cross-sectional area,<sup>313, 319</sup> especially following muscle wasting due to ageing or malnutrition.<sup>320</sup> These, however, are not necessarily relevant for the elite wheelchair racing population. Morphological similarities in bone mineral density and total body fat mass exist between the sample population and reference literature. Upper extremity bone mineral density values for the athletes in this research are comparable between low paraplegics and able-bodied controls, however, is reduced in the lower extremity of individuals with SCI.<sup>321-323</sup> Total body fat mass (as percentage total body weight) for wheelchair track and field athletes ( $20.9 \pm 4.4\%$ )<sup>324</sup> are consistent with the recommended guidelines for the (age and gender matched) average population ( $19.2 \pm 8.6\%$ ).<sup>325</sup> Therefore, increased segment masses can be related to an increase in skeletal muscle tissue.

Although scaling factors must be a non-zero, positive number (ensuring maximum isometric force generating capabilities  $> 0.0001$  N) to ensure system dynamics can be solved, practically, a scaling factor should always be greater than 1 for use in the upper extremity of wheelchair racing athletes. Lower values would be indicative of severe muscle atrophy, which is not present within the upper extremities of this population, but may be in tetraplegic athletes. It is acknowledged that lower scaling factors will be required for the lower extremities of athletes, and should hence be considered in future research.

Reported muscle activations overestimated what is previously presented in models of manual wheelchair propulsion. For example, Lin et al.<sup>311</sup> demonstrated muscle forces ranging between 0.4 N (triceps long head) through 343.6 N (infraspinatus) during the propulsion phase, and between 0.9 N (teres minor) and 118.9 N (middle deltoid) during the recovery phase, as obtained using a similar computational approach. As increased speed has been demonstrated to change wheelchair propulsion patterns<sup>58, 104, 326</sup> and increase joint loading (e.g. walking v running)<sup>105</sup> the observed differences can be partly attributed to previous research being performed at lower propulsion speeds, representative of manual wheelchair propulsion. Additional variation may also be the result of the more dynamic 'striking' motion employed by wheelchair racing athletes, as compared to the 'pushing' motion demonstrated in manual wheelchair propulsion.

The recommended practice was followed to minimise errors. However, some limitations are recognised for the current research. While these preclude the measurement of muscular forces, they do not prevent the estimation of relative muscle force (compared to a generic value) which can be used in the musculoskeletal model. Based on the relative insensitivity demonstrated at greater magnitudes of scaling factors, these limitations are not detrimental. It is acknowledged, however, that the results presented in this research are specific to the methods applied, and so although the particular results are not generalizable, the used process is.

Future research using subject-specific muscle parameters will improve the validity of the assessment of how muscles influence movement, especially when functional impairments are present. Use of musculoskeletal modelling can assist with both the designation of athlete-specific strength and conditioning programs, instruct methods to counteract athlete asymmetries, and predict the likelihood of applied motions generating injury. Findings are also applicable to the manual wheelchair using population, who also have a high capacity to benefit from modelling approaches as up to 73% of paraplegic manual wheelchair users exhibit shoulder pain.<sup>327</sup> Through the use of more relevant isometric force generating capacity input data, the reliability of simulations will improve.

---

#### 6.4.5 CONCLUSION

Increasing the maximum isometric force-generating capacity of muscles is recommended for the computational biomechanical assessment of wheelchair racing propulsion. The magnitude of increase is performed on an athlete-specific basis through multiple sensitivity analyses. Research demonstrated that the use of DXA scans might provide a streamlined approach to this, which may be of benefit when analysing some athletes. Avoiding the gross- overestimation of maximum isometric force-generating capacity of muscles is also recommended.

### 6.5 DISCUSSION

This chapter focused on the development of subject-specific musculoskeletal models for use in the biomechanical modelling of wheelchair racing propulsion. Subject-specific parameters were established from the analysis of DXA scans, which is a method emerging in the literature for estimating body segment inertial parameters. Although not as precise as some of the more traditionally used scanning technologies, DXA scans are an attractive alternative due to their practical feasibility, with many elite athletes having regular scans as part of monitoring body composition. The reliability of the DXA scanning approach was revealed to be sensitive to the processing methodologies (Section 6.2) which also revealed the inaccurate definition of body segment inertial parameters impacted on the joint reaction moments. This was further supported in Section 6.3 when comparing against able-bodied, non-athletic populations. This provided the first research to adapt musculoskeletal models to represent the physical characteristics of an elite wheelchair racing population, and demonstrated methodological flaws with previous literature which has been based upon able-bodied, non-athletic populations.

As suggested in the literature, DXA scans provided a valid method of estimating body segment inertial parameters. As observed in Section 6.2, the reliability of the inertial estimates is sensitive to the processing method. The definition of intensity thresholds is not disclosed in accompanying user manuals or commented on in the literature. However, understanding how this process is performed is of benefit to future processing for enhanced reliability. As this research only investigated extreme bounds, recommendations for future use cannot be provided. However, it can be suggested that best practice would ensure the collection and exportation of phantom scans with each athlete scan. These are DXA scans taken of objects with known mass and density. These would also assist in understanding how to define the intensity thresholds, as phantom scans can act as validation measures with known properties. As this research made use of pre-established DXA scans from an existing database, phantom scans were not available.

Although the analysis of DXA scans provides a validated approach for body segment inertial parameter definition *in-vivo*, the application may be limited to all athletes. Reliability of scans may be reduced in athletes with muscle spasticity who may not be able to achieve or sustain postures for the entire duration of the scan, as well as those with metal implants.<sup>283</sup> Mass cannot be quantified in regions where metallic implants are present, as they limit data transmission to the DXA receiver.<sup>283</sup> Due to the low dose of radiation emitted by each DXA scan, however, scans can safely be taken in multiple planes (i.e. frontal and sagittal) to estimate the mass of each limb segment accurately. As this research utilised data from a pre-established database, postural alignment served as a limitation for a single athlete, as the right thigh and left foot segments were excluded from the analysis, and a bilateral limb symmetry assumption was enforced. While large limb asymmetries presented in this study question the validity of this assumption, these errors are easily overcome in future applications.

This research established that the body mass distribution of wheelchair racing athletes differed significantly from that of able-bodied, non-athletic individuals. These parameters are currently used in musculoskeletal modelling research and have a significant impact on joint reaction force estimates. Clear between-athlete differences, particularly surrounding the volume of tissue in the lower extremities were also observed. Therefore, it can be suggested that for this population, from a small subset, a set of normative values representative of the whole population cannot be established. Thus, it is suggested that for the biomechanical analysis of wheelchair racing athletes, customised, subject-specific modelling approaches should always be applied. While the use of DXA scans were suggested in the literature to require less sophisticated software than other medical scanning approaches; it is not always permissible. In the absence of these, it is possible to use volumetric estimation methods as suggested by Zatsiorsky et al.<sup>328</sup> or Hanavan,<sup>146</sup> ensuring appropriate anatomical landmarks and measurements are obtained. However, it is also crucial to consider the morphological similarity between athletes and the population these volumetric equations are based upon, however. Alternatively, reference values from this research can be used for athletes with comparable anthropometries as an estimate.

The assumption that there was no change in the physiological architecture of muscles or the governing force-velocity relationships compared to an able-bodied population was used due to the population of this research demonstrating no upper extremity physical impairment (Section 2.1). However, it should be noted that these parameters may require alteration when investigating populations with impairments to the upper extremity, as seen in athletes with tetraplegia, or incomplete spinal cord lesions.

A concern with the simulation approach is the sensitivity of the model to the input parameters, which are mostly estimated. Although approaches such as sensitivity analyses can be performed to improve



---

the precision of these estimates, such as what was done for the reserve actuator contribution, it is important to highlight that the obtained results are influenced by this parameter. Therefore, when converting research into practice, it is done with consideration of the reliability and inherent uncertainties of the approach. Model verification was performed in light of this, with results presented in Appendix B.

No accurate or validated method is currently recognised in the literature for estimating the reaction loads between the hands and the pushrim during wheelchair racing propulsion. It is acknowledged that the estimated external loads may overestimate the actual values. Effects should be minimal, however, with the literature reporting that performing inverse dynamics using kinematic data alone for gait analysis provided reasonable estimates of ground reaction forces and moment, with errors in the sagittal plane of 6% compared to force plate data.<sup>293</sup> The joint torques estimated in this research are of the same order of magnitude as presented in the literature when normalised for speed. Mean absolute glenohumeral flexion/extension torque from this research was approximately 13.0 times greater ( $274 \text{ Nm} \pm 75.7 \text{ Nm}$ ) than other data presented in the literature ( $21.1 \text{ Nm} \pm 0.9 \text{ Nm}$ ).<sup>169</sup> This difference can be attributed to both the higher speed of propulsion presented in this research (8.1 m/s here compared to 1.4 m/s in literature), with the alteration in wheelchair propulsion mechanics due to speed frequently demonstrated in the literature.<sup>64, 306, 307</sup> This is significant as at lower speeds, propulsion is more of a pull-push action, whereby athletes grab the wheel, while at the speeds employed by wheelchair racing athletes, strokes are executed solely by the push phase.<sup>306, 307</sup>

## 6.6 IMPLICATIONS AND CONCLUSION

Wheelchair racing athletes demonstrate substantial between-athlete, and between-population variability, with strengths greater than what is currently defined in the musculoskeletal model. This research section demonstrated the importance of using subject-specific parameters for both the inertial (Section 6.2, Section 6.3) and maximum isometric strength generating capacity (Section 6.4) in musculoskeletal models for the computational analysis of wheelchair racing propulsion, which can both be obtained through the analysis of DXA Scans. The importance of appropriate processing of the DXA scan was also highlighted (Section 6.2). Due to the uniqueness of athlete impairment, it is unlikely that a normative database can be established to simplify future modelling. However, estimation of inertial parameters through the application of volumetric modelling techniques when DXA scans are unavailable, or base parameters off the data presented in this chapter may still offer improvements to the generic counterparts.

### *Key Findings:*

- The processing of DXA scans is subject to a defined intensity threshold, with bony segments found to be more sensitive.
- Generic scaling approaches based on able-body mass distribution, poorly estimated DXA obtained segment mass values of physically impaired athletes.
- Differences in output joint torques were observed between subject-specific (DXA) and generically scaled models, however, was not associated with limb segment.
- The balance between muscle activation and reserve activation converges to an increased maximum isometric force generating capacity is defined, which can also be estimated with the assistance of DXA scan data.
- Weakening a model provided physiologically invalid results for wheelchair racing propulsion.

### *Implications*

- Inadequate processing of DXA images does not estimate total body mass and its distribution correctly, and it is proposed that a standardised, objective method of determining threshold values is required.
- Parameters of able-bodied, non-athletic populations should not be used in the analysis of wheelchair propulsion biomechanics by physically impaired athletes.
- Future wheelchair propulsion research should incorporate subject specific in-vivo measurements to ensure confidence in the simulation outputs.
- The maximum isometric force generating capacity is likely to be greater for athletic populations, and the musculoskeletal model requires adjusting to reflect this.
- Reserve actuator contribution should be defined with care, as it will likely change the point of convergence (particularly if reserve actuators are set high).

---

---

**CHAPTER SEVEN:**

**QUANTIFYING THE  
MECHANICS OF  
WHEELCHAIR  
PROPULSION USING  
SIMULATION**

---

The contribution to the holistic comparison of performance and assessment of injury prevention strategies are presented in this chapter, addressing the final aim of the research. Two experimental studies are presented, which together demonstrate the potential benefits of having a coupled kinetic and computational biomechanical analysis approach. The first study looks into whether simulation approaches can be used as an injury prevention and management tool. The second study then addresses the fundamental aim of the thesis; investigating how customised seating interfaces influence performance. These studies and their research questions are summarised following and in Figure 7.1.

**Influence of customised seating interfaces on lower extremity wheelchair kinematics.**

**(Section 7.1)**

*Research Question:*

- What is the performance benefit of customised seating interfaces?

**Injury prevention of elite wheelchair racing athletes using simulation approaches.**

**(Section 7.2)**

*Research Question:*

- Can computational simulations be used to predict techniques which may be more at risk of putting athletes at risk of obtaining an injury?

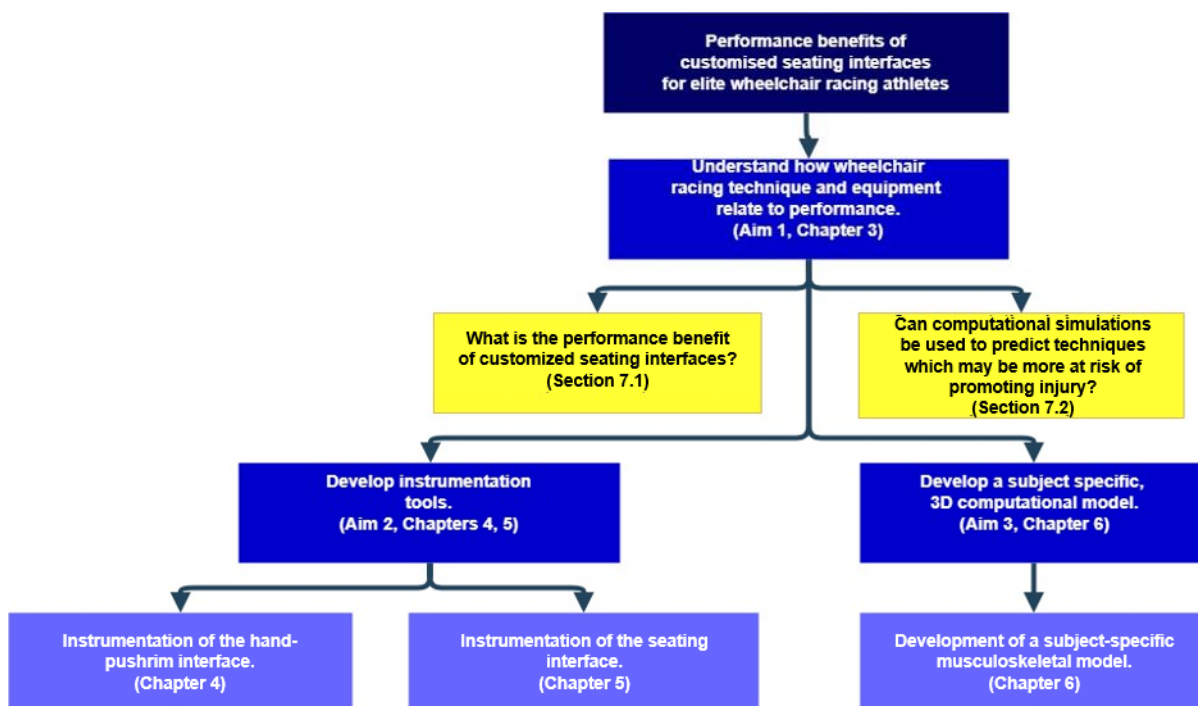


Figure 7.1: Relevance of the Chapter 7 (Quantifying the mechanics of racing propulsion using simulation) to the fundamental research question; what is the performance impact of customised seating interfaces on wheelchair racing propulsion?

---

## 7.1 INJURY PREVENTION OF ELITE WHEELCHAIR RACING ATHLETES USING SIMULATION APPROACHES

### 7.1.1 INTRODUCTION

Upper limb injuries are common amongst wheelchair athletes, particularly in the shoulder.<sup>119</sup> Literature has identified that wheelchair racing and road racing are amongst the sports with the s risk to athletes for sustaining a soft tissue injury.<sup>234</sup> Injuries to the upper extremity can both impede performance and limit the mobility of wheelchair-using individuals and athletes. It is therefore imperative that due diligence is taken to ensure athletes are employing propulsion techniques which have a low risk of promoting injury.

Soft tissue injuries have been demonstrated as a leading injury amongst athletes in wheelchair sports specifically wheelchair racers.<sup>234</sup> Monitoring muscle loading requires an inherent understanding of both the forces and activation pattern of each muscle, to determine how much it is contributing to the motion. As individual muscle forces and joint reaction moments cannot be measured directly, computer simulations using musculoskeletal models are required.

Athletes in wheelchair sports have demonstrated higher rates of the shoulder, elbow-arm, and forearm-wrist injuries as compared to other Paralympic athletes.<sup>234</sup> The high incidence of injury can be attributed to the nature of the shoulder girdle being ill-equipped for the kinematic requirements of wheelchair propulsion. The shoulder girdle, which is responsible for the majority of kinetic requirements of wheelchair propulsion, is structured to maximise freedom of movement.<sup>119</sup> However, in order to obtain maximum speed, athletes must apply large forces over short durations to achieve a high net impulse. The repeated, high loading of wheelchair propulsion contributes to injury in the shoulder-girdle construct.<sup>329</sup>

The specific aim of this study was to evaluate whether a coupled kinematic investigation and computational simulation approach could effectively discern whether kinematic aspects of the technique may lead to greater injury risk. As shoulder injuries have typically been diagnosed as a consequence of the repeated, high impact loadings, it was hypothesised in this study, that greater injury risk was associated with greater reaction joint moments.

### 7.1.2 METHODS

#### *Athlete Selection*

Two female wheelchair racing athletes from the national level senior program were recruited for this study (Athlete E: age = 24.4 years, mass = 52.9 kg, experience = 3 years, classification = T54; Athlete I: age = 33.7 years, mass = 48.0 kg, experience = 23 years, classification = T53). The experimental task and measurement system are consistent with methods presented in Section 6.1.

#### *Data Processing*

Hand speed at contact and release were obtained from taking the first derivative of the marker position data measured using motion capture. Push time, contact angle and release angle were obtained from manual digitisation of video data in Kinovea software.

#### *Musculoskeletal Model*

Computer simulations utilising the Wu Shoulder Musculoskeletal Model<sup>330</sup> were performed in OpenSim.<sup>133</sup> This model was developed after the Upper Extremity Dynamic Model used in Chapter Six. This model incorporates subject-specific inertial parameters of the torso segment. Based on the between-athlete variation in torso mass identified in Section 6.3, this was considered advantageous. Also, the Wu shoulder model allows independent scapula-humeral rhythm. Based on the highly dynamic motion of the shoulder, this was also considered beneficial in the analysis of wheelchair racing athletes.

The musculoskeletal model was adapted to incorporate athlete-specific segment mass, and maximum isometric force generating capacity data. Segment masses were obtained through the assessment of DXA scans, as detailed by Laschowski et al.,<sup>282</sup> while optimum isometric force generating capacity was established through an optimisation problem, iterating through strength factors. The optimum strength of the model was established through a convergence of muscle activation (Section 6.4). The range of motion analysed for this investigation is depicted in Figure 7.2. For trunk flexion angle, a value of  $-90^\circ$  has the trunk parallel to the ground, with a value of  $0^\circ$  representing the athlete is in a conventional upright seating posture.

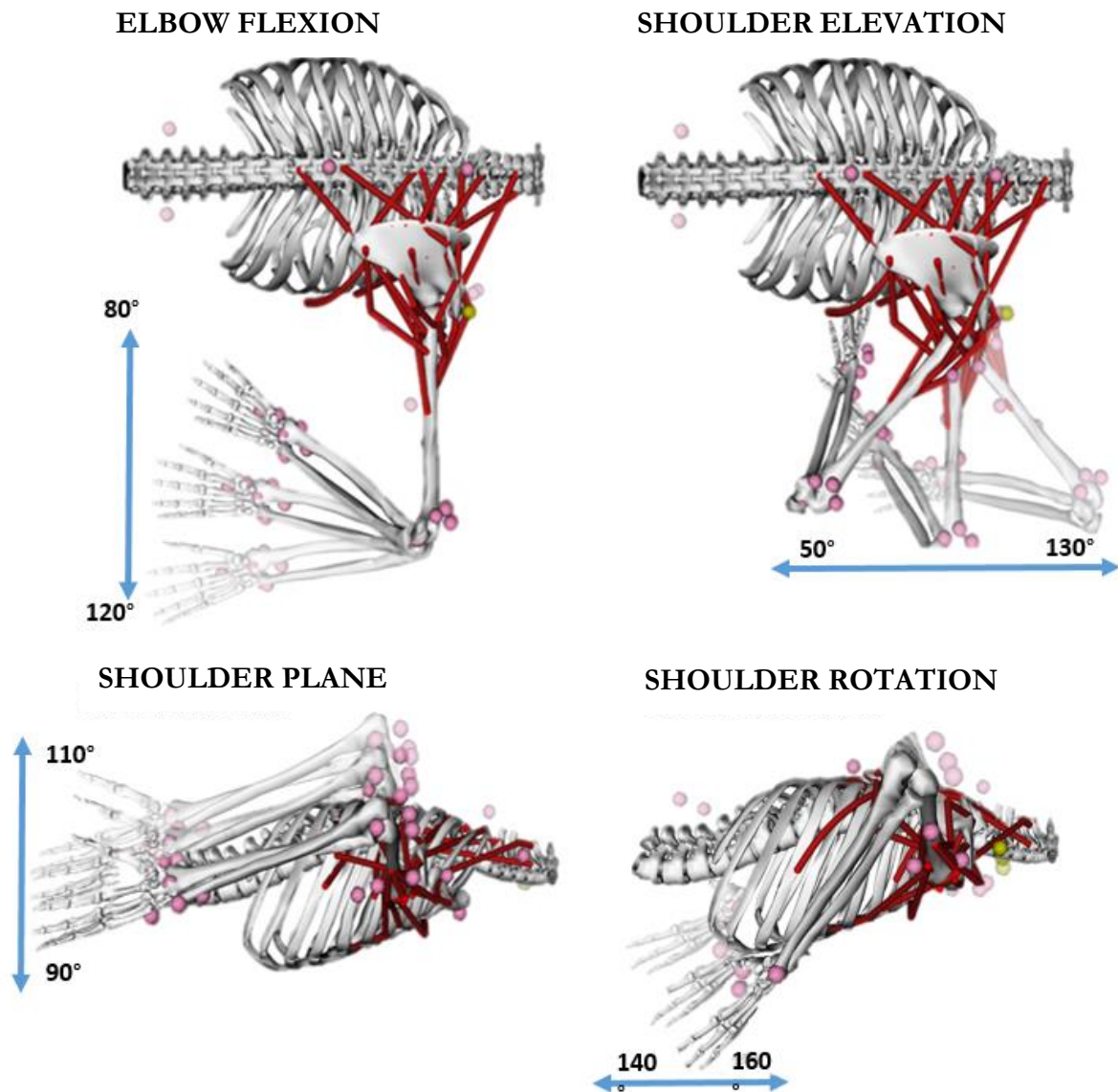


Figure 7.2: Joint range of motions explored in this investigation.

Inverse kinematics calculations in OpenSim were used to reveal the trunk, shoulder joint and elbow flexion at contact, with specific timestamps established directly from motion capture data. Reaction forces were estimated from the kinematic data,<sup>293</sup> whereby forces were estimated as a sum of the segment masses multiplied by their respective translational acceleration and were used to drive the inverse dynamics calculations to obtain net joint reaction moments (Section 6.1). An example of the propulsion motion, including applied forces, can be seen in Figure 7.3.

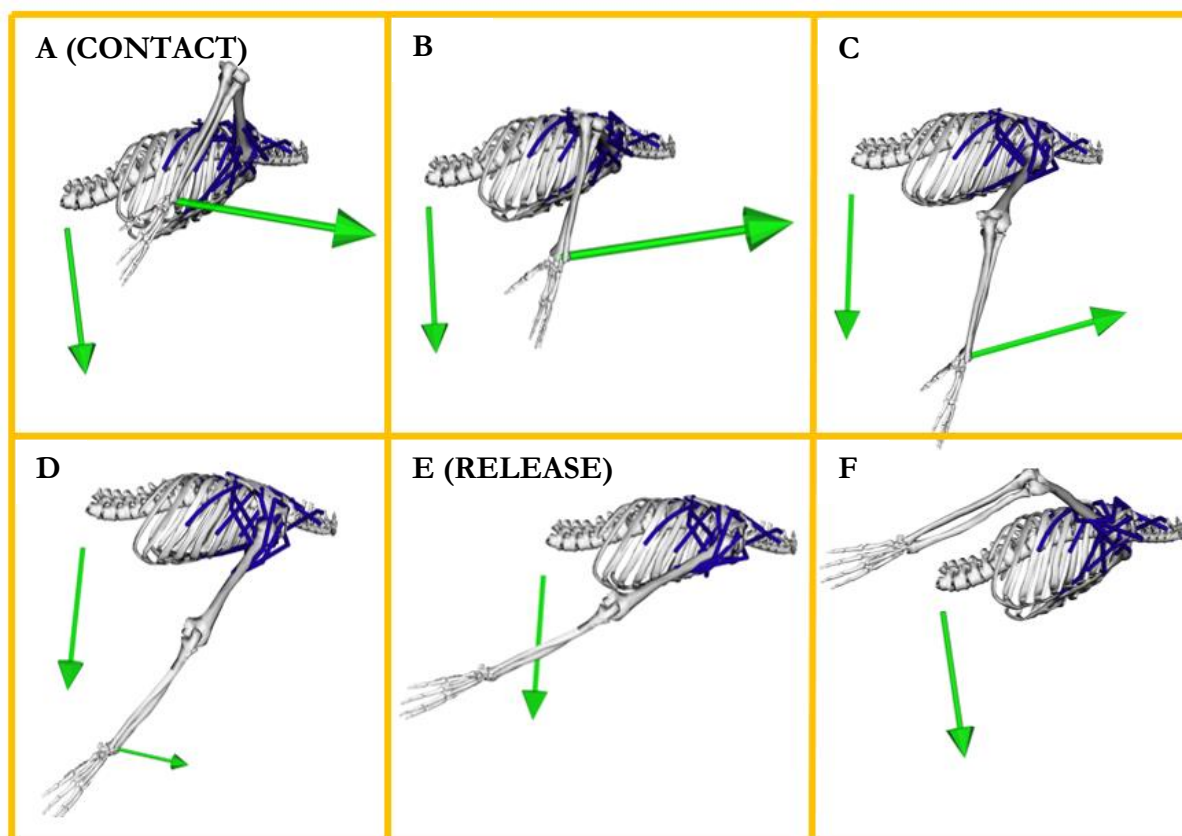


Figure 7.3: Example of a computational model of wheelchair racing propulsion. Arrows demonstrate the direction and magnitude of applied forces.

### *Statistical Analysis*

Multiple regression analyses were performed to identify interactions between reaction moments and kinematic parameters. All statistical calculations were performed using IBM SPSS Statistics 24 Software for Windows.

### 7.1.3 RESULTS

Intra- and inter-athlete kinematic variation was observed and is presented qualitatively in Figure 7.4, and quantitatively in Table 7.1 and Table 7.2. Key kinematic variations included release angle (Athlete E:  $218.9 \pm 7.3^\circ$ ; A2:  $180.9 \pm 7.9^\circ$ ), shoulder elevation (Athlete E:  $52.1 \pm 2.6^\circ$ ; A2:  $91.7 \pm 8.0^\circ$ ), shoulder plane (A1:  $-141.4 \pm 5.9^\circ$ ; A2:  $-107.8 \pm 2.0^\circ$ ), and elbow flexion (Athlete E:  $83.3 \pm 3.1^\circ$ ; A2:  $122.2 \pm 4.8^\circ$ ). Figure 7.4 demonstrates the different kinematic strategies employed by athletes with regards to head position and movement throughout the motion. As the head segment was not modelled, its movement variability is not discussed.



Table 7.1: Kinematic and kinetic characteristics of propulsion presented for Athlete E as mean  $\pm$  SD; *n* represents the number of push cycles recorded. Contact and Release angles are presented to no decimal places to reflect the precision of the collected data.

		<b>Athlete E</b> <b>22km/hr</b> <b>n = 15</b>	<b>Athlete E</b> <b>23km/hr</b> <b>n = 21</b>	<b>Athlete E</b> <b>24km/hr</b> <b>n = 19</b>
Hand Speed Contact	(m/s)	8.2 $\pm$ 0.6	8.5 $\pm$ 0.7	9.3 $\pm$ 0.7
Hand Speed Release	(m/s)	6.3 $\pm$ 1.3	6.6 $\pm$ 1.6	6.9 $\pm$ 1.5
Push Time	(s)	0.2 $\pm$ 0.0	0.2 $\pm$ 0.0	0.2 $\pm$ 0.0
Contact Angle	( $^{\circ}$ )	21 $\pm$ 5	24 $\pm$ 5	26 $\pm$ 4
Release Angle	( $^{\circ}$ )	188 $\pm$ 4	183 $\pm$ 7	175 $\pm$ 7
Trunk Flexion Angle*	( $^{\circ}$ )	-89.9 $\pm$ 0.0	-89.9 $\pm$ 0.1	-86.2 $\pm$ 1.1
Shoulder Elevation Angle*	( $^{\circ}$ )	97.1 $\pm$ 3.4	96.0 $\pm$ 4.5	81.5 $\pm$ 3.2
Shoulder Rotation Angle*	( $^{\circ}$ )	156.3 $\pm$ 4.9	153.3 $\pm$ 18.0	137.1 $\pm$ 3.3
Shoulder Plane Angle*	( $^{\circ}$ )	-108.4 $\pm$ 0.0	-108.2 $\pm$ 0.1	-106.4 $\pm$ 3.6
Elbow Flexion Angle*	( $^{\circ}$ )	125.1 $\pm$ 0.7	125.6 $\pm$ 1.0	115.3 $\pm$ 0.9
Reaction Force (Resultant)*	(N)	1077.8 $\pm$ 23.8	1066.9 $\pm$ 19.3	883.5 $\pm$ 15.6
Shoulder Elevation Reaction Moment*	(Nm)	-116.6 $\pm$ 4.5	-117.2 $\pm$ 6.3	-113.3 $\pm$ 4.3
Shoulder Rotation Reaction Moment *	(Nm)	62.7 $\pm$ 3.0	76.2 $\pm$ 3.7	72.6 $\pm$ 9.8
Shoulder Plane Reaction Moment*	(Nm)	114.1 $\pm$ 4.4	108.3 $\pm$ 3.6	108.3 $\pm$ 3.6

\*Represents data collected for a single side only.

Table 7.2: Kinematic and kinetic characteristics of propulsion presented for Athlete I as mean  $\pm$  SD; *n* represents the number of push cycles recorded. Contact and Release angles are presented to no decimal places to reflect the precision of the collected data.

		<b>Athlete I</b> <b>22km/hr</b> <b>n = 15</b>	<b>Athlete I</b> <b>23km/hr</b> <b>n = 16</b>	<b>Athlete I</b> <b>24km/hr</b> <b>n = 16</b>
Hand Speed Contact	(m/s)	7.3 $\pm$ 0.4	7.2 $\pm$ 0.2	7.4 $\pm$ 0.8
Hand Speed Release	(m/s)	4.5 $\pm$ 0.7	3.8 $\pm$ 0.8	5.1 $\pm$ 0.9
Push Time	(s)	0.3 $\pm$ 0.0	0.3 $\pm$ 0.0	0.3 $\pm$ 0.6
Contact Angle	( $^{\circ}$ )	25 $\pm$ 4	28 $\pm$ 4	28 $\pm$ 4
Release Angle	( $^{\circ}$ )	217 $\pm$ 8	221 $\pm$ 7	219 $\pm$ 7
Trunk Flexion Angle*	( $^{\circ}$ )	-91.7 $\pm$ 0.9	-93.4 $\pm$ 1.1	-92.8 $\pm$ 0.7
Shoulder Elevation Angle*	( $^{\circ}$ )	50.0 $\pm$ 1.0	52.6 $\pm$ 1.2	53.7 $\pm$ 2.4
Shoulder Rotation Angle*	( $^{\circ}$ )	157.1 $\pm$ 2.0	159.4 $\pm$ 1.2	160.9 $\pm$ 1.2
Shoulder Plane Angle*	( $^{\circ}$ )	-146.0 $\pm$ 1.0	-151.6 $\pm$ 1.0	-138.3 $\pm$ 5.8
Elbow Flexion Angle*	( $^{\circ}$ )	82.3 $\pm$ 3.2	85.0 $\pm$ 3.0	83.6 $\pm$ 2.9
Reaction Force (Resultant)*	(N)	844.2 $\pm$ 11.4	818.4 $\pm$ 10.6	825.2 $\pm$ 10.7
Shoulder Elevation Reaction Moment*	(Nm)	-321.9 $\pm$ 3.4	-322.2 $\pm$ 7.5	-326.8 $\pm$ 3.6
Shoulder Rotation Reaction Moment *	(Nm)	230.7 $\pm$ 6.3	211.3 $\pm$ 8.4	231.3 $\pm$ 3.2
Shoulder Plane Reaction Moment*	(Nm)	232.1 $\pm$ 3.4	243.2 $\pm$ 7.7	262.2 $\pm$ 5.5

\*Represents data collected for a single side only.

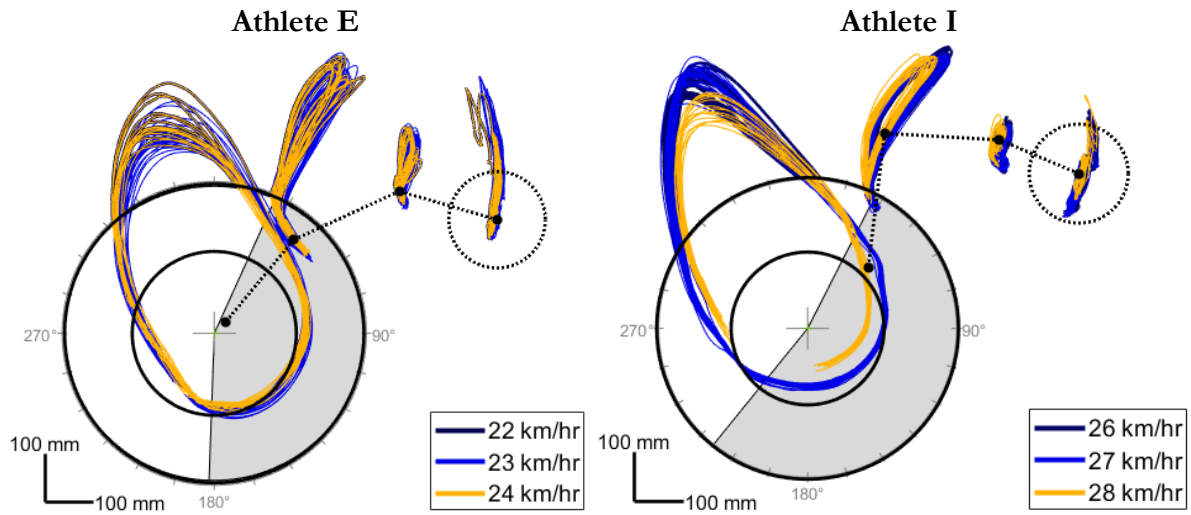


Figure 7.4: Kinematic comparison of motion for Athlete E (left) and Athlete I (right). Grey regions represent time in contact with the wheel, with guideline references located on the outside of the wheel. Segments presented represent the kinematic tracking of the head, shoulder, elbow and hand markers, respectively.

Statistical analysis revealed that the reported shoulder joint reaction moments correlated with the athlete (Table 7.3). Additional correlations were observed with elbow flexion angle (Rotation:  $r = -.981, p = .000$ ; Plane:  $r = -.970, p = .001$ ) and reaction force (Rotation:  $r = -.817, p = .024$ ; Plane:  $r = -.801, p = .028$ ).

Table 7.3: Statistical significance for shoulder reaction moments with kinematic parameters.

	<b>Shoulder Elevation Reaction Moment</b>	<b>Shoulder Rotation Reaction Moment</b>	<b>Shoulder Plane Reaction Moment</b>
Athlete	$r = -.947, p = .002$	$r = .992, p = .000$	$r = .988, p = .000$
Speed	$r = -.734, p = .048$	$r = .899, p = .007$	$r = .903, p = .007$
Hand Velocity at Contact	$r = .875, p = .011$	$r = -.866, p = .013$	$r = -.880, p = .010$
Hand Velocity at Release	$r = .977, p = .000$	$r = -.891, p = .009$	$r = -.891, p = .009$
Push Time	$r = -.866, p = .013$	$r = .940, p = .003$	$r = .965, p = .001$
Release Angle	$r = -.928, p = .000$	$r = .959, p = .001$	$r = .970, p = .001$
Trunk Flexion Angle	$r = -.784, p = .020$	$r = -.807, p = .026$	$r = -.834, p = .020$
Shoulder Elevation Angle	$r = .925, p = .004$	$r = -.963, p = .001$	$r = -.946, p = .002$

---

#### 7.2.4 DISCUSSION

This study aimed to ascertain whether kinematic characteristics of motion could increase injury risk, and was assessed through coupling kinematic and computational modelling approaches. Greater joint reaction moments at the shoulder was the inferred mechanism for injury risk. With greater joint reaction moments, greater stresses are applied to the muscles spanning these joints, potentially generating a higher risk of overuse strain injury. Hand velocity at contact and release, push time, and joint angles at contact were important contributors to higher joint reaction moments. The magnitude of the reaction force and the speed of propulsion were significantly correlated with a greater shoulder plane and rotation moments. Athletes did not present with shoulder injuries at the time of testing.

Clear variations in kinematic strategies were employed between the two athletes, with a clear point of distinction being the hand speed at contact. Athlete E demonstrated a greater hand speed at contact, as well as a shorter push time (approximately  $\frac{2}{3}$  that of Athlete I). In performance terms, this is indicative of a compromised transfer of force between the athlete and wheelchair. This may explain the reduced average race velocity as compared with Athlete I, who is a World Champion level athlete. Biomechanically, due to the shorter push time, and potentially greater hand speed at contact, Athlete E experiences a much greater impulse with each contact, which can be translated to the estimated reaction force data. It is interesting to observe, however, that despite this, all reported shoulder joint reaction moments are smaller in Athlete E. It can be inferred that Athlete E adopts a technique which minimises moment arms, effectively reducing the reaction loads passing through the arm and acting at the shoulder. It can hence be suggested that the largely different kinematic position at contact may be reducing the likelihood of the athlete in sustaining a soft tissue injury to the shoulder. It is important to highlight that athletes must optimise the balance between biomechanical stability for injury prevention, and the highly dynamic motions required for competitive advantage. Through utilising this coupled kinematic and modelling analysis approach, athletes can modify techniques with the aim of improved performance, however also reaping the benefits of reduced risk of soft tissue injury.

The clear inter-individual variations observed can be likened to the difference in classification, and the degree of trunk control (present in Athlete E only). Additionally, Athlete I demonstrated > 10 years of international experience. Inter-individual variations across speeds are consistent with the literature and can be explained by the fastest speed being representative of race velocity, while the other two are sub-maximal efforts, where athletes may have greater control over technique. When considering the kinematic parameters alone, Athlete I demonstrated greater consistency across each of the speeds, which can potentially be attributed to experience. It is assumed that as both athletes were female, performed at comparable speeds, and had a similar classification, the results presented in this study are more homogenous than would be characteristic of the entire population.

This study identified that elbow angle and shoulder elevation and plane angles are correlated with greater peak joint reaction moments. Hence, the continuation and expansion of this work in developing a database of normative values may better promote kinematic techniques which are less likely to result in athlete injury. However, these techniques will also be reliant on the unique physical impairments and capabilities of each athlete. Furthermore, this study examined a simplistic approach to the diagnosis of athlete injury, focusing solely on increased joint moments being the causative factor, without consideration of interaction effects with other performance aspects. It is also plausible that additional factors, including highly consistent techniques (repeatedly straining the same tissues), may also contribute to injury, and should be explored further.

It is acknowledged that the simulation of only the right-hand side of the body is a limitation of this study, as temporal asymmetries have been observed for both athletes. Verified musculoskeletal models of a full upper extremity, are currently not available within the OpenSim environment. Both athletes exhibit complete spinal cord injuries, with less pronounced asymmetries as compared to athletes with incomplete spinal cord lesions. Additionally, both athletes are competitive in classifications having full physical function in their upper extremities. Therefore, in terms of the musculoskeletal model definition, it can be inferred that there is a reasonable agreement between the left and right limbs, and it is unlikely that the reported kinematic parameters would vary largely.

Lateral rotation of the torso occurs throughout the motion, with the magnitude of this potentially exceeding what is observed in video data (Figure 7.5). While this rotation may be partly attributed to athlete asymmetry, it may also be a consequence of only modelling the right limb. No reaction loads were applied to the left shoulder. Movement in this plane could have been locked within the OpenSim modelling environment (restricting its motion to two dimension) to remove this error, however, was not desirable as it would mask any rotations caused due to asymmetries.

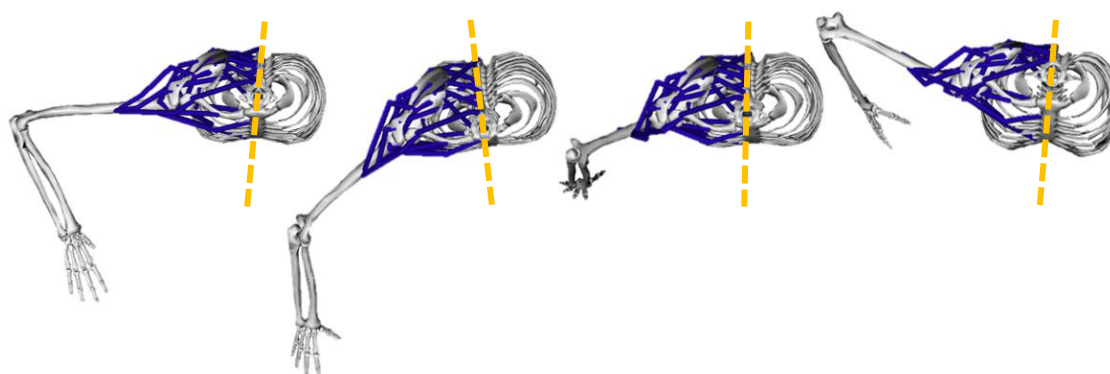


Figure 7.5: Torso rotation to the right side during propulsion. The dashed line between the centre of spine and sternum.

---

Multiple smaller models can be carefully amalgamated to create a larger model. For example, the OpenSim Upper Extremity (top left),<sup>164</sup> Wrist<sup>331</sup> and Lower Extremity model<sup>332</sup> can be combined to estimate the 3D joint reaction loadings under wheelchair propulsion (Figure 7.6). As the Upper Extremity and Wrist model were only created for the right limb, the assumption of limb symmetry is required for the development of the left limb. As different generic models source input parameters from different sources, it is possible that inconsistencies will exist between each of the different models. Future research is required to analyse the plausibility of this approach.

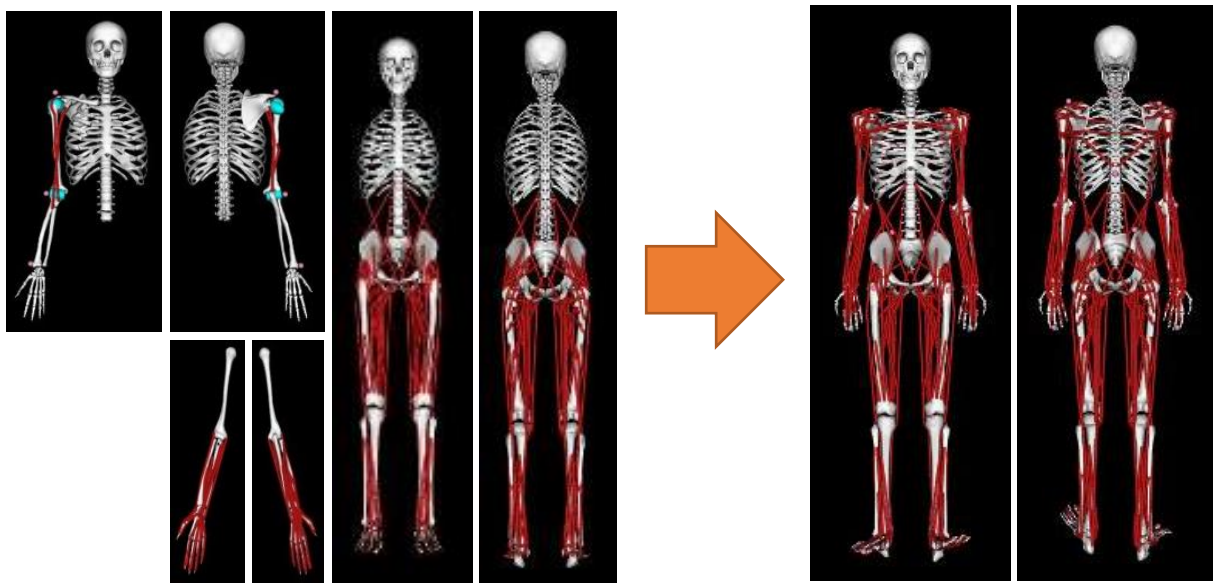


Figure 7.6: Amalgamation of existing verified models, including the Upper Extremity (top left),<sup>164</sup> Wrist<sup>331</sup> and Lower Extremity<sup>332</sup> to produce a full body model.

Another limitation with this study was that the input force estimates presented in Table 7.1 and Table 7.2 are much larger than what is presented in the literature and based on the linear extrapolation of the force-velocity plot presented in Figure 4.26. The large error may fundamentally be a consequence of extrapolating the methodology which demonstrated promising reliability for a low impact and speed gait motion, to a far more ballistic motion of wheelchair racing.

Further investigation into the source of errors also revealed an error introduced during the calculation of the centre of mass accelerations in OpenSim. While the independent scapula-humeral rhythm in the Wu Shoulder Model was considered an advancement to what was in the Upper Extremity Dynamic Model, it was revealed that it might have contributed to the large over-estimation of forces. As can be seen in Figure 7.7, the scapula moves away from the thorax near the release point. It is possible that this error is also the result of the magnitude of increased scaling.

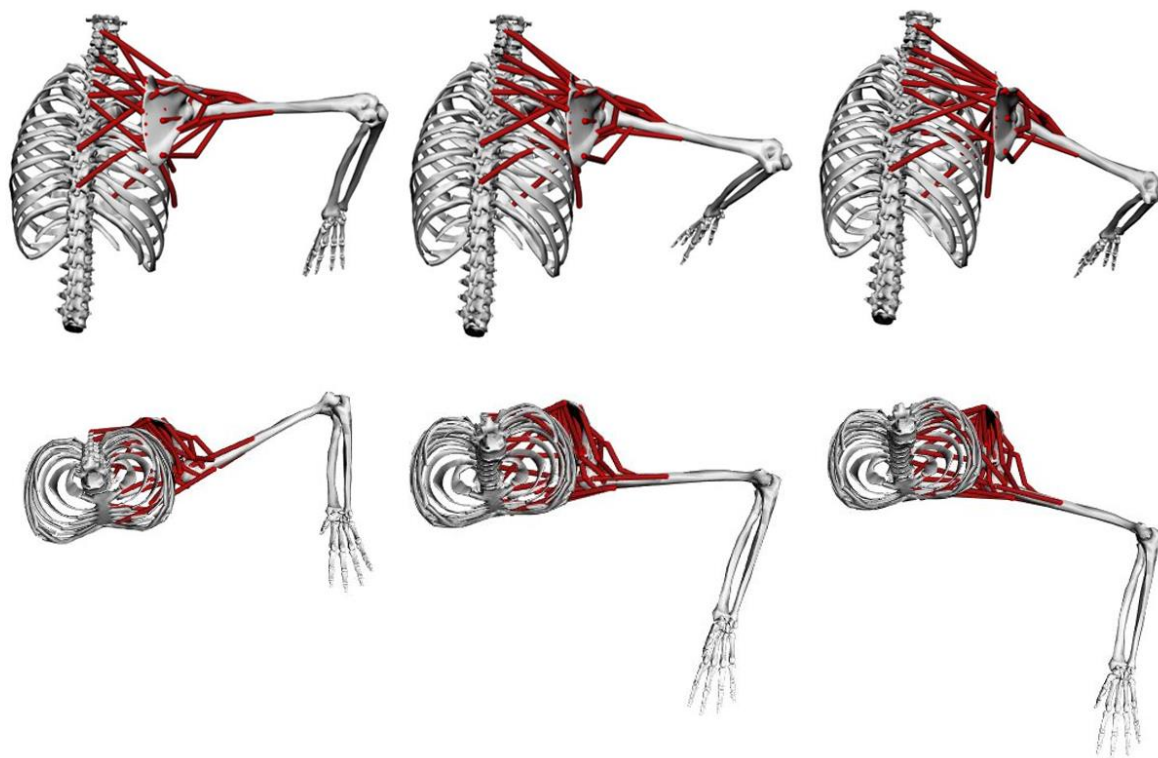


Figure 7.7: Scapula movement during propulsion from a top view (top) and rear view (bottom). Data is from Athlete J (Section 7.2).

For the athletes in this research, the torso segment masses were up to 1.70 times larger than the generic model (Section 6.4). A sensitivity study was performed on how important the scaling of the specific clavicle and scapula masses are to the overall reliability of the simulation (Appendix C.2). Increases of up to 7.61% in joint reaction moments resulted from a reduction in scapula mass by 10%. Therefore, the increase in torso mass in the musculoskeletal model of wheelchair racing athletes may be influential.

Locking the motion of the scapula onto the torso (thus removing the independent scapulohumeral rhythm), significantly reduced the magnitude of the centre of mass accelerations, which lead to a reduced input force (Figure 7.8). Although still higher than what would be anticipated from Figure 4.27, it is more reasonable. Additionally, locking the motion of the scapula also prevented the errors associated with the movement of the scapula away from the torso (Figure 7.6). Although the high magnitude of estimated forces used in this research may have impacted the statistical significance of the findings, as it was a systematic error, it is not anticipated that the overestimation of input forces would have impacted the trends identified. Thus, there is still merit in completing a coupled kinematic and computational modelling analysis, particularly when input forces of appropriate magnitude are included.

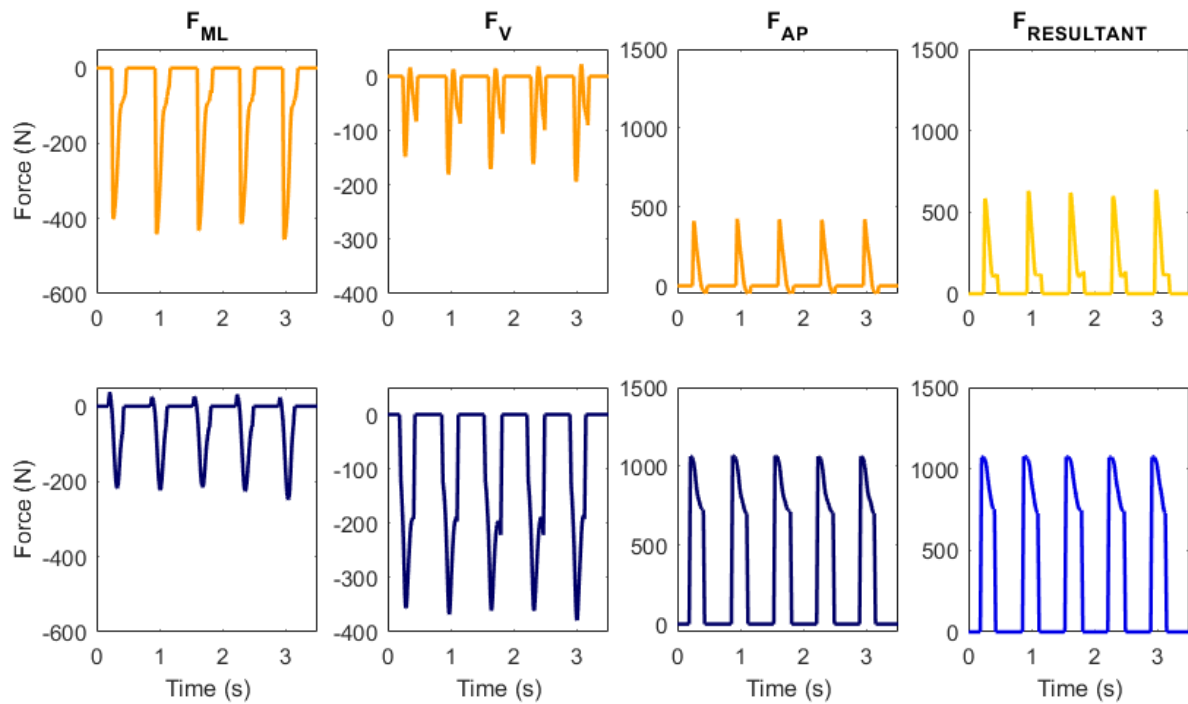


Figure 7.8: Comparison of reaction force estimates for unlocked (top) and locked (bottom) scapulothoracic joints, which resulted in the large overestimation of error in the results for Athlete I at 27 km/hr.

It is possible that errors may have been further emphasised by the high stiffness at the hand-pushrim interface due to the negligible damping provided from the use of thermoplastic gloves. This may have increased marker acceleration upon contact, which may have then propagated through to the calculation of the centre of mass accelerations of each of the limb segments. This can be observed from the instantaneous peak  $F_{\text{RESULTANT}}$  from the ‘locked’ condition in Figure 7.8, which may be eradicated through further data filtering.

## 7.2.5 CONCLUSION

This study has demonstrated the potential impact of using a coupled kinematic and modelling approach as a performance assessment tool to better ascertain relationships between kinematic technique and injury. Increased shoulder loading is a compounding effect of numerous kinematic parameters, with clear differences observed in the kinematic strategies utilised by the athletes in this study. By coupling regular kinematic feedback with a biomechanical model, it is possible to balance the performance and injury-risk requirements of propulsion.

### 7.2 INFLUENCE OF CUSTOMISED SEATING INTERFACES ON LOWER EXTREMITY WHEELCHAIR RACING KINEMATICS: A CASE STUDY

#### 7.2.1 INTRODUCTION

Optimising the athlete-wheelchair interface is critical for enhancing performance, and is achieved through best matching wheelchair geometry to unique athlete anthropometry. When buying a wheelchair, athletes can manipulate configuration parameters to best suit functional capacity. For example, athletes with reduced balance require higher knee placement, which is achieved with shorter seating (cage) depths.<sup>6</sup> However, the level of customisation in commercially available chairs does not always appropriately accommodate the anthropometric variations resulting from specific impairment. As a consequence, athletes may not have the stable base of support required for optimal propulsion.<sup>19</sup> The optimisation of an entire wheelchair to match unique athlete geometry is both time consuming and costly and precludes replacements to accommodate growth. The use of assistive technology can provide an efficient transition between the commercially available equipment and the unique athlete anthropometry. Customised seating interfaces provide a time and cost-effective solution, facilitating regular modifications to satisfy athlete growth. These solutions have been used extensively in clinical applications for enhanced stress distribution and injury prevention at the seating interface,<sup>74, 88, 222-224, 228, 232, 333-336</sup> however, these solutions have not been applied to sporting contexts. As such, this study examines how the inclusion of customised seating interfaces enhance athlete performance.

The inclusion of additional material at the seating interface has the potential to be detrimental to performance for two key reasons. Firstly, through the addition of increased aerodynamic resistance through the increased frontal area. Wheelchair racing athletes are subject to aerodynamic forces based on the high speeds they reach, with the kneeling posture adopted by wheelchair racing athletes almost halving this frontal area.<sup>9</sup> However, the customised seating interface does not contain much mass, and so the athlete does not sit much higher than in their conventional position. This also suggests that the centre of mass is not increased, which would make them more prone to increasing instability due to tipping.

Secondly, benefits of performance interfaces extend to improved head control, posture, reach, grasping and functional capabilities,<sup>86</sup> as well as allowing maximum force transfer through the entire range of motion.<sup>92</sup> Enhanced reach and grasping capabilities are crucial for effective force generation on the wheel. It is desired that athletes can use the entirety of the vertical plane of the pushrim for greatest force transfer.



---

This study aimed to investigate the performance impact of customised seating interfaces on wheelchair racing propulsion technique. It was hypothesised that through enhanced conformity at the seating interface, performance would be enhanced.

## 7.2.2 METHODS

### *Athlete Selection*

A single male athlete (Athlete J: age = 40 years; body mass = 62.4 kg; wheelchair mass = 6.7 kg; impairment: incomplete spinal cord injury) participated in this study after providing informed consent. The athlete was an experienced athlete, regularly competing in para-triathlons at an international level. The athlete adopted a seated position in his own racing wheelchair which was fixed on a single-roller ergometer system (Section 5.4).

### *Measurement System*

Propulsion kinematics pre- and post- customised seating interface intervention were captured through synchronised motion capture (sampling frequency = 250 Hz,) and high-speed video (Panasonic F15, Sampling Frequency 300 Hz, shutter speed 1/1000 s). Pre-intervention data was recorded using the athlete's conventional seating configuration, while post-intervention data were collected when the customised seating interface was included. High-speed camera footage captured the rear and sagittal (dominant side) planes of motion.

Markers were located on key anatomical landmarks, as well as the frame and wheel, (reflective tape rather than traditional spherical markers) to measure relative athlete and chair motion, as well as obtain an independent source of wheel speed, later converted to translational velocity. Marker placement was selected to be as unobtrusive as possible, while effectively measuring the range of motion at each joint. Four markers were located at the top of the seating bucket, where they were not obstructed and did not interfere with athlete motion. Five markers were located on each wheel: one at the centre, two located 180° apart on the pushrim, and two outer rim markers placed perpendicular to these. The cross arrangement (Figure 7.9) facilitates the use of relative trajectories to accommodate marker occlusion during wheel contact. Wheel based markers were made from flat strips of reflective tape to ensure no interference or loss of marker with motion.

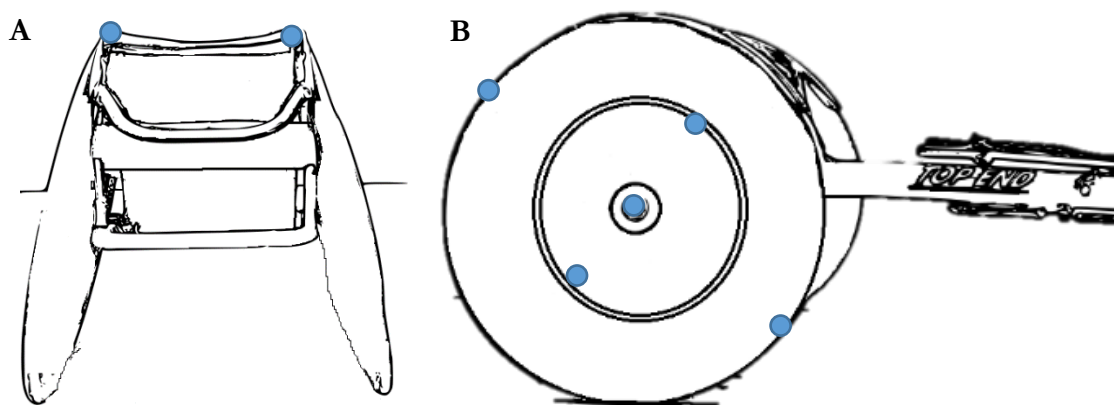


Figure 7.9: Marker (circles) configuration on A) the wheelchair frame (four, front two occluded) and B) wheel (five, same on both wheels).

A twenty-one marker-configuration was applied to the athlete (Figure 7.10): one marker on each of the shoulder (acromion process), elbow (styloid process), ulnar and radial wrist joints, and at the base of the 3rd metacarpal (adhered to the gloves). An individual marker was located on each of the C7 and T10 spinal processes, left and right posterior, superior iliac crests. On the lower extremity, one marker was located on each of the greater trochanters, knee, heel and big toe. Gaps in kinematic data (<25 ms) were interpolated using a cubic-spline interpolation. Despite cluster based marker configurations being more commonly implemented in modern literature than joint based, much of the modern literature regarding wheelchair kinematics adopt a plug-in marker-set approach.<sup>262, 337</sup>

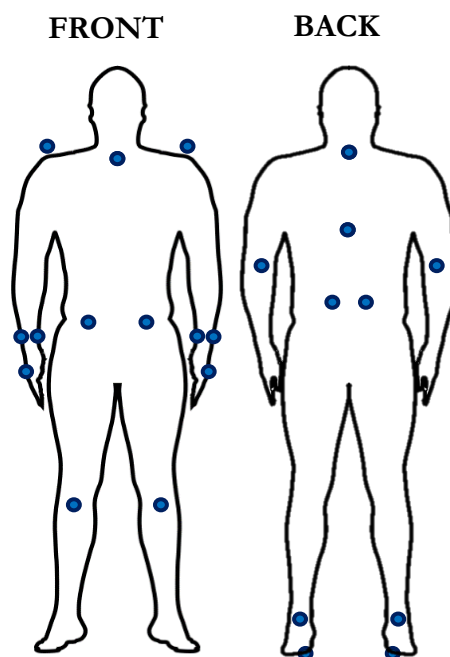


Figure 7.10: Motion capture marker placement on an athlete.

---

### *Experimental Propulsion Task*

A period of at least 15 minutes was provided to athletes before data collection to perform a self-directed warm up and acclimate with ergometer propulsion. Two stationary starts and steady-state trials at race pace (32 SPM) of 20 s were performed, with 2 minutes active recovery between trials, with the short duration of trials ensuring potential effects of fatigue on kinematic patterns were minimised. For the steady-state trial, data collection commenced after the athlete demonstrated consistent propulsion at speed, as determined through a velocimeter (Garmin Edge) located on the wheelchair frame. The three-dimensional kinematic data were filtered with a fourth-order Butterworth low-pass filter, zero lag, and a 7 Hz, - 6dB cut off frequency,<sup>262</sup> and processed using methods described in Section 4.2.

It is acknowledged that the use of the rollers is a limitation of the study. Biomechanically, it has been demonstrated that ergometers do not completely reflect the biomechanical and physiological requirements of propulsion.<sup>183</sup> For example, the lower rolling resistance means it is easier for athletes to accelerate, and as the wheelchairs are constrained to the rollers, athletes can neglect all steering requirements. However, findings from Section 5.4 demonstrated that a treadmill did not accurately represent overground propulsion, and hence as testing was refined to a laboratory (for the use of motion capture), rollers were used. These are still commonly used training tools suggesting their biomechanical relevance. Results were purposefully presented as relative comparisons, as it was assumed that any biomechanical variation introduced into the testing protocol would be consistent across both conditions.

### *Musculoskeletal Model*

Computer simulations utilising the Wu Shoulder Musculoskeletal Model<sup>330</sup> were performed in OpenSim.<sup>133</sup> The musculoskeletal model was adapted to incorporate athlete-specific segment mass (Section 6.3). No DXA data for this athlete was available in the prospectively maintained database identified previously. The collection of DXA data for this athlete was not feasible. Upper extremity body mass distribution was estimated from the average of the body mass distribution of three male athletes (Athlete K, Athlete L, and Athlete M). Segment masses were calculated based on multiplying the body mass distribution of segments against the measured athlete mass value. While it is acknowledged that this is a limitation, as none of the athletes had visible impairments to their upper extremity, were all male, and were all elite athletes, any errors introduced should be minor.

The generic model segment mass and inertia parameters were scaled by 1.29x for the thorax, clavicle and scapula, 1.51x for the humerus, 1.84x for the ulna and radius and 1.47x for the hand. As the

findings in Section 6.4, the maximum isometric force generating capacity upper extremity demonstrated close agreement with the difference in segment mass of the thorax with the generic, muscles were uniformly scaled by 1.3x. It is acknowledged that the scaling factor is lower in this study than what was presented in Chapter Six (1.50x for Athlete I and 1.7x for Athlete E). This can be partly attributed to the use of different models between Chapter Six and Chapter Seven.

### *Statistical Analysis*

Asymmetries in the lower extremities were deduced through statistical significance between the translations of the left and right limbs. Independent samples t-test were performed on cycle-based peak data between left and right markers in all three directions (AP, ML, V). All statistical calculations were performed using IBM SPSS Statistics 24 Software for Windows.

### 7.2.3 RESULTS

Unwanted translations of the lower extremity and torso were minimised through the inclusion of customised seating interfaces (Table 7.4). Pre and post designates performance prior to and after the inclusion of a customised seating interface, respectively. PSIS and knee marker motion was reduced by 59.42% and 41.46% respectively, with lateral translation of the spine reduced by up to 34.28%. Statistical significance was observed between the motions of all limbs between the old and new seating configurations. Statistically significant differences were observed for the toe (Race Pace: AP  $p = .000$ , Race Start: ML  $p = .004$ ), knee (Race Pace: AP  $p = .000$ , ML  $p = .012$ , V  $p = .000$ , Race Start: AP  $p = .000$ ), PSIS (Race Pace: AP  $p = .000$ , ML  $p = .000$ , V  $p = .000$ , Race Start: AP  $p = .008$ , V  $p = .000$ ) and C7 (Race Pace: AP  $p = .000$ , V  $p = .000$ , Race Start: AP  $p = .019$ , ML  $p = .009$ , V  $p = .000$ ).

Statistically significant differences in symmetry were observed at the knee and toe only, with these primarily observed in the old seating configuration (Toe: Race Pace ML:  $p = .000$ , V:  $p = .000$ , Race Start V:  $p = .008$ , Knee: Race Pace ML:  $p = .000$ , V:  $p = .000$ , Race Start ML:  $p = .054$ , V:  $p = .008$ ). Asymmetries were not mitigated within the new seating interface for Race Pace ML for both the toe and knee ( $p = .026$  and  $p = .026$ , respectively).

Asymmetry of the upper extremity was analysed through the use of cyclograms (Figure 7.11 and Figure 7.12). It is clear that low asymmetries were present in the upper extremities with these being minimised through the inclusion of a customised seating interface. Greatest motions are present further down the kinematic chain, demonstrating the sensitivity of the motion.

Table 7.4: Changes in forwards knee motion between old and new seating conditions. Positive values indicate a reduction in movement (post).

	Race Pace			Race Start			
		Pre (mm)	Post (mm)	%	Pre (mm)	Post (mm)	%
Toe	AP	10.5 ± 1.6	9.3 ± 1.1	11.8**	10.9 ± 2.2	9.1 ± 2.1	17.0
	ML	5.9 ± 3.3	8.1 ± 3.9	-36.2	5.6 ± 2.5	8.5 ± 3.3	-52.5**
	V	7.1 ± 2.9	11.7 ± 1.9	-65.3	6.6 ± 1.7	10.2 ± 2.0	-54.8
Knee	AP	12.9 ± 4.1	9.4 ± 1.1	26.8**	17.3 ± 3.9	10.1 ± 2.9	41.5**
	ML	6.0 ± 2.1	5.9 ± 1.6	0.7*	6.8 ± 2.2	6.7 ± 2.3	0.9
	V	17.6 ± 5.4	16.4 ± 1.7	6.5**	21.5 ± 3.2	18.0 ± 3.6	16.2
PSIS	AP	30.4 ± 15.5	12.4 ± 2.6	59.4**	41.8 ± 7.2	23.1 ± 8.3	44.7*
	ML	8.4 ± 3.3	7.9 ± 2.1	6.5**	9.4 ± 2.6	9.2 ± 2.6	2.7
	V	22.9 ± 3.5	21.8 ± 2.2	4.4**	23.7 ± 3.1	25.9 ± 6.6	-9.2**
C7	AP	41.9 ± 19.9	19.4 ± 5.9	53.8**	63.0 ± 9.1	36.5 ± 11.5	42.0*
	ML	13.7 ± 5.4	11.6 ± 7.5	15.2	17.0 ± 8.2	11.1 ± 4.1	34.3*
	V	129.8 ± 23.1	129.6 ± 8.3	0.2**	126.8 ± 15.5	128.5 ± 33.5	-1.3**

\* denotes  $p < .05$ , \*\* denotes  $p < .001$

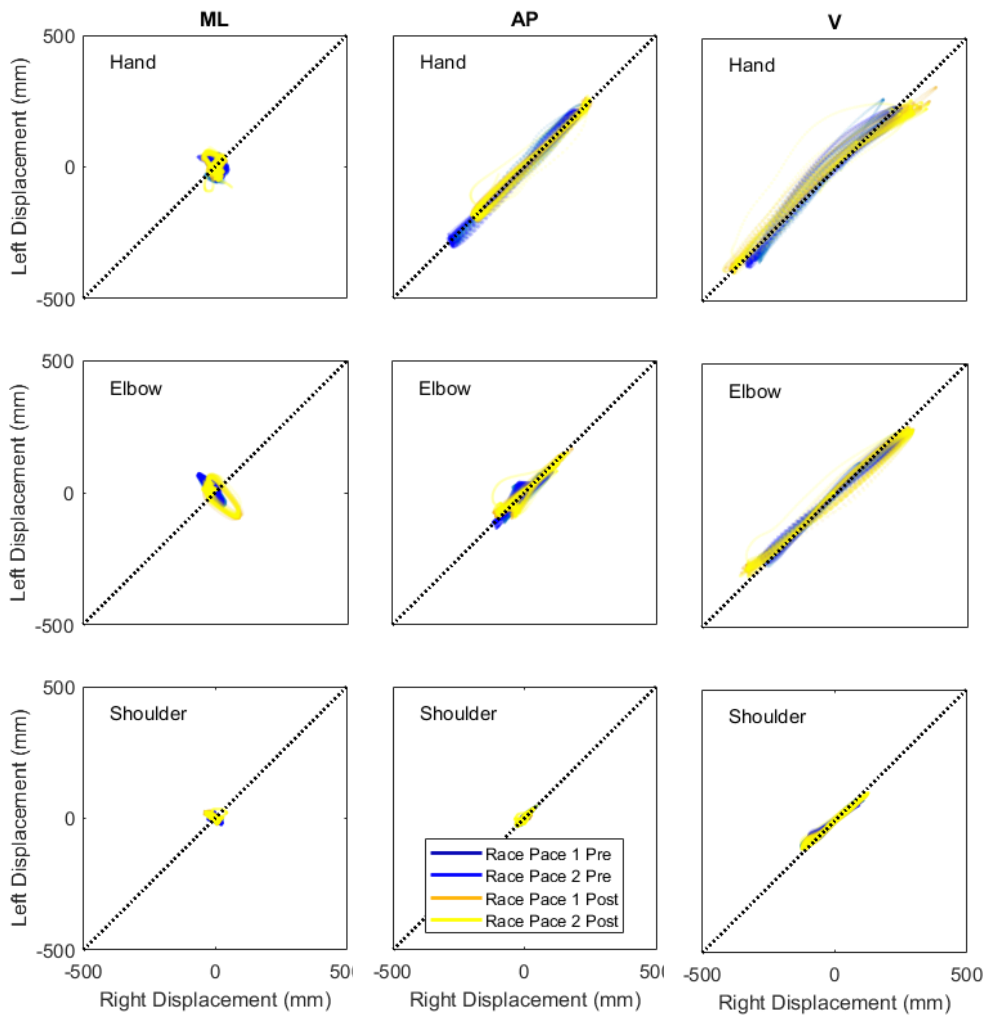


Figure 7.11: Cyclograms demonstrating reduced asymmetries at the hand during steady state conditions due to a customised seating interface.

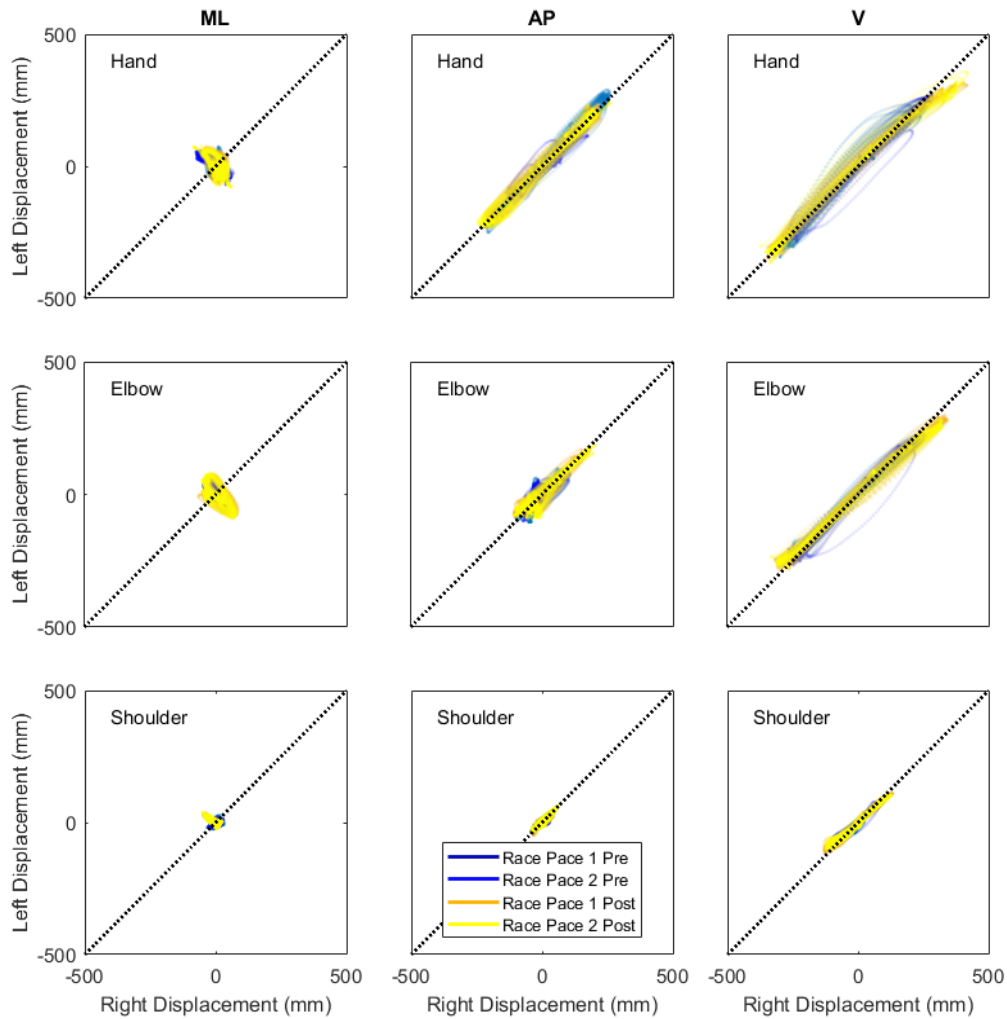


Figure 7.12: Cyclograms, demonstrating reduced asymmetries at the hand and elbow through the inclusion of the customised seating interface under race start conditions.

Clear variability was observed between the old and new seating conditions for both steady state (Figure 7.13) and starting motions (Figure 7.14). However, there were no considerable increases in peak moment in any of the modelled degrees of freedom, suggesting that the use of customised seating interfaces do not increase the risk of athlete injury. It can be seen particularly for the starting motion (Figure 7.13), that the distribution of data post-intervention was more normally distributed about 0 (Shoulder Plane Moment, Shoulder Reaction Moment) than pre-intervention. Additionally, there is a more symmetric loading between the left and right hands, in line with the reduced asymmetries observed from the analysis of the kinematic data. A higher magnitude of discrete data points from the post-intervention case, however, have a higher absolute value than was observed with the pre-intervention data, however as can be seen in Figure 7.13 and Figure 7.14, the occurrence of these were rare, suggesting they are movement artefact errors and can be neglected.

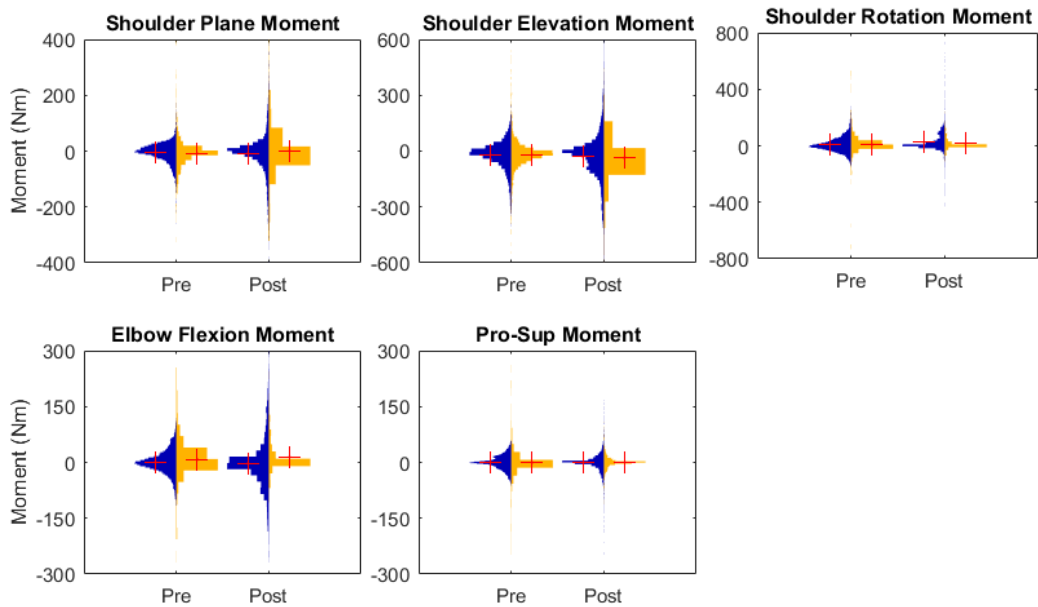


Figure 7.13: Violin plots demonstrating joint reaction moments differ between left (blue) and right (yellow) limbs during steady-state motion. The width of the violin plot for a particular moment indicates its relative frequency in the distribution.

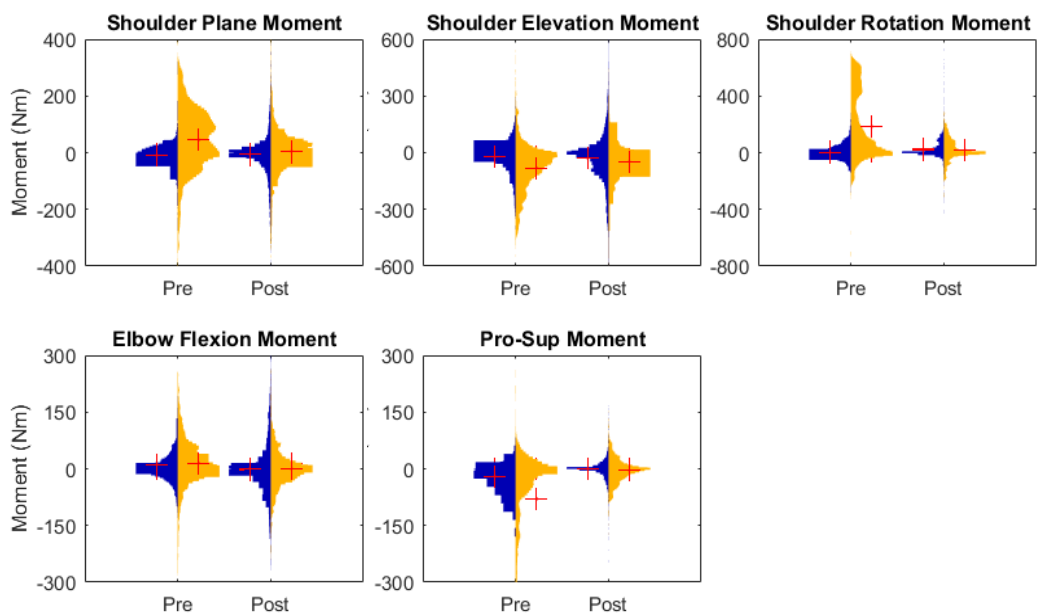


Figure 7.14: Violin plots demonstrating joint reaction moments differ between left (blue) and right (yellow) limbs during a starting motion.

Performance was observed to have a 3.7% improvement in mean race time since the inclusion of the customised seating interface. Figure 7.15 demonstrates the individual and mean performance times in the eight international competitions immediately before and after the inclusion of the seating interface. Improved performance translates to 0.36 s over 5,000 m.

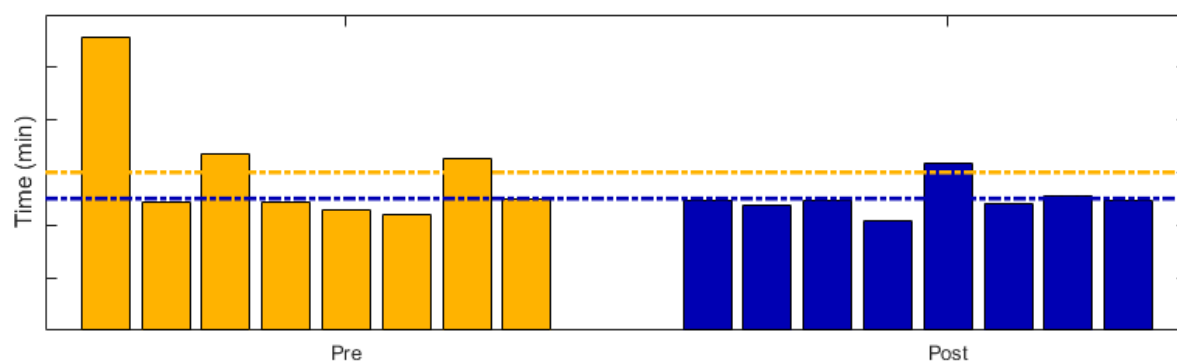


Figure 7.15: Performance impact of customised seating interfaces on performance. Dashed lines indicate mean time. Values are omitted to retain athlete anonymity.

#### 7.2.4 DISCUSSION

This study evaluated the performance impact of a customised seating interface for a single athlete. Customised seating interfaces were demonstrated to effectively increase the conformity at the seating interface, as demonstrated through the reductions in unwanted lower extremity movement. Additionally, lateral translations of the spine were reduced. No significant increases in joint loading were observed, suggesting the altered kinematic patterns acquired through the use of customised seating interfaces does not increase the risk of the athlete acquiring an injury risk. Finally, performance benefits were observed through a 3.7% reduction in competition time, which has a significant impact on race outcome. This study only investigated the seating interface, with no modifications to the existing wheelchair frame made.

The athlete in this study demonstrated lower extremity bilateral asymmetry, suggesting that the results from this study are greater than what may be observed across the whole population. However, based on the uniqueness of each athlete's impairment, their requirement on their equipment varies largely. Although the case study approach in this study cannot be formally generalised across the entire population, the findings of this study demonstrate the potential performance impact of customised seating interfaces.

Viscoelastic foam was the preferred material selection in this research. However, a problem with commonly used viscoelastic foams is that they lose their supportive properties with wear over time.<sup>91</sup> The specific manufacture of customised seating interfaces was outside the scope of this research. Further optimisation into material selection is justified for the future.

It was demonstrated in this study that lower extremity motion was substantially reduced following the inclusion of a customised seating interface. Although this is theoretically reducing the unwanted slipping and frictional rubbing motions which are not contributing to movement, previous literature



---

has demonstrated the potential use of the lower extremity as a form of leverage to gain a biomechanical advantage in propulsion.<sup>338</sup> As such it is suggested that the specific density of stiffness of foam may be related to the functional capacity of the lower extremity, and hence needs individual consideration. Further, the customised interface may need customisation for the race course itself. For example, performance times can be impacted by external factors (such as wind), as well as race geometry, with courses having tighter turns may require more support and control.

A key performance outcome of this study is that reductions in asymmetry (albeit minor) were observed immediately. From a skill acquisition perspective, it is possible that the values presented in this study underestimate the actual changes, which the athlete would experience after appropriate acclimation. It is currently unknown what the optimal acclimation period is. However, it is theorised that this is of the magnitude of months. However, the benefits of these immediate changes are that they require no cognitive control, and as such, the reduced asymmetries, and lower extremity translations are unlikely to be observed during competition or when fatigued. This suggests greater longevity in the outcome.

The increased peak moments from the inclusion of the customised seating interface may not imply increased injury risk. As suggested in Section 7.1, normative databases need to be established to inform whether increases are as a consequence of greater force transmission and hence performance, or whether they indicate injury risk. As can be seen in the violin plots, the majority of the data is of much smaller magnitude than the peak values are presented in Table 7.1 and Table 7.2. This is indicative of errors with the estimation of input forces, which as mentioned in Section 7.1, may have high instantaneous peaks due to the ballistic nature of contact between a hard, thermoplastic glove, and the pushrim.

The inclusion of muscular stresses would complement future research. A preliminary investigation into the modelling of muscular forces was performed in this research (Appendix C.3). However, based on the limitations surrounding the estimation of applied forces, and the propagation of errors throughout the OpenSim modelling workflow, the reliability of these estimates was questioned. Further refinement into the estimation of input forces (Section 4.5) and the scaling of the clavicle and scapula (Section C.2) are required to facilitate the estimation of these muscle stresses.

## 7.2.5 CONCLUSION

Customised seating interfaces can positively influence wheelchair propulsion motion. Performance increases are the result of reduced unwanted motions at the lower extremity, which lead to the increased symmetry of the upper extremity. Additionally, no substantial increases on joint reaction

loads (Figure 7.13 and Figure 7.14) were identified from the inclusion of customised seating interfaces, suggesting there is no additional risk of injury from their use.

### 7.3 IMPLICATIONS AND CONCLUSION

Computational modelling provides an advancement on traditional video observation, or motion capture analyses. By coupling the kinematic patterns with estimated kinetic loading, it is possible to associate technical strategies with injury risk (Section 7.1), and the influence of athlete equipment on performance (Section 7.2). While the process of performing computational analyses is laborious, for a sport such as wheelchair racing, where minimal sports science has been performed, the understanding of techniques invoking injury is of critical importance. Further research is required in the development and validation of appropriate musculoskeletal models and methods for estimating input forces to improve the reliability of this process.

#### *Key Findings:*

- Customised seating interfaces improve athlete performance, through the reduction in unwanted lateral translations of the lower extremity.
- Customised seating interfaces can improve whole body symmetry.
- Joint loadings are not increased through the inclusion of customised seating interfaces.
- Shoulder, elbow and torso angles can affect the loads acting at the shoulder.
- Greater applied loads at the hand rim do not necessarily translate to the shoulder.

#### *Implications:*

- The degree of conformity should be analysed in more detail to match performance.
- The level of performance impact may rely on the level of athlete impairment, and what anthropometric adaptations are present in the lower extremities.
- Coupled kinematic and modelling studies can be used to balance the performance and injury risk requirements of propulsion.
- Athletes can manipulate technique to ensure maximum force application, without injury risk. (E.g. High hand velocity at contact may reduce performance and increase injury risk).
- A normative database may be established to highlight techniques which are more prone to injury.

---

---

# CHAPTER EIGHT:

# CONCLUSION

---

## 8.1 OVERVIEW OF THE EXPERIMENTAL CHAPTERS

This research aimed to determine whether the inclusion of customised seating interfaces lead to improve the performance of wheelchair racing athletes. The performance was analysed using a computational modelling approach based on its ability to provide an understanding of both the kinematic advantage and injury risk of a specific technique. Computational modelling approaches are not novel methodologically in the analysis of sporting motions. However, they are for applications involving wheelchair athletes. The fundamental musculoskeletal model used typically reflects the musculoskeletal parameters of able-bodied, non-athletic populations, who are more conventionally analysed using these processes. The development of subject-specific musculoskeletal models representative of an elite wheelchair racing population was required to address the fundamental research aim. In addition to the musculoskeletal model, two experimental data sets (kinetics and kinematics) were used to drive the computational modelling approach. An exploration into practically-viable instrumentation solutions capable of measuring in-field performance (both propulsive and reaction forces) for input into the computational model was also required, as no commercially-available systems are currently appropriate for use with wheelchair racers. This can be reflected in the four key aims of the research, with the interrelation between these presented in Figure 8.1.

- Understand how various aspects of wheelchair racing technique and equipment relate to performance. (Chapter Three)
- Develop instrumentation tools capable of in-field data measurement. (Chapters Four and Five)
- Develop a subject-specific, 3D computational model. (Chapter Six)
- Quantify the mechanics of wheelchair propulsion using simulation. (Chapter Seven)

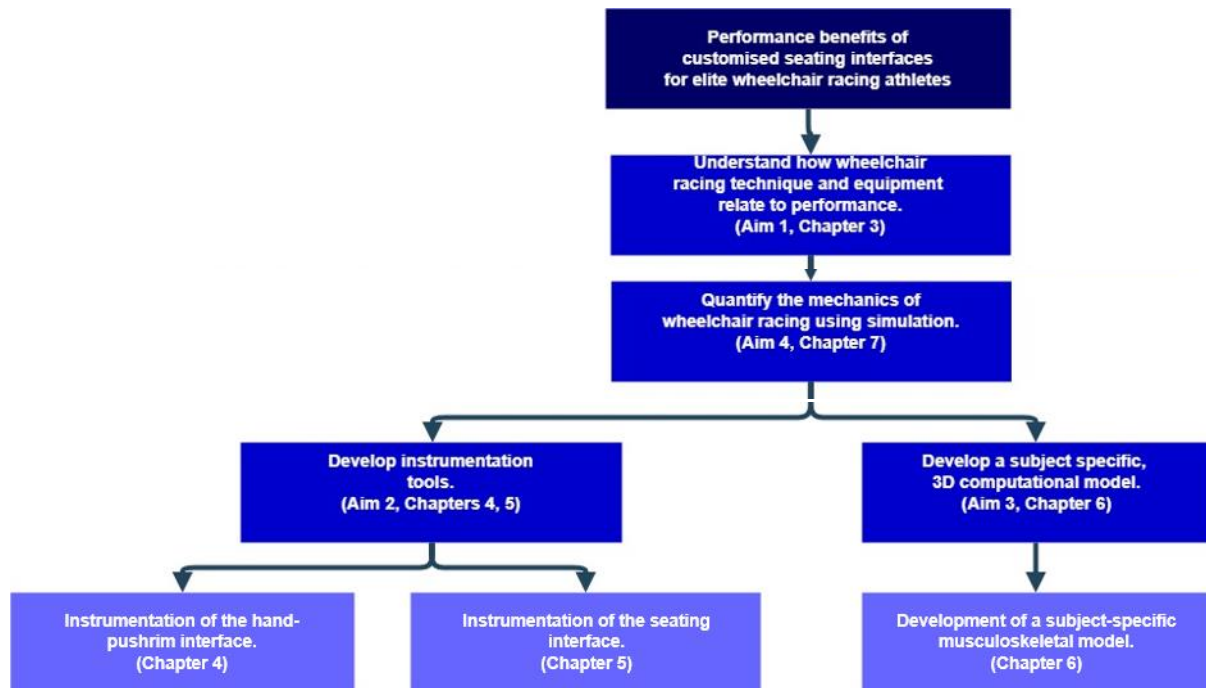


Figure 8.8.1: Relation of key research aims to overall research aim.

A series of experimental investigations, resulting in six journal papers, two conference proceedings, and six conference presentations were performed to answer each of these objectives holistically. The key findings for each of the studies, which led to the overall assessment of customised seating interfaces on wheelchair performance are summarised as follows.

### 8.1.1 UNDERSTAND HOW VARIOUS ASPECTS OF WHEELCHAIR RACING TECHNIQUE AND EQUIPMENT RELATE TO PERFORMANCE

The effective integration of specialised equipment into athletic applications is an iterative process requiring concurrent research and contributions from a multidisciplinary team. To ensure resources are being maximised, it is hence important to understand the magnitude of the potential performance gains relative to other factors affecting performance such as technique and equipment. It was,

therefore, essential to understand whether aerodynamic strategies dominate performance (as seating cushions may increase frontal area) and whether customised gloves promote asymmetries.

Some athletes elect to use customised thermoplastic gloves. These are commonly 3D printed based off the mould of a single hand, with the glove on the non-dominant hand being a mirror-image of the glove on the dominant hand. Athlete asymmetries were not found to increase through the use of these thermoplastic gloves. It can hence be assumed that the aetiology of athlete asymmetry is more so a consequence of athlete impairment and geometry rather than glove selection. This demonstrates the potential benefits of the use of customised seating interfaces for asymmetric athletes.

While some sports are dominated by aerodynamics, findings from Section 3.2 demonstrated that aerodynamic advantage might be compromised in order to achieve maximum force transmission to the wheelchair, and hence acceleration. The marginal increase in seating height and hence frontal area resulting from the inclusion of a customised seating interface are henceforth not anticipated to be of detriment to performance. The findings from these two studies highlighted that the use of a customised seating interface might lead to practically meaningful performance gains. The key findings from Chapter are summarised in Table 8.1.

Table 8.1: Key findings from Chapter Three: How important is the seating interface to athlete performance?

Section	Key Findings
3.2	<ul style="list-style-type: none"> <li>▪ No significant differences were observed in the degree of symmetry between soft and no glove conditions.</li> <li>▪ Hard gloves only influenced the level of symmetry of the propulsive impulse.</li> <li>▪ Symmetry was more affected by the use of gloves for T54 athletes, as compared with the T34 classified counterparts.</li> </ul>
3.3	<ul style="list-style-type: none"> <li>▪ Female performance improved with better aerodynamic positions, however aerodynamics were less critical for males who may better overcome additional resistive forces due to enhanced strength capabilities.</li> <li>▪ Although aerodynamics were not identified as the winning factor for males, improved aerodynamics, with no compromise to power generating capabilities can increase the potential of winning.</li> <li>▪ Overcorrection of aerodynamic positioning may artificially increase impairment, meaning athletes must select a technique best suited to their capabilities.</li> </ul>

### 8.1.2 DEVELOP INSTRUMENTATION TOOLS CAPABLE OF IN-FIELD DATA MEASUREMENT

Wheelchair motion is the result of an effective transfer of force from the hands to the pushrims on the wheelchair wheels. Substantial literature has explored the optimisation of these interactions to improve movement efficiency or velocity for both manual wheelchair users and athletes alike. These studies are typically performed in laboratory conditions, with propulsive forces measured using a SMARTWheel. However, due to the influence of mass on performance, and the lightweight nature of wheelchair racing frames, the use of a SMARTWheel does not translate to the assessment of wheelchair racing performance. Consequently, contemporary methods of measuring the hand-pushrim interactions are required for use within the computational model in this research. For completeness, the reaction forces at the seating interface are also required for input into the computational model. These have not typically been considered in previous literature detailing the biomechanics of wheelchair racing, however, are commonly explored in clinical applications which aim to minimise the risk of manual wheelchair users attaining pressure ulcers through alleviating peak pressures.

#### *Propulsive forces*

A literature review revealed the practical inadequacies of the commonly-used, commercially-available wheel-based instrumentation solutions, and the need for new technologies. To ensure integration within the daily training environment for the maximal benefit to performance preparation, any developed instrumentation must not be an encumbrance to performance. It was preferred that instrumentation was able to be efficiently and reliably operated by coaches and biomechanists, allowing nationally-based performance assessment. This supported the development of performance-based assessment protocols for the rapid growth in the understanding of optimisation of wheelchair racing technique. IMUs formed the primary instrumentation tool in this research, based on their light mass, ease of mounting, accessibility and cost, and previous success in the kinematic monitoring of wheelchair propulsion. The limited application of IMUs in the literature previously, which was predominantly court-sport and manual wheelchair propulsion oriented, merited the exploration of their efficacy in wheelchair racing.

Good agreement in contact timings was observed between IMU, video, and motion capture. The optimum placement location was on the frame, which was where the best results were achieved as determined by the best between method agreement. The IMU assessment approach facilitates an automated processing capability, which is an improvement to the currently used video analysis. An IMU located on the frame provided a robust solution across varied athlete and equipment

characteristics for this population sample. Detection reliability was positively associated with the SNR of the acceleration data. Therefore the use of IMUs may be limited for use with junior athletes or manual wheelchair users who have lower SNR (which is possibly due to lower stiffness equipment).

Good agreement in kinetic parameters between IMU data was observed under steady-state motion, with data from most athletes following a linear force-velocity relationship against previous research. IMUs were ineffective when used with wheelchairs having spoked wheels. The performance was best for measurements in the direction of motion. Although exact agreement was not observed, the IMU can provide an effective tool in the in-field assessment of propulsion kinetics. However, based on the data processing approaches implemented within this research, IMUs are not yet appropriate for use in computational modelling, due to the compounding and propagation of errors throughout the analysis. The key findings of the individual studies summarised in Table 8.2.

Table 8.2: Key findings from Chapter Four: Instrumentation using IMUs.

Section	Key Findings
4.1	<ul style="list-style-type: none"> <li>▪ IMUs are equally useful in identifying contact as compared with the ‘gold standard’ high-speed video observation method.</li> <li>▪ IMUs provide a method which is less susceptible to parallax and perspective errors than the current ‘gold standard’ methodology.</li> <li>▪ The characteristic response of IMUs changed across placement locations.</li> </ul>
4.3	<ul style="list-style-type: none"> <li>▪ Release points were not always identified, as they were of comparable magnitude to the underlying noise of the signal.</li> <li>▪ Release points were identified when athletes performed an inefficient technique, meaning IMUs may still be useful in kinematic monitoring for performance preparation.</li> <li>▪ Reliability of the IMU improved with speed, gender, athlete classification and age.</li> </ul>
4.4	<ul style="list-style-type: none"> <li>▪ Automated analysis requires more sophisticated data analysis than raw signal detection.</li> <li>▪ Acceleration response differs between the wheel and frame, with further differences based on specific placement on the wheel.</li> <li>▪ The reliability of the IMU methodology is reliant on the inherent SNR.</li> </ul>
4.5	<ul style="list-style-type: none"> <li>▪ IMUs can reliably estimate propulsive forces in the forwards direction but are less reliable in estimating out of plane forces in both the mediolateral (due to wheel camber) and vertical directions.</li> <li>▪ The reliability of the IMU increases with steady-state speed monitoring as compared with starting motions.</li> </ul>

### *Reaction forces*

The dynamic response at the seating interface of the wheelchair racing athlete has not been reported previously. Much of the literature detailing the biomechanical response of racing wheelchair propulsion has omitted the interactions at the seating interface, despite its importance frequently raised in the clinical literature involving manual wheelchair users. The gold standard measurement tool in this clinical research is a pressure mat. The translation of the use of pressure mapping technology from clinical to applied practice may have been limited by the vastly different geometries of the seating interface between wheelchairs used for ambulation, and racing wheelchairs.

Several performance aspects of a commercially-available pressure mat were explored, and these revealed there were no problems in measuring the athlete-wheelchair interactions at the seating interface, even when foam cushions were used. Preliminary findings also revealed the dangerously high pressures athletes are exposed to, as well as the potential for competitive advantage through effectively leveraging through the seating interface. This highlighted the need for athletes to introduce customised seating interfaces as part of regular wheelchair configuration to dissipate peak stresses and lower the risk of the athlete obtaining a pressure-related injury. Other key findings are presented in Table 8.3. From a modelling perspective; the key finding was that for steady-state, linear propulsion (as performed in this research), the reactions at the seating interface were not dynamic, but quasi-static. Thus, these reaction forces could be simplified as being a proportion of total body mass.

From a practical perspective, athletes demonstrated large within-trial variation in average pressure, peak pressure and contact area for the acceleration and agility (wheelchair rugby only) trials, suggesting the change in requirements of the seating interface for wheelchair athletes across different motions. This research suggests the need for greater individualisation of athlete-wheelchair seating interfaces to promote performance, as well as the importance of including these seating interactions in biomechanical analyses of wheelchair propulsion. Regular monitoring of pressure distribution and sport-specific demands will assist in wheelchair prescription and provide an improved understanding of individual seat design requirements associated with specific athlete impairments.



Table 8.3: Key findings from Chapter Five: Instrumentation using a pressure mat.

Section	Key Findings
5.2	<ul style="list-style-type: none"> <li>▪ A commercially available pressure mat can measure pressure at the wheelchair seat, while not being an encumbrance to athletes.</li> <li>▪ Dynamic interactions occur at the seating interface which may impact performance.</li> <li>▪ The assumption of constant mass at the seating interface is only valid under linear, steady-state propulsion.</li> </ul>
5.3	<ul style="list-style-type: none"> <li>▪ Implementation of a foam insert at the seating interface did not impede the recording capability of a pressure mat.</li> <li>▪ A minority of the sample size in this research currently use cushioned interfaces.</li> <li>▪ The inclusion of a foam insert at the seating interface altered athlete-wheelchair interaction, through a reduction in seating pressure (average and peak), and an increase in contact area.</li> </ul>
5.4	<ul style="list-style-type: none"> <li>▪ Pressure mapping technology can identify the direction of applied pressure at the seating interface.</li> <li>▪ Treadmill propulsion does not adequately represent the dynamic interactions at the seating interface compared to on-track performance.</li> <li>▪ Track steady-state and treadmill steady-state propulsion have similar variability, however, differ in absolute magnitude.</li> </ul>

### 8.1.3 DEVELOP A SUBJECT-SPECIFIC, 3D COMPUTATIONAL MODEL

Computational modelling provides an advanced analytical tool which is capable of both analysing performances and understanding the associated injury risk of movement technique. The direct application of these approaches is limited by the dominance of parameters from able-bodied, and non-athletic populations used in existing musculoskeletal models. Based on muscle loss from physical impairment, and hypertrophy, the physical anthropometry of wheelchair racing athletes was considered to differ substantially to the population samples these models are currently built upon. Due to the accumulation of errors in computational modelling, it is possible that the use of generic musculoskeletal models may invoke large errors, which would ultimately invalidate the results of a simulation. This research investigated the sensitivity of model predictions to increased personalisation of musculoskeletal models to more reliably analyse the influence of customised seating interfaces.

The majority of parameters used in large-scale models (such as optimal fibre length) cannot be practically measured as part of a regular biomechanical analysis. The use of DXA scans provides an attractive alternative facilitating the estimation of subject-specific inertial parameters in a far less time-expensive way than what is otherwise required from the processing of MRI scans, for example.

Substantial between-athlete body mass distribution variances (thigh mass between 7.8% and 22.4% total body mass), and between-limb asymmetries ( $< 62.4\%$  segment mass; 3.1 kg) were observed. Compared to non-athletic able-bodied anthropometric data, wheelchair racing athletes demonstrated greater mass in the upper extremities (up to 3.8% total body mass), and less in the lower extremities (up to 9.8% total body mass). Computational simulations were sensitive to individual body mass distribution, with joint torques increasing by up to 31.5% when the scaling of segment masses (measured or generic) differed by up to 2.3% total body mass. These data suggest non-athletic, able-bodied mass segment inertial parameters are inappropriate for analysing elite wheelchair racing motion and highlight the importance of the subject-specific modelling approaches.

Artificially weakening a model through the under-definition of maximum isometric force-generating capacity of muscles presented physiologically invalid simulation estimates. This may be the consequence of the use of generic parameters for an athletic population. Artificially strengthening a model excessively (4.0x) also demonstrated physiologically invalid muscle force values. The ideal scaling factors were 1.5x and 1.75x for Athletes E and I, respectively, which was comparable to the relative difference in limb masses between DXA data and anthropometric data in the literature (1.49x and 1.70x). This finding suggests that DXA may be used to estimate the required scaling factors to enhance the reliability of simulations for elite wheelchair racing athletes. The key findings from the development of a subject-specific, 3D computational model are presented in Table 8.4.

Table 8.4: Key findings from Chapter Six: Development of a subject-specific, 3D, musculoskeletal model.

Section	Key Findings
6.2	<ul style="list-style-type: none"> <li>▪ The processing of DXA scans is subject to a defined intensity threshold, with bony segments found to be more sensitive.</li> <li>▪ The machine-default threshold protocol was the most accurate method investigated.</li> <li>▪ Errors in segment mass definition can alter system dynamics.</li> </ul>
6.3	<ul style="list-style-type: none"> <li>▪ Large between-athlete variation and between-population variation in body mass distribution were observed.</li> <li>▪ Generic scaling approaches based on able-body mass distribution, poorly estimated DXA obtained segment mass values of physically impaired athletes.</li> <li>▪ Differences in output joint torques were observed between subject-specific and generically scaled models.</li> </ul>
6.4	<ul style="list-style-type: none"> <li>▪ The use of DXA scans can assist in defining the maximum isometric force-generating capacity of wheelchair athletes.</li> <li>▪ Weakening a model (reducing maximum isometric force-generating capacity) provided physiologically invalid results for wheelchair racing propulsion.</li> <li>▪ Muscle activation changed as scaling factor was increased in a non-proportional fashion.</li> </ul>

#### 8.1.4 QUANTIFY THE MECHANICAL BENEFITS OF CUSTOMISED SEATING INTERFACES FOR WHEELCHAIR RACING ATHLETES

Customised seating interfaces can improve conformity through increased contact area to reduce the incidence of pressure sore formation in manual wheelchair users. Despite the clinical benefits of customised seating interfaces, they are not yet commonly integrated into sporting wheelchairs. The findings from Chapter Five (a constant mass input can be used for the estimation of the reaction force at the seating interface for steady-state, linear propulsion), and Chapter Six (subject-specific musculoskeletal models) were used to drive the computational model to quantify mechanical performance of wheelchair racing (Chapter Seven). As the IMU was not suitable for use in the computational model, these were estimated using kinematic data.

Competition performance improved by 3.7% after implementation of a customised seating interface for the athlete investigated. This is a practically significant finding, as it has been demonstrated that medals were attained within a time frame of 0.28% of the winning time for the women's T54 1,500 m race at the London 2012 Paralympics.<sup>200</sup> Model predictions suggested that these performance gains may have been a consequence of increased propulsion efficiency resulting from the reduced lateral translation and unwanted movement in the seat. Additionally, despite the changes in posture invoked through manipulation of the seating interface, model predictions did not indicate significantly higher injury risk (as a consequence of enhanced joint loading and hence muscle strain). This suggests that the implementation of customised seating interfaces is both safe and effective and that they could start to be integrated into sports on a larger scale. As seating posture and hence spinal alignment are being altered, it is recommended that the introduction of these interfaces are performed in conjunction with multidisciplinary teams involving biomechanists, physiotherapists or occupational therapists to ensure safety and athlete wellbeing is upheld. The key findings from this aim are summarised in Table 8.5.

Table 8.5: Key findings from Chapter Seven: Quantify the mechanics of wheelchair racing propulsion using simulation.

Section	Key Findings
7.1	<ul style="list-style-type: none"> <li>▪ Different athletes employ different kinematic strategies.</li> <li>▪ Shoulder, elbow and torso angles can affect the loads acting at the shoulder.</li> <li>▪ Greater applied loads at the hand rim do not necessarily mean greater impact loads at the shoulder.</li> </ul>
7.2	<ul style="list-style-type: none"> <li>▪ Lateral translations of the lower extremity can be reduced when using customised seating interfaces.</li> <li>▪ Customised seating interfaces can improve whole body symmetry.</li> <li>▪ Joint loadings are not increased through the inclusion of customised seating interfaces.</li> </ul>

### 8.2 CONTRIBUTION TO SCIENTIFIC UNDERSTANDING AND FUTURE DIRECTIONS

Given the lack of computational modelling of wheelchair racing athletes previously identified in the scientific literature, this research has contributed significantly to the scientific understanding in this field. Additionally, the findings and tools developed are applicable to biomechanists, coaches and athletes for improved performance preparation, which may lead to improved performance outcome. Many of the findings presented in this research are preliminary and can be further developed through ongoing research to ensure maximal performance gains are delivered to the athletes.

The evidence of the ergonomic benefits of customised seating interfaces on elite wheelchair racing athletes was demonstrated in this research. Although the research presented in this research has substantially contributed to the field of study, some further questions have evolved which require continued evaluation. Repeat investigations should be completed with a larger population sample, possibly inclusive of a more diverse range of physical impairments, both within wheelchair racing and across other wheelchair sports. However, some methodological limitations were present within this research, which should be addressed prior to the large-scale evaluation of wheelchair racing propulsion using computational modelling approaches.

The research was predominantly constrained to wheelchair racing. As sporting wheelchairs are performance driven, there are substantial differences in designs. For example, wheelchair sports involving contact (Rugby and Basketball) both require much higher frame stiffness than is seen for wheelchair racers. Additionally, the kneeling position wheelchair racers adopt, and the use of a pushrim differs from other wheelchair sports. As such, it is anticipated that the response may vary across different wheelchair sports, and should be further investigated under conditions relevant to each sport. Nonetheless, wheelchair racing has been established as one of the most popular events at the Paralympics,<sup>245</sup> suggesting that this constraint does not limit the relevance of the obtained results.

Athletes were from classifications where there was no physical impairment to the upper extremity to maintain some homogeneity across modelling results. Use of more impaired athletes is likely to require more substantial adaption in the model, and thus should be performed as an extension to this research.

---

## 8.2.1 UNDERSTAND HOW VARIOUS ASPECTS OF WHEELCHAIR RACING TECHNIQUE AND EQUIPMENT RELATE TO PERFORMANCE

This research provided the first study to quantify the aerodynamic strategies used by wheelchair racing athletes in a competition setting and the impact of gloves on athlete asymmetry. Findings from Chapter Three justified the relevance of customised seating interfaces for wheelchair racing athletes (and hence the premise of this research), as the findings from both studies indicated the performance benefit of customised seating interfaces.

Further research into understanding how all of the elements of wheelchair racing (technique and equipment) is required to develop athlete performance in the sport further. The impact of structured technical interventions and customised seating solutions can be investigated using the instrumentation strategies presented in this thesis. Currently, a relatively homogenous athlete sample was used for the investigation of injury risk using computational modelling approaches. There are likely to be multiple mechanisms of action which promote injury, and a more diverse population sample may help differentiate between some of these effects due to the variation in function. Additionally, a broader population sample would further identify kinematic strategies which may promote injury risk as a consequence of high loading at the shoulder.

Aerodynamic testing of athletes with and without the use of customised seating interfaces was outside the scope of this project. While it is anticipated that changes in the frontal area from the inclusion of customised seating interfaces will be marginal, quantifying the increased drag forces will be beneficial.

## 8.2.2 DEVELOP INSTRUMENTATION TOOLS CAPABLE OF IN-FIELD DATA MEASUREMENT

The first-stage investigation conducted as part of this research explored the ability of IMUs to estimate propulsion forces, which are critical in determining the efficiency of the technique. The solution itself provided a lightweight and practically viable instrumentation tool, which demonstrated the potential to estimate the most practically significant propulsive forces.

Despite its simplicity, the application of a pressure mat at the seating interface provided many novel findings, substantially increasing the understanding of the interaction between wheelchair racing athletes and their equipment. Prior to the findings of Chapter Five, the interactions between the athlete and wheelchair were assumed to be quasi-static. Therefore, Chapter Five contributed to the understanding of the dynamic nature of the athlete-wheelchair interface during non-linear or non-steady-state propulsion. From this research, it is now understood that athletes can gain mechanical leverage from the operational use of one of their legs.

Of clinical importance was the high peak pressures at the seat of wheelchair racing athletes. Although quantification of their absolute magnitude was precluded by sensor saturation within the system used, the regions of high pressure were above the theoretical limit of tissue viability, highlighting the potential injury risk to athletes, if no preventative mechanisms are established.

The combined findings of Chapters Four and Chapter Five have demonstrated how commercially available sensors can be used to develop a comprehensive understanding of the whole-body dynamics of wheelchair racing propulsion.

The main limitation of this research was the estimation of the propulsive forces input to the model. Fundamentally, the development of instrumentation tools capable of measuring in-field propulsion forces for use in computational modelling is still required. The estimation of propulsive forces using kinematic data resulted in propulsive forces higher than what is currently presented in the literature. Further refinement of this methodology, particularly coupled with validation against the clinical gold standard instrumented wheels (SMARTWheel) is suggested. Through future validation and refinement of data processing, IMUs may be an effective instrumentation strategy for the collection of in-field performance data of wheelchair racing athletes.

Minor limitations in available instrumentation impacted on the processing of measured data, however, they did not prevent their collection. As such, future research may potentially benefit from the use of IMUs with a variable sensing range, which is more representative of the requirements of elite wheelchair propulsion or a pressure mat which allows the fragmentation of the seating area into sub-sections, such as the left and right sides to better measure athlete symmetry, or understand the direction of pressure application and centre of pressure location. Additionally, although the pressure mat used in this research was deemed sufficient in recording pressures at the seating interface, use of more sophisticated technologies which allow more comprehensive data analysis would be beneficial.

### 8.2.3 DEVELOP A SUBJECT-SPECIFIC, 3D COMPUTATIONAL MODEL

This research presented the first anthropometric dataset of elite wheelchair racing athletes, and how DXA scans can be used to provide a better estimate of the maximum force-generating capacity of elite athletes. Although not novel methodologically, this was the first research to use DXA scans to obtain subject-specific body segment inertial parameters of elite wheelchair racing athletes. This research quantified the magnitude of difference in body mass distribution between elite wheelchair racing athletes and the generic counterparts in which musculoskeletal models are traditionally derived from. Based on the associated modelling error when using generic musculoskeletal models, it is suggested

---

that subject-specific modelling approaches are required for the computational analysis of wheelchair racing propulsion. The methods presented in this research can inform future researchers how to adapt open-source musculoskeletal models to represent elite wheelchair athletes, which will considerably improve the reliability of future biomechanical analysis of racing wheelchair propulsion.

Accurately defined musculoskeletal models that can provide a three-dimensional description of the mechanics of movement, which are required based on the complexity of the human movement system. While the sophistication of these approaches is continually improving, the limitations on measuring all relevant model parameters mean a musculoskeletal model will always be a simplification of the real system, and errors are likely to result from mathematically optimising neurological control systems.

The adaptations to body segment inertial parameters and maximum isometric force generating capacity provide the foundation for the adaptation of a musculoskeletal model for use with wheelchair racing athletes. These parameters formulate a baseline for developing more comprehensive models, which although they have demonstrated the benefits of the approach, are not without their limitations. For example, perturbing all maximum isometric force generating parameters by the same percentage does not approximate the effect of personalisation. Future research should detail more specific scaling strategies. Before any future conclusions are drawn from the computational modelling approach of wheelchair racing athletes, further model validation is required, including the integration of EMG. While these cannot validate muscle forces themselves, previous literature has used them to verify activation patterns of muscles.

Ultimately a predictive biomechanical model incorporating the aforementioned subject-specific parameters could be developed to aid the fitting process of customised seating interfaces based on the understanding of associated propulsion kinematics and joint loadings.

#### 8.2.4 QUANTIFY THE MECHANICAL BENEFITS OF CUSTOMISED SEATING INTERFACES FOR WHEELCHAIR RACING ATHLETES

The findings presented in Chapter Seven have provided the first literature quantifying the mechanical benefits of customised seating interfaces. While no definitive conclusions can be made as only a case-study was performed, the detectable differences in performance times provide the rationale for further research into the optimisation of these for enhanced athlete performance. The need for coupled kinematic and computational biomechanical analysis approaches to correlate performance with injury risk to best inform technique changes was also highlighted.

An extension of the case study performed in Chapter Seven would improve understanding of how seating interfaces can impact a range of athletes. The athlete investigated presented with an incomplete spinal cord injury, having large asymmetry between leg masses. These findings imply that athletes having a greater physical impairment in the lower extremity will receive more benefit from customised seating interfaces. The extension to other wheelchair sports would also be beneficial.

To help explore the magnitude of the influence of customised seating interfaces, where feasible, future studies should aim to do more testing under competition scenarios. The rapid development of technology has meant outdoor motion capture systems are now available. This would address the limitations surrounding the mode of propulsion (which was identified in Chapter Five), and also better understand how athletes are interacting with the seat during these key acceleration phases.

The interaction between athletes and their wheelchairs differed, with further variation observed for different modes of propulsion. While research has demonstrated that customised seating interfaces can improve performance, the degree of performance gain can still be optimised. Material selection may serve as a critical element to delivering a seating interface which provides adequate support, yet maintains the natural ability of the athlete to generate momentum, and consequently requires further research. The change in athlete performance with the wear of the cushion should also be monitored.

Development of an extensive database would be useful to understand which aspects of performance can translate to enhanced performance, and which may invoke injury risk. For example, apparent differences in shoulder and elbow angle were observed between the two athletes. Perhaps this also relates to wheelchair configuration parameters such as camber and pushrim diameter.

### **8.3 CONCLUDING REMARKS**

This research has shown that customised seating interfaces have a measurable beneficial performance impact for wheelchair racing athletes. Customised seating interfaces were observed to have a 3.7% gain in performance time, which has major implications in elite sport. Additionally, athlete asymmetries were reduced, which resulted in improved movement efficiency, with kinematic improvements seen immediately with the individual.

The benefits of the use of holistic and subject-specific computational modelling approaches for the assessment of wheelchair racing performance has also been demonstrated throughout this research. The changes in muscle and joint reaction moment prediction as a result of individualising musculoskeletal models highlight the necessity to use subject-specific modelling approaches in future



---

wheelchair racing research. The feasibility of this is improved through the use of DXA scans, which offer a more simplified, and practically viable approach to estimating body segment inertial parameters than other medical imaging analysis techniques. Although the full extent of personalisation (due to both impairment and training) are difficult to include, the steps presented in this research offer an advancement to the generic modelling approaches currently available.

---

# REFERENCES

---

1. Cooper RA. Wheelchair racing sports science: A review. *Journal of Rehabilitation Research and Development*. 1990; 27: 295-312.
2. Sports Reference LLC. Athletics at the 1984 Los Angeles Summer Games. 2016. January 5. <https://www.sports-reference.com/olympics/summer/1984/ATH/mens-1500-metres-wheelchair.html>
3. Cooper RA and De Luigi AJ. Adaptive sports technology and biomechanics: wheelchairs. *PM & R*. 2014; 6: S31-9.
4. Sanderson DJ and Sommer HJ. Kinematic features of wheelchair propulsion. *Journal of Biomechanics*. 1985; 18: 423-9.
5. Cooper RA. The contribution of selected anthropometric and physiological variables to 10K performance of wheelchair racers: a preliminary study. *Journal of Rehabilitation Research and Development*. 1992; 29: 29-34.
6. Invacare. Wheelchair Racing Measurement Guidelines. 2015, p. 26.
7. Goosey-Tolfrey V and Mason B. Enhancing Wheelchair Sport Performance. In: Winnick J and Poretta D, (eds.). *Adapted Physical Education and Sport*. 6 ed. Champaign, Illinois: Human Kinetics, 2017, p. 574.
8. Hoffman MD, Millet GY, Hoch AZ and Candau RB. Assessment of wheelchair drag resistance using a coasting deceleration technique. *American Journal of Physical Medicine and Rehabilitation*. 2003; 82: 880-9.
9. Barbosa TM, Forte P, Estrela JE and Coelho E. Analysis of the aerodynamics by experimental testing of an elite wheelchair sprinter. *Procedia Engineering*. 2016; 147: 2-6.
10. Slowik JS, Requejo PS, Mulroy SJ and Neptune RR. The influence of wheelchair propulsion hand pattern on upper extremity muscle power and stress. *Journal of Biomechanics*. 2016; 49: 1554-61.
11. Fuss FK. Influence of mass on the speed of wheelchair racing. *Sports Engineering*. 2009; 12: 41-53.
12. Peters C and Knicker A. Analysis of factors influencing the start push in wheelchair racing. *International Society of Biomechanics in Sport*. Beijing, China2005, p. 480-2.
13. Invacare. Invacare Top End Eliminator Racing Chair User Manual. Ohio, USA2011.
14. Klaesner J, Morgan KA and Gray DB. The development of an instrumented wheelchair propulsion testing and training device. *Assistive Technology*. 2014; 26: 24-32.

- 
15. Mikel B. How BMW redesigned the racing chair for Paralympic athletes: (2016).
  16. Chua JJC, Fuss FK and Subic A. Rolling friction of a rugby wheelchair. *Procedia Engineering*. 2010; 2: 3071-6.
  17. Tolerico ML, Ding D, Cooper RA, et al. Assessing mobility characteristics and activity levels of manual wheelchair users. *Journal of Rehabilitation Research and Development*. 2007; 44: 561.
  18. Ridgway M, Pope C and Wilkerson J. A kinematic analysis of 800-meter wheelchair-racing techniques. *Adapted Physical Activity Quarterly*. 1988; 5: 96-107.
  19. Faulkner K. Enhancing the athlete interface for performance impact in wheelchair tennis. *Journal of Science and Medicine in Sport*. 2014; 18: e130.
  20. Official Website of the Paralympic Movement. Athletics. 2017. January 12. [https://www.paralympic.org/rio-2016/schedule-results/info-live-results/rio-2016/eng/zz/engzz\\_athletics-daily-competition-schedule.htm](https://www.paralympic.org/rio-2016/schedule-results/info-live-results/rio-2016/eng/zz/engzz_athletics-daily-competition-schedule.htm)
  21. World Para Athletics. Classification Rules and Regulations. In: ParalympicCommittee I, (ed.). 2017.
  22. Tweedy SM and Bourke J. International Paralympic Committee Athletics classification project for physical impairments; Final report - Stage 1. In: International Paralympic Committee Athletics, (ed.). Bonn, Germany 2010, p. 107.
  23. Lebidowska MK, Gaebler-Spira D, Burns RS and Fisk JR. Biomechanic characteristics of patients with spastic and dystonic hypertonia in cerebral palsy<sup>1</sup>. *Archives of Physical Medicine and Rehabilitation*. 85: 875-80.
  24. Bar-On L, Molenaers G, Aertbeli, et al. Spasticity and its contribution to hypertonia in cerebral palsy. *BioMed Research International*. 2015; 2015: 10.
  25. Martino G, Ivanenko YP, Serrao M, et al. Locomotor patterns in cerebellar ataxia. *Journal of Neurophysiology*. 2014; 112: 2810-21.
  26. Mulroy SJ, Farrokhi S, Newsam CJ and Perry J. Effects of spinal cord injury level on the activity of shoulder muscles during wheelchair propulsion: an electromyographic study. *Archives of Physical Medicine and Rehabilitation*. 2004; 85: 925-34.
  27. Brodwin MG, Siu FW, Howard J and Brodwin ER. *Medical, Psychosocial and Vocational Aspects of Disability; Third Edition*. Athens, Georgia: Elliott & Fitzpatrick, Inc., 2009.
  28. Bhambhani Y. Physiology of wheelchair racing in athletes with spinal cord injury. *Sports Medicine*. 2002; 32: 23-51.
  29. Maynard FM, Jr., Bracken MB, Creasey G, et al. International standards for neurological and functional classification of spinal cord injury. . *Spinal Cord*. 1997; 35: 266-74.
  30. Kocina P. Body composition of spinal cord injured adults. *Sports Medicine*. 1997; 23: 48-60.
  31. Dec KL, Sparrow KJ and McKeag DB. The Physically-Challenged Athlete. *Sports Medicine*. 2000; 29: 245-58.
  32. Toth C, McNeil S and Feasby T. Peripheral nervous system injuries in sport and recreation. *Sports Medicine*. 2005; 35: 717-38.
  33. Feinberg JH, Nadler SF and Krivickas LS. Peripheral Nerve Injuries in the Athlete. *Sports Medicine*. 1997; 24: 385-408.
  34. Watanabe L. Spina Bifida. Understanding the Impact & Choosing Mobility Solutions that Fit the Whole Child: (2010).
  35. van Koningsveld R, Steyerberg EW, Hughes RAC, Swan AV, van Doorn PA and Jacobs BC. A clinical prognostic scoring system for Guillain-Barré syndrome. *The Lancet Neurology*. 2007; 6: 589-94.
  36. Movement OWotP. Classification. April 11. <https://www.paralympic.org/triathlon/classification>
  37. ITU Executive Board. ITU Competition Rules. 2016.
  38. McCrory JL, Salacinski AJ, Hunt SE and Greenspan SL. Thigh muscle strength in senior athletes and healthy controls. *Journal of Strength and Conditioning Research*. 2009; 23: 2430-6.
  39. Taylor AW, McDonnell E and Brassard L. The effects of an arm ergometer training programme on wheelchair subjects. *Paraplegia*. 1986; 24: 105-14.
  40. Taylor AW, McDonnell E, Royer D, Loiselle tR, Lush N and Steadward R. Skeletal muscle analysis of wheelchair athletes. *Paraplegia*. 1979; 17: 456-60.
  41. Finley MA, Rasch EK, Keyser RE and Rodgers MM. The biomechanics of wheelchair propulsion in individuals with and without upper-limb impairment. *Journal of Rehabilitation Research and Development*. 2004; 41: 385-95.
-

42. Harbo T, Brincks J and Andersen H. Maximal isokinetic and isometric muscle strength of major muscle groups related to age, body mass, height, and sex in 178 healthy subjects. *European Journal of Applied Physiology*. 2012; 112: 267-75.
43. Ambrosio F, Boninger ML, Souza AL, Fitzgerald SG, Koontz AM and Cooper RA. Biomechanics and strength of manual wheelchair users. *The Journal of Spinal Cord Medicine*. 2005; 28.
44. Burnham RS, May L, Nelson E, Steadward R and Reid DC. Shoulder pain in wheelchair athletes. The role of muscle imbalance. *American Journal of Sports Medicine*. 1993; 21: 238-42.
45. Miyahara M, Sleivert GG and Gerrard DF. The relationship of strength and muscle balance to shoulder pain and impingement syndrome in elite quadriplegic wheelchair rugby players. *International Journal of Sports Medicine*. 1998; 19: 210-4.
46. Ellenbecker TS and Mattalino AJ. Concentric isokinetic shoulder internal and external rotation strength in professional baseball pitchers. *Journal of Orthopaedic and Sports Physical Therapy*. 1997; 25: 323-8.
47. Bernard PL, Codine P and Minier J. Isokinetic shoulder rotator muscles in wheelchair athletes. *Spinal Cord*. 2004; 42: 222-9.
48. Ruivo R, Pezarat-Correia P and Carita A. Elbow and shoulder muscles strength profile in judo athletes. *Isokinetics and Exercise Science*. 2012; 20: 41-5.
49. Connelly Maddux RE, Kibler WB and Uhl TL. Isokinetic peak torque and work values for the shoulder. *Journal of Orthopaedic and Sports Physical Therapy*. 1989; 10: 264-9.
50. Haisma JA, van der Woude LHV, Stam HJ, Bergen MP, Sluis TAR and Bussmann JBJ. Physical capacity in wheelchair-dependent persons with a spinal cord injury: a critical review of the literature. *Spinal Cord*. 2006; 44: 642-52.
51. Phillips BA, Lo SK and Mastaglia FL. Muscle force measured using "break" testing with a hand-held myometer in normal subjects aged 20 to 69 years. *Archives of Physical Medicine and Rehabilitation*. 2000; 81: 653-61.
52. Goosey-Tolfrey V. *Wheelchair Sport: A complete guide for athletes, coaches, and teachers*. Champaign, Illinois: Human Kinetics, 2010.
53. Rice I, Dysterheft J, Bleakney AW and Cooper RA. The influence of glove type on simulated wheelchair racing propulsion: A pilot study. *International Journal of Sports Medicine*. 2015; 37: 30-5.
54. International Paralympic Committee Athletics. Official Rules for Athletics 2006. 2006.
55. Boninger M, Cooper R, Robertson R and Shimada S. Three-dimensional pushrim forces during two speeds of wheelchair propulsion. *American Journal of Physical Medicine and Rehabilitation*. 1997; 76: 420-6.
56. Boninger ML, Baldwin M, Cooper RA, Koontz A and Chan L. Manual wheelchair pushrim biomechanics and axle position. *Archives of Physical Medicine and Rehabilitation*. 2000; 81: 608-13.
57. Boninger ML, Koontz AM, Sisto SA, et al. Pushrim biomechanics and injury prevention in spinal cord injury: recommendations based on CULP-SCI investigations. *Journal of Rehabilitation Research and Development*. 2005; 42: 9-19.
58. Boninger ML, Souza AL, Cooper RA, Fitzgerald SG, Koontz AM and Fay BT. Propulsion patterns and pushrim biomechanics in manual wheelchair propulsion. *Archives of Physical Medicine and Rehabilitation*. 2002; 83: 718-23.
59. Koontz AM, Roche BM, Collinger JL, Cooper RA and Boninger ML. Manual wheelchair propulsion patterns on natural surfaces during start-up propulsion. *Archives of Physical Medicine and Rehabilitation*. 2009; 90: 1916-23.
60. Koontz AM, Yang Y, Price R, et al. Multisite comparison of wheelchair propulsion kinetics in persons with paraplegia. *Journal of Rehabilitation Research & Development*. 2007; 44: 449-58.
61. Kwarciak AM, Sisto SA, Yarossi M, Price R, Komaroff E and Boninger ML. Redefining the manual wheelchair stroke cycle: identification and impact of nonpropulsive pushrim contact. *Archives of Physical Medicine and Rehabilitation*. 2009; 90.
62. Robertson RN, Boninger ML, Cooper RA and Shimada SD. Pushrim forces and joint kinetics during wheelchair propulsion. *Archives of Physical Medicine and Rehabilitation*. 1996; 77: 856-64.
63. Russell IM, Raina S, Requejo PS, Wilcox RR, Mulroy S and McNitt-Gray JL. Modifications in wheelchair propulsion technique with speed. *Frontiers in Bioengineering and Biotechnology*. 2015; 3: 171.
64. Wang YT, Deutsch H, Morse M, Hedrick B and Millikan T. Three-dimensional kinematics of wheelchair propulsion across racing speeds. *Adapted Physical Activity Quarterly*. 1995; 12: 78-89.
65. Okawa H, Tajima F, Makino K, et al. Kinetic factors determining wheelchair propulsion in marathon racers with paraplegia. *Spinal Cord*. 1999; 37: 542-7.

- 
66. Mandy A, Redhead L, McCudden C and Michaelis J. Position and movement of centre of force during propulsion of 3 different one arm drive wheelchairs by hemiplegic users. *Physical Medicine and Rehabilitation International*. 2015; 2: 1-7.
  67. Alm M, Saraste H and Norrbrink C. Shoulder pain in persons with thoracic spinal cord injury: Prevalence and characteristics. *Journal of Rehabilitation in Medicine*. 2008; 40: 277-83.
  68. Samuelsson KA, Tropp H and Gerdle B. Shoulder pain and its consequences in paraplegic spinal cord-injured, wheelchair users. *Spinal Cord*. 2004; 42: 41-6.
  69. Curtis KA, Drysdale GA, Lanza RD, Kolber M, Vitolo RS and West R. Shoulder pain in wheelchair users with tetraplegia and paraplegia. *Archives of Physical Medicine and Rehabilitation*. 1999; 80: 453-7.
  70. Soltau SL, Slowik JS, Requejo PS, Mulroy SJ and Neptune RR. An investigation of bilateral symmetry during manual wheelchair propulsion. *Frontiers in Bioengineering and Biotechnology*. 2015; 3: 86.
  71. Mason BS, Porcellato L, van der Woude LH and Goosey-Tolfrey VL. A qualitative examination of wheelchair configuration for optimal mobility performance in wheelchair sports: a pilot study. *Journal of Rehabilitation Medicine*. 2010; 42: 141-9.
  72. Bronzino J and Peterson D. Biomedical Engineering Fundamentals. In: Bronzino J, (ed.). *The Biomedical Engineering Handbook, Fourth Edition*. Boca Raton, Florida: CRC Press, 2006, p. 69-80.
  73. Wall J and Colley T. Preventing pressure ulcers among wheelchair users: Preliminary comments on the development of a self-administered risk assessment tool. *Journal of Tissue Viability*. 2003; 13: 48-56
  74. Apatsidis DP, Solomonidis SE and Michael SM. Pressure distribution at the seating interface of custom-molded wheelchair seats: Effect of various materials. *Archives of Physical Medicine and Rehabilitation*. 2002; 83: 1151-6.
  75. Grey JE, Harding KG and Enoch S. Pressure ulcers. *British Medical Journal*. 2006; 332: 472-5.
  76. Loerakker S. Aetiology of pressure ulcers. *Department of Biomedical Engineering*. Eindhoven University of Technology, 2007, p. 31.
  77. Linder-Ganz E, Yarnitzky G, Yizhar Z, Siev-Ner I and Gefen A. Real-time finite element monitoring of sub-dermal tissue stresses in individuals with spinal cord injury: toward prevention of pressure ulcers. *Annals of Biomedical Engineering*. 2009; 37: 387-400.
  78. Mutsuzaki H, Tachibana K, Shimizu Y, et al. Factors associated with deep tissue injury in male wheelchair basketball players of a Japanese national team. *Asia-Pacific Journal of Sports Medicine, Arthroscopy, Rehabilitation and Technology*. 2014; 1: 72-6.
  79. Gil-Agudo A, De la Peña-González A, Del Ama-Espinosa A, Pérez-Rizo E, Díaz-Domínguez E and Sánchez-Ramos A. Comparative study of pressure distribution at the user-cushion interface with different cushions in a population with spinal cord injury. *Clinical Biomechanics*. 2009; 24: 558-63.
  80. Wang YN, Bouten CV, Lee DA and Bader DL. Compression-induced damage in a muscle cell model in vitro. *Proceedings of the Institution of Mechanical Engineers Part H, Journal of Engineering in Medicine*. 2005; 219: 1-12.
  81. Conine TA, Hershler C, Daechsel D, Peel C and Pearson A. Pressure ulcer prophylaxis in elderly patients using polyurethane foam or Jay wheelchair cushions. *International Journal of Rehabilitation Research*. 1994; 17: 123-37.
  82. Invacare Corporation. Invacare IVC 9000 XT Wheelchair Price List and Order Form. In: Invacare Corporation, (ed.). OH, USA2011.
  83. Howarth D. Paralympic design: 3D-printed seats for wheelchair basketball. 2012. April 8. <https://www.dezeen.com/2012/09/05/paralympic-design-3d-printed-seats-for-wheelchair-basketball/>
  84. Kaelin B. Wheelchair basketball players get 3D printed seats. 2013. April 8. <http://www.3dprinterworld.com/article/wheelchair-basketball-players-get-3d-printed-seats>
  85. Wheelchair Basketball Canada. Equipment. 2018. April 8. <http://www.wheelchairbasketball.ca/the-sport/equipment/>
  86. Rasmussen J, Tørholm S and de Zee M. Computational analysis of the influence of seat pan inclination and friction on muscle activity and spinal joint forces. *International Journal of Industrial Ergonomics*. 2009; 39: 52-7.
  87. Levy A, Kopplin K and Gefen A. Computer simulations of efficacy of air-cell-based cushions in protecting against reoccurrence of pressure ulcers. *Journal of Rehabilitation Research and Development*. 2014; 51: 1297-319.
-

88. Lemaire ED, Upton D, Paialunga J, Martel G and Boucher J. Clinical analysis of a CAD/CAM system for custom seating: a comparison with hand-sculpting methods. *Journal of Rehabilitation Research and Development*. 1996; 33: 311-20.
89. Sprigle S, Chung KC and Brubaker CE. Reduction of sitting pressures with custom contoured cushions. *Journal of Rehabilitation Research and Development*. 1990; 27: 135-40.
90. Yuen HK and Garrett D. Comparison of three wheelchair cushions for effectiveness of pressure relief. *American Journal of Occupational Therapy*. 2001; 55: 470-5.
91. Bleganek J and Hetzel T. Race and Recreational Seating Interfaces.
92. Creaform and GeoMagic Come to the Aid of Australia's Kayak Team. 2012.
93. Gutierrez EM, Alm M, Hultling C and Saraste H. Measuring seating pressure, area, and asymmetry in persons with spinal cord injury. *European Spine Journal*. 2004; 13: 374-9.
94. Hurd WJ, Morrow MM, Kaufman KR and An KN. Biomechanic evaluation of upper-extremity symmetry during manual wheelchair propulsion over varied terrain. *Archives of Physical Medicine and Rehabilitation*. 2008; 89: 1996-2002.
95. Wang HK and Cochrane T. Mobility impairment, muscle imbalance, muscle weakness, scapular asymmetry and shoulder injury in elite volleyball athletes. *Journal of Sports Medicine and Physical Fitness*. 2001; 41: 403-10.
96. Boninger ML, Cooper RA, Baldwin MA, Shimada SD and Koontz A. Wheelchair pushrim kinetics: Body weight and median nerve function. *Archives of Physical Medicine and Rehabilitation*. 1999; 80: 910-5.
97. Cooper RA. An exploratory study of racing wheelchair propulsion dynamics. *Adapted Physical Activity Quarterly*. 1990; 7: 74-85.
98. Cooper RA, Boninger ML, Shimada SD and Lawrence BM. Glenohumeral joint kinematics and kinetics for three coordinate system representations during wheelchair propulsion. *American Journal of Physical Medicine and Rehabilitation*. 1999; 78: 435-46.
99. Cooper RA, Robertson RN, VanSickle DP, Boninger ML and Shimada SD. Methods for determining three-dimensional wheelchair pushrim forces and moments: a technical note. *Journal of Rehabilitation Research and Development*. 1997; 34: 162-70.
100. Charlton IW and Johnson GR. A model for the prediction of the forces at the glenohumeral joint. *Proceedings of the Institution of Mechanical Engineers, Part H: Journal of Engineering in Medicine*. 2006; 220: 801-12.
101. Dubowsky SR, Rasmussen J, Sisto SA and Langrana NA. Validation of a musculoskeletal model of wheelchair propulsion and its application to minimizing shoulder joint forces. *Journal of Biomechanics*. 2008; 41: 2981-8.
102. Kulig KP, Rao SSMS, Mulroy SJP, et al. Shoulder joint kinetics during the push phase of wheelchair propulsion. *Clinical Orthopaedics and Related Research September*. 1998; 354: 132-43.
103. Slowik JS, McNitt-Gray JL, Requejo PS, Mulroy SJ and Neptune RR. Compensatory strategies during manual wheelchair propulsion in response to weakness in individual muscle groups: A simulation study. *Clinical Biomechanics*. 2016; 33: 34-41.
104. Slowik JS, Requejo PS, Mulroy SJ and Neptune RR. The influence of speed and grade on wheelchair propulsion hand pattern. *Clinical Biomechanics*. 2015; 30: 927-32.
105. van den Bogert AJ, Read L and Nigg BM. An analysis of hip joint loading during walking, running, and skiing. *Medicine and Science in Sports and Exercise*. 1999; 31: 131-42.
106. Lombardi AdB and Dedini FG. Biomechanical model for the determination of forces on upper-extremity members during standard wheelchair propulsion. *Mathematical and Computer Modelling*. 2009; 49: 1288-94.
107. Neptune RR. Computer modeling and simulation of human movement. Applications in sport and rehabilitation. *Physical Medicine and Rehabilitation Clinics of North America*. 2000; 11: 417-34.
108. Senteler M, Weisse B, Rothenfluh DA and Snedeker JG. Intervertebral reaction force prediction using an enhanced assembly of OpenSim models. *Computer Methods in Biomechanics and Biomedical Engineering*. 2016; 19: 538-48.
109. Wilke HJ, Neef P, Caimi M, Hoogland T and Claes LE. New in vivo measurements of pressures in the intervertebral disc in daily life. *Spine (Phila Pa 1976)*. 1999; 24: 755-62.
110. Rohlmann A, Zander T, Bock B and Bergmann G. Effect of position and height of a mobile core type artificial disc on the biomechanical behaviour of the lumbar spine. *Proceedings of the Institution of Mechanical Engineers Part H, Journal of Engineering in Medicine*. 2008; 222: 229-39.

- 
111. Torráo JND, dos Santos MPS and Ferreira JAF. Instrumented knee joint implants: innovations and promising concepts. *Expert Review of Medical Devices*. 2015; 12: 571-84.
  112. Seth A, Sherman M, Reinbolt JA and Delp SL. OpenSim: a musculoskeletal modeling and simulation framework for in silico investigations and exchange. *Procedia IUTAM*. 2011; 2: 212-32.
  113. DiGiovine CP, Cooper RA, DiGiovine MM, Boninger ML and Robertson RN. Frequency analysis of kinematics of racing wheelchair propulsion. *IEEE Transactions on Rehabilitation Engineering*. 2000; 8: 2714-16.
  114. Goosey VL and Campbell IG. Symmetry of the elbow kinematics during racing wheelchair propulsion. *Ergonomics*. 1998; 41: 1810-20.
  115. Chow JW, Millikan TA, Carlton LG, Morse MI and Chae WS. Biomechanical comparison of two racing wheelchair propulsion techniques. *Medicine and Science in Sports and Exercise*. 2000; 33: 476-84.
  116. Moss AD, Fowler NE and Goosey-Tolfrey VL. The intra-push velocity profile of the over-ground racing wheelchair sprint start. *Journal of Biomechanics*. 2005; 38: 15-22.
  117. O'Connor T, Robertson RN and Cooper RA. Three-dimensional kinematic analysis and physiologic assessment of racing wheelchair propulsion. *Adapted Physical Activity Quarterly*. 1998; 15.
  118. Wang Y, Vrongistinos KD and Xu D. The relationship between consistency of propulsive cycles and maximum angular velocity during wheelchair racing. *Journal of Applied Biomechanics*. 2008; 24.
  119. Churton E and Keogh J. Constraints influencing sports wheelchair propulsion performance and injury risk. *BMC Sports Science, Medicine, and Rehabilitation*. 2013; 5: 1-10.
  120. Hamner SR, Seth A and Delp SL. Muscle contributions to propulsion and support during running. *Journal of Biomechanics*. 2010; 43: 2709-16.
  121. Liu MQ, Anderson FC, Schwartz MH and Delp SL. Muscle contributions to support and progression over a range of walking speeds. *Journal of Biomechanics*. 2008; 41: 3243-52.
  122. Neptune RR, Clark DJ and Kautz SA. Modular control of human walking: A simulation study. *Journal of Biomechanics*. 2009; 42: 1282-7.
  123. van der Woude LHV, Dallmeijer AJ, Janssen TWJ and Veeger D. Alternative modes of manual wheelchair ambulation: An overview. *American Journal of Physical Medicine and Rehabilitation*. 2001; 80: 765-77.
  124. Arnold AS and Delp SL. Computer modeling of gait abnormalities in cerebral palsy: application to treatment planning. *Theoretical Issues in Ergonomics Science*. 2005; 6: 305-12.
  125. Seth A, Sherman M, Reinbolt J and Delp SL. OpenSim: a musculoskeletal modeling and simulation framework for in silico investigations and exchange. *Procedia IUTAM*. 2011; 2: 212-32.
  126. Reinbolt JA, Haftka RT, Chmielewski TL and Fregly BJ. A computational framework to predict post-treatment outcome for gait-related disorders. *Medical Engineering and Physics*. 2008; 30: 434-43.
  127. Delp SL, Arnold AS, Speers RA and Moore CA. Hamstrings and psoas lengths during normal and crouch gait: implications for muscle-tendon surgery. *Journal of Orthopaedic Research*. 1996; 14: 144-51.
  128. Delp SL, Arnold AS and Piazza SJ. Graphics-based modeling and analysis of gait abnormalities. *Biomed Mater Eng*. 1998; 8: 227-40.
  129. Fregly BJ, Reinbolt JA, Rooney KL, Mitchell KH and Chmielewski TL. Design of Patient-Specific Gait Modifications for Knee Osteoarthritis Rehabilitation. *IEEE Transactions on Bio-medical Engineering*. 2007; 54: 1687-95.
  130. Valente G, Taddei F and Jonkers I. Influence of weak hip abductor muscles on joint contact forces during normal walking: probabilistic modeling analysis. *Journal of Biomechanics*. 2013; 46: 2186-93.
  131. Silverman AK and Neptune RR. Muscle and prosthesis contributions to amputee walking mechanics: A modeling study. *Journal of Biomechanics*. 2012; 45: 2271-8.
  132. Shelburne KB and Pandy MG. Determinants of cruciate-ligament loading during rehabilitation exercise. *Clinical Biomechanics*. 1998; 13: 403-13.
  133. Delp SL, Anderson FC, Arnold AS, et al. OpenSim: open-source software to create and analyze dynamic simulations of movement. *IEEE Transactions on Bio-medical Engineering*. 2007; 54: 1940-50.
  134. Langholz JB, Westman G and Karlsteen M. Musculoskeletal modelling in sports - Evaluation of different software tools with focus on swimming. *Procedia Engineering*. 2016; 147: 281-7.
  135. Delp SL, Loan JP, Hoy MG, Zajac FE, Topp EL and Rosen JM. An interactive graphics-based model of the lower extremity to study orthopaedic surgical procedures. *IEEE Transactions on Bio-medical Engineering*. 1990; 37: 757-67.
  136. Yamaguchi GT and Zajac FE. A planar model of the knee joint to characterize the knee extensor mechanism. *Journal of Biomechanics*. 1989; 22: 1-10.
-

137. Anderson FC and Pandy MG. A dynamic optimization solution for vertical jumping in three dimensions. *Computer Methods in Biomechanics and Biomedical Engineering*. 1999; 2: 201-31.
138. Anderson FC and Pandy MG. Static and dynamic optimization solutions for gait are practically equivalent. *Journal of Biomechanics*. 2001; 34: 153-61.
139. Anderson FC and Pandy MG. Dynamic optimization of human walking. *Journal of Biomechanical Engineering*. 2001; 123: 381-90.
140. Hicks JL, Uchida TK, Seth A, Rajagopal A and Delp SL. Is my model good enough? Best practices for verification and validation of musculoskeletal models and simulations of movement. *Journal of Biomechanical Engineering*. 2015; 137: 1-24.
141. Ganley KJ and Powers CM. Determination of lower extremity anthropometric parameters using dual energy X-ray absorptiometry: the influence on net joint moments during gait. *Clinical Biomechanics*. 2004; 19: 50-6.
142. Hainisch R, Gfoehler M, Zubayer-Ul-Karim M and Pandy MG. Method for determining musculotendon parameters in subject-specific musculoskeletal models of children developed from MRI data. *Multibody System Dynamics*. 2012; 28: 143-56.
143. Cheng CK, Chen HH, Chen CS, Chen CL and Chen CY. Segment inertial properties of Chinese adults determined from magnetic resonance imaging. *Clinical Biomechanics*. 2000; 15: 559-66.
144. Durkin JL and Dowling JJ. Analysis of body segment parameter differences between four human populations and the estimation errors of four popular mathematical models. *Journal of Biomechanical Engineering*. 2003; 125: 515-22.
145. Winter DA. Anthropometry. *Biomechanics and Motor Control of Human Movement*. Hoboken, New Jersey: John Wiley & Sons, Inc., 1990, p. 82-106.
146. Hanavan EP, Jr. A mathematical model of the human body. *AMRL-TR Aerospace Medical Research Laboratories (US)* 1964: 1-149.
147. Sutton L, Wallace J, Goosey-Tolfrey V, Scott M and Reilly T. Body composition of female wheelchair athletes. *International Journal of Sports Medicine*. 2009; 30: 259-65.
148. Pearsall DJ and Costigan PA. The effect of segment parameter error on gait analysis results. *Gait and Posture*. 1999; 9: 173-83.
149. Rao G, Amarantini D, Berton E and Favier D. Influence of body segments' parameters estimation models on inverse dynamics solutions during gait. *Journal of Biomechanics*. 2006; 39: 1531-6.
150. Li K, Zheng L, Tashman S and Zhang X. The inaccuracy of surface-measured model-derived tibiofemoral kinematics. *Journal of Biomechanics*. 2012; 45: 2719-23.
151. Lathrop RL, Chaudhari AMW and Siston RA. Comparative assessment of bone pose estimation using point cluster technique and OpenSim. *Journal of Biomechanical Engineering*. 2011; 133: 114503-.
152. OpenSim. OpenSim Documentation. 2017. January 13. <https://simtk-confluence.stanford.edu/display/OpenSim/>
153. Myers CA, Laz PJ, Shelburne KB and Davidson BS. A probabilistic approach to quantify the impact of uncertainty propagation in musculoskeletal simulations. *Annals of Biomedical Engineering*. 2014; 43: 1098-111.
154. Mogk JPM, Johanson ME, Hentz VR, Saul KR and Murray WM. A simulation analysis of the combined effects of muscle strength and surgical tensioning on lateral pinch force following brachioradialis to flexor pollicis longus transfer. *Journal of Biomechanics*. 2011; 44: 669-75.
155. Henninger HB, Reese SP, Anderson AE and Weiss JA. Validation of computational models in biomechanics. *Proceedings of the Institution of Mechanical Engineers Part H, Journal of Engineering in Medicine*. 2010; 224: 801-12.
156. Engel K, Herpers R and Hartmann U. Biomechanical Computer Models. In: Klika V, (ed.). *Theoretical Biomechanics*. Rijeka: InTech, 2011, p. Ch. 05.
157. Donnelly CJ, Lloyd DG, Elliott BC and Reinbolt JA. Optimizing whole-body kinematics to minimize valgus knee loading during sidestepping: Implications for ACL injury risk. *Journal of Biomechanics*. 2012; 45: 1491-7.
158. Leary M, Gruijters J, Mazur M, Subic A, Burton M and Fuss FK. A fundamental model of quasi-static wheelchair biomechanics. *Medical Engineering and Physics*. 2012; 34: 1278-86.



- 
159. Bolsterlee B, Veeger DHEJ and Chadwick EK. Clinical applications of musculoskeletal modelling for the shoulder and upper limb. *Medical & Biological Engineering and Computing*. 2013; 51: 953-63.
160. Hogfors C, Peterson B, Sigholm G and Herberts P. Biomechanical model of the human shoulder joint - II. The shoulder rhythm. *Journal of Biomechanics*. 1991; 24: 669-709.
161. Hogfors C, Sigholm G and Herberts P. Biomechanical model of the human shoulder--I. Elements. *Journal of Biomechanics*. 1987; 20: 157-66.
162. Nikooyan AA, Veeger HEJ, Westerhoff P, Graichen F, Bergmann G and van der Helm FCT. Validation of the Delft Shoulder and Elbow Model using in-vivo glenohumeral joint contact forces. *Journal of Biomechanics*. 2010; 43: 3007-14.
163. van der Helm FCT. A Finite Element Musculoskeletal Model of the Shoulder Mechanism. *Journal of Biomechanics*. 1994; 27: 551-69.
164. Holzbour KR, Murray WM and Delp SL. A model of the upper extremity for simulating musculoskeletal surgery and analyzing neuromuscular control. *Annals of Biomedical Engineering*. 2005; 33: 829-40.
165. Damsgaard M, Rasmussen J, Christensen ST, Surma E and de Zee M. Analysis of musculoskeletal systems in the AnyBody Modeling System. *Simulation Modelling Practice and Theory*. 2006; 14: 1100-11.
166. Garner BA and Pandy MG. Musculoskeletal model of the upper limb based on the visible human male dataset. *Computer Methods in Biomechanics and Biomedical Engineering*. 2001; 4: 93-126.
167. Dickerson CR, Chaffin DB and Hughes RE. A mathematical musculoskeletal shoulder model for proactive ergonomic analysis. *Computer Methods in Biomechanics and Biomedical Engineering*. 2007; 10: 389-400.
168. Odle M. Construction and assessment of a computer graphics-based model for wheelchair propulsion. *Biomedical and Health Sciences*. New Jersey Institute of Technology and Rutgers University, 2014, p. 224.
169. Veeger HEJ, Rozendaal LA and van der Helm FCT. Load on the shoulder in low intensity wheelchair propulsion. *Clinical Biomechanics*. 2002; 17: 211-8.
170. van Drongelen S, van der Woude LH, Janssen TW, Angenot EL, Chadwick EK and Veeger DH. Glenohumeral contact forces and muscle forces evaluated in wheelchair-related activities of daily living in able-bodied subjects versus subjects with paraplegia and tetraplegia. *Archives of Physical Medicine and Rehabilitation*. 2005; 86: 1434-40.
171. van Drongelen S, van der Woude LH, Janssen TW, Angenot EL, Chadwick EK and Veeger DH. Mechanical load on the upper extremity during wheelchair activities. *Archives of Physical Medicine and Rehabilitation*. 2005; 86: 1214-20.
172. Sullivan SR, Langrana NA and Sisto SA. Multibody computational biomechanical model of the upper body. *ASME 2005 International Design Engineering Technical Conferences & Computers and Information in Engineering Conference*. Long Beach, California, USA2005, p. 1-6.
173. Sullivan SR, Langrana NA and Sisto SA. Shoulder mechanics: Analytical modeling and validation. *American Society of Biomechanics*. Stanford, California2007.
174. Morrow MMB, Kaufman KR and An K-N. Shoulder model validation and joint contact forces during wheelchair activities. *Journal of Biomechanics*. 2010; 43: 2487-92.
175. Rankin JW, Kwarciak AM, Mark Richter W and Neptune RR. The influence of altering push force effectiveness on upper extremity demand during wheelchair propulsion. *Journal of Biomechanics*. 2010; 43: 2771-9.
176. Rankin JW, Richter WM and Neptune RR. Individual muscle contributions to push and recovery subtasks during wheelchair propulsion. *Journal of Biomechanics*. 2011; 44: 1246-52.
177. May LA, Burnham RS and Steadward RD. Assessment of isokinetic and hand-held dynamometer measures of shoulder rotator strength among individuals with spinal cord injury. *Archives of Physical Medicine and Rehabilitation*. 1997; 78: 251-5.
178. Blana D, Hincapie JG, Chadwick EK and Kirsch RF. A musculoskeletal model of the upper extremity for use in the development of neuroprosthetic systems. *Journal of Biomechanics*. 2008; 41: 1714-21.
179. Gilsdorf P, Patterson R, Fisher S and Appel N. Sitting forces and wheelchair mechanics. *Journal of Rehabilitation Research and Development*. 1990; 27: 239-46.
180. van der Slikke RM, Berger MA, Bregman DJ and Veeger D. Push characteristics in wheelchair court sport sprinting. *Procedia Engineering*. 2016; 147: 730-4.
181. Vanlandewijck YC, Verellen J and Tweedy S. Towards evidence-based classification in wheelchair sports: impact of seating position on wheelchair acceleration. *Journal of Sports Sciences*. 2011; 29: 1089-96.
-

- 
182. West CR, Campbell IG, Goosey-Tolfrey VL, Mason BS and Romer LM. Effects of abdominal binding on field-based exercise responses in Paralympic athletes with cervical spinal cord injury. *Journal of Science and Medicine in Sport*. 2014; 17: 351-5.
183. Mason B, Lenton J, Leicht C and Goosey-Tolfrey V. A physiological and biomechanical comparison of over-ground, treadmill and ergometer wheelchair propulsion. *Journal of Sports Sciences*. 2014; 32: 78-91.
184. Stephens CL and Engsborg JR. Comparison of overground and treadmill propulsion patterns of manual wheelchair users with tetraplegia. *Disability and Rehabilitation Assistive Technology*. 2010; 5: 420-7.
185. Hwang S, Kim S, Son J and Youngho K. Manual wheelchair propulsion torque and power outputs in different skill groups. *Journal of Biomechanical Science and Engineering*. 2012; 7: 349-57.
186. Yao F. Measurement and modeling of wheelchair propulsion ability for people with spinal cord injury. *Mechanical Engineering*. University of Canterbury, 2007, p. 1-138.
187. Vanlandewijck Y, Theisen D and Daly D. Wheelchair propulsion biomechanics: implications for wheelchair sports. *Sports Medicine*. 2001; 31.
188. Koontz AM, Cooper RA, Boninger ML, Yang Y, Impick BG and van der Woude LHV. A kinetic analysis of manual wheelchair propulsion during start up on select indoor and outdoor surfaces. *Journal of Rehabilitation Research and Development*. 2005; 42: 447-58.
189. Cooper RA. SMARTWheel: From concept to clinical practice. *Prosthetics and Orthotics International*. 2009; 33: 198-209.
190. Asato K, Cooper R, Robertson R and Ster J. SMARTWheels: Development and testing of a system for measuring manual wheelchair propulsion dynamics. *IEEE Transactions on Bio-medical Engineering*. 1993; 40: 1320-4.
191. Morrow MM, Hurd WJ, Kaufman KR and An KN. Shoulder demands in manual wheelchair users across a spectrum of activities. *Journal of Electromyography and Kinesiology*. 2010.
192. Collinger JL, Boninger M, Koontz AM, et al. Shoulder biomechanics during the push phase of wheelchair propulsion: A multisite study of persons with paraplegia. *Archives of Physical Medicine and Rehabilitation*. 2008; 89: 667-76.
193. Lenton JP, van der Woude LHV, Fowler NE, Nicholson G, Tolfrey K and Goosey-Tolfrey VL. Hand-rim forces and gross mechanical efficiency at various frequencies of wheelchair propulsion. *International Journal of Sports Medicine*. 2013; 34.
194. Vegter RJ, Lamoth CJ, de Groot S, Veeger DH and van der Woude LH. Variability in bimanual wheelchair propulsion: consistency of two instrumented wheels during handrim wheelchair propulsion on a motor driven treadmill. *Journal of NeuroEngineering and Rehabilitation*. 2013; 10.
195. Goosey-Tolfrey V, Fowler NE, Campbell IG and Iwnicki SD. A kinetic analysis of trained wheelchair racers during two speeds of propulsion. *Medical Engineering and Physics*. 2001; 23: 259-66.
196. Brubaker CE. Wheelchair prescription: An analysis of factors that affect mobility and performance. *Journal of Rehabilitation Research and Development*. 1986; 23: 19-26.
197. Sherman S. Rolling resistance in manual wheelchairs: applying the evidence. *Canadian Seating and Mobility Conference*. Toronto, Canada 2014, p. 39-41.
198. Medola FO, Elui VM, Santana Cda S and Fortulan CA. Aspects of manual wheelchair configuration affecting mobility: A review. *Journal of Physical Therapy Science*. 2014; 26: 313-8.
199. Bednarczyk JH. The effect of mass on the kinematics of steady state wheelchair propulsion in adults and children with spinal cord injury. *Physical Education and Recreation*. Vancouver, Canada: The University of British Columbia, 1993, p. 1-108.
200. Perret C. Elite-adapted wheelchair sports performance: a systematic review. *Disability and Rehabilitation*. 2015; 39: 164-72.
201. Bednarczyk JH and Sanderson DJ. Limitations of kinematics in the assessment of wheelchair propulsion in adults and children with spinal cord injury. *Physical Therapy*. 1995; 75: 281-9.
202. Symonds A, Holloway C, Suzuki T, Smitham P, Gall A and Taylor SJG. Identifying key experience-related differences in over-ground manual wheelchair propulsion biomechanics. *Journal of Rehabilitation and Assistive Technologies Engineering*. 2016; 3: 2055668316678362.
203. Symonds A, Taylor SJG and Holloway C. Sensewheel: an adjunct to wheelchair skills training. *Healthcare Technology Letters*. 2016; 3: 269-72.
-

- 
204. Bertucci W, Duc S, Villerius V, Pernin JN and Grappe F. Validity and reliability of the PowerTap mobile cycling powermeter when compared with the SRM Device. *International Journal of Sports Medicine*. 2005; 26: 868-73.
205. CycleOps. Owner's Manual PowerTapSL. 2013, p. 1-39.
206. Sabick MB, Kotajarvi BR and An KN. A new method to quantify demand on the upper extremity during manual wheelchair propulsion. *Archives of Physical Medicine and Rehabilitation*. 2004; 85: 1151-9.
207. Newsam CJ, Rao SS, Mulroy SJ, Gronley JK, Bontrager EL and Perry J. Three dimensional upper extremity motion during manual wheelchair propulsion in men with different levels of spinal cord injury. *Gait and Posture*. 1999; 10: 223-32.
208. Kulig K, Newsam CJ, Mulroy SJ, et al. The effect of level of spinal cord injury on shoulder joint kinetics during manual wheelchair propulsion. *Clinical Biomechanics*. 2001; 16: 744-51.
209. Moss AD, Fowler NE and Tolfrey VL. A telemetry based velocometer to measure wheelchair velocity. *Journal of Biomechanics*. 2003; 36: 253-7.
210. Fuss FK and Ow ZJ. Performance diagnostics with instrumented racing wheelchairs: Comparison of athletes of class T52 and T53. In: Kwon YK, Shim J, Shim JK and Shin IS, (eds.). *XXVI International Symposium on Biomechanics in Sports*. Seoul, Korea: Seoul National University, 2008, p. 320-3.
211. Chua JJC, Fuss FK and Subic A. Evaluation of different gyroscope sensors for smart wheelchair applications. *Procedia Engineering*. 2011; 13: 519-24.
212. Usma-Alvarez CC, Chua JJC, Fuss FK, Subic A and Burton M. Advanced performance analysis of the Illinois agility test based on the tangential velocity and turning radius in wheelchair rugby athletes. *Sports Technology*. 2010; 3: 204-14.
213. Fuss FK, Subic A and Chua JJC. Analysis of wheelchair rugby accelerations with fractal dimensions. *Procedia Engineering*. 2012; 34: 439-42.
214. Lemerle P, Klinger A, Cristalli A and Geuder M. Application of pressure mapping techniques to measure push and gripping forces with precision. *Ergonomics*. 2008; 51: 168-91.
215. Rodgers MM, Gayle GW, Figoni SF, Kobayashi M, Lieh J and Glaser RM. Biomechanics of wheelchair propulsion during fatigue. *Archives of Physical Medicine and Rehabilitation*. 1994; 75: 85-93.
216. van der Slikke RM, Berger MA, Bregman DJ, Lagerberg AH and Veeger HE. Opportunities for measuring wheelchair kinematics in match settings; reliability of a three inertial sensor configuration. *Journal of Biomechanics*. 2015; 48: 3398-405.
217. Pansiot J, Zhang ZQ, Lo B and Yang G. WISDOM: Wheelchair inertial sensors for displacement and orientation monitoring. *Measurement Science and Technology*. 2011; 22: 105801.
218. Bergamini E, Morelli F, Marchetti F, et al. Wheelchair propulsion biomechanics in junior basketball players: A method for the evaluation of the efficacy of a specific training program. *BioMed Research International*. 2015; 2015: Article ID: 275965.
219. IMeasureU. Product Specification In: IMeasureU, (ed.).
220. Dallmeijer AJ and Kappe YJ. Anaerobic power output and propulsion technique in spinal cord injured subjects during. *Journal of Rehabilitation Research and Development*. 1994; 31: 120-8.
221. Sauret C, Vaslin P, Dabonneville M and Cid M. Drag force mechanical power during an actual propulsion cycle on a manual wheelchair. *Innovation and Research in BioMedical Engineering*. 2009; 30: 3-9.
222. Stinson M and Crawford S. Wheelchair seating and pressure mapping. In: Soderback I, (ed.). *International Handbook of Occupational Therapy Interventions*. Switzerland: Springer International Publishing, 2015, p. 221-31.
223. Stinson MD, Porter-Armstrong A and Eakin P. Seat-interface pressure: a pilot study of the relationship to gender, body mass index, and seating position. *Archives of Physical Medicine and Rehabilitation*. 2003; 84: 405-9.
224. Stinson M and Crawford S. Optimal positioning: Wheelchair seating comfort and pressure mapping. In: Soderback I, (ed.). *International Handbook of Occupational Therapy Interventions*. New York: Springer, 2009, p. 83-90.
225. Stinson MD, Porter A and Eakin P. Measuring interface pressure - a laboratory based investigation into the effects of repositioning and sitting. *American Journal of Occupational Therapy*. 2002; 56: 185-90.
226. Gil-Agudo A, De la Pena-Gonzalez A, Del Ama-Espinosa A, Perez-Rizo E, Diaz-Dominguez E and Sanchez-Ramos A. Comparative study of pressure distribution at the user-cushion interface with different cushions in a population with spinal cord injury. *Clinical Biomechanics*. 2009; 24: 558-63.
-

227. Tam EW, Mak AF, Lam WN, Evans JH and Chow YY. Pelvic movement and interface pressure distribution during manual wheelchair propulsion. *Archives of Physical Medicine and Rehabilitation*. 2003; 84: 1466-72.
228. Ferrarin M, Andreoni G and Pedotti A. Comparative biomechanical evaluation of different wheelchair seat cushions. *Journal of Rehabilitation Research and Development*. 2000; 37: 315-24.
229. Ferguson-Pell M and Cardi MD. Prototype development and comparative evaluation of wheelchair pressure mapping system. *Assistive Technology*. 1993; 5: 78-91.
230. Rouhani H, Favre J, Crevoisier X and Aminian K. Ambulatory assessment of 3D ground reaction force using plantar pressure distribution. *Gait and Posture*. 2010; 32: 311-6.
231. Jung Y, Jung M, Lee K and Koo S. Ground reaction force estimation using an insole-type pressure mat and joint kinematics during walking. *Journal of Biomechanics*. 2014; 47: 2693-9.
232. Lacoste M, Therrien M, Cote JN, Shrier I, Labelle H and Prince F. Assessment of seated postural control in children: comparison of a force platform versus a pressure mapping system. *Archives of Physical Medicine and Rehabilitation*. 2006; 87: 1623-9.
233. Schofield R, Porter-Armstrong A and Stinson M. Reviewing the literature on the effectiveness of pressure relieving movements. *Nursing Research and Practice*. 2013; 2013: 13.
234. Curtis KA and Dillon DA. Survey of wheelchair athletic injuries: Common patterns and prevention. *Paraplegia*. 1985; 23: 170-5.
235. Cooper R, Robertson R, VanSickle D, Boninger ML and Shimada S. Methods for determining three-dimensional wheelchair pushrim forces and moments : A technical note. *Journal of Rehabilitation Research and Development*. 1997; 34: 162-70.
236. LaMere TJ and Labanowich S. The history of sport wheelchairs, part III: The racing wheelchair 1976 - 1983. *Sports'N Spokes*. 1984; 10: 12-6.
237. International Triathlon Union. ITU Paratriathlon Classification Rules. In: Board IE, (ed.). *ITU Competition Rules*. 2015.
238. Gorce P and Louis N. Wheelchair propulsion kinematics in beginners and expert users: influence of wheelchair settings. *Clinical Biomechanics*. 2012; 27: 7-15.
239. Fay BT, Boninger M, Cooper R, Koontz A and Baldwin M. Gender differences in the kinematic features of manual wheelchair propulsion. *Proceedings of the 1999 RESNA Conference*. Long Beach, California 1999, p. 376-8.
240. Crespo-Ruiz BM, Del Ama-Espinosa AJ and Gil-Agudo AM. Relation between kinematic analysis of wheelchair propulsion and wheelchair functional basketball classification. *Adapted Physical Activity Quarterly*. 2011; 28: 157-72.
241. Starrs P, Chohan A, Fewtrell D, Richards J and Selfe J. Biomechanical differences between experienced and inexperienced wheelchair users during sport. *Prosthet Orthot Int*. 2012; 36: 324-31.
242. Kloosterman MG, Eising H, Schaake L, Buurke JH and Rietman JS. Comparison of shoulder load during power-assisted and purely hand-rim wheelchair propulsion. *Clinical Biomechanics*. 2012; 27: 428-35.
243. International Paralympic Committee. Records World Para Athletics. 2018. August 1. <https://www.paralympic.org/world-records/athletics>
244. Fuss FK, Subic A, Strangwood M and Mehta R. *Routledge Handbook of Sports Technology and Engineering*. London, United Kingdom: Routledge, 2014.
245. Forte P, Tiago BM and Marinho D. Technologic Appliance and Performance Concerns in Wheelchair Racing - Helping Paralympic Athletes to Excel. In: Liu DC, (ed.). *New Perspectives in Fluid Dynamics*. InTech, 2015, p. 101-21.
246. Burke ER. *Science of Cycling*. Champaign, United States: Human Kinetics, 1988, p.1 - 224.
247. Hedrick B, Wang YT, Moeinzadeh M and Adrian M. Aerodynamic positioning and performance in wheelchair racing. *Adapted Physical Activity Quarterly*. 1990; 7: 41-51.
248. Costa GB, Rubio MP, Belloch SL and Soriano PP. Case study: effect of handrim diameter on performance in a paralympic wheelchair athlete. *Adapted Physical Activity Quarterly*. 2009; 26.
249. Chow JW and Chae W. Kinematic analysis of the 100 m wheelchair race. *Journal of Biomechanics*. 2007; 40.
250. Atkinson G and Nevill AM. Statistical methods for assessing measurement error (reliability) in variables relevant to sports medicine. *Sports Medicine*. 1998; 26: 217-38.
251. ITU World Triathlon Series. 2017 Gold Coast ITU World Paratriathlon Series. 2017. June 2. <http://wts.triathlon.org/results/>

- 
252. Wheelchair Sports NSW. 2017 Summer Down Under. 2014. June 2. <http://wsnsw.org.au/2017-summer-down-under/>
253. Sinclair J, Taylor PJ and Hobbs SJ. Digital filtering of three-dimensional lower extremity kinematics: An assessment. *Journal of Human Kinetics*. 2013; 39: 25-36.
254. Andena L, Aleo S, Caimmi F, Mariani S, Briatico-Vangosa F and Pavan A. A 3D numerical model for the optimization of running tracks performance. *Procedia Engineering*. 2016; 147: 854-9.
255. Elliott BC, Alderson JA and Denver ER. System and modelling errors in motion analysis: Implications for the measurement of the elbow angle in cricket bowling. *Journal of Biomechanics*. 2007; 40: 2679-85.
256. Kainz H. Evaluation of direct and inverse kinematic modelling for typical and cerebral palsy gait. *School of Allied Health Sciences and Centre for Musculoskeletal Research, Menzies Health Institute Queensland*. Queensland, Australia: Griffith University, 2016, p. 245.
257. Hanneman SK. Design, Analysis and Interpretation of Method-Comparison Studies. *AACN Advanced Critical Care*. 2008; 19: 223-34.
258. Hopkins WG. A scale of magnitudes for effect statistics. 2002. May 18. <http://www.sportsci.org/resource/stats/effectmag.html>
259. Field A. *Discovering statistics using SPSS*. Thousand Oaks, California: SAGE Publications, 2009.
260. Tupling SJ, Davis GM, Pierrynowski MR and Shephard RJ. Arm strength and impulse generation: Initiation of wheelchair movement by the physically disabled. *Ergonomics*. 1986; 29: 303-11.
261. Rodgers MM, Keyser RE, Rasch EK, Gorman PH and Russell PJ. Influence of training on biomechanics of wheelchair propulsion. *Journal of Rehabilitation Research and Development*. 2001; 38: 505-11.
262. Koontz AM, Cooper RA, Boninger ML, Souza AL and Fay BT. Shoulder kinematics and kinetics during two speeds of wheelchair propulsion. *Journal of Rehabilitation Research and Development*. 2002; 39: 635-49.
263. Bregman DJ, van Drongelen S and Veeger HE. Is effective force application in handrim wheelchair propulsion also efficient? *Clinical Biomechanics*. 2009; 24: 13-9.
264. Moon Y, Chandrasekaran J, Hsu IMK, Rice IM, Hsiao-Wecksler ET and Sosnoff JJ. Variability of peak shoulder force during wheelchair propulsion in manual wheelchair users with and without shoulder pain. *Clinical Biomechanics*. 2013; 28: 1-27.
265. van der Woude LH, Bakker WH, Elkhuizen JW, Veeger HE and Gwinn T. Propulsion technique and anaerobic work capacity in elite wheelchair athletes: cross-sectional analysis. *American Journal of Physical Medicine and Rehabilitation*. 1998; 77: 222-34.
266. Gil-Agudo A, Del Ama-Espinosa A, Perez-Rizo E, Perez-Nombela S and Pablo Rodriguez-Rodriguez L. Upper limb joint kinetics during manual wheelchair propulsion in patients with different levels of spinal cord injury. *Journal of Biomechanics*. 2010; 43: 2508-15.
267. Keller TS, Weisberger AM, Ray JL, Hasan SS, Shiavi RG and Spengler DM. Relationship between vertical ground reaction force and speed during walking, slow jogging, and running. *Clinical Biomechanics*. 1996; 11: 253-9.
268. Laing AC and Robinovitch SN. Low stiffness floors can attenuate fall-related femoral impact forces by up to 50% without substantially impairing balance in older women. *Accident Analysis & Prevention*. 2009; 41: 642-50.
269. Novaproducts Global. Sports and Gym Flooring. *Website*. 2017.
270. Li T, Du Y, Ji W, Liu Z and Cai C. Short communication: Automated testing of accelerometer transverse sensitivity with a flexure-based XY compliant stage. *Mechanical Sciences*. 2016; 7: 149-53.
271. Finch M and BESIER TF. Lower limb loading assessment systems and methods. Google Patents, 2015.
272. Piezotronics P. Installation and Operating Manual.
273. Kistler Group. Force plates and accessories. In: Kistler, (ed.). 2015, p. 32.
274. Kwarciak AM, Turner JT, Guo L and Richter WM. Comparing handrim biomechanics for treadmill and overground wheelchair propulsion. *Spinal Cord*. 2011; 49: 457-62.
275. Cardoso M, Girouard M, McKinnon C, Callaghan JP and Albert WJ. Quantifying the postural demands of patrol officers: a field study. *International Journal of Occupational Safety and Ergonomics*. 2017; 23: 185-97.
276. Davis K and Sprigle S. The science of interface papping - Updates for clinical application. *24th International Seating Symposium*. Vancouver, British Columbia: Georgia Institute of Technology, 2008, p. 4.
-

- 
277. TekScan. I-Scan Product Selection Guide. 2015.
278. Kutilek P, Svoboda Z and Smrcka P. Evaluation of bilateral asymmetry of the muscular forces using OpenSim software and bilateral cyclograms. In: Březina T and Jabłoński R, (eds.). *Mechatronics 2013 Recent Technological Scientific Advantages*. Brno, Czech Republic: Springer, 2013.
279. Nana A, Slater GJ, Hopkins WG and Burke LM. Effects of exercise sessions on DXA measurements of body composition in active people. *Medicine and Science in Sports and Exercise*. 2013; 45: 178-85.
280. Clauser CE, McConville JT and Young JW. Weight, volume, and center of mass segments of the human body. *Journal of Occupational and Environmental Medicine*. 1969; 13: 270.
281. Dempster WT. Space Requirements of the Seated Operator. In: Centre WAD, (ed.). Ohio: Air Research and Development Command, United States Air Force, 1955, p. 55-159.
282. Laschowski B and McPhee J. Body segment parameters of Paralympic athletes from dual-energy X-ray absorptiometry. *Sports Engineering*. 2016; 19: 155-62.
283. Laschowski B and McPhee J. Quantifying body segment parameters using dual-energy x-ray absorptiometry: A Paralympic wheelchair curler case report. *Procedia Engineering*. 2016; 147: 163-7.
284. Rossi M, Lyttle A, El-Sallam A, Benjanuvatra N and Blanksby B. Body segment inertial parameters of elite swimmers Using DXA and indirect methods. *Journal of Sports Science and Medicine*. 2013; 12: 761-75.
285. Zatsiorsky V. *Kinetics of Human Motion*. Champaign, Illinois 2002.
286. Bell DR, Sanfilippo JL, Binkley N and Heiderscheit BC. Lean mass asymmetry influences force and power asymmetry during jumping in collegiate athletes. *Journal of Strength and Conditioning Research*. 2014; 28: 884-91.
287. Saul KR, Hu X, Goehler CM, et al. Benchmarking of dynamic simulation predictions in two software platforms using an upper limb musculoskeletal model. *Computer Methods in Biomechanics and Biomedical Engineering*. 2014; 18: 1445-58.
288. Crowninshield RD and Brand RA. A physiologically based criterion of muscle force prediction in locomotion. *Journal of Biomechanics*. 1981; 14: 793-801.
289. Laschowski B, Mehrabi N and McPhee J. Optimization-based motor control of a Paralympic wheelchair athlete. *Sports Engineering*. 2018.
290. Chinappen-Horsley U, Blake GM, Fogelman I and Spector TD. A method for determining skeletal lengths from DXA images. *BMC Musculoskeletal Disorders*. 2007; 8: 113.
291. Bortoletto R, Pagello E and Piovesan D. Effects of reserve actuators on optimization solutions: From muscle force to joint stiffness. *2015 IEEE International Conference on Rehabilitation Robotics (ICORR)*. Nanyang Technological University, Singapore 2015, p. 973-8.
292. Bruno AG, Bouxsein ML and Anderson DE. Development and validation of a musculoskeletal model of the fully articulated thoracolumbar spine and rib cage. *Journal of Biomechanical Engineering*. 2015; 137: 081003.
293. Ren L, Jones RK and Howard D. Whole body inverse dynamics over a complete gait cycle based only on measured kinematics. *Journal of Biomechanics*. 2008; 41: 2750-9.
294. Garteiser P, Doblas S, Towner RA and Griffin TM. Calibration of a semi-automated segmenting method for quantification of adipose tissue compartments from magnetic resonance images of mice. *Metabolism - Clinical and Experimental*. 2013; 62: 1686-95.
295. Keil M, Totosy de Zepetnek JO, Brooke-Wavell K and Goosey-Tolfrey VL. Measurement precision of body composition variables in elite wheelchair athletes, using dual-energy X-ray absorptiometry. *European Journal of Sport Science*. 2016; 16: 65-71.
296. Lussier L, Knight J, Bell G, Lohman T and Morris AF. Body composition comparison in two elite female wheelchair athletes. *Paraplegia*. 1983; 21: 16-22.
297. Braune W and Fischer O. The center of gravity of the human body as related to the German Infantryman. In: Service. LNTI, (ed.). *ATI 138 452*. Springfield, VA 1889.
298. Chen S-C, Hsieh H-J, Lu T-W and Tseng C-H. A method for estimating subject-specific body segment inertial parameters in human movement analysis. *Gait & Posture*. 2011; 33: 695-700.
299. Fujikawa K. The center of gravity in the parts of human body. *Okajimas Folia Anatomica Japonica*. 1963; 39: 117-25.
300. Harless E. The static moments of the component masses of the human body. *Treatises of the Mathematics - Physics Class*. Royal Bavarian Academy of Sciences: Wright-Patterson Air Force Base
-

---

1860, p. 257-94.

301. Jensen RK. Changes in segment inertia proportions between 4 and 20 years. *Journal of Biomechanics*. 1989; 22: 529-36.
302. Jensen RK. Body segment mass, radius and radius of gyration proportions of children. *Journal of Biomechanics*. 1986; 19: 359-68.
303. Jensen RK. Distribution of mass to the segments of elderly males and females. *Journal of Biomechanics*. 1994; 27: 89-96.
304. Ma Y, Lee K, Li L and Kwon J. Nonlinear regression equations for segmental mass-inertial characteristics of Korean adults estimated using three-dimensional range scan data. *Applied Ergonomics*. 2011; 42: 297-308.
305. Pavol MJ, Owings TM and Grabiner MD. Body segment inertial parameter estimation for the general population of older adults. *Journal of Biomechanics*. 2002; 35: 707-12.
306. Goosey V, Campbell IG and Fowler NE. Effect of push frequency on the economy of wheelchair racers. *Medicine and Science in Sports and Exercise*. 2000; 32: 174-81.
307. Vanlandewijck YC, Spaepen AJ and Lysens RJ. Wheelchair propulsion efficiency- movement pattern adaptations to speed changes. *Medicine and Science in Sports and Exercise*. 1994; 26: 1373-81.
308. Milgrom C, Schaffler M, Gilbert S and van Holsbeeck M. Rotator-cuff changes in asymptomatic adults. The effect of age, hand dominance and gender. *Journal of Bone and Joint Surgery*. 1995; 77: 296-8.
309. Bernard P-L, Peruchon E, Micallef J-P, Hertog C and Rabischong P. Balance and stabilization capability of paraplegic wheelchair athletes. *Journal of Rehabilitation Research and Development*. 1994; 31: 287.
310. Caruso JF, Brown LE and Tufano JJ. The reproducibility of isokinetic dynamometry data. *Isokinetics and Exercise Science*. 2012; 20: 239-53.
311. Lin H-T, Su F-C, Wu H-W and An K-N. Muscle forces analysis in the shoulder mechanism during wheelchair propulsion. *Proceedings of the Institution of Mechanical Engineers, Part H: Journal of Engineering in Medicine*. 2004; 218: 213-21.
312. Tries J. EMG feedback for the treatment of upper-extremity dysfunction: Can it be effective? *Biofeedback and Self-regulation*. 1989; 14: 21-53.
313. Knarr BA, Ramsay JW, Buchanan TS, Higginson JS and Binder-Macleod SA. Muscle volume as a predictor of maximum force generating ability in the plantar flexors post-stroke. *Muscle & nerve*. 2013; 48: 971-6.
314. O'Brien TD, Reeves ND, Baltzopoulos V, Jones DA and Maganaris CN. In vivo measurements of muscle specific tension in adults and children. *Experimental Physiology*. 2010; 95: 202-10.
315. Lictwark D. strengthscaler.m. *opensim-core*. github2012, p. component of Opensim.
316. Bulbulian R, Johnson RE, Gruber JJ and Darabos B. Body composition in paraplegic male athletes. *Medicine and Science in Sports and Exercise*. 1987; 19: 195-201.
317. Arnet U, van Drongelen S, van der Woude LHV and Veeger DHEJ. Shoulder load during handcycling at different incline and speed conditions. *Clinical Biomechanics*. 2012; 27: 1-6.
318. Chadwick EK, Blana D, Kirsch RF and Van den Bogert AJ. Real-time simulation of three-dimensional shoulder girdle and arm dynamics. *IEEE Transactions on Bio-medical Engineering*. 2014; 61: 1947-56.
319. Jones EJ, Bishop PA, Woods AK and Green JM. Cross-Sectional Area and Muscular Strength. *Sports Medicine*. 2008; 38: 987-94.
320. Bruce SA, Phillips SK and Woledge RC. Interpreting the relation between force and cross-sectional area in human muscle. *Medicine and Science in Sports and Exercise*. 1997; 29: 677-83.
321. Dionyssiotis Y. Changes in bone density and strength of the tibia and alterations of lean and fat mass in chronic paraplegic men. *Doctoral Dissertaion Laboratory for Research of the Musculoskeletal System*. Athens: University of Athens, 2008.
322. Dionyssiotis Y. Body Composition in Paraplegia. In: Dianyssiotis Y, (ed.). *Topics in Paraplegia*. InTech, 2014.
323. Miyahara K, Wang DH, Mori K, et al. Effect of sports activity on bone mineral density in wheelchair athletes. *Journal of Bone and Mineral Metabolism*. 2008; 26: 101-6.
324. Aguado-Henche S, Carrascosa-Sánchez J, Cristóbal-Aguado S and Clemente de Arriba C. Normative values for body compartments of sedentary white people. *MOJ Anatomy and Physiology*. 2017; 4: 1:9.

325. Inukai Y, Takahashi K, Wang DH and Kira S. Assessment of total and segmental body composition in spinal cord-injured athletes in Okayama prefecture of Japan. *Acta Med Okayama*. 2006; 60: 99-106.
326. Shimada SD, Robertson RN, Boninger ML and Cooper RA. Kinematic characterization of wheelchair propulsion. *Journal of Rehabilitation Research and Development*. 1998; 35.
327. Mercer JL, Boninger M, Koontz A, Ren D, Dyson-Hudson T and Cooper R. Shoulder joint kinetics and pathology in manual wheelchair users. *Clinical Biomechanics*. 2006; 21: 781-9.
328. Zatsiorsky V, Seluyanov V and Chugunova L. In vivo body segment inertial parameters determination using a gamma-scanner method. In: Berme N and Cappozzo A, (eds.). *Biomechanics of Human Movement: Applications in Rehabilitations, Sports and Ergonomics*. Bertec, Ohio 1990, p. 187-202.
329. Curtis KA and Black K. Shoulder pain in female wheelchair basketball players. *Journal of Orthopaedic and Sports Physical Therapy*. 1999; 29: 225-31.
330. Wu W, Lee PVS, Bryant AL, Galea M and Ackland DC. Subject-specific musculoskeletal modeling in the evaluation of shoulder muscle and joint function. *Journal of Biomechanics*. 2016; 49: 3626-34.
331. Gonzalez RV, Buchanan TS and Delp SL. How muscle architecture and moment arms affect wrist flexion-extension moments. *Journal of Biomechanics*. 1997; 30: 705-12.
332. Arnold EM, Ward SR, Lieber RL and Delp SL. A model of the lower limb for analysis of human movement. *Annals of Biomedical Engineering*. 2010; 38: 269-79.
333. Chung J, Evans J, Lee C, et al. Effectiveness of adaptive seating on sitting posture and postural control in children with cerebral palsy. *Pediatric Physical Therapies*. 2008; 20: 303-17.
334. Ferguson JE, Wittig BL, Payette M, Goldish GD and Hansen AH. Pilot study of strap-based custom wheelchair seating system in persons with spinal cord injury. *Journal of Rehabilitation Research and Development*. 2014; 51: 1255-64.
335. Masse LC, Lamotagne M and O'Riain MD. Biomechanical analysis of wheelchair propulsion for various seating positions. *Journal of Rehabilitation Research and Development*. 1992; 29: 12-28.
336. Stankovits S. The impact of seating and positioning on the development of repetitive strain injuries of the upper extremity in wheelchair athletes. *Work*. 2000; 15.
337. Rudins A, Laskowski ER, Growney ES, Cahalan TD and An KN. Kinematics of the elbow during wheelchair propulsion: a comparison of two wheelchairs and two stroking techniques. *Archives of Physical Medicine and Rehabilitation*. 1997; 78: 1204-10.
338. Lewis AR, Haydon DS, Phillips EJ, Grimshaw PN, Robertson WSP and Portus M. Monitoring seating interface pressure in wheelchair sports. *Sports Engineering*. 2018.
339. Anderson AE, Ellis BJ and Weiss JA. Verification, validation and sensitivity studies in computational biomechanics. *Computer Methods in Biomechanics and Biomedical Engineering*. 2007; 10: 171-84.
340. Andersen MS, Benoit DL, Damsgaard M, Ramsey DK and Rasmussen J. Do kinematic models reduce the effects of soft tissue artefacts in skin marker-based motion analysis? An in vivo study of knee kinematics. *Journal of Biomechanics*. 2010; 43: 268-73.
341. Oberkampf WL, Trucano TG and Hirsch C. Verification, validation, and predictive capability in computational engineering and physics. *Applied Mechanics Reviews*. 2004; 57: 345-84.
342. Tsai TY, Lu TW, Kuo MY and Lin CC. Effects of soft tissue artifacts on the calculated kinematics and kinetics of the knee during stair-ascent. *Journal of Biomechanics*. 2011; 44: 1182-8.
343. Stagni R, Fantozzi S, Cappello A and Leardini A. Quantification of soft tissue artefact in motion analysis by combining 3D fluoroscopy and stereophotogrammetry: a study on two subjects. *Clinical Biomechanics*. 2005; 20: 320-9.
344. Peters A, Galna B, Sangeux M, Morris M and Baker R. Quantification of soft tissue artifact in lower limb human motion analysis: a systematic review. *Gait and Posture*. 2010; 31: 1-8.
345. Prinold JA, Masjedi M, Johnson GR and Bull AM. Musculoskeletal shoulder models: a technical review and proposals for research foci. *Proceedings of the Institution of Mechanical Engineers Part H, Journal of Engineering in Medicine*. 2013; 227: 1041-57.
346. Prinold JA, Shaheen AF and Bull AM. Skin-fixed scapula trackers: a comparison of two dynamic methods across a range of calibration positions. *Journal of Biomechanics*. 2011; 44: 2004-7.
347. Karduna AR, McClure PW, Michener LA and Sennett B. Dynamic measurements of three-dimensional scapular kinematics: a validation study. *Journal of Biomechanical Engineering*. 2001; 123: 184-90.
348. Charlton IW. A model for the prediction of the forces at the glenohumeral joint. University of Newcastle upon Tyne, 2003.



- 
349. Happee R and Van der Helm FC. The control of shoulder muscles during goal directed movements, an inverse dynamic analysis. *Journal of Biomechanics*. 1995; 28: 1179-91.
350. de Groot JH. The variability of shoulder motions recorded by means of palpation. *Clinical Biomechanics*. 1997; 12: 461-72.
351. Remy CD and Thelen DG. Optimal Estimation of Dynamically Consistent Kinematics and Kinetics for Forward Dynamic Simulation of Gait. *Journal of Biomechanical Engineering*. 2009; 131: 031005-.
352. Duffell LD, Hope N and McGregor AH. Comparison of kinematic and kinetic parameters calculated using a cluster-based model and Vicon's plug-in gait. *Proceedings of the Institution of Mechanical Engineers Part H, Journal of Engineering in Medicine*. 2014; 228: 206-10.
353. Cooper RA, DiGiovine CP, Boninger ML, Shimada SD, Koontz AM and Baldwin MA. Filter frequency selection for manual wheelchair biomechanics. *Journal of Rehabilitation Research and Development*. 2002; 39: 323-6.
354. Bland JM and Altman DG. Statistical methods for assessing agreement between two methods of clinical measurement. *Lancet*. 1986; 1: 307-10.
355. Winter DA. *Biomechanics and motor control of human movement*. Hoboken, New Jersey: Wiley, 2009.
356. Iino Y and Kojima T. Validity of the top-down approach of inverse dynamics analysis in fast and large rotational trunk movements. *Journal of Applied Biomechanics*. 2012; 28: 420-30.
357. Shan G and Bohn C. Anthropometrical data and coefficients of regression related to gender and race. *Applied Ergonomics*. 2003; 34: 327-37.
358. Moissenet F, Chèze L and Dumas R. Influence of the level of muscular redundancy on the validity of a musculoskeletal model. *Journal of Biomechanical Engineering*. 2016; 138: 021019--6.
359. Samaan MA, Weinhandl JT, Bawab SY and Ringleb SI. Determining residual reduction algorithm kinematic tracking weights for a sidestep cut via numerical optimization. *Computer Methods in Biomechanics and Biomedical Engineering*. 2016; 19: 1721-9.
360. Kaufman KR, Kovacevic N, Irby SE and Colwell CW. Instrumented implant for measuring tibiofemoral forces. *Journal of Biomechanics*. 1996; 29: 667-71.
361. D'Lima DD, Fregly BJ and Colwell CW. Implantable sensor technology: measuring bone and joint biomechanics of daily life in vivo. *Arthritis Research and Therapy*. 2013; 15: 203-.
362. van Drongelen S, de Groot S, Veeger HE, et al. Upper extremity musculoskeletal pain during and after rehabilitation in wheelchair-using persons with a spinal cord injury. *Spinal Cord*. 2006; 44.
363. van Drongelen S, van der Woude LHV, Janssen TWJ, Angenot ELD, Chadwick EKJ and Veeger HEJ. Glenohumeral joint loading in tetraplegia during weight relief lifting: A simulation study. *Clinical Biomechanics*. 2006; 21: 128-37.
364. Morrow MM, Rankin JW, Neptune RR and Kaufman KR. A comparison of static and dynamic optimization muscle force predictions during wheelchair propulsion. *Journal of Biomechanics*. 2014; 47: 3459-65.
365. Rankin JW, Kwarciak AM, Richter WM and Neptune RR. The influence of wheelchair propulsion technique on upper extremity muscle demand: a simulation study. *Clinical Biomechanics*. 2012; 27: 879-86.
366. Rankin JW, M KA, M RW and Neptune RR. Muscle function during the push phase of wheelchair propulsion. *American Society of Biomechanics*. Providence, Rhode Island 2010.
367. Knarr BA, Zeni JA and Higginson JS. Comparison of electromyography and joint moment as indicators of co-contraction. *Journal of electromyography and kinesiology : official journal of the International Society of Electrophysiological Kinesiology*. 2012; 22: 607-11.
368. McConville JT and Air Force Aerospace Medical Research Laboratory (U.S.). *Anthropometric relationships of body and body segment moments of inertia*. Washington, D.C. : Springfield, Va: Wright-Patterson Air Force Base, Ohio 1981.
369. de Leva P. Adjustments to Zatsiorsky-Seluyanov's segment inertia parameters. *Journal of Biomechanics*. 1996; 29: 1223-30.
370. Nikooyan AA, Veeger HEJ, Westerhoff P, et al. An EMG-driven musculoskeletal model of the shoulder. *Human Movement Science*. 2012; 31: 429-47.
371. Klein Breteler MD, Spoor CW and Van der Helm FC. Measuring muscle and joint geometry parameters of a shoulder for modeling purposes. *Journal of Biomechanics*. 1999; 32: 1191-7.
372. Reich J and Daunicht WJ. A rigid body model of the forearm. *Journal of Biomechanics*. 2000; 33: 1159-68.
-

373. Karlsson D and Peterson B. Towards a model for force predictions in the human shoulder. *Journal of Biomechanics*. 1992; 25: 189-99.
374. Makhous M, Hogfors C, Siemienski A and Peterson B. Total shoulder and relative muscle strength in the scapular plane. *Journal of Biomechanics*. 1999; 32: 1213-20.
375. Scheys L, Desloovere K, Suetens P and Jonkers I. Level of subject-specific detail in musculoskeletal models affects hip moment arm length calculation during gait in pediatric subjects with increased femoral anteversion. *Journal of Biomechanics*. 2011; 44: 1346-53.
376. Favre P, Sheikh R, Fucentese SF and Jacob HA. An algorithm for estimation of shoulder muscle forces for clinical use. *Clinical Biomechanics*. 2005; 20: 822-33.
377. Wolffson DM. Scapula shape and muscle function, with special reference to the vertebral border. *American Journal of Physical Anthropology*. 1950; 8: 331-41.
378. Krobot A, Janura M and Elfmark M. Functional categorization of the individual morphology of the scapula. *Medical and Biological Engineering and Computing*. 2009; 47: 497-506.
379. Garner BA and Pandy MG. Estimation of musculotendon properties in the human upper limb. *Annals of Biomedical Engineering*. 2003; 31: 207-20.
380. Scovil CY and Ronsky JL. Sensitivity of a Hill-based muscle model to perturbations in model parameters. *Journal of Biomechanics*. 2006; 39: 2055-63.
381. Cutti AG, Paolini G, Troncossi M, Cappello A and Davalli A. Soft tissue artefact assessment in humeral axial rotation. *Gait and Posture*. 2005; 21: 341-9.
382. Lempereur M, Leboeuf F, Brochard S, Rousset J, Burdin V and Remy-Neris O. In vivo estimation of the glenohumeral joint centre by functional methods: accuracy and repeatability assessment. *Journal of Biomechanics*. 2010; 43: 370-4.
383. Stokdijk M, Nagels J and Rozing PM. The glenohumeral joint rotation centre in vivo. *Journal of Biomechanics*. 2000; 33: 1629-36.
384. Xu H, Merryweather A, Blawieck D, Mao Q and Wang T. The effect of toe marker placement error on joint kinematics and muscle forces using OpenSim gait simulation. *Biomed Mater Eng*. 2015; 26 Suppl 1: S685-91.
385. Rabuffetti M, Baroni G, Ferrarin M, Ferrigno G and Pedotti A. Self-marking of anatomical landmarks for on-orbit experimental motion analysis compared to expert direct-marking. *Human Movement Science*. 2002; 21: 439-55.
386. Della Croce U, Leardini A, Chiari L and Cappozzo A. Human movement analysis using stereophotogrammetry: Part 4: Assessment of anatomical landmark misplacement and its effects on joint kinematics. *Gait and Posture*. 2005; 21: 226-37.
387. Della Croce U, Cappozzo A and Kerrigan DC. Pelvis and lower limb anatomical landmark calibration precision and its propagation to bone geometry and joint angles. *Medical & Biological Engineering & Computing*. 1999; 37: 155-61.
388. Seth A, Matias R, Veloso AP and Delp SL. A biomechanical model of the scapulothoracic joint to accurately capture scapular kinematics during shoulder movements. *PLoS One*. 2016; 11: e0141028.
389. Lee JH, Asakawa DS, Dennerlein JT and Jindrich DL. Finger muscle attachments for an OpenSim upper-extremity model. *PLoS One*. 2015; 10: e0121712.
390. Kuo AD. Choosing Your Steps Carefully. *IEEE Robotics and Automation Magazine*. 2007; 14: 18-29.
391. Abdulrahman A, Iqbal K and White G. Improving inverse dynamics accuracy in a planar walking model based on stable reference point. *Journal of Robotics*. 2014; 2014: 1-9.
392. Xiao M and Higginson J. Sensitivity of estimated muscle force in forward simulation of normal walking. *Journal of Applied Biomechanics*. 2010; 26: 142-9.
393. Langenderfer JE, Laz PJ, Petrella AJ and Rullkoetter PJ. An efficient probabilistic methodology for incorporating uncertainty in body segment parameters and anatomical landmarks in joint loadings estimated from inverse dynamics. *Journal of Biomechanical Engineering*. 2008; 130: 1-7.
394. Ackland DC, Lin Y-C and Pandy MG. Sensitivity of model predictions of muscle function to changes in moment arms and muscle-tendon properties: A Monte-Carlo analysis. *Journal of Biomechanics*. 2012; 45: 1463-71.
395. Valente G, Pitto L, Testi D, et al. Are Subject-Specific Musculoskeletal Models Robust to the Uncertainties in Parameter Identification? *PLoS ONE*. 2014; 9: e112625.
396. Durkin JL and Dowling JJ. Body segment parameter estimation of the human lower leg using an elliptical model with validation from DEXA. *Annals of Biomedical Engineering*. 2006; 34: 1483-93.

- 
397. Kelly TL, Berger N and Richardson TL. DXA body composition: theory and practice. *Applied Radiation and Isotopes*. 1998; 49: 511-3.
398. Lee MK, Le NS, Fang AC and Koh MT. Measurement of body segment parameters using dual energy X-ray absorptiometry and three-dimensional geometry: an application in gait analysis. *Journal of Biomechanics*. 2009; 42: 217-22.
399. Slosman DO, Casez JP, Pichard C, et al. Assessment of whole-body composition with dual-energy x-ray absorptiometry. *Radiology*. 1992; 185: 593-8.
400. Durkin JL, Dowling JJ and Andrews DM. The measurement of body segment inertial parameters using dual energy X-ray absorptiometry. *Journal of Biomechanics*. 2002; 35: 1575-80.
401. Wu G, Siegler S, Allard P, et al. ISB recommendation on definitions of joint coordinate system of various joints for the reporting of human joint motion--part I: ankle, hip, and spine. International Society of Biomechanics. *Journal of Biomechanics*. 2002; 35: 543-8.
402. Martin PE, Mungiole M, Marzke MW and Longhill JM. The use of magnetic resonance imaging for measuring segment inertial properties. *Journal of Biomechanics*. 1989; 22: 367-76.
403. Clarkson S, Choppin S, Hart J, Heller B and Wheat J. Calculating body segment inertia parameters from a single rapid scan using the microsoft kinect. *3rd International Conference on 3D Body Scanning Technologies*. Lugano, Switzerland 2012, p. 11.
404. Mungiole M and Martin PE. Estimating segment inertial properties: comparison of magnetic resonance imaging with existing methods. *Journal of Biomechanics*. 1990; 23: 1039-46.
405. Pearsall DJ, Reid JG and Livingston LA. Segmental inertial parameters of the human trunk as determined from computed tomography. *Annals of Biomedical Engineering*. 1996; 24: 198-210.
406. Huang HK and Suarez FR. Evaluation of cross-sectional geometry and mass density distributions of humans and laboratory animals using computerized tomography. *Journal of Biomechanics* 1983; 16: 821-32.
407. Dumas R, Cheze L and Verriest JP. Adjustments to McConville et al. and Young et al. body segment inertial parameters. *Journal of Biomechanics*. 2007; 40: 543-53.
408. Chandler RF, Clauser CE, Mcconville JT, Reynolds H, M and Young JW. Investigation of inertial properties of the human body. *Aerospace Medical Research Laboratory*. 1975: 70-137.
409. Zatsiorsky V and Seluyanov V. The mass and inertia characteristics of the main segments of the human body. In: Matsui H and HKobayashi K, (eds.). *Biomechanics VIII-B*. Champaign, Illinois: Human Kinetics, 1983, p. 1152-9.
410. Zatsiorsky V and Seluyanov V. Estimation of the mass and inertia characteristics of the human body by means of the best predictive regression equations. In: Winter DA, (ed.). *Biomechanics IX-B*. Champaign, Illinois: Human Kinetics, 1985.
411. Wicke J and Dumas GA. Influence of the volume and density functions within geometric models for estimating trunk inertial parameters. *Journal of Applied Biomechanics*. 2010; 26: 26-31.
412. Wicke J and Dumas GA. A new geometric-based model to accurately estimate arm and leg inertial estimates. *Journal of Biomechanics*. 2014; 47: 1869-75.
413. Yeadon MR and Morlock M. The appropriate use of regression equations for the estimation of segmental inertia parameters. *Journal of Biomechanics*. 1989; 22: 683-9.
414. Rodgers M, Tummarakota S and Lieh J. Three-dimensional dynamic analysis of wheelchair propulsion. *Journal of Applied Biomechanics*. 1998; 14: 80-92.
415. Slavens BA, Schnorenberg AJ, Aurit CM, et al. Evaluation of pediatric manual wheelchair mobility using advanced biomechanical methods. *BioMed Research International*. 2015; 2015: 634768.
416. Hill A. *First and Last Experiments in Muscle Mechanics*. Cambridge University Press, London: Cambridge University Press, 1970.
417. Haeufle DFB, Günther M, Bayer A and Schmitt S. Hill-type muscle model with serial damping and eccentric force-velocity relation. *Journal of Biomechanics*. 2014; 47: 1531-6.
418. Asadi Nikooyan A, Veeger HEJ, Chadwick EKJ, Praagman M and van der Helm FCT. Development of a comprehensive musculoskeletal model of the shoulder and elbow. *Medical and Biological Engineering and Computing*. 2011; 49: 1425-35.
419. Minekus J. Kinematical model of the human elbow. Leiden: Leiden University, 1997.
-

420. Veeger HE, Van der Helm FC, Van der Woude LH, Pronk GM and Rozendal RH. Inertia and muscle contraction parameters for musculoskeletal modelling of the shoulder mechanism. *Journal of Biomechanics*. 1991; 24: 615-29.
421. Veeger HE, Yu B, An KN and Rozendal RH. Parameters for modeling the upper extremity. *Journal of Biomechanics*. 1997; 30: 647-52.
422. Wood JE, Meek SG and Jacobsen SC. Quantitation of human shoulder anatomy for prosthetic arm control--I. Surface modelling. *Journal of Biomechanics*. 1989; 22: 273-92.
423. Chang YW, Hughes RE, Su FC, Itoi E and An KN. Prediction of muscle force involved in shoulder internal rotation. *Journal of Shoulder and Elbow Surgery*. 2000; 9: 188-95.
424. Hind K, Oldroyd B and Truscott JG. In vivo precision of the GE Lunar iDXA densitometer for the measurement of total body composition and fat distribution in adults. *European Journal of Clinical Nutrition*. 2011; 65: 140-2.
425. Jeukendrup A and Gleeson M. *Sport Nutrition - 2nd Edition. An Introduction to Energy Production and Performance*. Champaign, Illinois: Human Kinetics, 2010.
426. Akman A, Demirkan F, Sabir N, Oto M, Yorukoglu C and Kiter E. Femoral bowing plane adaptation to femoral anteversion. *Indian Journal of Orthopaedics*. 2017; 51: 49-54.
427. Arnold AS, Blemker SS and Delp SL. Evaluation of a deformable musculoskeletal model for estimating muscle-tendon lengths during crouch gait. *Annals of Biomedical Engineering*. 2001; 29: 263-74.
428. Zhang J, Fernandez J, Hislop-Jambrich J and Besier TF. Lower limb estimation from sparse landmarks using an articulated shape model. *Journal of Biomechanics*. 2016; 49: 3875-81.
429. Qi L, Wakeling J, Grange S and Ferguson-Pell M. Changes in surface electromyography signals and kinetics associated with progression of fatigue at two speeds during wheelchair propulsion. *Journal of Rehabilitation Research and Development*. 2012; 49: 23-34.
430. Howarth SJ, Pronovost LM, Polgar JM, Dickerson CR and Callaghan JP. Use of a geared wheelchair wheel to reduce propulsive muscular demand during ramp ascent: Analysis of muscle activation and kinematics. *Clinical Biomechanics*. 2010; 25: 21-8.
431. Louis N and Gorce P. Surface electromyography activity of upper limb muscle during wheelchair propulsion: Influence of wheelchair configuration. *Clinical Biomechanics*. 2010; 25: 879-85.
432. Veeger HE, van der Woude LH and Rozendal RH. A computerized wheelchair ergometer. Results of a comparison study. *Scandinavian Journal of Rehabilitation Medicine*. 1992; 24.
433. Limroongreungrat W, Wang YT, Chang L-s, Geil MD and Johnson JT. An instrumented wheel system for measuring 3-D pushrim kinetics during racing wheelchair propulsion. *Res Sports Med: An International Journal*. 2009; 17.

---

---

**APPENDIX A:**

**COMPUTATIONAL  
MODELLING IN  
OPENSIM**

---

Computational modelling has a sequential workflow, with this research utilising three computational stages: inverse kinematics, inverse dynamics and static optimisation (Figure A.1). At each analytical step, a series of matrix operations are performed incorporating the movement data collected in Chapters Four and Five and incorporating the subject-specific physical parameters introduced in Chapter Six. This chapter provides an overview of each of the calculation steps used within the computational modelling workflow; inverse kinematics (Section A.1), inverse dynamics (Section A.2) and static optimisation (Section A.3). Common error sources for each of these calculation processes are documented within each of these sections, with additional comments as to how these potential error sources were controlled within this research.

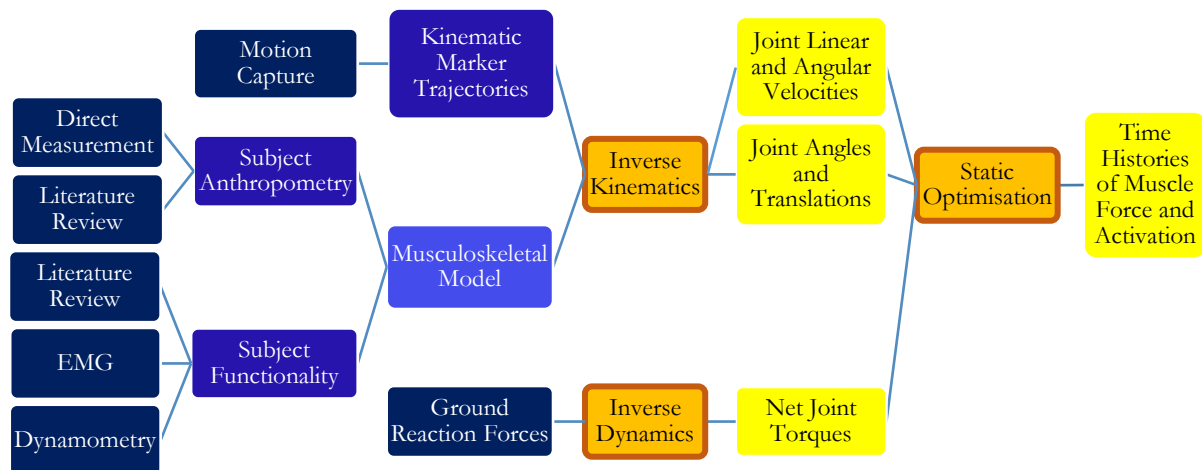


Figure A.1: Flowchart of the modelling process demonstrating the required inputs (left, dark boxes), the processes (outlined boxes), and the resulting outputs (right, light boxes)...

## A.1 INVERSE KINEMATICS

Inverse kinematics calculations estimate the requirements of all the anatomical structures (e.g. limb segments) required for producing the observed motion, subject to the constraints imposed through the defined boundary conditions.<sup>133</sup> A generalised set of joint motions (angles, velocities and accelerations) is computed for each time stamp of experimental data. The fundamental inputs for inverse kinematics include the kinematic marker trajectories (obtained using motion capture) and the musculoskeletal model (Figure A.2).

During this process, the three-dimensional coordinates of marker position are resolved onto the known landmarks on rigid body segments.<sup>112</sup> The orientation of the musculoskeletal model is established using a global weighted least-squares optimisation method. This minimises the distances between the generalised coordinates of the rigid segment virtual markers and the recorded positions of the experimental markers.<sup>133, 151</sup> The weighting for each marker can be manually adjusted for each simulation, such that greater weighting is placed on markers with a known location (such as near a bony landmark). For cluster based marker systems, lower weighting can hence be placed on the segment clusters, which have a more arbitrary location.

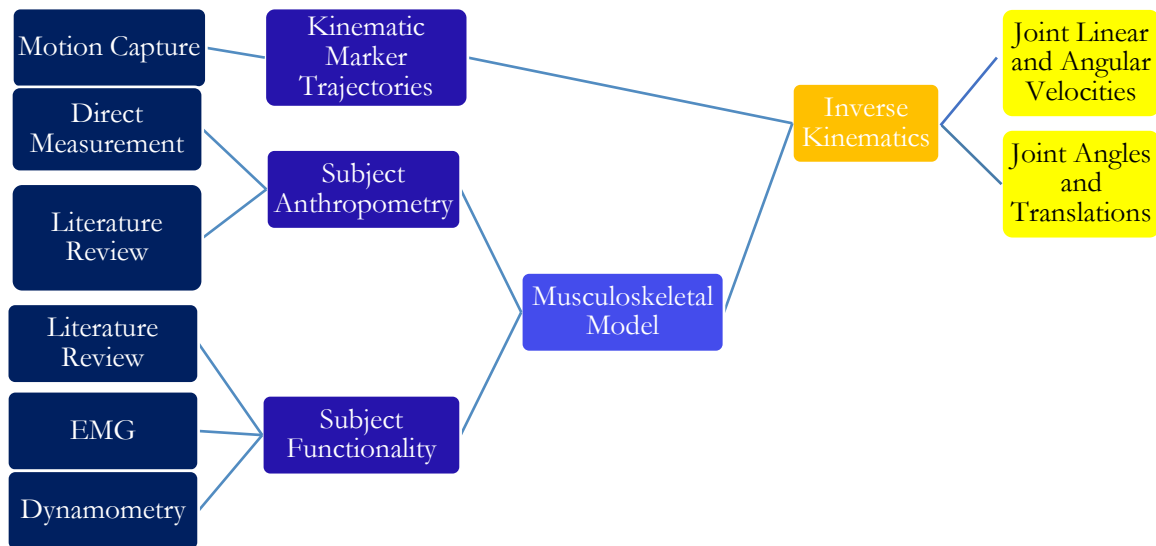


Figure A.2: Required inputs (left) for inverse kinematics calculations and the resulting output measures (right).

The presence of modelling error and uncertainty are associated with a loss in modelling accuracy.<sup>339</sup> For example, errors associated with the pre-processing of data has the potential for compounding in later calculations, resulting in the misclassification of information.<sup>151</sup> Additional examples of the error and sensitivity of model outputs to marker placement are summarised in Table A.1. For inverse kinematics results, errors can be established in both the development of the musculoskeletal model and in the collection and the processing of kinematic data. Consequently, methods for the development of subject-specific musculoskeletal models were explored in this research (Chapter Six) to minimise potential error sources.

Marker placement (both physical and theoretical) serves as the most prominent error source for the joint angles calculated using inverse kinematics. Inaccuracies of surface marker-based model-derived kinematics predominantly result from the presence of soft tissue artefacts and model inadequacies.<sup>150, 151, 340</sup> Soft tissue artefacts are the result of relative displacement of the marker to the bony landmark in which it was placed and is most commonly due to the presence of skin or adipose tissue.<sup>153, 341</sup> While the effects of soft tissue artefacts on kinematic variables have been well characterised and recognised,<sup>342</sup> the resulting accuracies of the surface measured model derived kinematics remain relatively unknown. This gap in knowledge may result from the activity-dependent nature of soft tissue artefacts, which are more pronounced at higher speed motions.<sup>150, 343, 344</sup> OpenSim endeavours to minimise the effects of soft tissue artefacts through incorporating residual measures in their underlying formulations.<sup>151</sup> This residual term is calculated for each marker within OpenSim and represents the difference between the placement of the assumed and virtual marker locations.

Table A.1: Observed kinematic uncertainties and impact on the model and ensuing calculations. Table initially presented in Prinold et al. <sup>345</sup> and has been extended in this review. Gaps in the table occur when model output sensitivity was not explicitly mentioned in the literature and does not indicate results are immune to these considerations.

Parameters And Methods	Accuracy And Error	Sensitivity Of Model Output	Reference
Scapula and Clavicle Kinematics	Scapula $\pm 4^\circ$ and clavicle $\pm 2^\circ$ . <sup>346, 347.</sup> The optimisation of kinematics is a significant factor that is poorly studied.	Primary input, thus high. <sup>100, 162, 348</sup> Static scapula compared with regression, <sup>349</sup> segment lengths, scapula kinematics, <sup>100</sup> and scapula lateral rotations <sup>178</sup> have shown a significant effect on model outputs.	Prinold et al. <sup>345</sup>
Large Bone Kinematics	Humerus, forearm and thorax $\pm 2^\circ$ . Palpation error. <sup>350</sup>	Sensitive when used as a constraint for the scapular kinematics.	
Scapulothoracic Gliding Plane	A good fit is shown for original geometries. <sup>348</sup> Scalability is unclear.	Sensitive when used as a constraint for the scapular kinematics. <sup>100</sup>	
Hip, Knee and Ankle Kinematics	Experimental data tracked within a maximum of $3^\circ$ .		Liu et al. <sup>121</sup>
	Maximum RMS deviation of $1.5^\circ$ for all joint angles over the gait cycle.		Hamner et al. <sup>120</sup>
	RMS differences are exceeding $15^\circ$ , with averages around $4^\circ$ .		Lathrop et al. <sup>151</sup>
	RMS differences during running were $9.1 \pm 3.2^\circ$ .		Li et al. <sup>150</sup>
Reduction of Noise	White noise in the range of 6-9 mm. Improved the accuracy of joint moment estimations when residuals removed.	For a 9 mm SD noise, the moment estimation error was reduced by approximately 59% at the lower back and by 23% at the hip (flexion/extension moments).	Remy and Thelen <sup>351</sup>
Confidence Bounds in Gait	The combined effect of uncertainty resulted in mean confidence bounds (5-95%) of $2.7^\circ$ - $6.4^\circ$ .		Myers et al. <sup>153</sup>

In a physical sense, marker placement on bony landmarks should be avoided (except for static markers) to minimise the extent of skin movement artefacts. For example, marker placement directly over the lateral and medial epicondyles of the elbow during cricket bowling has been criticised.<sup>255</sup> Cluster-based marker models are emerging in the literature. Static markers located on bony landmarks are removed following calibration, minimising errors due to soft tissue artefact. Additionally, cluster-based marker models are less reliant on marker placement,<sup>352</sup> reducing inter-trial and inter-subject errors.



The controversy over the extent and timing of data processing has long existed within biomechanics research. Methods for determining an appropriate cut off frequency for use in low pass filters have been established by both Cooper et al. <sup>353</sup> (manual wheelchair propulsion) and DiGiovine et al. <sup>113</sup> (wheelchair racing propulsion). Verification of data outputs should be performed to ensure the integrity of data following data-processing techniques. Best accuracy of joint angle measurements can be achieved through direct measurement approaches. Lathrop et al. <sup>151</sup> have identified intercortical pins, external fixation devices, stereo radiography, and fluoroscopic techniques as alternative methods for the precise measurement of joint angles. Joint kinematics can be more practically compared to simulation outputs and raw motion capture data. Accuracy can be quantified through the level of agreement between data sets, as performed by Bland Altman plots, and Wilcoxon Matched-Pairs Signed-Ranks Tests.<sup>114</sup> Guidelines for assessing the reliability of results recommend that the kinematics be within two standard deviations of published data for a similar motion.<sup>140</sup> Due to the variance of wheelchair propulsion styles presented in the literature, this is limited. Bland Altman plots are used extensively throughout literature to evaluate the correlation between two measurement types which are both subject to error.<sup>257</sup> These plots present the relationship between two data sets, which should be high when comparing two data sets measuring the same parameter.<sup>354</sup> It should be noted that a high correlation does not necessarily imply a high level of agreement between the two datasets.

## A.2 INVERSE DYNAMICS

Inverse dynamics is calculated using the known motion (angles, velocities and accelerations) and inertia of the model to solve the equations of motion for the unknown generalised forces. The output joint reactions (inter-segmental moments) represent the total force acting across a joint, and not the bone on bone force, which is the actual force acting across the articulating surfaces of the joint and includes the effect of muscle activity.<sup>355</sup> The underlying equation of motion is subject to the dynamic equilibrium and boundary conditions being satisfied (Figure A.3) and is presented in Equation A.1.

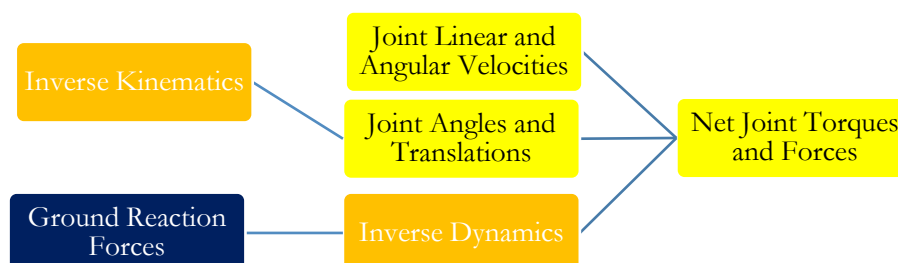


Figure A.3: Required inputs for inverse dynamics calculations and the resulting output measures.

$$M(q)\ddot{q} + C(q)\dot{q} + G(q) = \tau \quad \text{Equation A.1}$$

Where  $N$  is the number of degrees of freedom;

$q, \dot{q}, \ddot{q} \in \mathbb{R}^N$  are the vectors of generalised positions, velocities and accelerations, respectively;

$M(q) \in \mathbb{R}^N$  is the system mass matrix;

$C(q, \dot{q}) \in \mathbb{R}^N$  is the vector of Coriolis and centrifugal forces

$G(q) \in \mathbb{R}^N$  is the vector of gravitational forces; and

$\tau \in \mathbb{R}^N$  is the vector of generalised forces.

Inverse dynamics can either be performed through the top-down approach (using kinematic data of the upper body) or the bottom-up approach (using the kinematic data of the lower limbs and ground reaction data), with the latter approach more accurate.<sup>356</sup> OpenSim opts to use the bottom-up method, possibly due to the enhanced accuracy, but also due to the predominant use for gait analysis and the availability of ground reaction data. The top-down approach can also be used when reaction force data cannot be obtained.<sup>356</sup>

Minimal errors are introduced during the inverse dynamics calculation process, but are instead a consequence of the inputs driving the simulation (Table A.2).<sup>345</sup> Mass and inertial properties of limb segments are required to convert the kinematic trajectories obtained from inverse kinematics into force and torque values. The availability of input data and the capability to accurately define all parameters influencing motion is restricted by the practical and ethical limitations surrounding their direct measurement. Use of subject-specific body segment mass estimations was included as part of this research (Chapter Six) as they are one of the most influential input parameters with regards to accuracy.<sup>154</sup>

Table A.2: Observed kinetic uncertainties and impact on the model and ensuing calculations. Table initially presented in Prinold et al. <sup>345</sup> and has been extended in this review. Gaps in the table occur when model output sensitivity was not explicitly mentioned in the literature and does not indicate results are immune to these considerations.

Parameters and Methods	Accuracy and Error	Sensitivity of Model Output	Reference
BSP (moment of inertia, mass)	Significant error upon scaling, up to 20% in segment mass. <sup>357</sup>	Low in relation to the input force created in high output tasks (e.g. Pull-ups). High when external forces are low since the primary input to inverse dynamics. <sup>149</sup>	Prinold et al. <sup>345</sup>
Inverse Dynamics (joint torques)	Negligible (errors from inputs).	Highly sensitive to noise at high speed. Smoothing of kinematics can reduce this. <sup>349</sup> The timing of smoothing has little effect.	
Confidence Bounds in Gait	The combined effect of uncertainty resulted in mean confidence bounds (5-95%) of 2.7-8.1 Nm.		Myers et al. <sup>153</sup>

Errors can also be introduced through the measurement or estimation of input forces. Traditionally, OpenSim is used for the analysis of gait, where force plate data is used, and hence this is not a common error source. However, the force plate is not always a practically viable approach for use within wheelchair racing, and so alternate instrumentation solutions were explored in this research (Chapters Four and Five). Although an IMU provided a reliable measure of contact time and estimated force with appropriate reliability in the direction of motion, it was poor at estimating out of plane forces, and so was not used as a modelling input in this research. Instead, kinetic data were estimated from the kinematic data recorded using motion capture (Section 4.2) to minimise error sources.

Inverse dynamics is calculated using Newtonian Mechanics, more specifically the summation of forces and moments at the joints of a link segment model. The inclusion of muscles in analyses generates a redundancy problem as there are more unknowns than there are boundary conditions. Literature by Moissenet et al. <sup>358</sup> has demonstrated that increased muscular redundancy (the number of muscles defined) corresponds with greater accuracy. Due to the presence of errors in the experimental motion data and the inaccuracies in the musculoskeletal model, Newton's second law is not satisfied.<sup>133</sup> Residual forces are applied to models to reduce inconsistencies existing between model and experimental data, with a weighting applied to each degree of freedom to reduce the overall inconsistencies between data sets.<sup>359</sup> Reduced residual algorithms can be implemented to prevent these residual forces from becoming large. It was also suggested by Hicks et al. <sup>140</sup> that residual forces of the experimental simulation should be within 5% of the net external forces measured.

Verification of output data is restricted as the direct measurement of joint reaction data is practically limited. Surgical implantation of specialised instrumentation can be used to facilitate the direct measurement of dynamic joint loads<sup>360</sup> of the hip joint, spine, shoulder joint and knee joint, as well as in bone and cartilage.<sup>361</sup> However, this process requires the use of invasive sensors surgical reconstruction.<sup>361</sup> As direct measurement techniques are infeasible; verification is limited to comparisons with literature. It was suggested that the measured forces should be within two standard deviations of experimental joint forces, as obtained through instrumented implants for similar motions,<sup>140</sup> similarly to inverse kinematics. However, care should be taken in ensuring comparisons are made against motions of comparable dynamics. For example, significant variations in the kinematics, kinetics and ground reaction forces of the ankle, knee and hip were identified by the literature of Hamner et al.<sup>120</sup> and other literature, based on the greater dynamic requirements of the motion. A similar magnitude of variation would be anticipated between manual wheelchair propulsion (commonly around 1.1 m/s), compared to wheelchair racing (up to 8.6 m/s). Although neither of these methods is capable of holistically identifying the impacts of errors on analysis or quantifying their magnitude, close observation can assist in their minimisation.

### A.3 STATIC OPTIMISATION

Static optimisation further resolves the net joint moments obtained through inverse dynamics into an estimated time history of activations and forces of all muscles included in the computational model (Figure A.4). These techniques are commonly used for the solving of indeterminate force distribution problems, such as at the shoulder joint complex during wheelchair propulsion.<sup>101, 169-171, 174, 175, 191, 311, 362-366</sup>

The contribution of individual or lumped muscle groups is estimated through decomposition of the net joint forces obtained through inverse dynamics methods. These forces are resolved by minimising the sum of squared muscle activations (Equation 6.4).<sup>133</sup> As each step in time is considered in isolation, both the time-dependent nature of muscles<sup>364</sup> and the activation dynamics and tendon compliances<sup>140</sup> are neglected. These considerations aside, it has been demonstrated that equivalent force predictions exist for both the static and dynamic cases.<sup>138, 139, 364</sup>

Similar to inverse dynamics, errors are the consequence of the propagation of the errors and uncertainties introduced at earlier stages. The degree of solver can be defined when performing static optimisation calculations. Varying the degree of solving alters the convergence time and quality of the simulation, but should have no direct influence on the quality of the results.<sup>133</sup>

---

Recommended practice suggests inverse kinematics results should be filtered prior to being used in static optimisation calculations, whereby they should be presented as a smooth signal to prevent the calculation from failing. As mentioned previously, close inspection of the impact of the filtering process is warranted and should be accompanied by sensitivity analyses to ensure the raw data are not artificially altered.

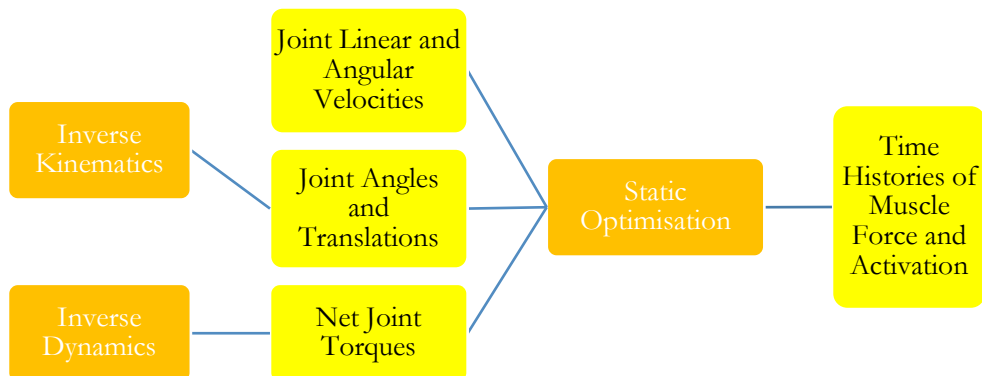


Figure A.4: Required inputs for Static Optimisation calculations and the resulting output measures. Yellow boxes contain the required input parameters, and orange boxes are the computational tool employed by OpenSim.

Muscle activation data collected through electromyography (EMG) can be used to assist in the verification of the static optimisation outputs. This data can be used to analyse the agreement between the timing and magnitude patterns of muscle activations, as was performed by Knarr et al.<sup>367</sup>. Due to the random nature of muscle excitations, it is unlikely that these two data sets will present a perfect correlation. However trend wise similarities, as observed for the co-contraction index can provide confidence that the model simulation is performing as it should. Whilst EMG can be used to gauge the activity of muscles; it does not directly correlate with muscle force for dynamic measurement,<sup>311</sup> and so are better suited to analyses regarding excitation timings, such as in the work of Mulroy et al.<sup>26</sup> and Tries.<sup>312</sup> EMG data can also be incorporated into the modelling process. These are given higher weightings than the estimated activations during static optimisation equations. This can reduce the reliance on earlier estimations, which may ultimately limit the influence of the propagation of errors. This method is only effective when the measured electromyography data has sufficient accuracy. For example, the superficial placement of the electrodes required for electromyography is susceptible to the same skin movement artefacts as the marker placements.

#### **A.4 CONCLUSION**

It is well accepted that inherent errors are present within computational analyses on account of the strict practical limitations preventing the collection of experimental data. In the majority of cases, errors are considered to be within acceptable bounds and not detrimental to the reliability of the resultant estimates. The magnitude of these errors correlates with the dynamic extent of movement measured. The propagation of errors in highly dynamic activities, such as sprinting, identifies concerns of the computational modelling approach. The majority of errors are introduced at the model development stage on account of the superfluous parameters requiring estimation or modification to reflect the particular characteristics and capabilities of the individual who performed the movement.

---

---

## APPENDIX B:

# MUSCULOSKELETAL MODEL DEVELOPMENT

---

A musculoskeletal model consists of rigid bodies connected by joints which have muscles spanning across them to generate the moments and forces responsible for the motion.<sup>133</sup> This is used to provide a visual representation of all included computational elements (such as bones and joints) and boundary constraints (such as ranges of joint motion).<sup>125</sup> Musculoskeletal models demonstrate varying levels of complexity depending on the intended application and range from a wrist model,<sup>331</sup> through to a full-body model,<sup>120</sup> with some even considering aspects of neuromuscular control. This complexity is driven by the number of modelling constituents defined. Model development in OpenSim requires the definition of musculoskeletal elements via XML code. This chapter provides an extended literature review detailing which input parameters are contained within a musculoskeletal model (Section B.1), the impact of parameter perturbation on simulation output (Section B.2), how subject-specific inertial parameters (Section B.3) and maximum isometric force-generating capacities can be estimated (Section B.4), and the estimation of joint reference frames (Section B.5).

There are four major elements required in the models; bones, joints, muscle actuators, as well as contact elements and ligaments (Table B.1). Even small models, such as the Wrist model requires over 1000 input parameters to be defined for the 29 bones, 29 joints and 25 muscles.<sup>331</sup>

Table B.1: Required parameters for the development of a computational model in the OpenSim environment. List of computational counterparts acquired from the XML file for the gait2392\_scaled.osim file.<sup>135-139</sup>

Structure	Required Parameters
BODY SET Bones (Rigid Bodies)	MASS PROPERTIES - Mass - Mass Centre - Inertia (xx,yy,zz,xy,xz,yz)
CONSTRAINT SET Joints (Constraints, Mobilisers and Forces)	JOINTS - Type (Weld, Pin, Slider, Ball, Ellipsoid, Free, Custom) - Parent Body - Location and orientation in the Parent body GENERALISED COORDINATES - Motion Type (Translational, Rotational, Coupled) - Default and initial value, default speed value, range - Clamped (Constrain motion to be within the range values) - Locked (Constrain motion to initial value – i.e. No movement)
MARKER SET	- Body segment marker resides on - Location in body - Fixed (Or allowed to move when performing scaling etc.)
OBJECTS Ligaments and Muscle Actuators (Forces)	MUSCLE ARCHITECTURE - Origin, insertion and via points MUSCLE PARAMETERS - Maximum force actuator can produce - Maximum isometric force fibres can generate - Optimal fibre length, resting tendon length, optimal pennation angle (angle between tendon and fibres at optimal length), maximum contraction velocity, activation and deactivation time, tendon and passive muscle strain at maximum isometric muscle force, shape factor for Gaussian active muscle force-length relationship, exponential shape factor for passive muscle force-length relationship, force-velocity shape factor, maximum normalised lengthening force

Often, input parameters rely on relationships established in the literature, such as that of McConville and Air Force Aerospace Medical Research Laboratory (U.S.)<sup>368</sup>, Dempster<sup>281</sup>, or Hanavan.<sup>146</sup> Segment mass parameters or lengths are commonly presented relative to the total body, such as the anthropometric data set presented by de Leva.<sup>369</sup> Musculoskeletal models currently utilised in wheelchair literature and available in OpenSim utilise the anthropometric table approach (Table B.2).



Table B.2: Source of BSIP in the most common shoulder and upper extremity models, demonstrating the reliance on cadaver studies, despite the questions in the literature regarding their reliability.

Model	Reference Publication	BSIP Estimation Method	Source of Inertial Parameters
Delft Shoulder and Elbow Model	Blana et al. <sup>178</sup> Nikooyan et al. <sup>370</sup> van der Helm <sup>163</sup>	Anthropometric tables (cadaver studies)	Klein Breteler et al. <sup>371</sup>
Upper Extremity Dynamic Model	Saul et al. <sup>287</sup>	Anthropometric tables (cadaver studies)	McConville and Air Force Aerospace Medical Research Laboratory (U.S.) <sup>368</sup> Reich and Daunicht <sup>372</sup> Blana et al. <sup>178</sup> , as derived from Clauser et al. <sup>280</sup>
Holzbaur's Upper Extremity Model	Holzbaur et al. <sup>164</sup>	Anthropometric tables (cadaver studies)	Klein Breteler et al. <sup>371</sup> as derived from Clauser et al. <sup>280</sup>
Newcastle Shoulder Model	Charlton and Johnson <sup>100</sup>	Anthropometric tables (cadaver studies)	de Leva <sup>369</sup>
Swedish Shoulder Model	Karlsson and Peterson <sup>373</sup> Makhsous et al. <sup>374</sup>	Morphological measurements	Based on the model of Hogfors et al. <sup>160</sup> , Hogfors et al. <sup>161</sup>
Dickerson's Model	Dickerson et al. <sup>167</sup>	Regression prediction equations	Zatsiorsky <sup>285</sup>

## B.1 SUBJECT-SPECIFIC MODELLING APPROACHES

A comparative study by Scheys et al. <sup>375</sup> has revealed differences in flexion moment arm length in models with varying levels of detail. However, these differences were not always statistically significant. Musculoskeletal models are highly sensitive to their input parameters (Table B.3), and so appropriate scientific rigour is required when making subject-specific perturbations.

APPENDIX B: MUSCULOSKELETAL MODEL DEVELOPMENT

Table B.3: Model Definition result errors as presented in the literature. Note, the table is an extension of what was presented in Prinold et al.<sup>345</sup> Gaps in the table occur when model output sensitivity was not explicitly mentioned in the literature and does not indicate results are immune to these considerations.

Parameters and Methods	Accuracy and Error	Sensitivity of Model Output	Reference
Segment Lengths (joint centres)	Landmark palpation repeatability $\pm 2$ mm. <sup>376</sup> Joints offset from palpated surface landmarks lead to additional error. Scapula has a complex 3D shape, <sup>377</sup> leading to larger errors. Coupled nature of segments leads to accumulated error.	Sensitive to clavicle length; important role in kinematics. <sup>100</sup> Sensitive to scapula size, given the number of muscle attachments and the shape variability across subjects. <sup>377, 378</sup>	Prinold et al. 345
Bony Landmarks (not joint centre)	Accurate if directly digitised ( $\pm 2$ mm). <sup>350</sup> Inaccurate for scapula (if homogeneously scaled). <sup>377</sup>	Affects the contact force between the scapula and the thorax. Sensitivity is unclear. Also similar sensitivity as with segment lengths.	
Musculotendon Model	Input parameter accuracy unclear. Cadaveric studies <sup>371</sup> and in vivo measures from maximal voluntary contractions and other measurements used. <sup>166, 379</sup>	Highly sensitive to the force-length relationship. <sup>380</sup> Low sensitivity to force-velocity in activities of daily living. <sup>348</sup> Sensitive to high output activities. <sup>349</sup>	
Glenohumeral Centre of Rotation	3 - 4.6 mm error <sup>381</sup> < 8.3 mm repeatability. <sup>382</sup> Reliable and valid. <sup>383</sup>	Change in force of up to 300% (linked to the retroversion angle). <sup>377</sup> Highly sensitive. 42.9% difference in kinematics and 17.8% in muscle forces when markers moved 5.5 cm from reference points, and 0.6% - 7.8% in kinematics with 1 cm marker movements as well as muscle forces varying between 0.8% through 4%.	Xu et al. 384
Toe Marker Placement	Variation in marker placement and anatomical landmarks vary up to 5 cm due to inadequate identification and presence of shoes.	Impact of movement artefact was 1.8 times greater than any other propagated source.	
Marker Placement	Marker placement on loose skin or adipose tissue. Marker placement variability (mm, $\pm$ 2SD) X: 0.7 (5 <sup>th</sup> metatarsal head)-12.2(greater trochanter), Y: 1.4 (distal medial condyle femur) – 11.5 (right		Myers et al. 153 Rabuffetti et al. 385, Della Croce et al. 386, Della

Muscle Attachment Points	anterior superior iliac spine), Z: 2.9 (distal lateral condyle femur) – 17.9 (greater trochanter).		Croce et al. <sup>387</sup>	
	Mean error between model reconstruction and bone pin experiments: 0.4 - 2.4mm.		Seth et al. <sup>388</sup>	
	Measured and calculated moment arms varied between 48.5% - 99.5% (mean 75.5%) for intrinsic and extrinsic finger muscles.	Muscle attachment point differences within 7.1% of the average length of the muscle-tendon paths and so suitable for use in many applications.		Lee et al. <sup>389</sup>
	Differences in modelled and experimentally measured muscle attachments were less than 4.9 mm.			
	The Euclidian distance between joint reference frames approximately 14.9 mm.	Precise joint angles are dependent on joint centre location, <sup>355</sup> hence errors impact on joint angle trajectory measurements. <sup>390</sup>	Abdulrahman et al. <sup>391</sup>	

## B.2 PERTURBATION OF MUSCULOSKELETAL MODEL PARAMETERS

A considerable amount of literature has been published on musculoskeletal model personalisation. However, no literature currently exists with regards to what adaptation of input parameters required for musculoskeletal modelling of wheelchair racing athletes.

Xiao and Higginson<sup>392</sup> demonstrated that during walking, perturbation of maximum isometric forces had normalised differences of -1.362, and 1.267 for -10% and +10% perturbations respectively. Differences in internal rotation torque of -15.4% were observed between wheelchair athletes and able-bodied athletes (Figure 2.1), and 10.8% between wheelchair athletes and non-athletic individuals. Consequently, due to the sensitivity of defined maximum isometric forces, there exists the potential for significant propagation of errors throughout the modelling workflow, particularly considering the high speeds of racing propulsion. The literature of Xiao and Higginson <sup>392</sup> only noted this difference for the Gluteus Maximus muscle, however, which may be indicative of the size and contribution of the muscle towards motion. This may suggest that for this research, only the muscles of the upper extremity, which are so dominant in wheelchair propulsion require adaptation, which would drastically simplify model development.

### B.3 ESTIMATING BODY SEGMENT INERTIAL PARAMETERS

Numerous methods have been explored for the measurement of body segment inertial parameters, each placing a different weighting on the time-accuracy optimisation (Table B.4 through Table B.7)). Estimation methods have improved and will continue to improve in line with technological advancements. These methods are either direct (such as cadaver measurements or the processing of medical imaging scans) or indirect (using mathematical relationships, based on measured data).

Subject-specific modelling techniques have emerged in more recent literature; however, such approaches have yet to be extended into wheelchair sports literature. Such approaches allow individual musculoskeletal anatomy and properties, tissue volumes, and musculotendon architecture parameters<sup>130</sup> to be defined for each subject. Whilst theoretically the customisation of all parameters to accurately replicate each subject is considered ideal, realistically parameter customisation on a large scale is difficult, if not impossible.<sup>159</sup> Parametric identification and definition is a time-consuming process, with unavoidable uncertainties introduced due to the aforementioned limitations in validation.<sup>130</sup> Consequently, parametric customisation should be restricted to the most influential parameters, as determined through sensitivity analyses.<sup>130, 393</sup> These analyses provide an attractive tool for understanding the impact of changing input parameters on the overall result and should be performed on all parameters most influential to subject-specific model development.<sup>393-395</sup> For example, it has been identified that statistically significant correlations exist with respect to segment mass, maximum isometric force and tendon slack length, with low sensitivities to the moment of inertia.<sup>130, 153, 393-395</sup> The inclusion of strength of impaired limbs has been identified as the most influential.<sup>124</sup> However, these are yet to quantify the uncertainties of subject-specific models wholly, and how their combined effect may compromise model predictions.<sup>395</sup>

When available, direct measurements provide the most precise method for obtaining parameters. These can be obtained using direct measurements on limbs of cadavers, or living subjects through processes of medical image reconstruction (e.g., magnetic resonance imaging, MRI). MRI can be implemented for the measurements of muscle volumes and attachments,<sup>154</sup> as opposed to by the regression estimations present in generic models. Although these have been demonstrated to have high accuracy, medical scanning technologies were not developed for use in musculoskeletal modelling approaches, and as such demonstrate some limitations. These limitations include being, time-consuming, expensive, and may impose large doses of ionising radiation on the athlete (computed tomography).<sup>283, 284, 295</sup> Ultimately, these practical limitations suggest that alternative scanning methods may be required for the measurement of *in vivo* body segment parameters of living subjects. DXA scans provide an attractive alternative, with greater accessibility, and safety (lower radiation dose) than other

medical scanning methodologies.<sup>144, 282-284, 396-400</sup> Analysis of DXA data provides accurate and direct estimates of two-dimensional body segment parameters of humans.<sup>144, 396, 398, 400</sup> Masses are estimated through the correlation of areal density data with the DXA grayscale image, establishing a relationship between the pixel colour gradient and the mass with which it represents.<sup>284</sup> When these are not available, ensuring compliance with the International Society of Biomechanics standards of body and joint coordinate systems may also increase confidence in the obtained results.<sup>395, 401</sup>

Table B.4: Limitations and specific applications of a number of direct BSIP estimation methods performed *ex vivo*.

Limitations	Reference	Method	Application
Up to 5% fluid loss from dissection process. <sup>282</sup>	Clauser et al. <sup>280</sup>		Koontz et al. <sup>262</sup>
			Kulig et al. <sup>102</sup>
Parameters vary from living state. <sup>143, 148, 402</sup> Gender and population type bias, limiting generalisation. <sup>403</sup>	Dempster <sup>281</sup>	Water immersion techniques using dissected cadavers obtaining volume, mass, CoG and MoI.	Saul et al. <sup>287</sup>
			Holzbaur et al. <sup>164</sup>
			Morrow et al. <sup>191</sup>
	Winter <sup>145</sup>	Adapted from Dempster <sup>281</sup>	Morrow, et al. <sup>13</sup> Sabick et al. <sup>206</sup> Sauret et al. <sup>221</sup> Robertson et al. <sup>62</sup>

Table B.5: Limitations and specific applications of a number of direct BSIP estimation methods performed *in vivo*. For medical scanning techniques, GRay represents gamma ray, CT; Computed Tomography, MRI; Magnetic resonance imaging.

Limitations	Reference	Method	Application
Large expense & operational costs. <sup>143, 298, 404, 405</sup>	GRay Zatsiorsky et al. <sup>328</sup>	100 male and 15 female living subjects of varying age to estimate mass, CoM and Ixx, Iyy, Izz.	
			Pearsall et al. <sup>405</sup>
Data processing labour demands. <sup>284</sup>	CT Huang and Suarez <sup>406</sup>	Pixel intensity values correlated to tissue densities.	
Limited accessibility to specialised equipment. <sup>284, 403</sup>	CT Cheng et al. <sup>143</sup>	Mass density and density of pixel across the manually digitised cross-section.	N/A: Animal Study
			Tissues were differentiated, mass and volume summed through integration.
Health risks owing to high exposure to radiation. <sup>143, 284</sup>	MRI Martin et al. <sup>402</sup>	Volume measures combined with cross-sectional images of 8 baboon cadavers.	
			Mungiole and Martin <sup>404</sup>
		Sum individual masses for each of the tissue sections, using density data of Clauser et al. <sup>280</sup>	N/A: Animal Study

Table B.6: Limitations and specific applications of a number of indirect BSIP estimation methods performed *in vivo* using regression equations.

Limitations	Reference	Method	Application
Limited by population based upon (e.g. cadavers). <sup>407</sup>  Limited by uniform densities. <sup>407</sup>  Highly simplified representations. <sup>144, 403</sup>	Chandler et al. <sup>408</sup>	Linear relationships between total body mass and separate segment masses obtained through cadaver dissection.	
	McConville and Air Force Aerospace Medical Research Laboratory (U.S.) <sup>368</sup>	Bodies of 31 males photographically segmented into 24 parts, with volumes established stereometrically.	
	Durkin and Dowling <sup>144</sup>	Linear regression equations developed using mass, CM location and radius of gyration values determined through DXA.	
	Zatsiorsky and Seluyanov <sup>409</sup>	Use whole body mass and height as predictors (based on 100 young Caucasian males).	
	Zatsiorsky and Seluyanov <sup>410</sup>	Uses anthropometric measures of specific segments.	

Table B.7: Limitations and specific applications of a number of indirect BSIP estimation methods performed *in vivo* using geometric models.

Limitations	Reference	Method	Application
Time-consuming for the subject (the 95 measurements for Yeadon model requires >40mins). <sup>403</sup>  Geometric assumptions produce cavities, and consequently large volume errors. <sup>411, 412</sup>  Simple geometries not reflective of the specific anthropometry of an individual.	Durkin and Dowling <sup>396</sup>	Ensemble average of mass distribution from DXA scans (frontal and sagittal plane) of 40 subjects from 4 populations.	
	Yeadon and Morlock <sup>413</sup>	Cylindrical and stadium shaped solids are representing segments. (Assume the uniform density of Dempster. <sup>281</sup> )	
	Zatsiorsky et al. <sup>328</sup>	Assumes each segment to be a circular cylinder, with segment-specific quasi-density values.	
	Hanavan <sup>146</sup>	15 segment model using cylinders with elliptical bases, rotational ellipsoid, spheres and truncated cones.	Koontz et al. <sup>262</sup> Cooper et al. <sup>98</sup> Rodgers et al. <sup>414</sup> Mercer et al. <sup>327</sup>
	Yeadon and Morlock <sup>413</sup>	40 segments, assuming uniform density, volume and mass can be estimated using stadium solids and anthropometric measurements.	Kulig et al. <sup>102</sup> Slavens et al. <sup>415</sup>

## B.4 ESTIMATING MAXIMUM FORCE GENERATING CAPACITY OF SKELETAL MUSCLES

As the inclusion of strength of impaired limbs has been identified as influential,<sup>124</sup> perturbation of muscular parameters is essential for modelling of wheelchair racing athletes. The well-established hill type muscle relationships<sup>416</sup> are commonly used in OpenSim. A simplified explanation of the model has been provided by Haeufle et al.<sup>417</sup> The model itself consists of three elements; a contractile element incorporating force-length and force-velocity parameters, as well as a series and a parallel element. The model takes inputs of muscle-tendon complex length, contraction velocity and neural muscle stimulation to produce a one-dimensional force, which is applied between the origin and insertion points of a model.

The maximum force a muscle can produce is a function of both its specific tension (force generated per unit of cross-sectional area) and its physiological cross-sectional area. Measuring the cross-sectional area of muscles can be a difficult and time-consuming task and so is commonly estimated. Some of the methods used to do this in the literature are presented in Table B.8.

Table B.8: Estimation procedures for muscle physical cross-sectional area (PCSA).

Reference	Aim	Type	Data Source
Asadi Nikooyan et al. <sup>418</sup>	Development of a musculoskeletal model of the shoulder and elbow.	Morphological data and muscle parameters from cadaver studies.	Klein Breteler et al. <sup>371</sup> Minekus <sup>419</sup>
Veeger et al. <sup>169</sup>	Load on the shoulder in low-intensity wheelchair propulsion.	PCSA data from cadaver studies, and the task performed by young subjects.	Veeger et al. <sup>420</sup>
van Drongelen et al. <sup>170</sup>	Glenohumeral joint loading in tetraplegia during weight relief lifting.	Multiply PCSA by a force of 100 N/cm <sup>2</sup> .	Veeger et al. <sup>420</sup> Veeger et al. <sup>421</sup>
Lin et al. <sup>311</sup>	Muscle force analysis in the shoulder mechanism during wheelchair propulsion.	Proportional to the cross-sectional area of muscle, maximum stress set to 115.97 N/m <sup>2</sup> .	Wood et al. <sup>422</sup> Chang et al. <sup>423</sup>

Magnetic Resonance Imaging or CT can present more accurate measurements of muscle size, however, these techniques are not always practically feasible. These methods are associated with considerable expense and operational costs, data processing labour demands, limited access to specialised equipment and health risks owing to high radiation exposure from some of these methods.<sup>284</sup> Additionally, wheelchair athletes with muscle spasticity may not be capable of maintaining the required body position

over the scan duration. As discussed previously, DXA presents a more practically viable approach with standard scan duration just 6 min and 30 s.<sup>424</sup>

Morphological equivalence is required for between-population comparisons. Morphological variations between paraplegic athletes and able-bodied individuals have been reported previously. This has included paraplegic athletes having a lower bone mineral density in the lower extremity (76.5% of controls),<sup>323</sup> and higher skeletal mass in the upper extremities.<sup>147, 283, 316</sup> However, comparable bone mineral density has been observed between low-lesion level paraplegics (such as what the athletes in this research are), and controls.<sup>321</sup> Similarly, fat mass in the arms and trunk for wheelchair athletes has been reported to be approximately 20%,<sup>323, 325</sup> which is comparable to the 15-20% body fat range suggested as acceptable by Jeukendrup and Gleeson.<sup>425</sup> Hence, morphological similarities can be assumed between the wheelchair athlete and the general population.

## **B.5 ESTIMATING JOINT REFERENCE FRAMES**

Estimation of bone positioning and joint orientations are further diversified through the presence of subject-specific differences in bone geometries such as anteversion, bowing or torsion. For example, the natural bowing in the shaft of the femur leads to a variable shape of the proximal femur, reflective of physiologic variations.<sup>426</sup> Such bone features are present in both wheelchair populations and able-bodied populations. However, as anatomical reference frames within the OpenSim environment are embedded within the generic bone models, they are inept at accommodating these variations.<sup>151</sup> These anatomical differences alter the definition of the reference frames utilised for joint angle calculations, hence limiting simulation accuracy.<sup>427</sup> Reference frames may better be defined through the use of clinical scanning technologies as they are better equipped to reconstruct the limbs and their constituents than what is presented in the generic models. For example, Zhang et al.<sup>428</sup> improved upon standard scaling methods using an articulated statistical shape model of the left lower limb. Lower limb bone geometry, pose, and muscle attachment regions were estimated more accurately based on seven commonly used motion-capture landmarks. However, such processes do come at the cost of substantially increased model development time. Estimating joint reference frames was outside the scope of this research.



---

## APPENDIX C:

# VALIDATION AND VERIFICATION OF INVERSE DYNAMICS MODELS

---

Validation and verification measures determine the degree in which the computational model represents the real world problem and underlying mathematics, respectively.<sup>155</sup> No gold standards are currently defined for how validation and verification are to be performed.<sup>155</sup> Validation procedures are limited by the restrictions on *in vivo* measurements, thus promoting the use of model verification. There exist a number of different statistical measures assessing various aspects of modelling uncertainties. One of the most prevalent methods is the use of probabilistic analyses, such as the use of confidence bounds and sensitivity factors to quantify impacts associated with the uncertainties generated through parametric estimation and measurement of motion.<sup>153</sup> A number of sensitivity analyses were performed to ascertain the reliability of the modelling process implemented.

**Definition of reserve actuators (Section C.1)***Research Question:*

- What magnitude of reserve forces are required to simulate wheelchair racing propulsion for elite wheelchair racing athletes successfully?

**Verification of musculoskeletal model adaptations for use with wheelchair racing athletes. (Section C.2)***Research Question:*

- Is the increased scaling of the scapula and clavicle (in line with increased torso mass) likely to introduce errors into the computational workflow?

**Upper extremity muscle demand for wheelchair racing propulsion technique. (Section C.3)***Research Question:*

- How well does the muscle coordination strategies and stresses match what is in the literature?

**C.1 DEFINITION OF RESERVE ACTUATORS**

As only a subset of muscles is included within the musculoskeletal model, it is possible that not all the forces acting at the joint will be able to be accommodated by the muscles spanning it. Reserve actuators are defined to compensate this force. A number of parameters control the reserve actuators, including maximum allowed value, and the optimal force produced by the actuator. As a cost function is used to solve the problem, higher reserve actuator optimal force values are cheaper to use. This suggests that the model may recruit the reserve actuators in preference to the muscles. OpenSim documentation recommends that peak reserve actuator torques be less than 10% of the peak torque joint.<sup>152</sup> However, if larger reserve forces are required for a successful simulation, the maximum control value can be increased, but will be penalised in the cost function for doing so.

A sensitivity analysis was performed to determine the required reserve actuator magnitude, as reserve actuator forces greater than 10% of the peak torque joint was required. It was hypothesised that a convergence analysis approach could be used to reveal the optimal selection of reserve actuation based on reserve force values.

### Methods

A convergence analysis was performed using the same simulation protocol presented in Section 6.4. Reserve actuator optimal forces were set at 50 N, 100 N, 150 N, 200 N and 500 N. Reserve forces (acting at the joints) were analysed at each of the degrees of freedom within the model.

### Results

The variation in reserve forces is presented graphically in Figure C.1. Low reserve actuator values (< 200 N) were observed to have low sensitivity, with minimal variation between different values. The model was sensitive to reserve actuators when defined to be 500 N. At this value; it can be seen that there is a different characteristic response in both the shoulder rotation reserve force, and pronation-supination force, suggesting an over-dependence on the reserve actuators, as they are so cheap to use.

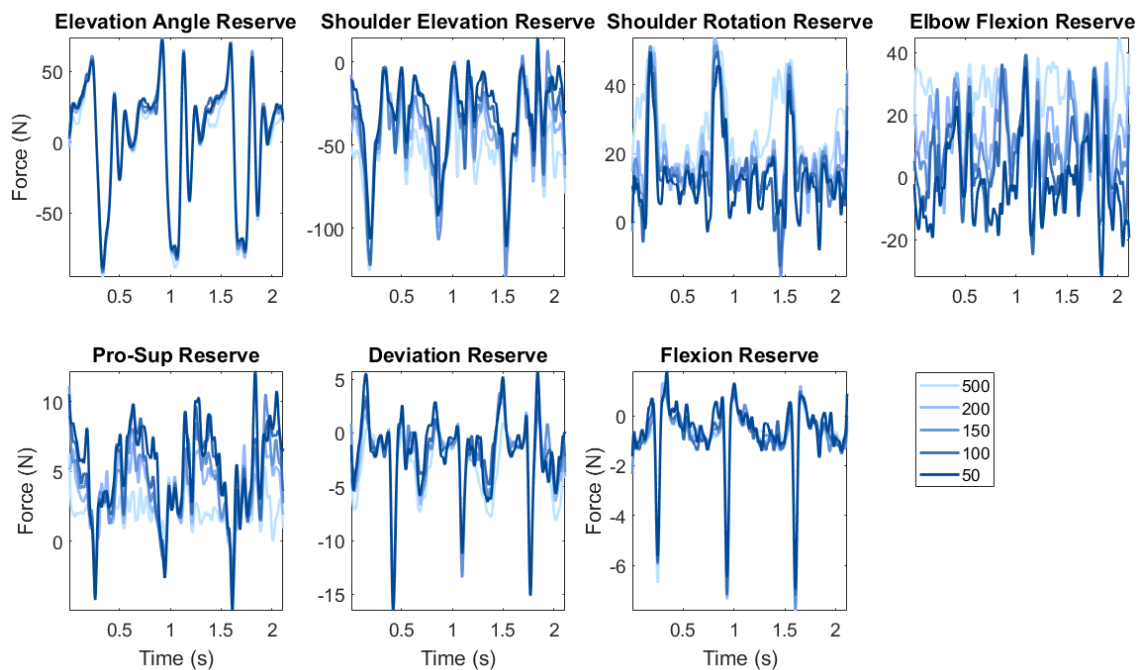


Figure C.1: Comparison of reserve actuator with defining various levels of optimal force in reserve actuators.

*Discussion*

Reserve actuators were identified to change the system dynamics when set too high. As the solver is a cost-based function which minimises activations, defining such a large optimal force value in the reserve actuators will make the simulation rely too heavily on the reserve actuators, and not the muscles. For the musculoskeletal model used, the median maximum isometric force generating capacity was 251.2 N for the unscaled model. A reserve actuator value was designated as 200 N, such that it was less than this median value. As can be seen from Figure C.1, this choice has little impact on results. Based on the reaction force values reported in Table 7.1 and Table 7.2, reserve actuator forces are approximately 20% of the input torque.

The large reliance on reserve actuators in this research may be a consequence of the large instantaneous peaks, which should have been filtered out of the kinetic data prior to performing the analysis. It may also be possible that the shoulder models currently available within the OpenSim environment are not ready for use in such dynamic applications yet, and should not be used when higher precision data is required. If inadequate reserve actuator force is provided, the simulation does not solve correctly, with errors appearing that the muscles have insufficient strength to complete the required task.

*Conclusion*

The value of optimal force defined for each of the reserve actuators has an impact on how muscles are recruited to complete a task. Values which are too high are undesirable as they change the dynamics of motion. Values too low may also be unable to complete the motion. An iterative process investigating both the reserve forces and the activations on the muscles should be performed to determine the required value for each simulation.

## **C.2 VERIFICATION OF MUSCULOSKELETAL MODEL ADAPTIONS FOR USE WITH WHEELCHAIR RACING ATHLETES**

To date, computational modelling has predominantly been used in the literature involving the lower extremity. Of the limited literature available for the upper extremity, and specifically for wheelchair propulsion, the use of OpenSim to analyse sporting propulsion is novel. As a consequence, there is limited validation at the speeds observed in this research. In addition, there are a number of uncertainties which have yet to be addressed in the literature, including the explicit scaling of the scapula and clavicle in relation to the remainder of the trunk segment.

---

## C.2.1 SCALING OF THE SCAPULA AND CLAVICLE

### *Introduction*

The upper extremity dynamic model used for the analysis consisted of seven bodies requiring mass and inertial input. These included the thorax, clavicle, scapula, humerus, ulna, radius and hand, with the ulna and radius each comprising half of the forearm mass. Although subject-specific masses were obtained for each of the limbs, within the upper extremity dynamic model, values needed to be estimated for the scapula and clavicle.

Across different models, there exists a difference in the distribution of the scapula mass relative to the thorax. For example, this is 2.5% in the Wu shoulder model and 3.5% in the dynamic arm simulator model. There is no mass in the torso for the upper extremity dynamic model, so the same ratio cannot be presented. However absolute mass is similar to that in the dynamic arm simulator model. Similarly, the clavicle is 1.0% of the torso mass in the Wu shoulder model and 0.8% in the dynamic arm simulator model.

No literature was identified which establishes how the scapula and clavicle should be scaled with increasing torso mass, and how this may differ with morphological composition. In the absence of this information, the default torso-scapula-clavicle scaling protocols were used within this research based on the overall mass of the torso segment obtained from the analysis of DXA scans.

This investigation aimed to understand the relative sensitivity of the scaling of the scapula and clavicle on the overall joint reaction moments, to understand the possible errors introduced through scaling. It was hypothesised that as the scapula and clavicle are small, and are not dynamic in their movements, there will be a low sensitivity to the defined value of these parameters.

### *Methods*

A sensitivity analysis was performed for each of the scapula and clavicle using the dynamic arm simulator model within OpenSim. Using the same simulation protocol, as outlined previously, the scapula and clavicle mass were altered by  $\pm 10\%$  and  $20\%$  increments. Kinetic and kinematic data were obtained using athletes E and I using the methods described in Sections 4.2 and Section 6.2, whilst subject-specific mass and strength characteristics were defined using the values presented in Section 6.3 and Section 6.4. Trunk mass was held constant (at a subject-specific value) with the distribution between the scapula, clavicle and remainder of the trunk altered.

Kinematic trajectories (inverse kinematics results), joint reaction moments (inverse dynamics) and muscle activations and forces (static optimisation) were normalised against the unscaled simulation to present relative differences.

### Results

Kinematics results did not alter due to changes in scapula mass, whilst mean absolute RMS differences were 1.2% when the clavicle was scaled. Minor variations in joint reaction moments occurred as a consequence of scaling the scapula (Figure C.2). For the majority of modelled degrees of freedom, the increased mass of the scapula led to an increased output parameter, and vice-versa. Observed differences were  $< 10\%$  for all instances, with the highest sensitivities noted for the wrist. Similar trends were observed for the clavicle.

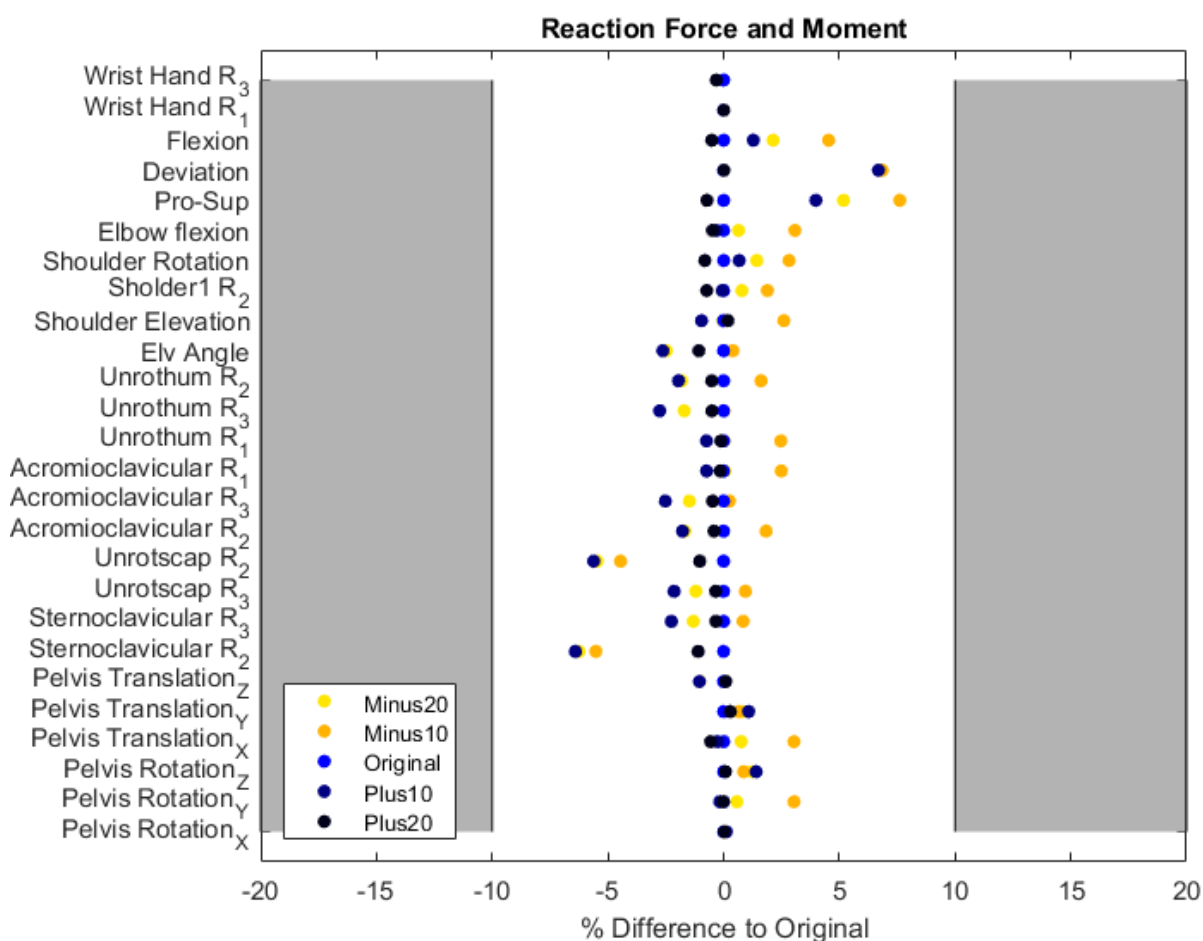


Figure C.2: Differences in reaction forces or moments for each of the modelled ROM for scaled values compared to default.

A minor correlation exists between the magnitude of change in muscle forces and activations based on the mass of the scapula and clavicle (Table C.1). It can be seen that the model is more sensitive to the scaling of the clavicle than the scapula. It is clear, however, that the model is highly sensitive to any change in scapula mass and inertia. Both muscle activation and force are correlated, as would be anticipated.

Table C.1: Mean absolute RMS differences between original and scaled conditions on static optimisation when scapula scaled.

Scaling Factor	Scapula		Clavicle	
	Muscle Force (% Difference to Original)	Muscle Activation (% Difference to Original)	Muscle Force (% Difference to Original)	Muscle Activation (% Difference to Original)
-20%	21.9	20.4	49.3	43.3
-10%	-18.9	18.3	19.4	18.6
10%	21.9	20.5	52.9	51.5
20%	22.3	21.7	17.2	16.0

### Discussion

The sensitivity of the simulation outputs compared to the ratio of trunk to scapula to clavicle mass was analysed to understand potential errors introduced into the model. As presented in the literature review, there was an apparent error propagation throughout the simulation workflow, with substantial potential errors in muscle force and activation estimates.

A small variation in joint kinematics due to scapula and clavicle mass were anticipated, as this calculation is more related to marker placement, with little variation in mass distribution due to the low mass of the scapula (1.1 kg) and clavicle. However, based on the scaling protocols, increased mass is accompanied by increased size, meaning the joint centres are moved relative to the origin. This can also explain why there are such large errors with the static optimisation results, as increased scapula or clavicle size changes the origin and insertion points of a muscle, and hence its line of action relative to the joint centre.

No clear trends were observed with increased mass of either the scapula or clavicle with specific output parameters from any of the analyses. As such, it can be suggested that changes in the distribution of mass within the torso segment has the capacity to alter the system dynamics. Hence, the simulation has a high sensitivity to the value of these parameters. As the models have obtained these parameters from cadaver studies, the values used in this research are relevant. However, future investigations should investigate how to obtain subject-specific values for the relative mass of the scapula and clavicle.

It is also important to understand how the distribution of these masses varies with scaling. For example, a reasonably constant scaling would be anticipated when scaling between a child and adult due to bone growth. However, for athletes, the skeletal mass increases in the torso, which is not necessarily accompanied by bone growth, suggesting that this scaling would not be consistent.

### *Conclusion*

A sensitivity analysis was performed to understand how kinematics, joint reaction moments, and muscle forces alter with a change of scapula and clavicle mass. It was identified that these outputs are highly sensitive to the input masses. Research presented in this thesis was performed using default mass distributions of the torso. It is acknowledged that this may have introduced errors, and that future investigation should examine how clavicle and scapula mass can be estimated for use in computational modelling.

## **C.3 UPPER EXTREMITY MUSCLE DEMAND OF WHEELCHAIR RACING PROPULSION TECHNIQUE**

Wheelchair racing propulsion is a highly dynamic and physically straining activity, utilising much of the upper extremity and back musculature.<sup>123</sup> The significance of the rotator cuff muscles, biceps, triceps, serratus anterior muscles, trapezius and pronator quadratus on propulsion have been demonstrated<sup>169</sup> either through computational simulation<sup>100, 169, 311, 363-366</sup> or EMG<sup>26, 429-431</sup> analysis, with the deltoids frequently considered the most influential. The anterior deltoid (along with the pectoralis major) has been identified as the prime movers for the push phase,<sup>311</sup> while the middle and posterior deltoids are considered crucial for the recovery phase.<sup>335, 432</sup>

While many muscle groups have been considered influential towards the motion, muscles of the shoulder, particularly deltoids are frequently regarded as the most influential. Lin et al.<sup>311</sup> identified the anterior deltoid and pectoralis major as the prime movers for the push phase, while Veeger et al.<sup>432</sup> and Masse et al.<sup>335</sup> have demonstrated the middle and posterior deltoids being crucial for the recovery phase.<sup>432</sup> Veeger et al.<sup>169</sup> further described the significance of the rotator cuff muscles as well as the biceps, triceps, serratus anterior, trapezius and pronator quadratus on propulsion. The key muscles analysed through either computational analysis or electromyography are summarised in Table C.2.



Table C.2 Muscles and the number of muscle elements modelled in computational modelling and EMG literature.

Reference Model	Computational Model							EMG			
	100	363	311	365	366	169	364	430	429	431	26
Trapezius	2	1				1		1	1	1	1
Levator Scapulae	1					1					
Rhomboid Minor	1					1					
Rhomboid Major	1	1									
Serratus Anterior	1	1				1					1
Pectoralis Minor	1	1									
Latissimus Dorsi	1	1	1		3	1	3	1		1	
Pectorialis Major	2	1	2	4	3	1	3	1	1	1	1
Deltoides	2	1	3	3	3	2	3	2	3	2	3
Supraspinatus	1	1	1	1	1	1	1				1
Infraspinatus	1		1	1	1	1	1				1
Subscapularis	1	1	1	1	1	1	1				
Teres Minor	1	1	1	1	1		1				
Teres Major	1	1	1		1		1				
Coracobrachialis	1	1			1		1				
Biceps Breve	1			1	1		1				
Biceps Long	1		1	1	1	1	1				
Triceps	4	2	1	3	3	1	3	1	1	1	1
Brachialis	1	1		1	1	1	1				
Anconeus	1			1	1		1				
Brachioradialis	1	1		1	1		1				
Supinator	2			1	1						
Pronator Teres	2			1	1	1					
Pronator Quadratus	1			1	1	1					
Biceps Brachii		1						1	1	1	1
Suprascapularis		1									1

Verification was performed on the obtained outputs to ensure that the simulation protocol utilised by this research is providing reliable outputs. This verification compared the obtained values to three simulation studies performed on wheelchair propulsion currently presented in the literature, as well as checked the physiological validity of the obtained results.

The instantaneous stress of muscles during the push and recovery phases of manual wheelchair propulsion has been investigated previously in the literature. Muscle recruitment strategies from this research Figure C.3 are consistent with literature by Slowik et al. <sup>10</sup>, whereby the subscapularis muscles and deltoid muscles are under the highest amount of strain. When looking at the magnitudes of these strains, once again data is of consistent magnitude to reported literature,<sup>103</sup> however, there exists a variation in how muscles are loaded.

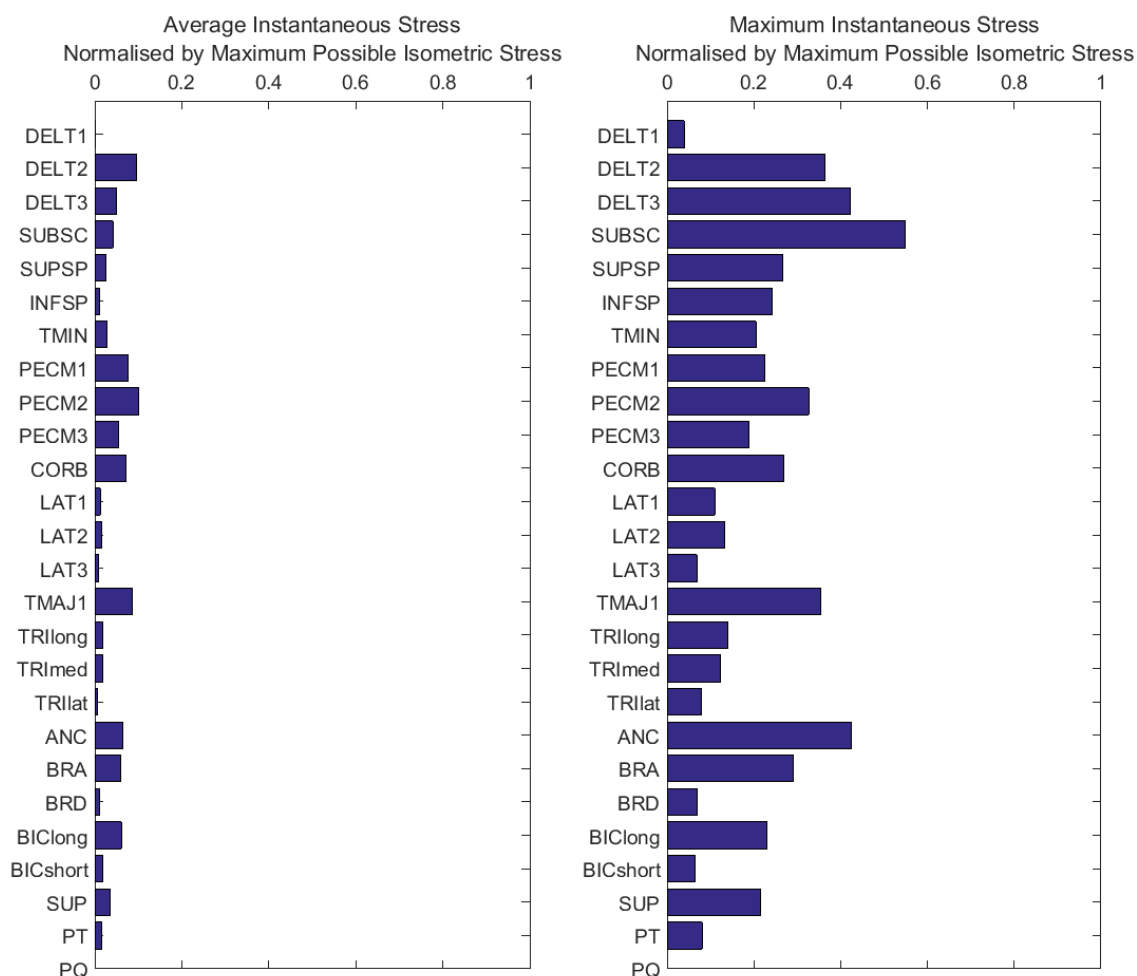


Figure C.3: Average (left) and maximum (right) instantaneous stress for the simulated muscles during wheelchair racing propulsion for Athlete E at 22 km/hr. Delt: deltoid, SUBSC: subscapularis, SUPSP: supraspinatus, INFSP: infraspinatus, TMIN: teres minor, PECM: pectoralis major, CORB: coracobrachialis, LAT: latissimus dorsi, TMAJ: teres major, TRI: triceps, ANC: anconeus, BRA: brachialis, BRD: brachioradialis, BIC: bicep, SUP: supinator, PT: pronator teres, and PQ: pronator quadratus.

In the literature, subscapularis muscles present the most substantial average instantaneous stress (muscle force divided by the maximum isometric force-generating capacity), followed by the pronator quadratus. This is not observed in this research, however, with both of these muscles having low instantaneous stresses. Such differences may be explained by the difference in posture between wheelchair racing (kneeling) and manual wheelchair (conventional, upright) propulsion.

For Athlete I, at 27 km/hr (7.5 m/s), resultant peak forces were approximately 280 N, and at 28 km/hr (7.8 m/s) were 271.6 N, with instantaneous peak values closer to 1130 N (Figure C.4). These are higher than measured values in the literature, where peak tangential forces of 158 N at 20.3 km/hr (5.64 m/s) were reported for propulsion performed on a wheelchair ergometer,<sup>195</sup> with peak radial forces of 166.2 N reported for propulsion at 15.8 km/hr (4.4 m/s) on a wheelchair stationary roller.<sup>433</sup> Peak forces may be higher than reported in the literature as a consequence of the increased speed of testing, but

---

may also be a consequence of the estimation method used in this research. Limitations in this method may be due to the high accelerations at impact, which may not translate directly to increased force. For example, the use of hard, thermoplastic gloves increases stiffness, meaning greater contact accelerations will be measured through the hands than if some of this force were damped through padded gloves. It can be seen that this change in damping does not translate to the amount of force applied. However, as the magnitudes are comparable to the values presented in the literature, it can be inferred that errors in force estimations are likely present. However, they are not detrimental to the research.

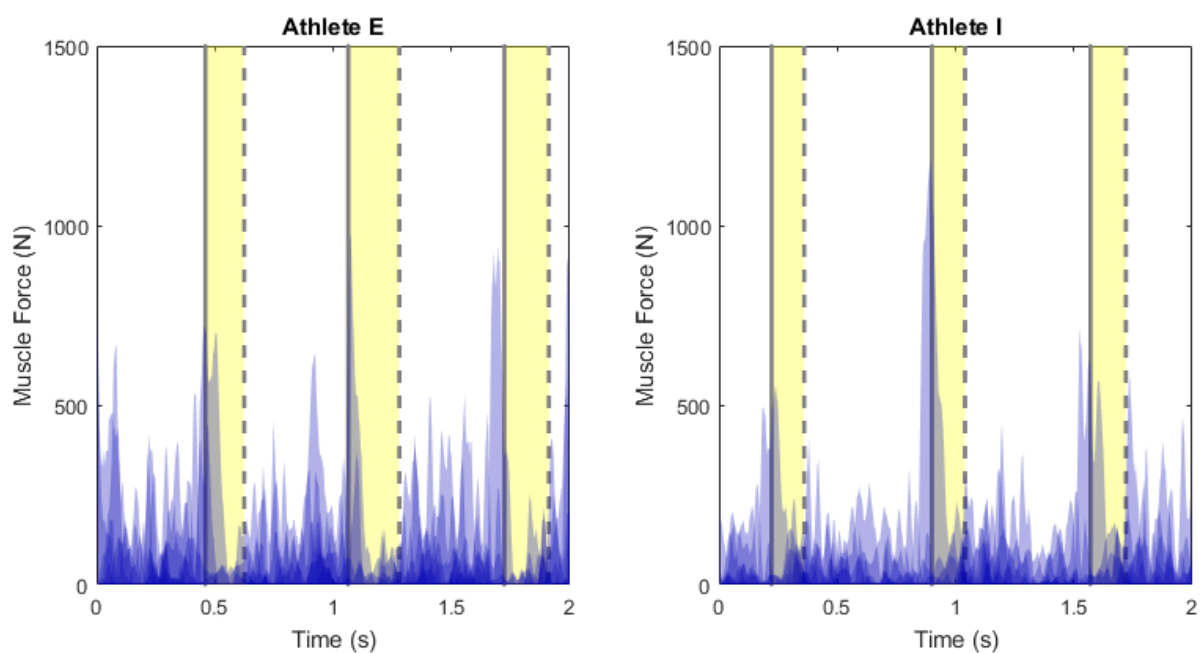


Figure C.4: Muscle force during propulsion (shaded) and recovery phases. Darker regions mean more muscles are being recruited to complete the task.